

UNCLASSIFIED

AD NUMBER

AD822284

LIMITATION CHANGES

TO:

Approved for public release; distribution is unlimited. Document partially illegible.

FROM:

Distribution authorized to U.S. Gov't. agencies and their contractors; Critical Technology; OCT 1967. Other requests shall be referred to Air Force Rome Air Development Center, EMLI, Griffiss AFB, NY 13440. Document partially illegible. This document contains export-controlled technical data.

AUTHORITY

RADC, USAF ltr, 17 Sep 1971

THIS PAGE IS UNCLASSIFIED

AD822284

RADC-TR- 67-465
Final Report



(RAT SCAT) LARGE OBJECT STUDY

Dr. Charles C. Freeny

William P. Cahill

General Dynamics

TECHNICAL REPORT NO. RADC-TR- 67-465
October 1967

This document is subject to special
export controls and each transmittal
to foreign governments, foreign na-
tionals or representatives thereto may
be made only with prior approval of
RADC (FMLI), GAFB, N.Y. 13440

Rome Air Development Center
Air Force Systems Command
Griffiss Air Force Base, New York

When US Government drawings, specifications, or other data are used for any purpose other than a definitely related government procurement operation, the government thereby incurs no responsibility nor any obligation whatsoever; and the fact that the government may have formulated, furnished, or in any way supplied the said drawings, specifications, or other data is not to be regarded, by implication or otherwise, as in any manner licensing the holder or any other person or corporation, or conveying any rights or permission to manufacturer use, or sell any patented invention that may in any way be related thereto.

Do not retain this copy. Return to drawing.

(RAT SCAT) LARGE OBJECT STUDY

Dr. Charles C. Freeny

William P. Cahill

General Dynamics

**This document is subject to special
export controls and each transmittal
to foreign governments, foreign na-
tionals or representatives thereto may
be made only with prior approval of
RADC (EMLI), GAFB, N.Y. 13440**

FOREWORD

This final report was prepared by Dr. Charles C. Freeny and William P. Cahill of General Dynamics, P.O. Box 748, Fort Worth, Texas, under Contract AF30(602)-4300, project number 6503, task 650301. Secondary report number is FZE-670. RADC project engineer is Donald M. Montana (ENASP).

This technical report has been reviewed by the Foreign Disclosure Policy Office (ENLI). It is not releasable to the Clearinghouse for Federal Scientific and Technical Information because it contains information embargoed from release to Sino-Soviet Bloc Countries by AFR 400-10, "Strategic Trade Control Program."

This report has been reviewed and is approved.



Approved:

DONALD M. MONTANA
Program Director's Office
Space Surveillance and Instrumentation Branch



Approved:

JOSEPH FALLIK
Chief, Space Surveillance and
Instrumentation Branch
Surveillance and Control Division

FOR THE COMMANDER:


IRVING J. GABELMAN
Chief, Advanced Studies Group

ABSTRACT

The investigation reported herein has been directed to defining an optimum means of implementing a capability for measurement of large-object radar cross section at the Radar Target Scattering Site, White Sands Missile Range. The required capability is that of accommodating targets up to 60 feet in length, over a frequency range of 0.03 to 12 gigahertz, and maintaining the present RAT SCAT measurement accuracy. The primary trade-off feature in this study was the requirement for range length, which exceeded 16 miles in the case of the most straight-forward approach to large-object measurement. This condition is commonly defined by $R \geq 2D^2/\lambda$ when D is the minimum target dimension and λ is the radar wavelength.

Four basic measurement methods were analyzed in this investigation: (1) scaling, wherein the target size and range length are reduced via the well-known scaling laws, (2) long range and high power, wherein a range length of $2D^2/\lambda$ is used, (3) antenna far field simulation, wherein a dielectric lens is used to partially correct the phase of the incident illuminating field, and (4) analytical correction of near field data, wherein data obtained at $R < 2D^2/\lambda$ is analytically processed to obtain data equivalent to that at $R = 2D^2/\lambda$.

The study conclusions are based on extensive theoretical investigation and experimental testing. Over 200,000 IBM 7090 computations and 250 experiments were performed. A trade-off study was conducted in order to uniformly evaluate the impact of the selection of the several methods. The final selection represents a combination of the long-range and high power, and antenna far-field simulation methods. The sensitive target length and frequency regions were determined to be 30 feet $\leq D \leq$ 60 feet and 4 gigahertz $\leq F \leq$ 12 gigahertz. With these bounds, the latter method is specified for the regions (1) $D > 40$ feet, $F > 4$ gigahertz and (2) $F > 8$ gigahertz. Other methods were eliminated in the trade-off study on the basis of the cost required to achieve the necessary range length or measurement accuracy.

TABLE OF CONTENTS

<u>Section</u>	<u>Title</u>	<u>Page</u>
	Introduction and Summary	1
1.	Technical Investigation	5
1.1	Scaling	6
1.1.1	General	6
1.1.2	Sensitivity Requirements	10
1.1.3	Scaling Frequency	11
1.1.4	Perfect Conductor Scaling	12
1.1.5	Dielectric Scaling	19
1.1.6	Target Support Requirements	24
1.1.7	Equipment Requirements	28
1.1.8	Conclusions	29
1.2	Long Range and High Power	107
1.2.1	General	107
1.2.2	Design Cross Section Level	107
1.2.3	Sensitivity Requirements	108
1.2.4	Antenna Height Effects	110
1.2.5	Target Support Requirements	115
1.2.6	Equipment Requirements	118
1.2.7	Conclusions	126
1.3	Antenna Far Field Simulation	159
1.3.1	General	159
1.3.2	Lens Design	159
1.3.3	Lens Radar Cross Section	166
1.3.4	Lens Physical Properties	167
1.3.5	Lens Fabrication Tolerances	170
1.3.6	Equipment Requirements	174
1.3.7	Conclusions	175
1.4	Analytical Correction of Near Field Data	191
1.4.1	General	191
1.4.2	Range Length Effects	191
1.4.3	Equipment Requirements	195
1.4.4	Conclusions	195

<u>Section</u>	<u>Title</u>	<u>Page</u>
2.	Trade-Off Study	221
2.1	General	221
2.2	Operational Models	223
2.3	General Trade-Off Parameters	227
2.4	Trade-Off Parameters	229
2.5	Conclusions	237
3.	Recommendations	248
3.1	General	248
3.2	Measurement Subsystems	249
3.3	Measurement Procedures	253
3.4	Ancillary Equipments	256
Appendix A	Physical Optics Computer Program Description	269
Appendix B	Near Field Error Computer Program Description	273
References		289

LIST OF FIGURES

<u>Number</u>	<u>Title</u>	<u>Page</u>
1.1-1	Scaling Frequency Flexibility	31
1.1-2	Target Types Used in Computer Study	32
1.1-3	Anomaly Magnitudes	33
1.1-4	Cost vs Tolerance Data	34
1.1-5	Gross Section Error for Target 1	35
1.1-6	Peak Envelope Error for Target 1	36
1.1-7	Lobe Width Error for Target 1	37
1.1-8	Cross Section Error for Target 2	38
1.1-9	Peak Envelope Error for Target 2	39
1.1-10	Lobe Width Error for Target 2	40
1.1-11	Cross Section Error for Target 3	41
1.1-12	Peak Envelope Error for Target 3	42
1.1-13	Lobe Width Error for Target 3	43
1.1-14	Cross Section Error for Target 4	44
1.1-15	Peak Envelope Error for Target 4	45
1.1-16	Lobe Width Error for Target 4	46
1.1-17	Cross Section Error for Target 5	47
1.1-18	Peak Envelope Error for Target 5	48
1.1-19	Lobe Width Error for Target 5	49
1.1-20	Cross Section Error for Target 6	50
1.1-21	Peak Envelope Error for Target 6	51

LIST OF FIGURES
(Sheet 2)

<u>Number</u>	<u>Title</u>	<u>Page</u>
1.1-22	Lobe Width Error for Target 6	52
1.1-23	Cross Section Error for Target 7	53
1.1-24	Peak Envelope Error for Target 7	54
1.1-25	Lobe Width Error for Target 7	55
1.1-26	Cross Section Error for Target 8	56
1.1-27	Peak Envelope Error for Target 8	57
1.1-28	Lobe Width Error for Target 8	58
1.1-29	Cross Section Error for Target 9	59
1.1-30	Peak Envelope Error for Target 9	60
1.1-31	Lobe Width Error for Target 9	61
1.1-32	Cross Section of Target 1 ($k_a = 314$)	62
1.1-33	Cross Section of Target 2 ($k_a = 2198$)	63
1.1-34	Cross Section of Target 3 ($k_a = 2198$)	64
1.1-35	Cross Section of Target 4 ($k_a = 2198$)	65
1.1-36	Cross Section of Target 5 ($k_a = 1760$)	66
1.1-37	Cross Section of Target 6 ($k_a = 2198$)	67
1.1-38	Cross Section of Target 7 ($k_a = 2198$)	68
1.1-39	Cross Section of Target 8 ($k_a = 2198$)	69
1.1-40	Cross Section of Target 9 ($k_a = 2198$)	70

LIST OF FIGURES
(Sheet 3)

<u>Number</u>	<u>Title</u>	<u>Page</u>
1.1-41	Target Configurations	71
1.1-42	Typical Aerospace Vehicle Mock-Up	72
1.1-43	Typical Target Appendages	73
1.1-44	Experimental Data on Target 2A Perturbation Level 0, Fin P-1	74
1.1-45	Experimental Data on Target 2A Perturbation Level 1, Fin P-1	75
1.1-46	Experimental Data on Target 9A Perturbation Level 0 (Spheres B-1)	76
1.1-47	Experimental Data on Target 9A Perturbation Level 2 (Spheres B-2)	77
1.1-48	Cone Cylinder Radar Cross Section Data, Target 2A (Near 2 degrees)	78
1.1-49	Cone Cylinder Radar Cross Section Data, Target 2A (Near 18 degrees)	79
1.1-50	Cone Cylinder Radar Cross Section Data, Target 2A (Near 36 degrees)	80
1.1-51	Error Distributions on Target 2A with Fin Perturbations	81
1.1-52	Error Distribution on Target 8A with Fin Perturbations	82
1.1-53	Error Distributions on Target 9A with Sphere Perturbations	83

LIST OF FIGURES
(Sheet 4)

<u>Number</u>	<u>Title</u>	<u>Page</u>
1.1-54	Cumulative Probability Density on Material Dielectric Constant	84
1.1-55	Cumulative Probability Density on Loss Tangent	85
1.1-56	Frequency Dependence of Dielectric Constant	86
1.1-57	Frequency Dependence of Loss Tangent	87
1.1-58	Dielectric Scaling Coefficient Error	88
1.1-59	Effect of $\tan \delta$ on Dielectric Sphere Scaling	89
1.1-60	Effect of Dielectric Constant on Dielectric Sphere Scaling	90
1.1-61	Dielectric Sphere Cross Section for $\tan \delta = 0.002$ (small kt)	91
1.1-62	Dielectric Sphere Cross Section for $\tan \delta = 0.002$ (large kt)	92
1.1-63	Perturbation Cross Section Error Effect	93
1.1-64	Dielectric Component Target Data ($\lambda/4$ thickness Teflon Material)	94
1.1-65	Dielectric Component Target Data ($\lambda/4$ thickness Polyethelene Material)	95
1.1-66	Cumulative Density on Dielectric Scaling Error (35 GHz)	96

LIST OF FIGURES
(Sheet 5)

<u>Number</u>	<u>Title</u>	<u>Page</u>
1.1-67	Cumulative Density on Dielectric Scaling Error (10.75 GHz)	97
1.1-68	Frequency Dependence of Styrofoam Column Cross Section	98
1.1-69	Hollow Target Support Column Geometry	99
1.1-70	Hollow Styrofoam Column Cross Section Reduction	100
1.1-71	Column Cross Section Reduction Requirements for 35-GHz Scaling	101
1.1-72	Target Support Columns	102
1.1-73	Tilted Styrofoam Column Data (X-Band)	103
1.1-74	Tilted Styrofoam Column Data (Ka-Band)	104
1.1-75	Vertical, Hollow Styrofoam Column Data (X-Band)	105
1.2-1	Average Cross Section for Representative Large Targets	129
1.2-2	Cross Section of Target 1	130
1.2-3	Cross Section of Target 2	131
1.2-4	Cross Section of Target 3	132
1.2-5	Cross Section of Target 4	133
1.2-6	Cross Section of Target 5	134
1.2-7	Cross Section of Target 6	135

LIST OF FIGURES
(Sheet 6)

<u>Number</u>	<u>Title</u>	<u>Page</u>
1.2-8	Cross Section of Target 7	136
1.2-9	Cross Section of Target 8	137
1.2-10	Cross Section of Target 9	138
1.2-11	Long Range and High Power Sensitivity Requirements	139
1.2-12	Vertical Plane Field Probes	140
1.2-13	Terrain Elevation Contour	141
1.2-14	Vertical Plane Near Field Error Model (Horizontal Cylinder Model)	142
1.2-15	Vertical Plane Near Field Error (Vertical Cylinder Model)	143
1.2-16	Vertical Plane Near Field Error (Two Scatterer Model)	144
1.2-17	Antenna Height Reduction Error Levels	145
1.2-18	Cumulative Error Density with 20-Percent Antenna Height Reduction	146
1.2-19	Cumulative Error Density with 30-Percent Antenna Height Reduction	147
1.2-20	Cumulative Error Density with 40-Percent Antenna Height Reduction	148
1.2-21	Vertical Plane Gradient Experimental Data (Ideal Antenna Height)	149
1.2-22	Vertical Plane Gradient Experimental Data with 30-Percent Antenna Height Reduction	150

LIST OF FIGURES
(Sheet 7)

<u>Number</u>	<u>Title</u>	<u>Page</u>
1.2-23	Large Target Styrofoam Support Cross Section Data	151
1.2-24	Real-Time Vector Subtraction Range Geometry	152
1.2-25	Real-Time Vector Subtraction Block Diagram	153
1.2-26	Target Cross Section Data for Noise Subtraction	154
1.2-27	Target-Plus-Noise Data for Noise Subtraction	155
1.2-28	Analog Noise Subtraction Block Diagram	156
1.2-29	Data Rate and Interval	157
1.3-1	Dielectric Lens Geometry	177
1.3-2	Dielectric Lens Design Parameter	178
1.3-3	Lens Width Requirements	179
1.3-4	Lens Thickness Requirements	180
1.3-5	Weight of Dielectric Lens	181
1.3-6	Lens Wind Loading	182
1.3-7	Near-Field Aperture Pattern	183
1.3-8	Dielectric Lens Phase Contour Correction	184
1.3-9	Range Geometry Using Lens	185

LIST OF FIGURES
(Sheet 8)

<u>Number</u>	<u>Title</u>	<u>Page</u>
1.3-10	Lens Height Requirements	186
1.3-11	Frequency Limitation in Fixed Range Operation Using Lens	187
1.3-12	Lens Construction Tolerance Require- ments	188
1.3-13	Lens Surface Variation Geometry	189
1.3-14	Lens Surface Variation Requirements	190
1.4-1	Near Field Error Computer Program	198
1.4-2	Normalized Size vs Frequency and Target Length	199
1.4-3	Cross Section at Selected Ranges (100 λ Cylinder Near 0 Degrees)	200
1.4-4	Cross Section at Selected Ranges (100 λ Cylinder Near 7 Degrees)	201
1.4-5	Cross Section at Selected Ranges (100 λ Cylinder Near 20 Degrees)	202
1.4-6	Cross Section at Selected Ranges (100 λ Cylinder Near 30 Degrees)	203
1.4-7	Cross Section at Selected Ranges (500 λ Cylinder Near 0 Degrees)	204
1.4-8	Cross Section at Selected Ranges (500 λ Cylinder Near 7 Degrees)	205

LIST OF FIGURES
(Sheet 9)

<u>Number</u>	<u>Title</u>	<u>Page</u>
1.4-9	Cross Section at Selected Ranges (500 λ Cylinder Near 20 Degrees)	206
1.4-10	Cross Section at Selected Ranges (500 λ Cylinder Near 30 Degrees)	207
1.4-11	Cross Section for Selected Antenna Sizes (100 λ Cylinder Near 30 Degrees)	208
1.4-12	Cross Section for Selected Antenna Sizes (500 λ Cylinder Near 30 Degrees)	209
1.4-13	Measurement versus Theory (Range = D^2/λ)	210
1.4-14	Measurement versus Theory (Range = $4D^2/\lambda$)	211
1.4-15	Cumulative Error Density on the General Case Cylinder	212
1.4-16	Cumulative Error Density on 60-Inch Cylinder	213
1.4-17	Cumulative Error Density on Target 2A	214
1.4-18	Cumulative Error Density on Target 9A	215
1.4-19	Experimental Data on 60-Inch Cylinder, Range Position 0	216
1-4-20	Experimental Data on 60-Inch Cylinder, Range Position 2	217
1.4-21	Experimental Data on Target 9A, Range Position 0	218
1.4-22	Experimental Data on Target 9A, Range Position 2	219

LIST OF FIGURES

(Sheet 10)

<u>Number</u>	<u>Title</u>	<u>Page</u>
2.1-1	Procedure Flow Diagram for Trade Off Study	238
2.2-1	Cumulative Density on Measurement Frequency	239
2.2-2	Cumulative Density on Target Length	240
2.2-3	Cumulative Density on Target Length Squared	240
2.2-4	Cumulative Density on D^2/λ	241
2.2-5	Measurement Time as a function of Target Length	242
2.2-6	Total Range Hours as a Function of Target Length	243
2.3-1	Range Length Requirements	244
2.3-2	Antenna-Target Height Requirements	245
2.3-3	Sensitivity Requirements	246
2.3-4	Sensitivity Improvement Requirements	247
3.2-1	Basic RAT SCAT Equipment Additions	259
3.2-2	Phase Measurement Block Diagram	260
3.2-3	Basic Coherent Integration Block Diagram	261
3.2-4	Dielectric Lens Specifications	262

LIST OF FIGURES

(Sheet 11)

<u>Number</u>	<u>Title</u>	<u>Page</u>
3.3-1	Dielectric Lens Mounting	263
3.3-2	Target-Lens Separation Envelope	264
3.3-3	Antenna-Lens Separation Envelope	265
3.3-4	Long-Range Length Operational Envelope	266
3.3-5	Recommended Range Layout	267
A-1	Basic Computer Logic	272
B-1	Subroutine 1 Program H-86	285
B-2	Subroutine 2 Program H-86	286
B-3	Subroutine 3 Program H-86	287
B-4	Subroutine 4 Program H-86	288

LIST OF TABLES

<u>NUMBER</u>	<u>TITLE</u>	<u>PAGE</u>
1.1-1	Scaling Method Measurement Equipment	11
1.1-2	Target and Perturbation Level Parameters	15
1.2-1	Large Target Cross Section Characteristics	109
1.2-2	Calibration Data Adjustment	115
1.2-3	Range Capability Improvement Costs	118
1.2-4	Equipment Sensitivity Improvements	120
1.2-5	Long-Range and High-Power Sensitivity Cost Data	123
1.2-6	Long-Range and High-Power Method Equipment Requirements	128
1.3-1	Antenna Far Field Simulation Method Equipments	174
1.4-1	Parameters Values for Near Field Error Program	194
1.4-2	Sensitivity Equipment Requirements	195
2.2-1	Target Length and Frequency Band Allocations	226
2.4-1	Technique Option I	230
2.4-2	Technique Option II	232
2.4-3	Technique Option III	234
2.4-4	Technique Option IV	235
3.2-1	Large Object Implementation Design Summary	247
3.2-2	System Implementation Components	251

LIST OF TABLES

<u>Number</u>	<u>Title</u>	<u>Page</u>
3.4-1	Preliminary Rotator Specifications	256
A-1	Equations for Five Basic Types of Surface	271
B-1	Validation Data for Subroutine II	284

EVALUATION

The objective of this effort is to gather data necessary and sufficient to establish the criteria upon which the long range planning of the RAT SCAT Facility can be based. The difficulties of performing radar cross section (RCS) measurements on very large objects are well known and established facts. The solutions (and many have been considered singly and in combination) invariably lead to complicated and costly forms of instrumentation or analysis. Prior to the arbitrary implementation of any particular solution at the Radar Target Scattering Range (RAT SCAT), it was felt prudent to complete a trade-off study of cost vs the accuracy of resulting RCS data. A valid conclusion could only be reached if all aspects of the various solutions to the problem including the initial implementation costs, recurring costs, and the operation and maintenance of the range were included in the study. This accounts for the scope of the effort and the thoroughness of the reported results. The ultimate usefulness of this work is therefore technical guidelines for future RAT SCAT upgrading in the most cost effective manner to achieve a specified measurement accuracy goal.

Donald M. Montana

DONALD M. MONTANA
Contract Engineer

INTRODUCTION AND SUMMARY

This technical report contains a description of the theoretical and experimental study conducted and the results obtained in the measurement of large objects at the Radar Target Scattering Site (RAT SCAT), White Sands Missile Range. The objective set for this effort was to determine the magnitude and complexity of the addition to and modification of the existing RAT SCAT facility necessary (1) to obtain radar cross section data on targets up to 60 feet in length and (2) maintain the quality of the measurement data so that it is comparable to the quality of the data obtained on smaller targets. This study consisted of a methodical comparison of the several possible solutions of the near field problem via a theoretical investigation and experimental measurements and field tests performed at the Fort Worth Division radar range and the RAT SCAT facility.

The present capability of accurately measuring the full-scale static radar cross section of very large vehicles over the RAT SCAT frequency range of 0.03 to 12 gigahertz is extremely limited. Reasonably accurate radar cross section measurements are commonly based on the criterion that the target-to-radar range equal the overall target length squared times the reciprocal of the operating wavelength ($R = 2D^2/\lambda$). Thus as target length increases, the maximum frequency available for accurate measurement decreases rapidly.

On the basis of previous RAT SCAT experience, it appears that there are two distinct classes of vehicles to be measured: (1) nose cones and other small aerospace objects which are well within the capability of the RAT SCAT equipment and (2) large payloads or entire vehicles, including propulsion packages, whose physical dimensions exceed the design limits of the measurement equipment. The latter group is of interest in this study since only limited frequency coverage can presently be furnished for measuring this type of object. Consequently, effort was specifically placed on defining the most practical method of obtaining measurements of ± 1 dB quality of a large object, 30 to 60 feet in length, at the RAT SCAT facility. This work included a theoretical investigation of several possible methods, an experimental investigation conducted to validate the theoretical results, and a trade-off study which resulted in the selection of the most promising approaches for future implementation at RAT SCAT.

The theoretical and experimental investigation, reported in Section I of this report, consisted in evaluating the following measurement methods:

1. Scaling techniques
2. Long range and high power technique
3. Simulation of far-field conditions by use of a unique antenna configuration
4. Analytical correction of near-field data to approximate far-field results.

The evaluation of the above methods was oriented toward determining

1. The degree of accuracy theoretically possible
2. The speed with which data can be acquired
3. The relative cost (both initial cost and operating cost)
4. The type of personnel required to obtain good data on an operational basis (engineers or technicians).

The experimental investigation was oriented toward validating candidate solutions on the basis of how closely the theoretically determined accuracy can be approximated under real-world conditions.

Section II contains a description of the trade-off study. This effort was based on the theoretical evaluation and experimental testing, and it resulted in the selection of the most suitable method of performing radar cross section measurements on large objects. The factors given primary consideration in selecting a method were

1. Adaptability to field operation
2. Accuracy
3. Cost (initial cost and operating cost).

The conclusions and recommendations reached in this study are discussed in Section 3. The recommendations take the form of a specification of the RAT SCAT equipment modifications required and a specification of necessary procedures.

In summary, the long-range and high-power method was selected as the primary means of large object radar cross section measurement. This approach allows a direct extension of the measurement procedures presently used at RAT SCAT and the equipment sensitivity is adequate with minor modifications from Band 0 (30 mega-

hertz) through Band 5 (4 gigahertz) and in Band 6 over the target length region of 30- to 40-feet; a maximum range length of 30,000 feet is required in this case. To accommodate the remaining target sizes and frequencies, a new range length of 21,000 feet was selected and a technique was chosen which makes use of a dielectric lens to correct the field phase curvature which at the higher frequencies becomes excessive. Tests conducted at RAT SCAT confirmed the feasibility of operation at these range lengths and the expected accuracy is considered sufficient to offset the disadvantages introduced by using the lens of additional range setup time and time lost due to inclement weather conditions. In addition, the small utilization rate required of the lens significantly reduces the impact of these disadvantages.

The long range and high power investigation indicated that the range length associated costs such as control cable and sensitivity improvement equipments were significantly greater than the cost of the dielectric lens and the increased cost of measurement time required using the lens.

In the scaling method investigation, the errors were found to be excessive except under conditions where target fabrication costs were excessive; in addition, a severe problem was found to exist in the area of target support reduction requirements at the higher frequencies (35 gigahertz, was highest frequency considered based on availability of power). The analytical correction of near field data method was found to be unfeasible because of the random nature of the errors introduced at range lengths significantly less than $2D^2/\lambda$. Although the actual error levels encountered using range lengths on the order of D^2/λ were not large, on the average, the errors incurred at individual aspects were considered excessive.

SECTION I

TECHNICAL INVESTIGATION

Details of the theoretical and experimental study are discussed in this section in terms of the four basic methods investigated. The primary emphasis is placed on range length requirements (and corresponding equipment sensitivity requirements) and the impact of the selection of a technique on measurement accuracy, adaptability to field operations, and cost.

Except in the case of special measurement techniques, the range length requirement is based on providing a sufficiently uniform phase illumination function at the target. This effect is recognized as a limitation on the accuracy of radar cross section measurements. The criterion commonly employed to reduce this error to an acceptable level is that of allowing $R \geq 2D^2/\lambda$ where R is the range length, D is the minimum target dimension, and λ is the radar wavelength. Thus it is necessary to provide very long range lengths or means of correcting the incident phase front in some cases of large object measurements.

On the basis of the present RAT SCAT capability, the limitation on accuracy is commonly specified as a normally distributed error function whose standard deviation is 1 dB. It is assumed that normally distributed errors are introduced by use of a technique or associated features that differ from those presently used at RAT SCAT, the acceptable error can be specified by a standard deviation on the order of 0.5 dB. This level represents the total permissible additional degradation of the measurement data.

Adaptability to field operations is a measure of how well present RAT SCAT equipments and procedures meet the requirements for the measurement of large objects.

The costs associated with each of the measurement methods under consideration necessarily include both initial and recurring costs. Significant factors include initial cost of method implementation and other costs peculiar to each technique.

Since the long range and high power method is retained as the basic measurement approach, equipment or process items common to all methods are included in the discussion associated with this method.

1.1 Scaling

1.1.1 General

To obtain radar cross section data, electrodynamic similitude laws have been extensively used to scale targets for measurements at short ranges and selected frequencies rather than continuous frequency coverage and/or long ranges. Consequently, the major advantages and disadvantages of the scaling technique are widely publicized. However, not much quantitative information is available for ascertaining the practical generality, the accuracies, and the cost of using scaling at RAT SCAT to obtain data on targets to 60 feet in length at frequencies between .03 and 12 gigahertz to the accuracies required. In particular, the advantages of scaling relative to the overall study are the reductions in range length and target handling time, and the primary disadvantages are related to equipment and target fabrication costs. Hence, the objective set for this theoretical investigation was to obtain, in conjunction with available data, sufficient information to make a high-confidence, realistic evaluation of the applicability of solving the RAT SCAT large-target problem via scaling.

The conditions for scaling or electrodynamic similitude have been delineated by Stratton (Reference 1), and they can be reduced to the form of two characteristic parameters C_1 and C_2 which must be invariant to a change in scale.

$$\mu \epsilon \left(\frac{l}{T} \right)^2 = C_1, \quad \mu \Delta \frac{l^2}{T} = C_2 \quad (1.1-1)$$

where

- μ = permeability
- ϵ = permittivity
- Δ = conductivity
- l = characteristic dimension
- T = wave period.

The case of interest in scaling is commonly that of target fabrication based on highly conductive and/or perfect dielectric

materials. In these cases, the scaling law normally used is obtained from the above relation containing C_1 . The practical consideration in these cases is that of maintaining a constant l/λ . In this case, it can be demonstrated that the cross section relationship is

$$\sigma_s = \sigma_0 s^2 \quad (1.1-2)$$

where S and 0 subscripts respectively refer to scaled and full-scale targets, and S is the scaling factor. Hence, in the cases where the conductivity is zero or infinite, the only consideration is the practical ability to maintain a constant l/λ ratio by using the same material on the model as that used on the full-scale target since the cross sections of the scaled and full-scale targets are related in a simple manner. However, in all cases, the conductivity is in the range $0 < \Delta < \infty$. Hence, to be exact, the relation involving C_2 must also be satisfied; consequently, Δ_s must equal Δ_0/S . The effect of this approximation depends upon the type of scatter as well as the range of Δ . For example, in the large ka region where the scattering is primarily specular, the cross section of a medium-to-large dielectric constant target can be approximated by

$$\sigma = \sigma_m \Gamma^2 \quad (1.1-3)$$

where

σ_m = cross section of perfect conducting target of same configuration

$$\Gamma = \left(\sqrt{\epsilon_r} \sqrt{1 - j \frac{60 \Delta \lambda}{\epsilon_r}} - 1 \right) / \left(\sqrt{\epsilon_r} \sqrt{1 - j \frac{60 \Delta \lambda}{\epsilon_r}} + 1 \right)$$

= plane surface reflection factor

ϵ_r = dielectric constant

It can be seen that only in a limited range will the influence of Δ noticeably affect the cross section. In addition, if the scale factor is correctly selected, depending upon λ , ϵ_r , and

Δ , the cross section error caused by not scaling conductivity can be minimized.

In contrast to the above example just discussed is the case of a low-dielectric constant, low-loss material. In Equation 1.1-4 is the expression which has been found to describe the minimum cross section return from a styrofoam right circular cylinder (Reference 2).

$$\sigma = L^2 (k_0 d)^3 (15)^2 (\Delta^1)^2 (\epsilon_r - 1)^2 / 2 \quad (1.1-4)$$

L = Length of column

d = Diameter of column

Δ^1 = Number proportional to conductivity and independent of frequency

k = $2\pi/\lambda$

ϵ_r = Relative dielectric constant of styrofoam.

If Equation 1.1-4 is used to compute the cross section on the basis of the scaling laws, σ_S is equal to σ_0 since $\Delta^1 S$ is equal to Δ^1_0/S . This apparent discrepancy is due to the dependence of the styrofoam conductivity on frequency. Hence in this case, if the conductivity was doubled, the scaled model cross section would be in error by $20 \log S$ if the normal cross section scaling law stated in Equation 1.1-2 was used. This example indicates that the frequency dependence of materials and targets must at least be considered when the cross section is directly dependent upon the material constants. These cases are likely to be prevalent in the examination of absorbers and minimum cross sections of low-loss materials, as illustrated in the above example. Although the majority of targets are likely to be of the large-conductivity class (metal), the techniques and feasibility of handling material problems is considered in the investigation in order to ascertain correctly the generality and cost of using scaling to obtain accurate cross section data on large targets.

Another limitation on the selection of the scale factor or scaled frequency is related to the sensitivity requirements imposed upon the measurement system. The influence of scaling on range and consequently on power requirements can be seen by considering a modified form of the radar range equation:

$$\frac{P_R}{P_t} = K^1 \frac{\sigma \lambda^2}{R^4} \quad (1.1-5)$$

where

P_R = received power
 P_t = transmitted power
 σ = radar cross section
 λ = operating wavelength
 R = range.

It will be noted that, in this equation form, antenna gain is constant under the assumption that the maximum practical gain will be used. If an accuracy requirement is assumed to be of the form

$$R = \frac{\rho D^2}{\lambda} \quad (1.1-6)$$

where ρ is a constant, Equation 1.1-5 can be written

$$\frac{P_R}{P_t} = K \frac{\sigma_o \lambda_o^6}{D_o^8}$$

for the full-scale case. Since the scale factor S can be expressed as

$$S = \frac{\lambda_s}{\lambda_o} = \frac{D_s}{D_o} = \left[\frac{\sigma_s}{\sigma_o} \right]^{\frac{1}{2}} \quad (1.1-7)$$

then

$$\frac{P_R}{P_t} = K \frac{\sigma_s \lambda_s^6}{D_s^8}$$

The influence of scaling on the range required can be seen by consideration of Equation 1.1-6. Upon substitution of the usual scaling relations, Equation 1.1-6 becomes

$$R_s/R_o = S \quad (1.1-8)$$

Thus it can be seen that use of the scaling technique reduces the severity of the minimum range requirements. On the basis of the above relationship, it can be seen that, under the assumed conditions, scaling introduces no change in radar sensitivity requirements over the full-scale requirements, but it reduces the range requirement in proportion to the scale factor. However, it should be noted that obtaining the required sensitivity is more costly at the higher frequencies and the maximum scaled $2 D^2/\lambda$ can be large.

Another important feature in the scaling investigation is that of target support requirements. As indicated by Equation 1.1-2, the scaled cross section decreases at a rate of 20 dB per decade of scale factor (or frequency), and in Equation 1.1-4, the minimum cross section of the styrofoam columns increases at a rate of 30 dB per decade of frequency for a given column size. Thus, there is a potential target-to-support column cross section margin reduction of 50 dB per decade of frequency change, and this change can introduce severe errors.

Significant aspects of these features are discussed in detail in the following paragraphs. The results of the investigation are limited to the characteristic dimension region of $300 \leq ka \leq 5000$ and the scaling factor region $0.05 \leq S \leq 0.5$. The errors resulting from a limited degree of attention to detail in model fabrication are presented in terms of cross section magnitude, peak envelope, and lobe structure errors. This categorization of errors is appropriate because of the fine lobe structure associated with the large ka values for which this measurement method is most appropriate.

1.1.2 Sensitivity Requirements

As indicated in paragraph 1.1.1, the equipment sensitivity requirements are invariant to the scale factor imposed. Therefore, the sensitivity requirements defined for the more tractable full-scale case can be used to define requirements for the case in which a range length of $2 D^2/\lambda$ is maintained. Data germane to this requirement is subsequently discussed in paragraph 1.2.2 and 1.2.3 in which the design radar cross section of -30 dBsm and the maximum sensitivity factor of 74 dBW₂ (Figure 1.2-11) are defined. This sensitivity factor is defined as $PG^2/(NF)(B)$ where P is the peak power transmitted, G is the antenna gain, NF is the system noise figure, and B is the noise bandwidth. A description of the required radar system features is presented in Table 1.1-1.

Table 1.1-1 SCALING METHOD MEASUREMENT EQUIPMENTS

Frequency	35 GHz
Bandwidth*(1 MHz)	61 dB
Noise Figure	15 dB
Antenna Gain	48 dB
Power	53 dBW
$\frac{PG^2}{(B)(NF)}$	73 dBW
Area Cost	\$200,000

*Based on a 9-dB noise improvement over a 10-gigahertz bandwidth

The tabulated data are 1 dB less than the maximum requirement, but it is anticipated that an additional 1 dB can be made available. In any case, the system will allow measurement of more than 99 percent of the target and frequency combinations expected.

1.1.3 Scaling Frequencies

The selection of scaling frequencies is based on the considerations associated with the degree of flexibility provided and the availability of equipments. An examination of the high-power equipment available for operation at 12 gigahertz and above resulted in an obvious preliminary selection of the frequencies 12, 17, 35, and 80 gigahertz. On the basis of the equipment available, including moderate development effort, the 80-gigahertz frequency is not attractive and may not be feasible because of the limited power available and such practical problems as waveguide breakdown.

The degree of flexibility is based on the availability of scaling factors in the range $0.1 \leq S \leq 0.5$. The 0.5 boundary is assigned on the basis that reduction in the range length to more than 0.5 is not an attractive solution, and the 0.1 boundary

is assigned on the basis of the potential problems with target supports which are discussed in paragraph 1.1.6. In any case, the choice of scaling frequency is not a sensitive function of the boundaries selected. The flexibility in the choice of 12- and 35-gigahertz scaling frequencies is illustrated in Figure 1.1-1 in terms of the alternate full-scale frequencies as a function of the use of the selected full-scale frequency as a scaling reference. On the basis of these data, it can be seen that, if a target is scaled from 12 to 35 gigahertz, the highest alternate full-scale frequency for use with the same target model is 4.1 gigahertz. This value represents the case of using a scaled frequency of 12 gigahertz. Thus, for the case selected, data could not be obtained over the range $4.1 \leq F_0 \leq 12$ by using a single model. Similarly, a target model, based on a reference full-scale frequency scaled to 12 gigahertz, will allow the simulation of (1) any full-scale frequency below the reference (since RAT SCAT coverage will be continuous below 12 gigahertz) and (2) a spot frequency at which 35-gigahertz scaling can be used. This spot frequency is shown as the curve labeled equivalent 35 gigahertz in Figure 1.1-1. Thus it can be seen that, in measurement frequencies in the range greater than 6 gigahertz, one model will be required for each full-scale frequency, but below 6 gigahertz one model will suffice in addition to possibly providing a correct scale factor for one full-scale frequency higher than 6 gigahertz for use at the 35-gigahertz scaling frequency. An examination of the operational data shown in subsection 1.5 will reveal that 75 percent of the time the required measurement frequency will be less than 6 gigahertz and that, on the basis of RAT SCAT experience, the average number of frequencies required in a measurement program is approximately 5. Thus it appears that 2 target models with different scale factors will suffice for the average measurement program.

It is clear that the use of an 80-gigahertz scaling frequency would limit the flexibility more than use of the 35-gigahertz scaling frequency because of the more extreme scaling factors required. A scaling frequency in the vicinity of 17 gigahertz will allow greater flexibility but will require scaling factors significantly greater than the 0.5 boundary assigned in order to scale from a 12-gigahertz full-scale frequency.

1.1.4 Perfect Conductor Scaling

The objectives set for this task were those of realistically simulating and evaluating the effects of the model inaccuracies anticipated in scaling large, perfectly conducting targets for

measurement at frequencies of 35 gigahertz and below 12 gigahertz. The steps used in meeting these objectives can be summarized as (1) the computation of cross section by using physical optics formulas for representative types of large objects, (2) the introduction of realistic construction inaccuracies and the recomputation of cross section, (3) the use of the data attained in steps 1 and 2 to define a realistic range of target aspect angles, ka regions, and construction accuracies, (4) the analysis and subsequent relation of the simulated measurement errors generated in steps 1, 2, and 3 to technical feasibility and model cost, and (5) a comparison of theoretical and experimental data.

The computer program used to perform the sequential computations is described in Appendix A. Approximately 150,000 computations were made to obtain data for the purposes described above. A total of nine geometries were used to represent the class of large (30- to 60-foot), perfectly conducting targets of interest. The electrical size (ka) range used in studying each of these targets was between 10 and 5000, and the cross section was examined at no less than 150 aspects in order to generate the complex patterns representative of large objects.

The target configurations used in the computer study are depicted in Figure 1.1-2 (solid lines). Also noted in the figure (dashed lines) are the construction anomalies which were simulated in each case. The type anomalies indicated in Figure 1.1-2 are considered typical of those which will be encountered in model fabrication, and combinations were selected on the basis of those considered to be representative of anomalies which would actually be encountered in practice. The magnitudes of the anomalies were selected to cover a range of construction tolerances between costly precision machine shop models and relatively inexpensive models on which normal tolerances on the detailed components might be exceeded several orders of magnitude. In addition, the magnitudes of the anomalies were selected to be somewhat larger than those indicated for state-of-art machine shop practice in order to account for human errors along with errors in obtaining accurate full-scale drawings and/or measurements. In this approach, each of the anomaly magnitudes used in the study is considered to be representative in that they should not be exceeded more than 5 percent of the time.

The anomaly magnitudes used in the study are indicated in Figure 1.1-3 in terms of tolerances in inches versus percent of the base-scale factor of each of the scale factors used in the study. Also indicated in the figure are the scale-model size

ranges associated with each of the scale factors. The fact that scale factor and model size are interrelated is a consequence of the size limits placed on the full-scale targets (30 to 60 feet). Also, the two sets of curves (one for low values of base scale factor and the other for the high values) are a consequence of placing realistic tolerances on the basic shape sizes (low values) and on the detailed items, such as nuts, bolts, and small appendages (high values). The actual values computed appear in Table 1.1-2.

The data presented in Figure 1.1-3 are related to model cost in Figure 1.1-4. The scale of the cost axis in the figure is considered a realistic area estimate at this time; it is based on model cost information obtained from current or recently completed programs in which models were fabricated for cross section measurements. Also, the cost data on relatively simple geometries and that on models involving the assembly of many detailed parts were averaged to arrive at a single cost scale as a function of model size and tolerances. Hence the cost data related to a given model size and tolerance should be low for a complex target and high for a simple model.

To relate the information presented in Figure 1.1-4 to the measurement error which can be expected on the basis of a given model cost and target size, it is necessary to use the error data presented in Figures 1.1-5 through 1.1-31. The error data presented in these figures were obtained by using the targets depicted in Figure 1.1-2 and the anomaly magnitude ranges shown in Figure 1.1-3. In the case of each target type, error data are presented in terms of (1) cumulative error (70 percentile or the 10 point), (2) peak envelope error, and (3) lobe-width error. These three types of error data are presented in Figures 1.1-5, 1.1-6, and 1.1-7 for the case of the cone-cylinder type of target. The subsequent figures contain data on the remaining target types.

The cumulative error data were obtained by averaging the cross section error computed for at least 150 aspect angles at each k_a and for each target anomaly magnitude. The peak envelope error was obtained in a similar manner; however, use was made only of those data obtained in the aspect vicinity of the peak cross section values of the reference (i.e., the cross section values of the perturbed geometry were compared with the reference geometry in the vicinities of the lobe maximums). The lobewidth errors were obtained by (1) comparing the lobe widths of the perturbed geometry with those of the reference in corresponding aspect regions and (2) averaging the results.

Table 1.1-2 PERFECT CONDUCTOR SCALING ANALYTICAL TARGETS DESCRIPTION (SHEET 1)

Target	Configuration	DIMENSIONS - Wavelengths									
		Ka=314	Ka=440	Ka=628	Ka=785	Ka=942	Ka=1256	Ka=1570			
#1	Cone	10x3.33		20x6.66		30x9.99	40x13.32	50x16.65			
	Cylinder	40x3.33		80x6.66		120x9.99	160x13.32	200x16.65			
#2	Cone	10x3.33	14x4.662	20x6.66	25x8.325	30x9.99	40x13.32	50x16.65			
	Cylinder	40x3.33	56x4.662	80x6.66	100x8.325	120x9.99	160x13.32	200x16.65			
#3	Plate	1.11x3.33	1.554x4.662	2.22x6.66	2.775x8.325	3.33x9.99	4.44x13.32	5.55x16.65			
	Cone	10.7x5.7	14.98x7.98	21.4x11.4		32.1x17.1	42.8x22.8	53.5x28.5			
#4	Frustum	1.8	2.52	3.6		5.4	7.2	9			
	Cylinder	37.5x6.25	52.5x8.75	75x12.5		82.5x18.75	150x25	187.5x31.25			
#6	Cone	21.4x5.7	29.96x7.98	42.8x11.4		64.2x17.1	85.6x22.8	107x28.5			
	Frustum	3.6	5.04	7.2		7.8	14.4	18			
#7	Cylinder	25x6.25	35x8.75	50x12.5		75x18.75	100x25	125x31.25			
	Plate	10x2.0	14x2.8	20x4		30x6	40x8	50x10			
#8	Cone	16.67x3		33.33x6			66.66x12				
	Frustum	25x3		50x6			100x12				
#9	Cylinder	8.33x3x4		16.66x6x8			33.32x12x16				
	Cone	16.67x6		33.33x12			66.66x24				
#10	Cylinder	33.33x6	23.33x8.4	66.66x12			133.32x24				
	Small Cylinder	16.67x.6	23.33x.84	33.33x1.2			66.66x2.4				
#11	Hemisphere	1.5	2.1	3.0			6				
	Hemisphere	3.11	4.354	6.22		9.33	12.44	15.55			
#12	Cylinder	8.33x3.11	11.66x4.354	16.66x6.22		24.99x9.33	33.32x12.44	41.65x15.55			
	Frustum	5.22x3.633	7.308x5.0862	10.44x7.266		15.66x10.899	20.88x14.532	26.11x18.165			
#13	Sphere #1	.075	.075	.1		.1	.1875	.1875			
	Sphere #2	.075	.075	.1		.1	.1875	.1875			
#14	Sphere #3	.075	.075	.1		.1	.1875	.1875			
	Cone	5x5.5	7.0x7.5	10x11		15x16.5	20x22	25x27.5			
#15	Cylinder	10x5.5	14x7.5	20x11		30x16.5	40x22	50x27.5			
	Frustum	5x6x5.5	7.0x7.5x8.4	10x11x12		15x16.5x18	20x22x24	25x27.5x30			
#16	Cylinder	20x6	28x8.4	40x12		60x18	80x24	100x30			
	Cylinder	10x.6	14x.84	20x1.2		30x1.8	40x2.4	50x3.0			
#17	Sphere #1	.075	.075	.1		.1	.1875	.1875			
	Sphere #2	.075	.075	.1		.1	.1875	.1875			
#18	Sphere #3	.075	.075	.1		.1	.1875	.1875			
	Cylinder										
#19	Frustum										
	Cylinder										
#20	Hemisphere										
#21	Cylinder	Ka=251		Ka=502			Ka=1004				
	Frustum	16x5		32x10			64x20				
#22	Cylinder	4		8			16				
	Hemisphere	8x4		16x8			32x16				
#23		4		8			16				

Table 1.1-2 PERFECT CONDUCTOR SCALING ANALYTICAL TARGETS DESCRIPTION (SHEET 2)

Target	Configuration	DIMENSIONS - Wavelengths									
		Ka=2198	Ka=2669	Ka=3140	Ka=3460	Ka=3768	Ka=4396				
#1	Cone	70x23.31	85x28.305	100x33.3		120x39.96	140x46.62				
	Cylinder	280x23.31	340x28.305	400x33.3		480x39.96	560x46.62				
#2	Cone	70x23.31	85x28.305	100x33.3		120x39.96	140x46.62				
	Cylinder	280x23.31	340x28.305	400x33.3		480x39.96	560x46.62				
#3	Plate	7.77x23.31	9.435x28.305	11.1x33.3		13.32x39.96	15.54x46.62				
	Cone	74.9x37.9	90.95x48.45	107x57	117.7x62.7	128.4x68.4	149.8x79.8				
#4	Frustum	12.6	15.3	18.0	19.8	21.6	25.2				
	Cylinder	262.5x43.75	18.75x53.125	375x62.5	412.5x68.75	450x75	52.5x87.5				
#6	Frustum	149.8x39.9		214x57	235.4x62.7		300.6x79.8				
	Cylinder	25.2		36	39.6		50.4				
#7	Plate	70x14		100x20	110x22		140x28				
	Cone	116.69x21		166.7x30			233.38x42				
#8	Frustum	175x21		250x30			350x42				
	Cylinder	58.31x21x28		83.3x30x40			116.62x42x56				
#9	Cone	116.69x42		166.7x60			233.38x84				
	Cylinder	233.31x42		333.3x60			466.62x84				
#10	Small Cylinder	116.69x4.2		166.7x6			233.38x8.4				
	Hemisphere	10.5		15			21				
#11	Hemisphere	21.77	26.435	31.1	34.21	37.32	43.54				
	Cylinder	58.31x21.77	70.805x26.435	83.3x31.1	91.63x34.21	99.96x37.32	116.62x43.54				
#12	Frustum	36.54x25.431	44.37x30.8805	52.2x36.33	57.42x39.963	62.64x43.596	73.08x50.862				
	Sphere #1	.1875	.3	.3	.3	.5	.5				
#13	Sphere #2	.1875	.3	.3	.3	.5	.5				
	Sphere #3	.1875	.3	.3	.3	.5	.5				
#14	Cone	35x38.5	42.5x46.75	50x55	55x60.5	60x66	70x77				
	Cylinder	70x38.5	85x46.75	100x55	110x60.5	120x66	140x77				
#15	Frustum	35x38.5x42	42.5x46.75x51	50x55x60	55x60.5x66	60x66x72	70x77x84				
	Cylinder	140x42	170x51	200x60	220x66	240x72	280x84				
#16	Cylinder	70x4.2	85x5.1	100x6.0	110x6.6	120x7.2	140x8.4				
	Sphere #1	.1875	.3	.3	.3	.5	.5				
#17	Sphere #2	.1875	.3	.3	.3	.5	.5				
	Sphere #3	.1875	.3	.3	.3	.5	.5				
#18	Cylinder	Ka=1760		Ka=2510			Ka=3514				
	Frustum	112x35		160x50			224x70				
#19	Cylinder	28		40			56				
	Frustum	56x28		90x40			112x56				
#20	Cylinder	28		46			56				
	Hemisphere										

In Figures 1.1-32 through 1.1-40 typical cross section data are shown for the case of each of the nine target types used in the study. In each of the cases shown, the cross section data of the unperturbed geometry is presented along with the data for the worst case anomaly used in the aspect region and for the k_a value indicated on each figure.

By combining the error data presented in Figures 1.1-5 through 1.1-32 with the cost information presented in Figure 1.1-4, the expected cost of obtaining high-quality data via the scaling technique can be ascertained once the acceptable error limits are selected and the number of models and k_a region per model are selected.

The experimental program devoted to perfect conductor scaling was based on obtaining validation data on targets similar to target types 2, 8, and 9, as illustrated in Figure 1.1-2. The actual configurations used in the program are illustrated in Figure 1.1-41. Photographs of typical target components are presented in Figures 1.1-42 and 1.1-43; typical data obtained at 35 gigahertz are illustrated in Figures 1.1-44 through 1.1-47. Figures 1.1-44 and 1.1-46 contain reference data on targets 2A and 9A, and Figures 1.1-45 and 1.1-47 represent the results obtained from imposing the indicated perturbation levels on each of the targets.

Theoretical data obtained on target 2A are shown in Figures 1.1-48 through 1.1-50. In this example, an attempt was made to accurately duplicate the target configuration for the measurement and the computed data. This example indicates the fine grain structure of the pattern, even at the low k_a value of 1200, when it is compared with the experimental pattern shown in Figures 1.1-44 or 1.1-45. It should be noted that these patterns are expanded by a factor of 2 so that the minor divisions on the abscissa represent one degree of azimuth rather than the commoner 2-degree increment.

The error data derived from the experimental data is shown in Figures 1.1-51 through 1.1-53. These data are in the form of the cumulative density distribution on the error in dB between a reference configuration and the same configuration after a perturbation has been introduced. Because of the relatively unstable point-to-point data obtained from the measurement of large- k_a targets, especially at the high frequency of 35 gigahertz, a number of repeated runs were made in order to obtain

a measure of the statistics of the basic measurement system. As a result of this effort, a number of cumulative density curves were obtained with an average standard deviation of 1.07 dB. This value was used in interpreting the error data to obtain an accurate measure of the influence of the perturbations through the common relationship

$$\sigma_p = \left[\sigma_M^2 - (1.07)^2 \right]^{1/2} \quad (1.1-9)$$

for distributions which are approximately Gaussian. The results of this process are plotted as extra data points on the theoretical data shown in Figures 1.1-9, 1.1-27, and 1.1-30. The values obtained are compatible and within the error spread predicted as a result of the theoretical analysis.

An additional consideration in the scaling of targets is that of the requirements for the material used in fabrication and the material used as a coating to simulate the characteristics of metal targets. In the case of target fabrication in which common construction materials, such as aluminum, are used no consideration of surface material is necessary because the conductivity of the material is a large value (on the order of 10^7 mhos per meter) and in this range the influence of small changes in conductivity is negligible, especially when the primary scattering is specular. In addition, computations were made at the Fort Worth Division by applying the rigorous scattering formulation for a sphere, whose conductivity was finite, and the results were used to demonstrate that the influence of a wide range of large conductivities was negligible in the case of all scattering mechanisms of the sphere.

Experience in target construction at GD/FW has indicated that reasonable care in coating nonmetallic targets will produce satisfactory results, although no definitive program has been conducted to evaluate the total effect of coating materials. Previously conducted tests have included the measurement of right circular cylinders coated with a high-quality silver preparation in which the data obtained closely approximated the physical optics cross section predictions. In addition, from a theoretical viewpoint, there appears to be no problem in providing an adequate coating on nonmetallic targets either

in terms of conductivity or thickness. The tendency for RF energy to remain near the surface of a conductor reduces the requirement for care in joint construction as well as that in metallic coating thickness. This feature is commonly described in terms of the skin depth, d , given by

$$d = (\pi f \mu \Delta)^{-1/2} \quad (1.1-10)$$

where f is the frequency, μ is the material permeability, and Δ is the conductivity. It can be seen from Equation 1.1-10 that the skin depth is small in the frequency and conductivity range of interest. For example, at a frequency of 35 gigahertz and a conductivity of 10^7 mhos per meter, d is only about 8.5×10^{-5} cm; thus it can be seen that several skin depths can be obtained with normal processing.

1.1.5 Dielectric Scaling

The basic approach in the area of dielectric scaling has been that of (1) examination of the range of expected values of material electrical properties, (2) application of these values to the scaling models, and (3) examination of the dielectric component contribution to the total target cross section. The analytical formulation of the electrical properties used in the analysis is of the form $\exp(-i k^* r)$ where k^* is the complex propagation constant commonly represented by $k_0 (\epsilon_r^*)^{1/2} = k_0 (\epsilon_r - i \epsilon_r \tan \delta)^{1/2}$ where ϵ_r is the material dielectric constant and $\tan \delta$ is the loss tangent. As previously discussed, the scaling laws are commonly employed by maintaining a constant ratio of L/λ and a constant ϵ and μ . Consequently, $\tan \delta$ must remain constant for exact scaling.

The two analytical models used in the analysis for dielectric scaling evaluation are based on (1) the usual definition of the reflection coefficient and (2) the radar cross section of a dielectric sphere whose conductivity is finite. The error forms are established on the basis of the fact that, in ideal scaling, no change in the reflection coefficient will occur and the sphere cross section will change as the square of the scale factor. Thus the error E in the reflection coefficient model

is

$$E = 20 \log \frac{\epsilon'_{1s}}{\epsilon'_{1o}} = \frac{\sqrt{\epsilon_r^*} - 1}{\sqrt{\epsilon_r^*} + 1}$$

and in the spherical model

$$E = 10 \log \frac{\epsilon_s}{\epsilon_o s^2} \quad (1.1-11)$$

where S is the scale factor and the s and o subscripts are used to designate the scaled and base configuration, respectively. The results of the analysis indicate that the reflection coefficient model will produce an indication of considerably smaller errors than the spherical model.

In order to define the range of electrical properties of interest in the analysis, a survey of the range of parameters in common materials was conducted, and the results shown in Figures 1.1-54 through 1.1-57 were obtained. An examination of these data indicates that a large-percentage change should be expected in the loss tangent especially when a scaling frequency of 35 gigahertz is considered. This condition is particularly apparent in the data in Figure 1.1-57 (the dashed lines indicate areas of uncertainty). However, an examination of the form of reflection coefficient equation (Equation 1.1-11) will reveal the fact that the results obtained by using this model are not critical in terms of the value of the loss tangent since the dielectric constant is much greater than the loss tangent in the range of values of interest. The results obtained by using the dielectric spherical model were found to be sensitive to all parameters.

The theoretical results of the dielectric scaling analysis are shown in Figures 1.1-58 through 1.1-61. The results shown in Figure 1.1-58 are based on the reflection coefficient error model. In this model, the effects of $\tan \delta$ are insignificant so that the influence of changes in dielectric properties can be related to the dielectric constant alone. An examination of these data indicate that the worst-case error is not severe. In the

extreme cases, the ratios of the scaled and the full-scale dielectric constant are 2 and 0.5, and the magnitude of the error will be less than 3 and 4 dB, respectively; the effect of this order of error on the overall target cross section will of course be small if the dielectric components are physically small relative to the target size.

In the spherical models, the influence of electrical property changes is illustrated in Figures 1.1-58 through 1.1-62. To obtain these data, 7100 lossy dielectric sphere computations were made on the Fort Worth Division IBM 7090. Computations were made over the previously designated range of parameters by varying the dielectric constant in steps of 0.1 and $\tan \delta$ in steps of 0.003. The variation in the radius of the sphere was $\lambda/4$ to 3λ . In order to provide a systematic means of analyzing the data and presenting the results, the data was analyzed in terms of the error introduced by a change of 0.003 (increasing) in $\tan \delta$ for a given kt where k is the propagation constant of the material and t is the diameter (analog of overall material thickness). The data displayed in Figure 1.1-59 forms the envelope of the maximum error level encountered at the lowest kt value. In referring to a given error ϵ_i at a particular kt , the error will be less than ϵ_i at a smaller kt . In general terms, the error resulting from changes in $\tan \delta$ is monotonic and well behaved so that the onset of the sensitive areas are defined.

The influence of a change of 0.1 (decreasing) in the dielectric constant is shown in Figure 1.1-50. The data display is based on the peak envelope error with $\tan \delta = 0.002$ and also for the cases of $0.002 \leq \tan \delta \leq 0.026$. The results indicate that the errors introduced by ϵ_r changes are much more severe than those caused by $\tan \delta$ changes. This result is expected because of the relative values of ϵ_r and $\tan \delta$. It is of interest to note that, in view of the general class of materials which could be used in target fabrication, the maximum change expected in the dielectric constant is 10 percent (e.g., 5 to 4.5) over the frequency range of interest (See Figure 1.1-54). This fact can be used to advantage if the kt region of interest is not located in a critical region. The data shown in Figures 1.1-61 and -62 indicate the sensitivity of the cross section to changes in ka for the case of $\tan \delta = 0.002$. The data computed indicates that the errors introduced by a change in the dielectric constant are severe in the cases where the sphere model is applicable. The severity of the problem is such that no general rule can be established and each application must be

considered individually. In general, it appears that the closest possible tolerance should be maintained. However, the implication of the foregoing observation must be placed in the proper perspective by considering (1) the number of times this model will be applicable, and (2) the cross section level of the dielectric component relative to the overall target cross section.

The acceptable latitude in the material property values is potentially enhanced by the fact that the dielectric component may not be a significant contributor relative to the basic target cross section level. Evidently there is a category of perturbations which are small enough that any attempt at scaling or possibly complete omission of the perturbation would suffice. This feature is illustrated in Figure 1.1-63 wherein the maximum error resulting from an error in the cross section level of a minor perturbation is plotted as a function of the scattering from the minor perturbation relative to that of other scatterers. The data is presented in the form of constant contours of 0.5- and 1-dB maximum error levels. The data shown in this figure was derived on the basis of assuming that the total scattered power was of the form

$$\sigma_t = (Ae^{i\theta} + Be^{i\phi})^2 \quad (1.1-12)$$

If the amplitude of B is in error by the factor α , the maximum resultant error is given by the ratio of the resultant signal at the phase angle of maximum sensitivity to this type of error. Thus the maximum error can be written

$$E = \frac{(1 - \alpha)^2}{(1 - \alpha)^2} \quad (1.1-13)$$

where $\alpha = B/A$.

The portion of the experimental program oriented toward providing validation data on dielectric components was conducted by using target 9A with a layer of dielectric material attached to Cy-3 and Cy-5. In this configuration, the dielectric component of the target represents a significant portion of the scattering contribution of the target. The electrical properties of the

material, commercial grade teflon and polyethylene, were measured, and the materials were accurately machined to the dimension indicated in the figures. Data were obtained at X-Band (10.75 gigahertz) and at Ka-Band (35 gigahertz). Typical Ka-band results are shown in Figures 1.1-64 and 1.1-65 for the case of $\lambda/4$ thickness material of the two types selected. These data and similar runs are compared on the basis of the cumulative density on error in Figures 1.1-66 and 1.1-67. The results indicate that the dielectric scaling problem is as severe as that predicted on the basis of the theoretical results. The actual 1σ point on these curves of Ka-Band data must be obtained by using equation 1.1-9, but the adjustment required in the case of the X-Band data is insignificant because of the smaller target dimensions and the stability of the X-Band equipment. It appears that the primary scattering mechanism is specular since the severest effects are produced by materials with a $\lambda/4$ thickness (two-way phase shift of 180 degrees). Therefore, the reflection coefficient model appears to be most applicable to this target configuration. However, the resulting errors greatly exceed those indicated by the data in Figure 1.1-64 because of the complex nature of the target; i.e., the interference pattern from the several scattering centers will be severely influenced by a small change in the phase or amplitude of the scattering of one or more of the contributors.

The results indicate that there is no general solution to the accuracy requirements associated with scaling dielectric materials. Rather, each situation must be treated individually. Moreover, the accuracy requirements associated with common dielectric components are extreme, especially when it is necessary to maintain at least 3 separate parameters to the close tolerances which can be inferred from the previous discussion. Accuracy requirements will commonly impose the limitation of a maximum deviation of 2 percent in a parameter or dimensional value. Although there is a wide range of common materials available for selection, the probability of realizing all requirements simultaneously is low. In addition, contacts with potential manufacturers have indicated that unreasonably large costs would occur if an electrical parameter (ϵ_r or $\tan\delta$) with a tolerance closer than ± 10 percent was guaranteed. The most promising source of materials with electrical parameter specifications by the user appears to be U. S. Polymeric, Inc., Santa Ana, California.

1.1.6 Target Support Requirements

A potentially severe limitation on the utility of the scaling technique is that of the radar cross section levels of the styrofoam (cellular plastic) target supports. Reference 2 contains a derivation of the minimum radar cross section obtained by "tuning" a right circular styrofoam cylinder, and the results indicate a significant reduction in the radar cross section. However, the predicted reduction is limited by the material conductivity. This feature is particularly significant when a scaling technique is used since the frequency dependence of the cross section of the target and the polyfoam support act to reduce the differences in the relative signal levels as the frequency is increased.

On the basis of the theoretical prediction of the effects of conductivity and the results obtained from experimentally determining the frequency dependence of the conductivity of styrofoam, the minimum cross section of a right circular column is proportional to the third power of the frequency ($k d$). Thus, the selection of a typical, unmodified, styrofoam column for use in a scaling application can be expected to exhibit a minimum cross section which is larger by a factor of S^{-3} at the scaling frequency. This feature is illustrated in Figure 1.1-68 on the basis of experimental data obtained in the RAT SCAT R&D program (Reference 3). This factor, plus the fact that the cross section of the scaled target will be reduced by a factor of S^2 , can theoretically result in a 50-dB-per-decade reduction in the target-support cross section margin.

Two means of reducing the cross section of styrofoam for use in the scaling technique are available. The first is that of reducing the size of the support column. This approach is attractive since a drastic reduction in target weight can be realized in the scaled target. However, the use of this approach will not produce sufficient reduction in cross section. The data shown in Figure 1.1-68 is based on a support column whose rating is about 800 pounds, and a reduction in column size will have a severe influence on the load-bearing capability of the column. The common criterion used in rating columns is based on buckling failure, and in this case the load-bearing capability is proportional to the fourth power of the diameter. A scaled, 60-foot target maybe expected to approach the 800-pound weight cited; therefore, the reduction in column cross section must be based on modification of the column configuration.

A modification available in the fabrication of support columns is that of forming a right cylindrical shell. This process does not severely affect the buckling properties of the column, but provides an additional parameter to minimize the effects of the conductivity of the material to produce a significant reduction in the cross section.

The analytical model used in cross section prediction is based on particle scattering and is given in Reference 2 as

$$\sigma = \sigma_s \left| \int_0^{\infty} e^{-12ky} n(y) dy \right|^2 \quad (1.1-14)$$

where $n(y)$ in the integrand is the number of particles per unit depth, σ_s is the particle radar cross section, and k is equal to $2\pi/\lambda$. Although the cross section expression can vanish under ideal circumstances, the use of a realistic model which includes the use of the dielectric loss tangent results in a nonvanishing, coherent component.

The expression in Equation 1.1-14 can be written in a more useful form by expanding the σ_s term. The particle cross section to be used is that of the spherical shell,

$$\sigma_s = 4\pi t^2 (ka)^4 (\epsilon - 1)^2 \quad (1.1-15)$$

where

t = shell thickness

a = sphere radius

ϵ = dielectric constant of shell material.

Equation 1.1-15 can be written in a more tractable form by substituting a relationship between the bulk cellular plastic

material dielectric constant, ϵ_b , and the constituent material dielectric constant (Reference 2),

$$(\epsilon_b - 1) = (\epsilon - 1) \left[1 - \left(\frac{b}{a} \right)^2 \right] \quad (1.1-16)$$

where $b - a$ = shell thickness. If it is assumed that the spherical shells are uniformly distributed with a density of

$$N/V = 1/(8 a^3)$$

the $\mathcal{N}(y)$ can be represented by $N A(y)/V$ where $A(y)$ is the projected geometrical cross sectional area at y .

The backscattering from the column can now be written as

$$\sigma = \frac{\pi k^4}{64} (\epsilon_b - 1)^2 \left| \int_0^\infty A(y) e^{-12ky} dy \right|^2 \quad (1.1-17)$$

In the case of the cylindrical structure (see Figure 1.1-69) the area function can be written as

$$A(y) = 2L (a^2 - y^2)^{\frac{1}{2}}, \quad -a \leq y \leq -b \quad (1.1-18)$$

$$b \leq y \leq a$$

$$A(y) = 2L \left[(a^2 - y^2)^{\frac{1}{2}} - (b^2 - y^2)^{\frac{1}{2}} \right], \quad -b \leq y \leq b$$

When the appropriate $A(y)$ is inserted in Equation 1.1-17, the following is obtained:

$$\sigma = \frac{\pi^3 k^2 L^2}{64} \left[a J_1(2k^*a) - b J_1(2k^*b) \right]^2 \quad (1.1-19)$$

where $k^* = k_0 (1 - i \tan \delta)^{\frac{1}{2}} \approx k_0 (1 - i \frac{\tan \delta}{2})$ and J_1 is the first-order Bessel function.

To predict the effect of this type of support construction relative to experimental data on the solid cylinder ($b = 0$), the expression of interest is the ratio, R , of the respective minimum cross section levels. When the high-frequency approximation,

$$J_1(z) = (\pi z)^{-\frac{1}{2}} (\sin z - \cos z)$$

is used, this ratio becomes

$$R = \frac{\cos(2ka - 3\pi/4) + ika \tan \delta \sin(2ka - 3\pi/4) - (b/a)^{\frac{1}{2}} \cos(2kb - 3\pi/4)}{\cos(2ka - 3\pi/4) + ika \tan \delta \sin(2ka - 3\pi/4)} \quad (1.1-20)$$

where $\tan \delta$ is small.

In this expression the effects of conductivity are minimized when $2ka - 3\pi/4 = n\pi$, and equation 1.1-20 becomes

$$R = 1 - (b/a)^{\frac{1}{2}} \quad (1.1-21)$$

Thus it appears that the limit of cross section reduction by use of this approach is dependent only on the wall thickness. However, in practice, it will be necessary to apply careful construction techniques in order to approximate the reduction theoretically possible. A plot of equation 1.1-21 is presented in Figure 1.1-70. A comparison of these data and the reduction required (Figure 1.1-71) indicates that this approach will produce only marginal results, and the results of the experimental program verify this observation.

The experimental program devoted to the dielectric column was based on Ka- and X-band measurements on two right circular column configurations and two typical target cradle configurations. The columns were measured in both vertical and tilted positions. The results of the experimental program strongly indicate that the

results obtained by tilting the columns offer definite advantages over column tuning. The experimental results are presented in Figure 1.1-68. The Ka-Band data measurements do not necessarily represent minimum cross section values because of the difficulty in tuning the Ka-Band magnetron and the sensitivity level of the measurement system. The test columns are shown in Figure 1.1-72.

Typical examples of the experimental data obtained are shown in Figures 1.1-73 through 1.1-75. The effects of tilting the column are illustrated in Figures 1.1-73 and 1.1-74. The only potentially undesirable aspect of the pattern is the "broad side" peak obtained, but careful target orientation should obviate this effect. In addition, it was noted that a maximum reduction in this peak of about 10 dB could be made by tuning the system frequency at this azimuth angle.

The data in Figure 1.1-75 illustrates the effects of mechanical tolerances on the results obtained by using a hollow styrofoam column. In this example, the return from the column was nulled by tuning the transmitter frequency, but the sinusoidal pattern appeared as the column was rotated. The jig used to fabricate this column was set up to produce a column accuracy of 0.05 inch which should be adequate for X-band. However, it is not possible to accurately measure the dimension of the styrofoam material; consequently, the actual mechanical tolerances can be influenced by column deformation during and after machining.

An additional consideration is the backscatter contribution from the target support cradle which is commonly placed between the target and the basic support column. Unlike portions of the basic column, this device is fully illuminated by virtue of being placed near the center of the vertical plane pattern and can therefore contribute significantly to the support system backscatter. Test results indicate that a 3- to 5-dB increase in the configuration can be expected when a target cradle is used.

1.1.7 Equipment Requirements

Equipments required to implement the scaling method are limited to the system delineated in Table 1.1-1 and range length associated components such as those delineated in paragraph 1.1.8.

1.1.8 Conclusions

The conclusions reached in the investigation of the scaling method as a potentially cost effective means of large object radar cross section measurement are delineated below in terms of (1) adaptability of field operation, (2) accuracy, and (3) cost.

The range of parameters used in the investigation was limited to the point at which it became apparent that the cost effectiveness of other methods exceeded that of the scaling method.

1.1.8.1 Adaptability to Field Operation. The scaling method of large object measurement is readily adaptable to the present RAT SCAT operation if the target fabrication task is excluded. The reduced target size and weight results in a reduction in target mounting time (dependent on target weight and length); however, on the basis of the experience in operating the 35-gigahertz system at the Fort Worth Division, additional time (15 percent) is required for equipment setup and the data runs as a result of the relative instability of the high-frequency measurement system. Otherwise, the operational procedures and system components are identical to those presently used at RAT SCAT.

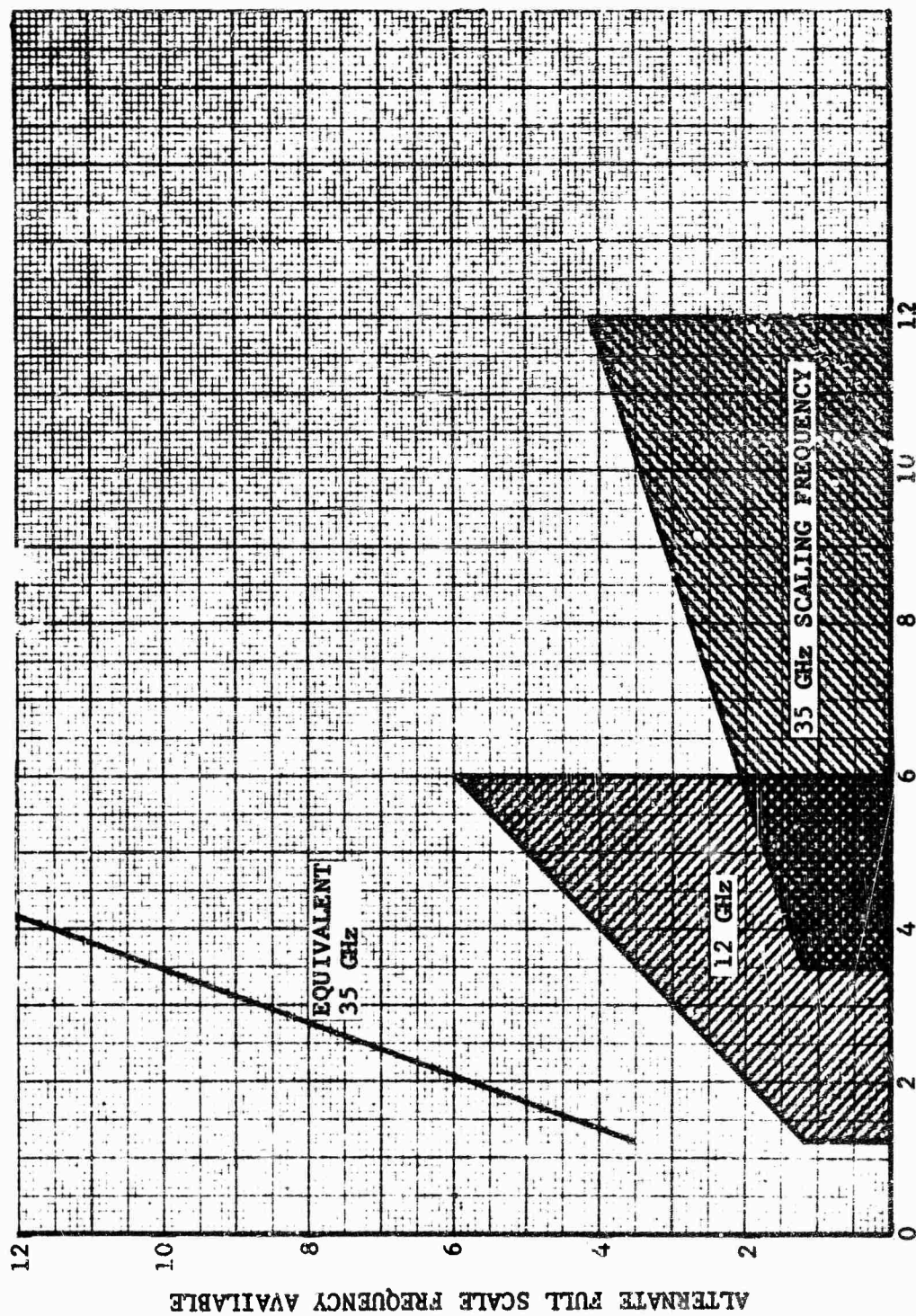
1.1.8.2 Accuracy. In the scaling measurement method, the accuracy available is a sensitive factor of the cost allowed for target fabrication. By using the most accurate target fabrication criteria investigated, the 1σ (standard deviation) of the error is approximately 1.1 dB in Band 6 and 1.5 dB in Band 7. These error levels do not include those associated with dielectric material scaling or target support cross section levels which have been shown to be severe error sources. The error estimate is based on the average magnitude error over the kL range applicable to each band. The trade-off study results indicate that this level of error is not competitive with other methods on a cost effectiveness basis (subsection 2.4).

1.1.8.3 Cost. The most significant cost features associated with the scaling method are the costs of system implementation and target fabrication. An area estimate of \$200,000 (refer to Table 1.1-1) has been established for the system; target fabrication costs are shown in Figure 1.1-4. As described in subsection 2.4, the primary area of applicability for this method is the range $40 \text{ feet} \leq D \leq 60 \text{ feet}$ in Band 6 (4 to 8 gigahertz) and $30 \text{ feet} \leq D \leq 60 \text{ feet}$ in Band 7 (8 to 12 gigahertz). On the basis of the

operational model subsequently presented in subsection 2.2, the model cost is \$176,000 and \$609,000 in Bands 6 and 7, respectively, over a 5-year period. The estimate is based on the average model size over the applicable scale factors, the two models required per measurement program, and the perturbation level 1 cost data.

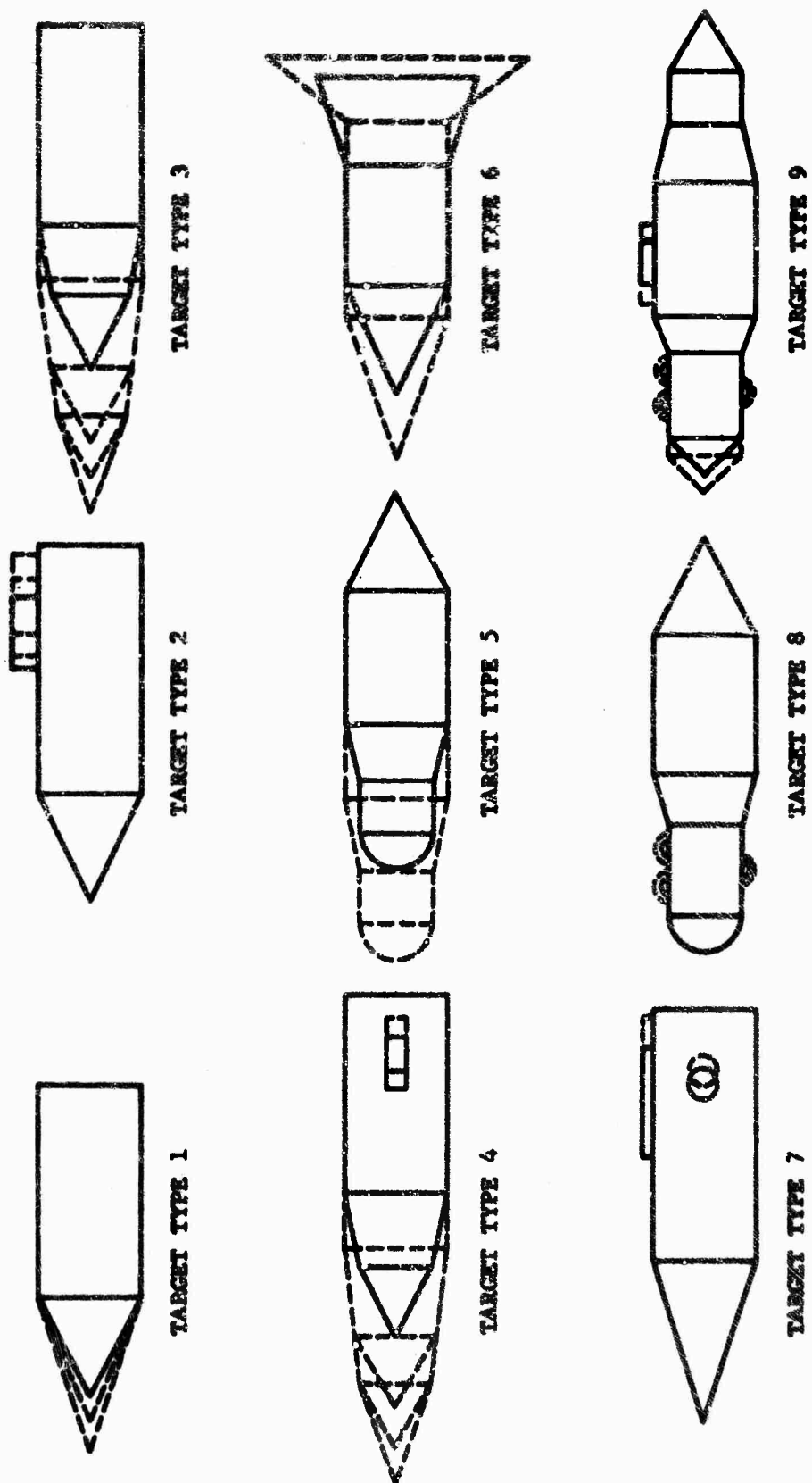
Other cost considerations include the range length associated costs and the target handling cost as described in paragraphs 1.2-8 and subsection 2.3. These include a cost of \$2 per foot of rotator control and signal lines and roadway construction over a range length of 28,000 feet.

1.1.8.4 Other Considerations. Other considerations which influence the overall utility of the scaling methods include the relative instability of the higher frequency systems and the fact that some system components are operated near the state of the art limitation; consequently, the probability of excessive recurring costs is increased, especially in case of the high power magnetron required (see Table 1.1-1).



FULL SCALE FREQUENCY SCALING REFERENCE - GHz

Fig. 1.1-1 SCALING FREQUENCY FLEXIBILITY



NOTE: DASHED LINES INDICATE PERTURBATION TYPES

Fig. 1.1-2 TARGET TYPES USED IN COMPUTER STUDY

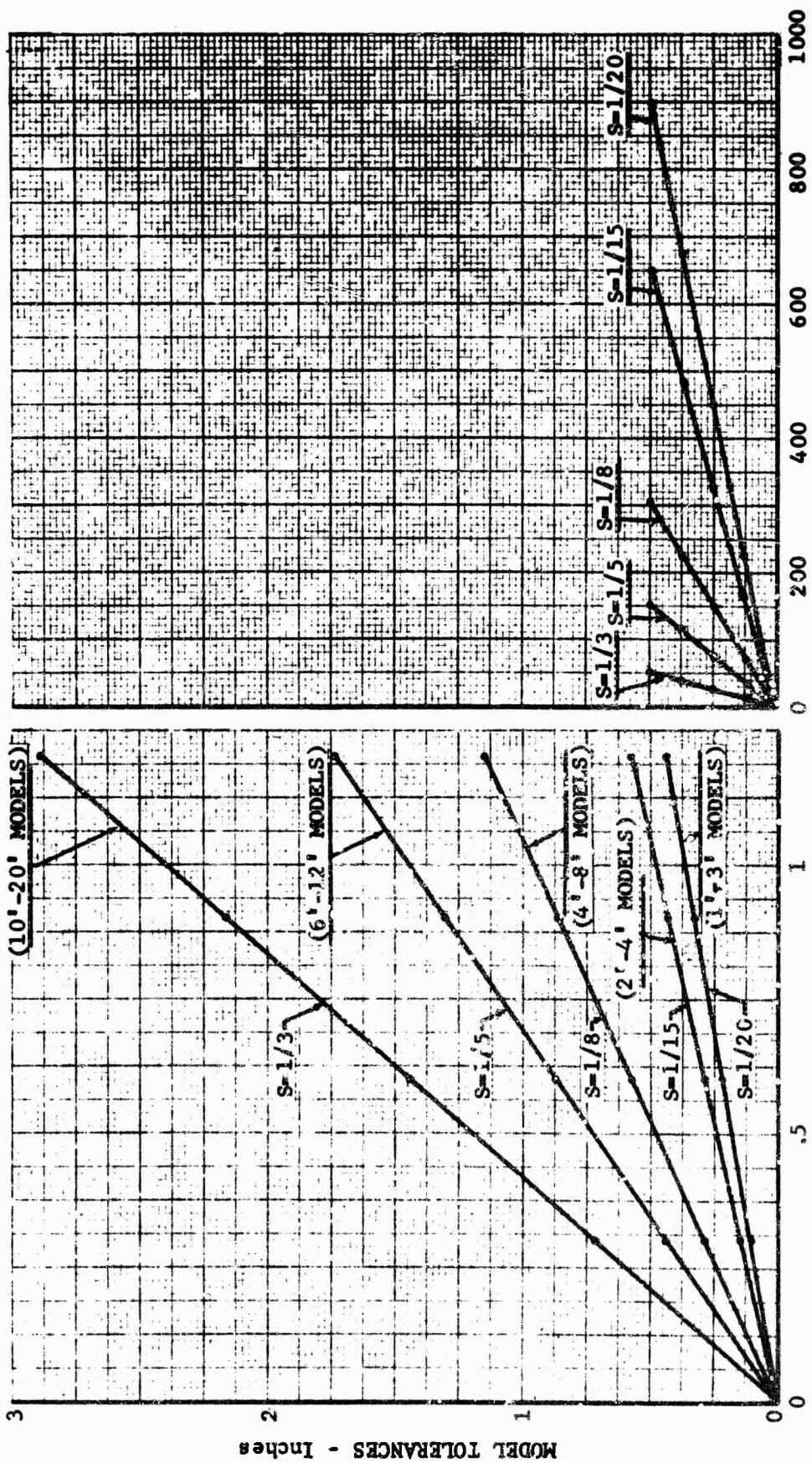


Fig. 1.1-7 ANOMOLY MAGNITUDES

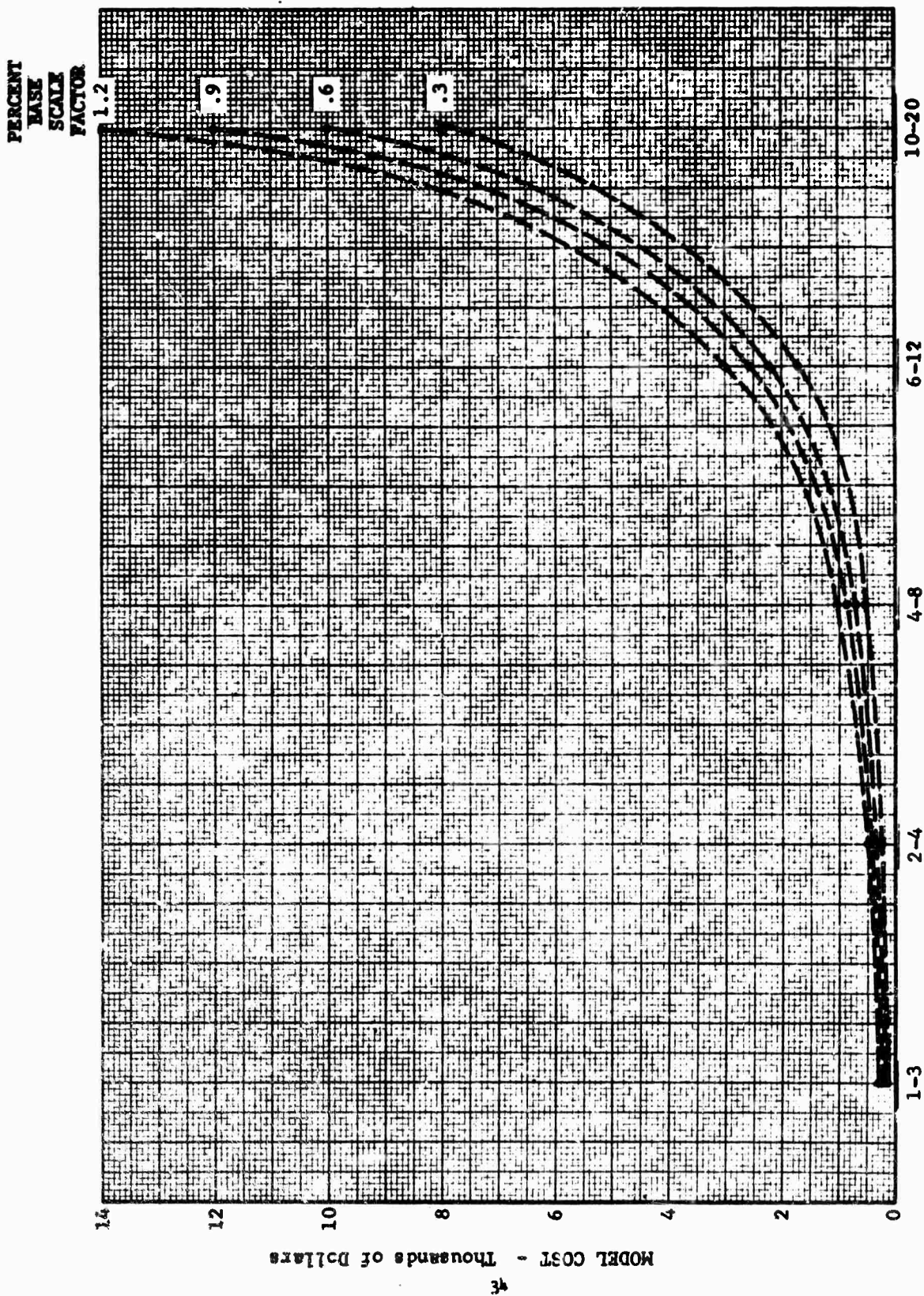


Fig. 1.1-4 COST VS. TOLERANCE DATA

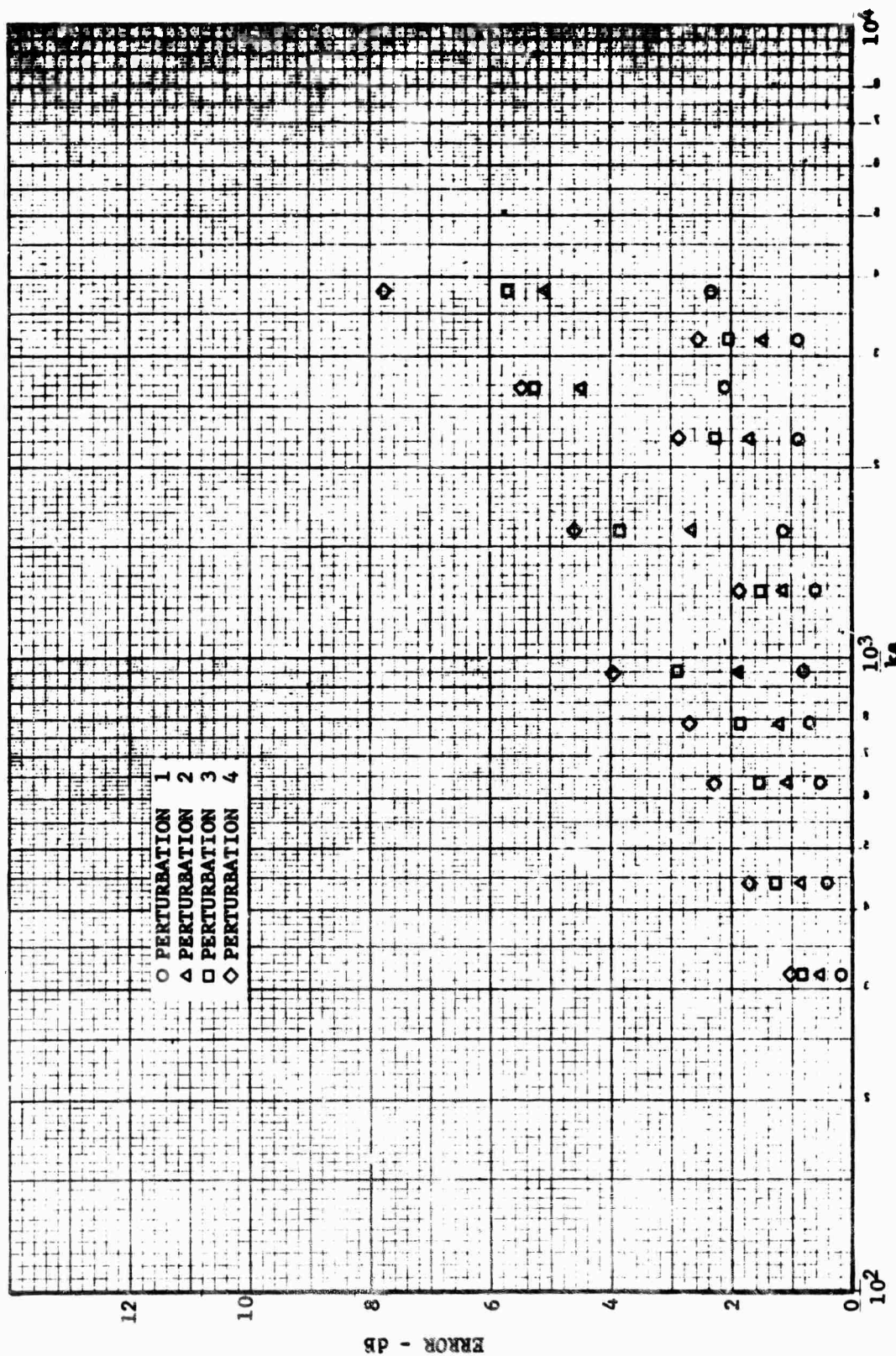


Fig. 1.1-5 CROSS SECTION ERROR FOR TARGET 1

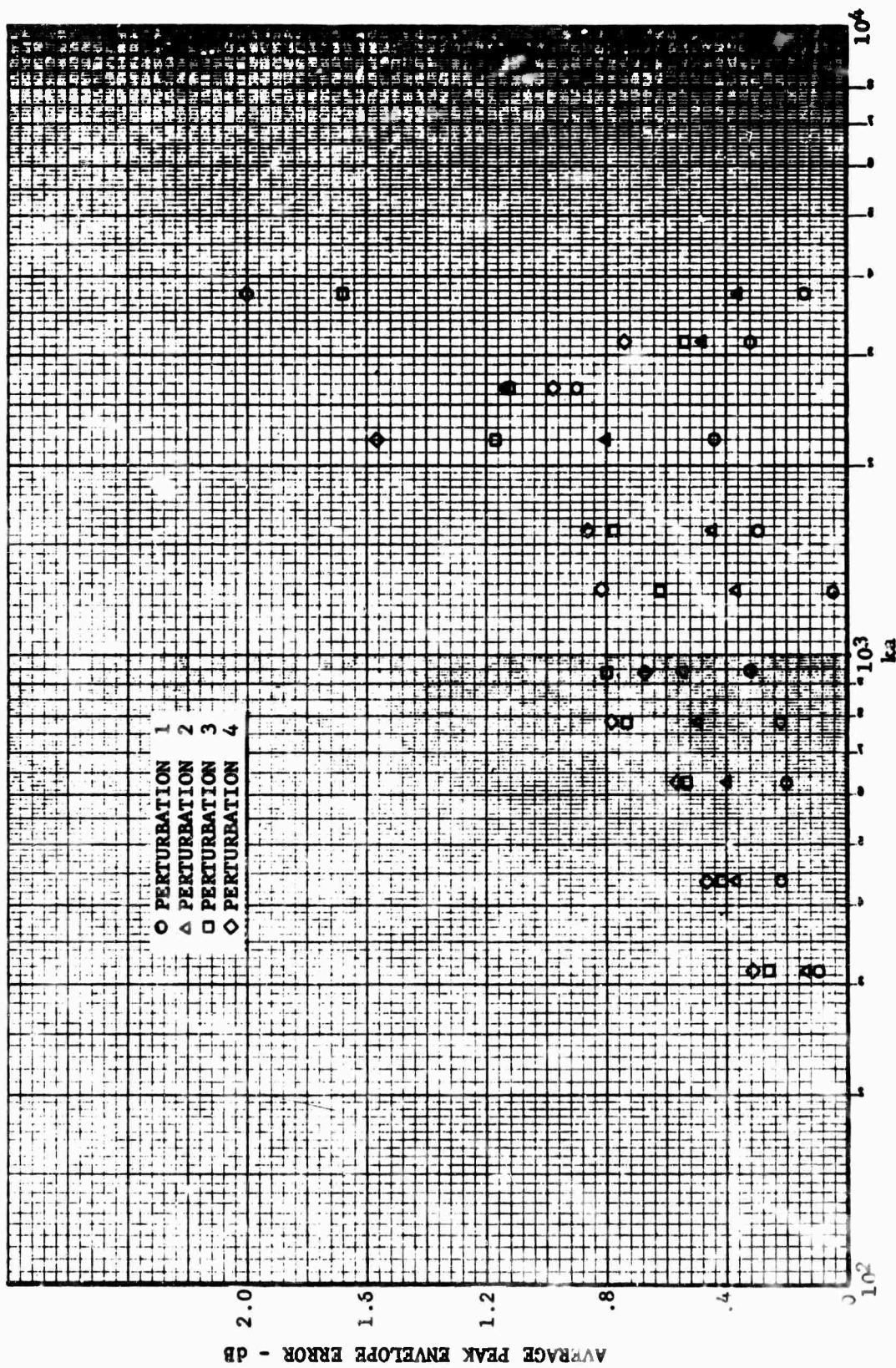


Fig. 1.1-6 PEAK ENVELOPE ERROR FOR TARGET 1

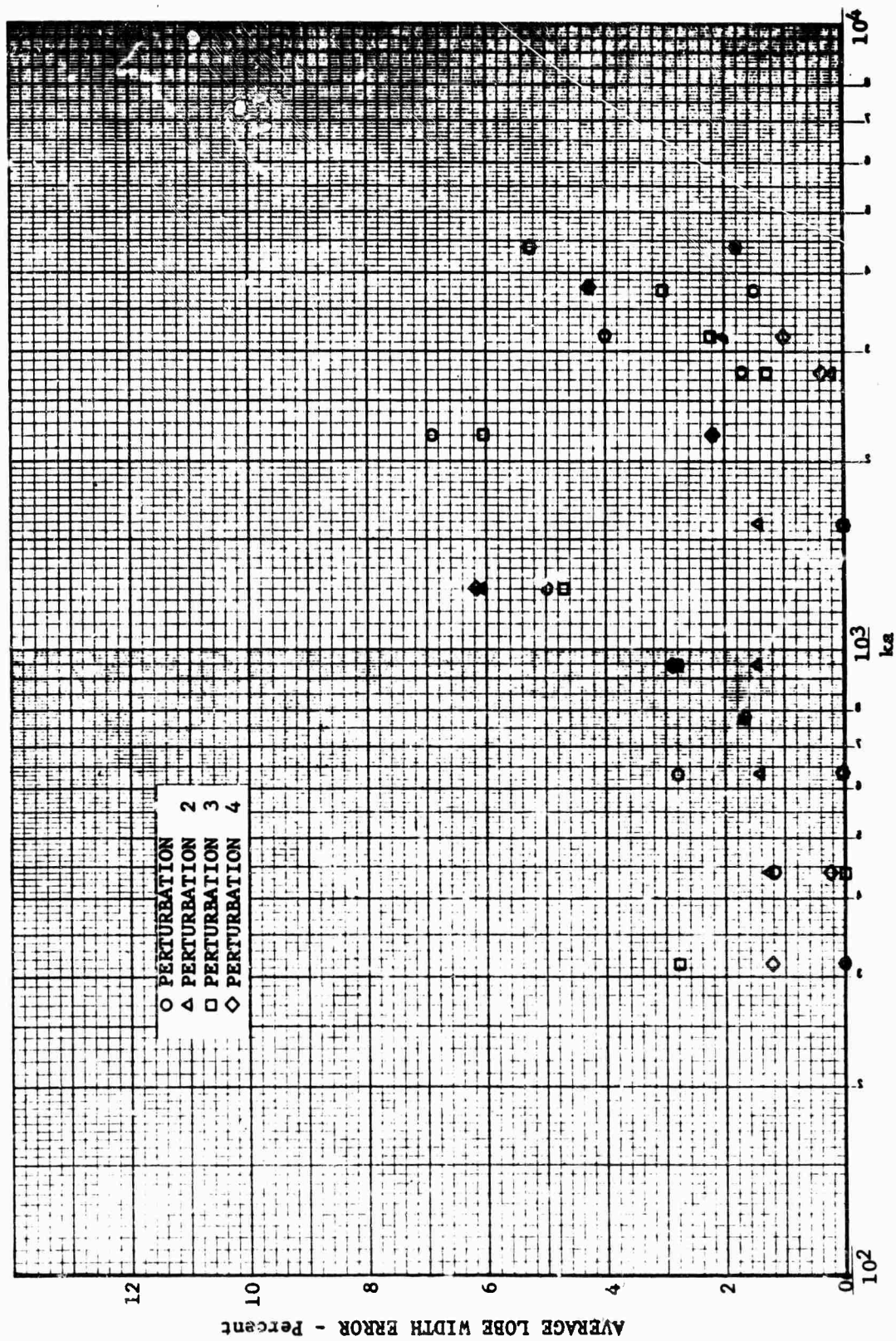


Fig. 1.1-7 LOBE WIDTH ERROR FOR TARGET 1

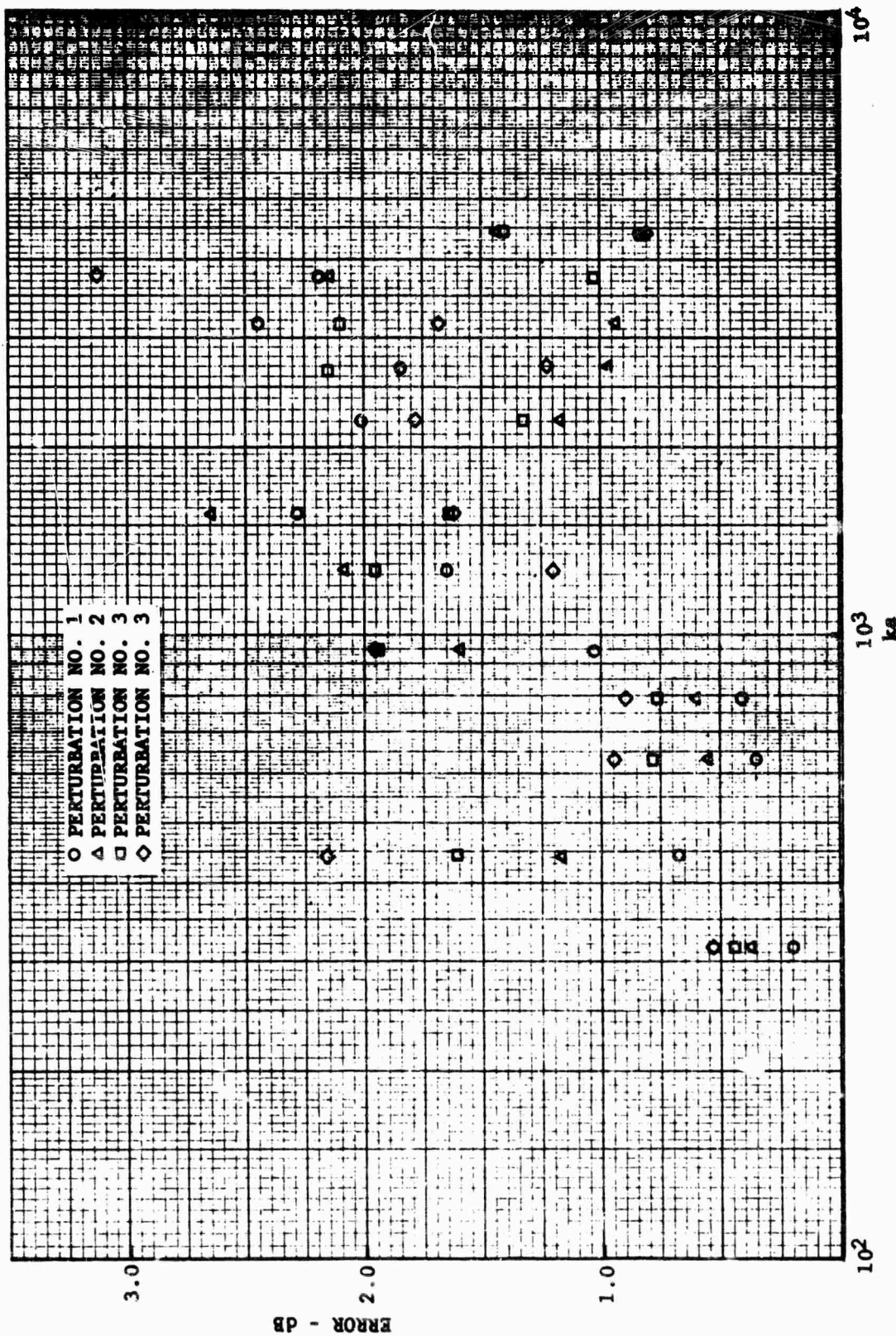


Fig. 1.1-8 CROSS SECTION ERROR FOR TARGET 2

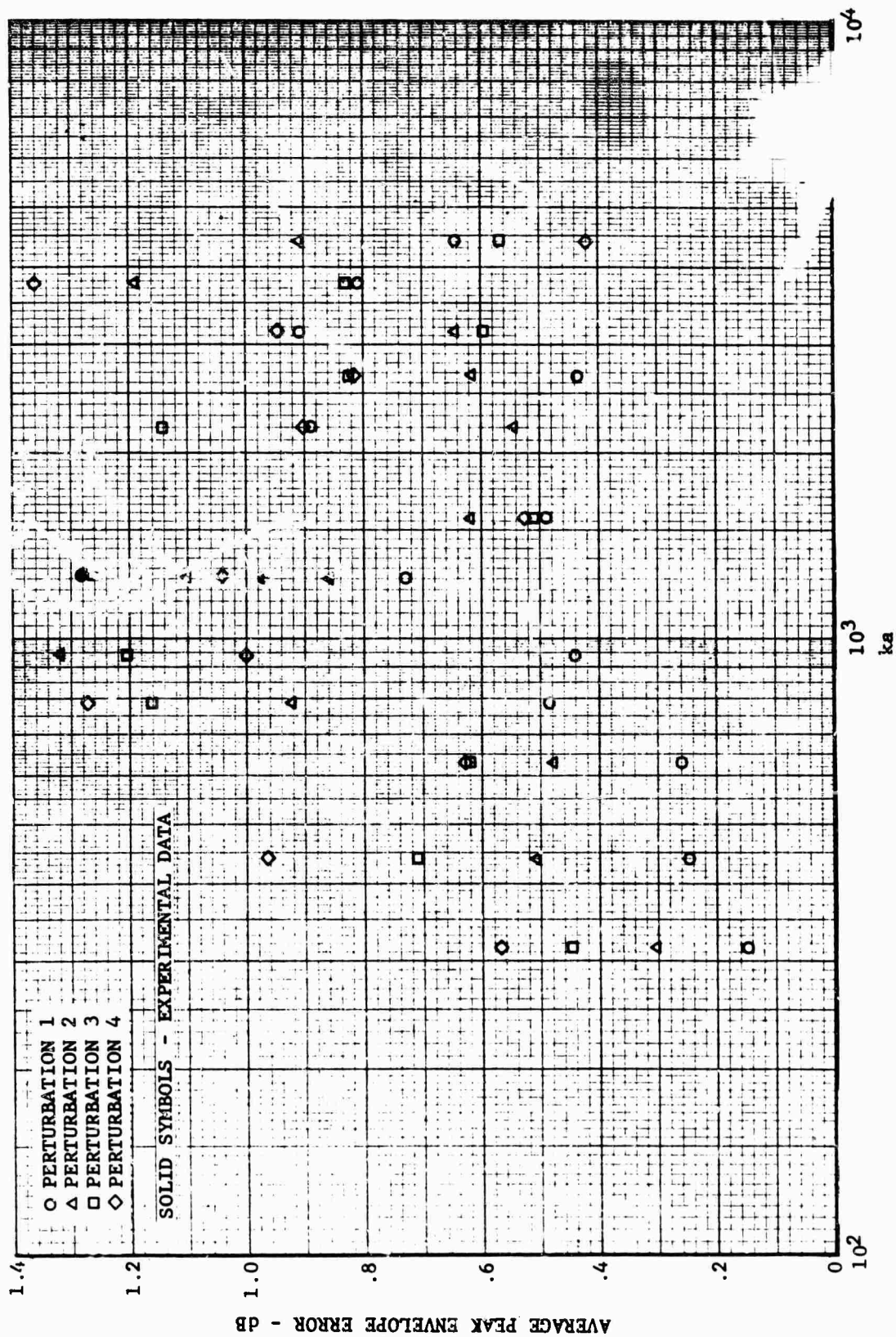


Fig. 1.1-9 PEAK ENVELOPE ERROR FOR TARGET 2

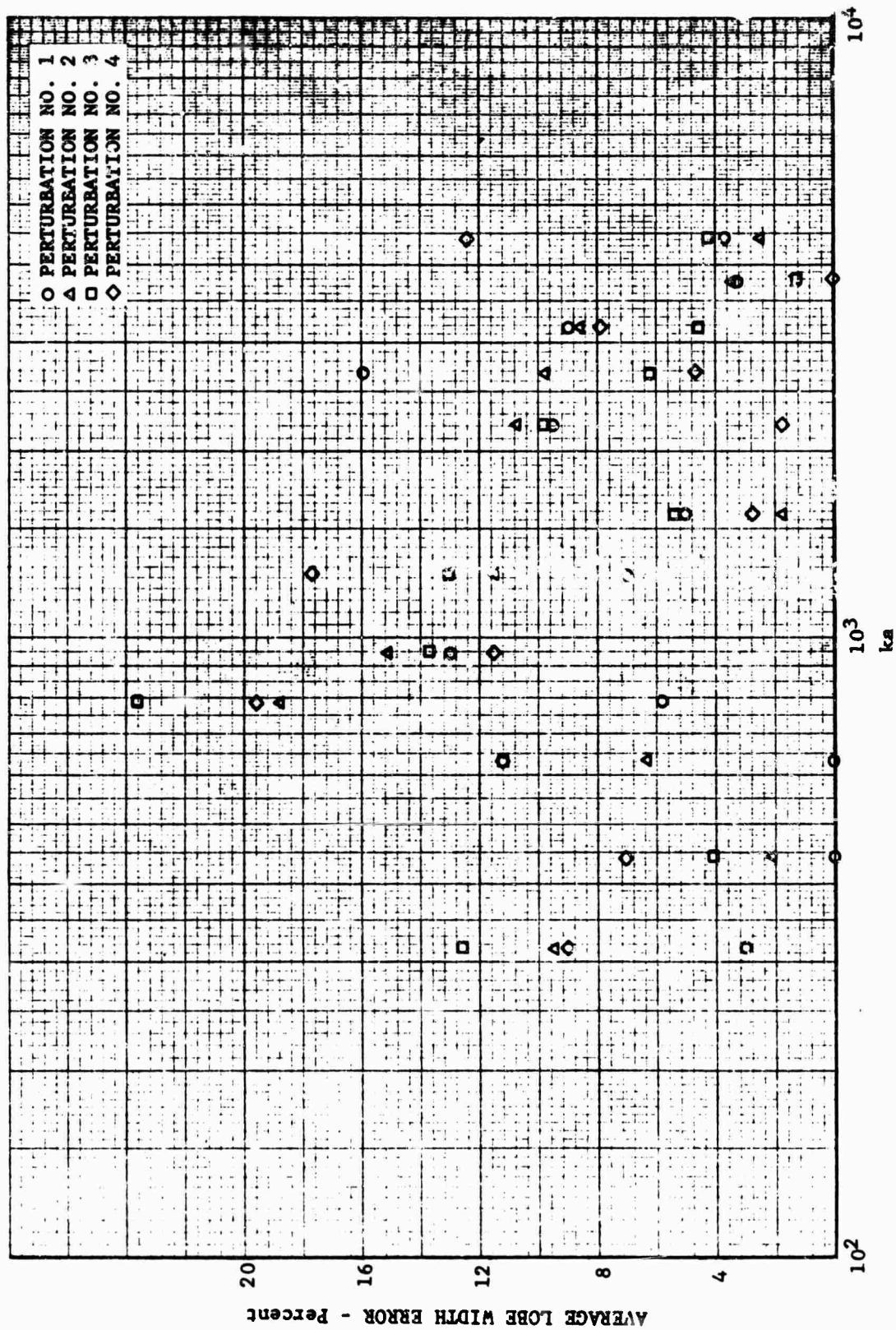


Fig. 1.1-10 LOBE WIDTH ERROR FOR TARGET 2

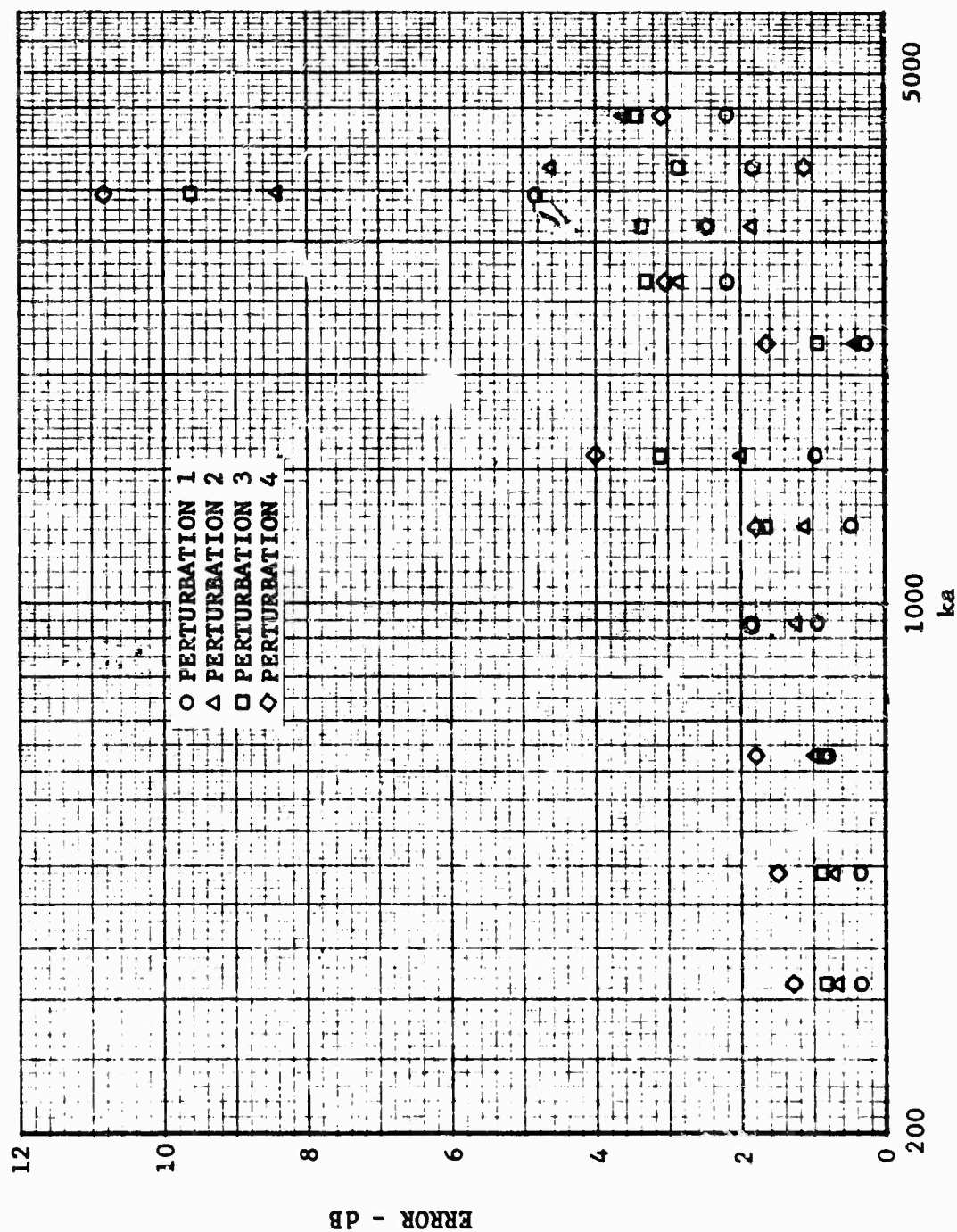


Fig. 1.1-11 CROSS SECTION ERROR FOR TARGET 3

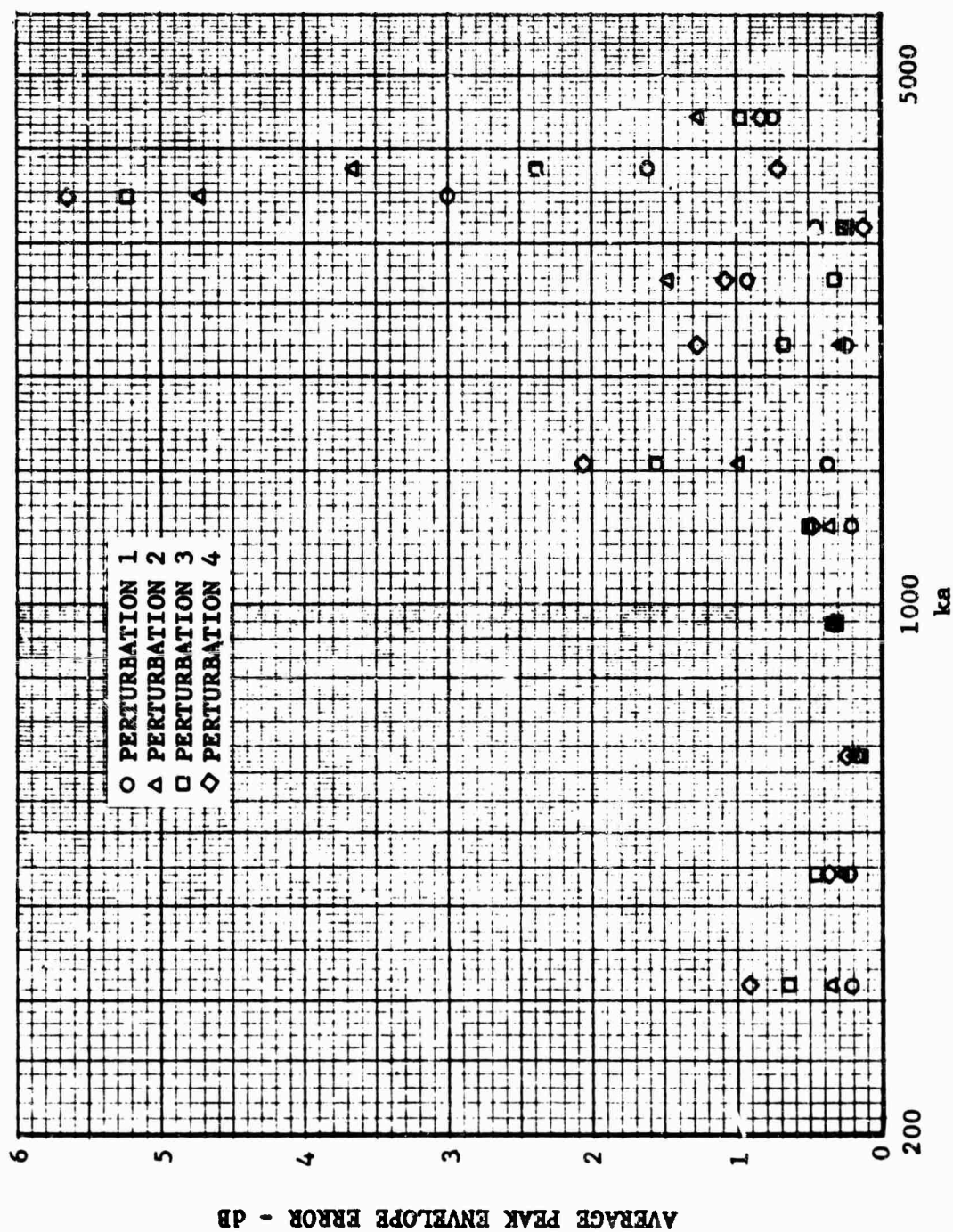


Fig. 1.1-12 PEAK ENVELOPE ERROR FOR TARGET 3

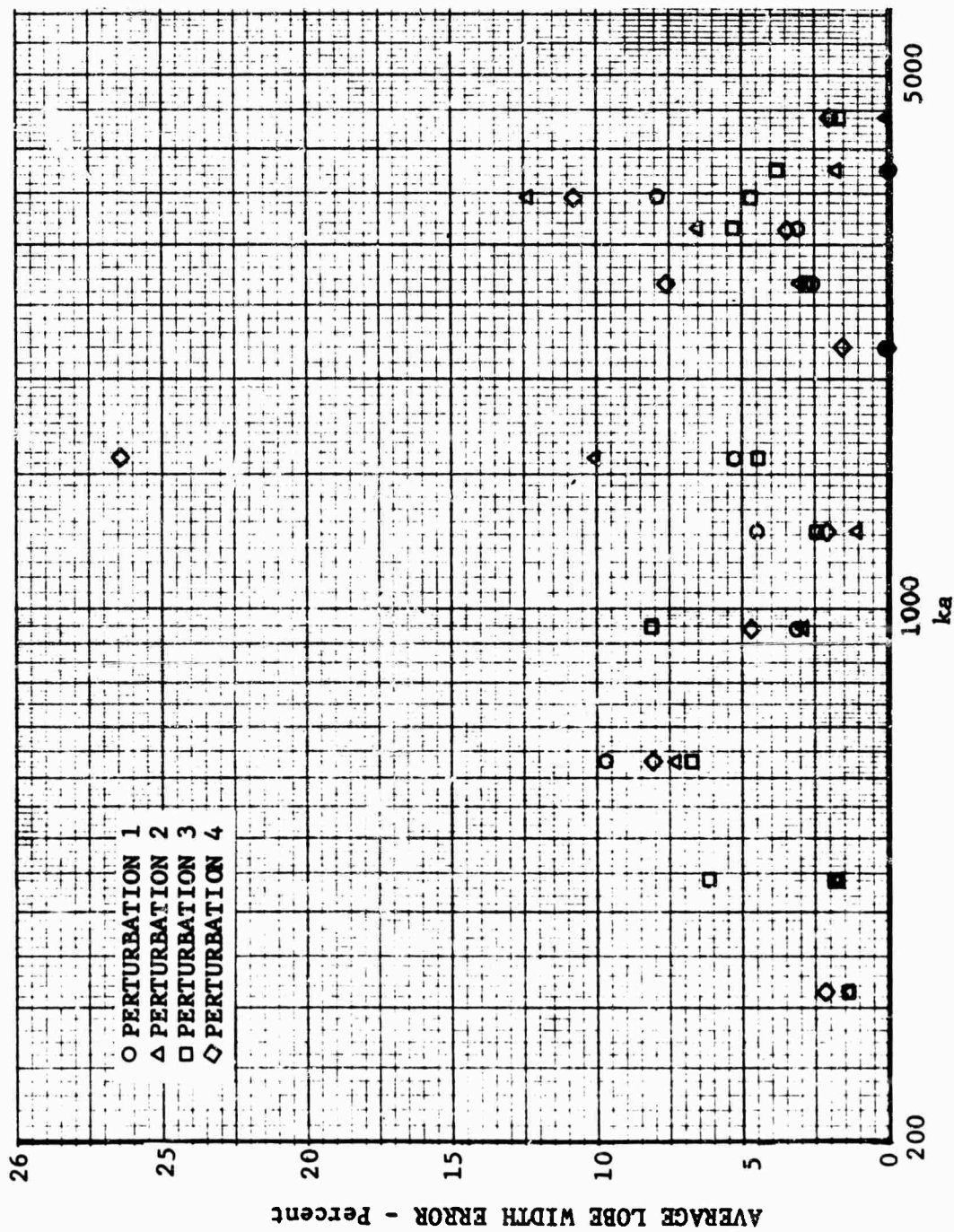


Fig. 1.1-13 LOBE WIDTH ERROR FOR TARGET 3

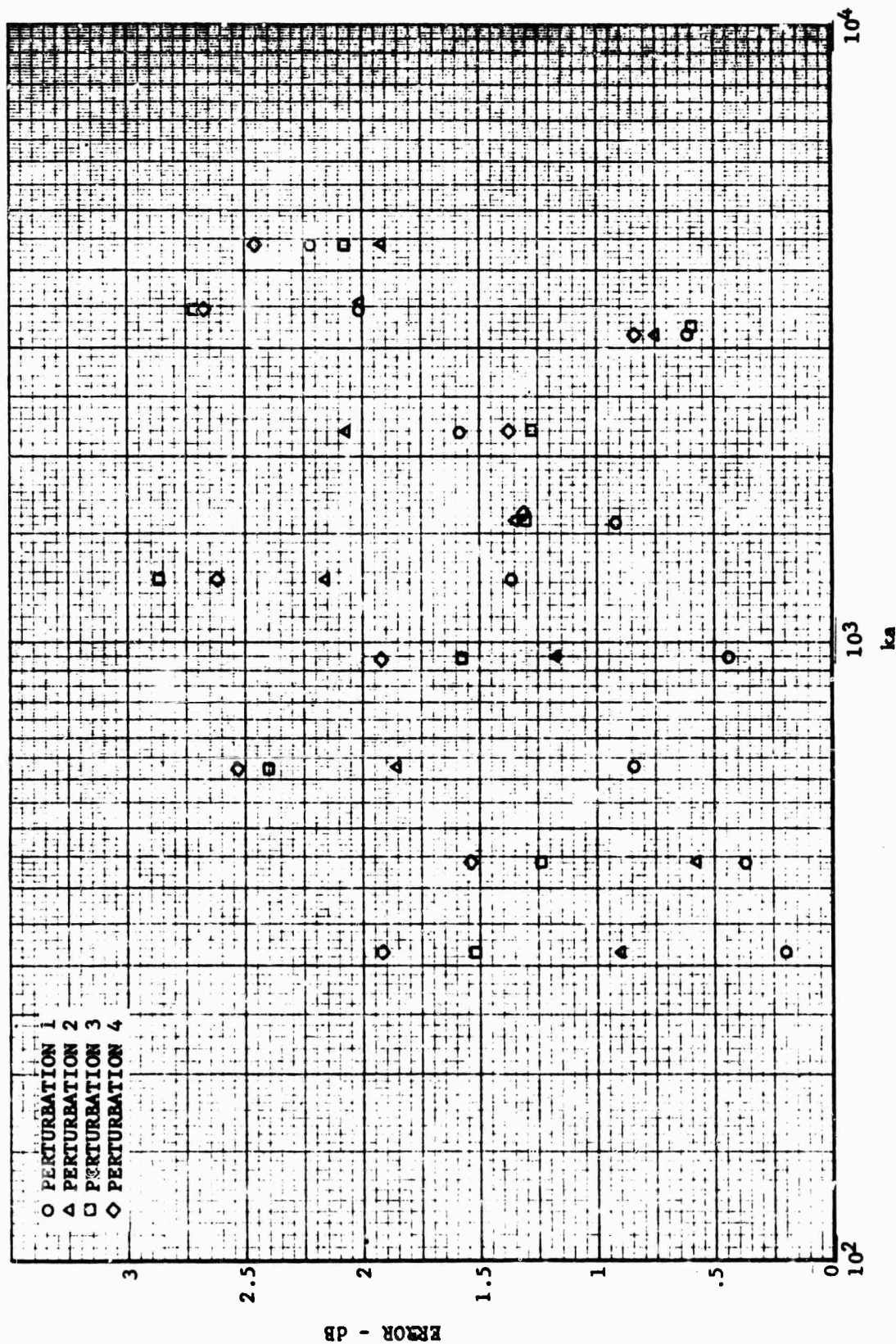


Fig. 1.1-14 CROSS SECTION ERROR FOR TARGET 4

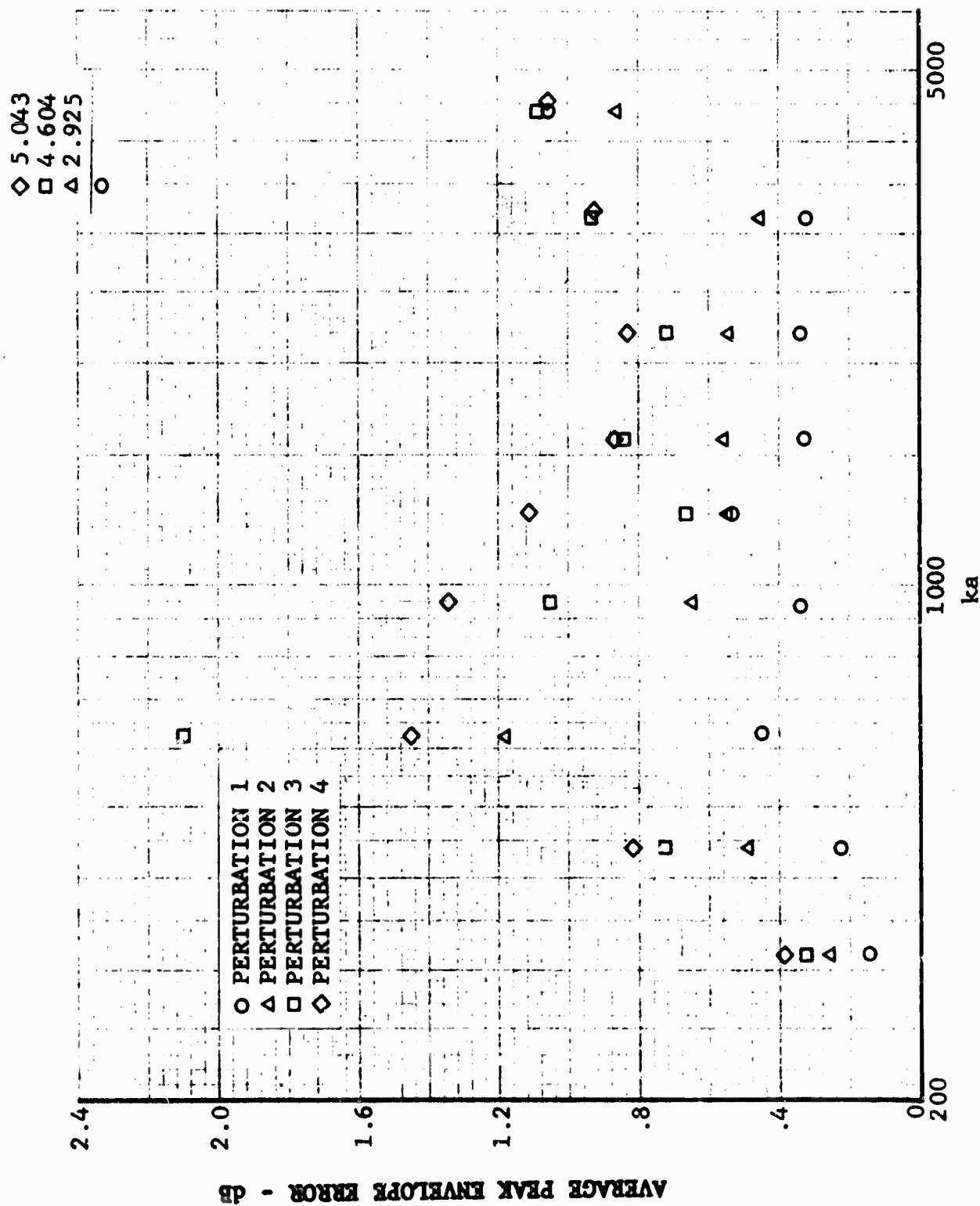


Fig. 1.1-15 PEAK ENVELOPE ERROR FOR TARGET 4

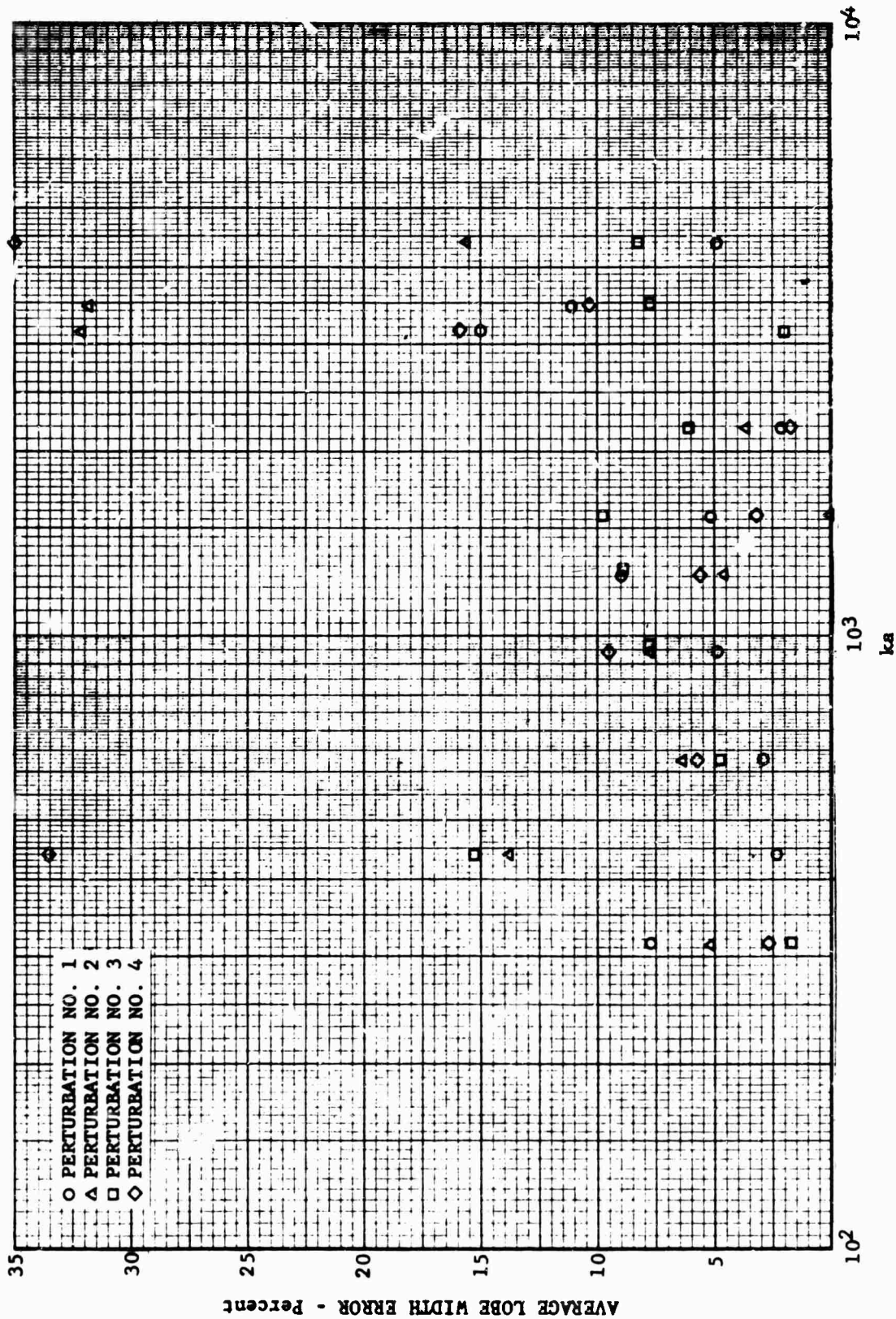


Fig. 1.1-16 LOBE WIDTH ERROR FOR TARGET 4

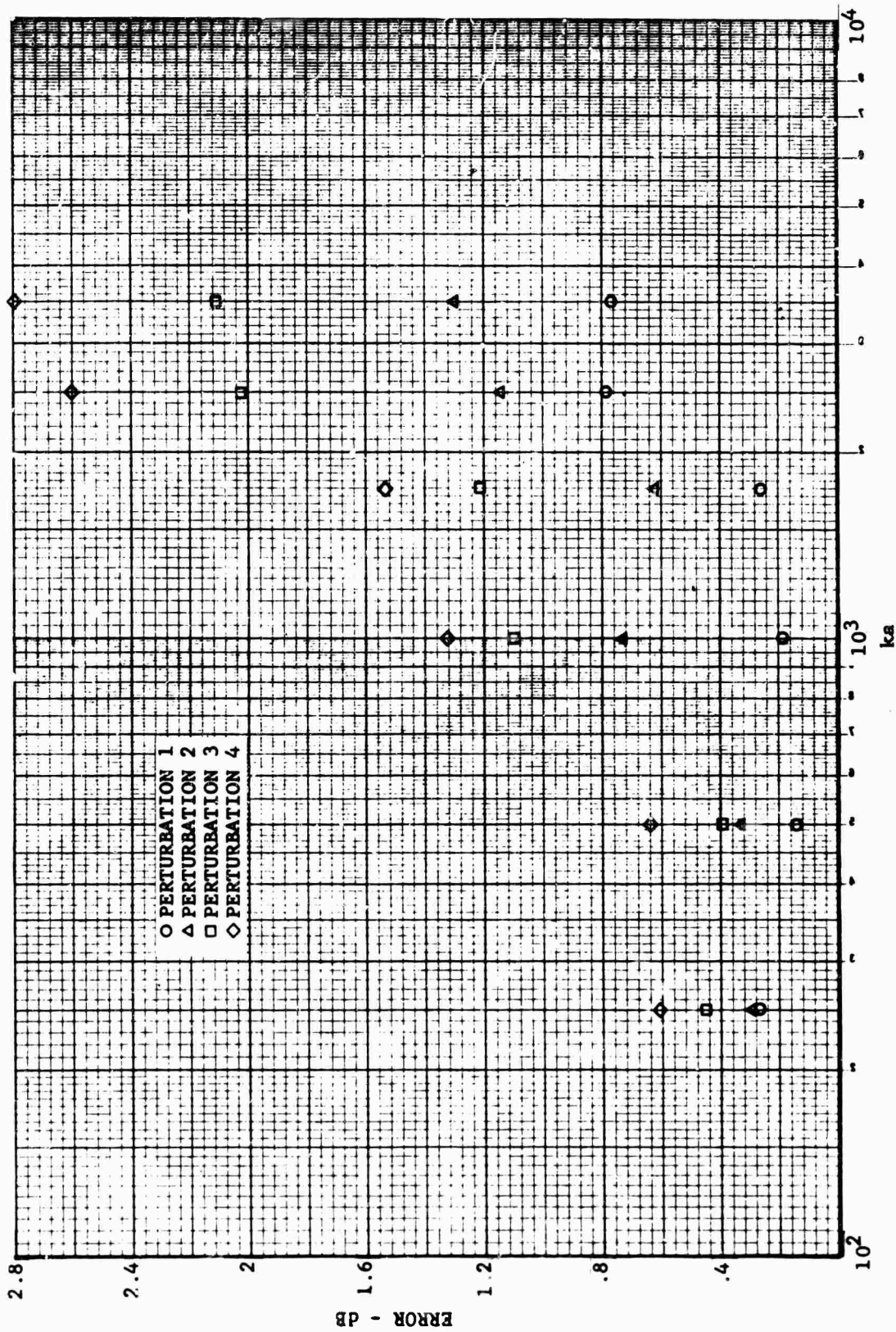


Fig. 1.1-17 CROSS SECTION ERROR FOR TARGET 5

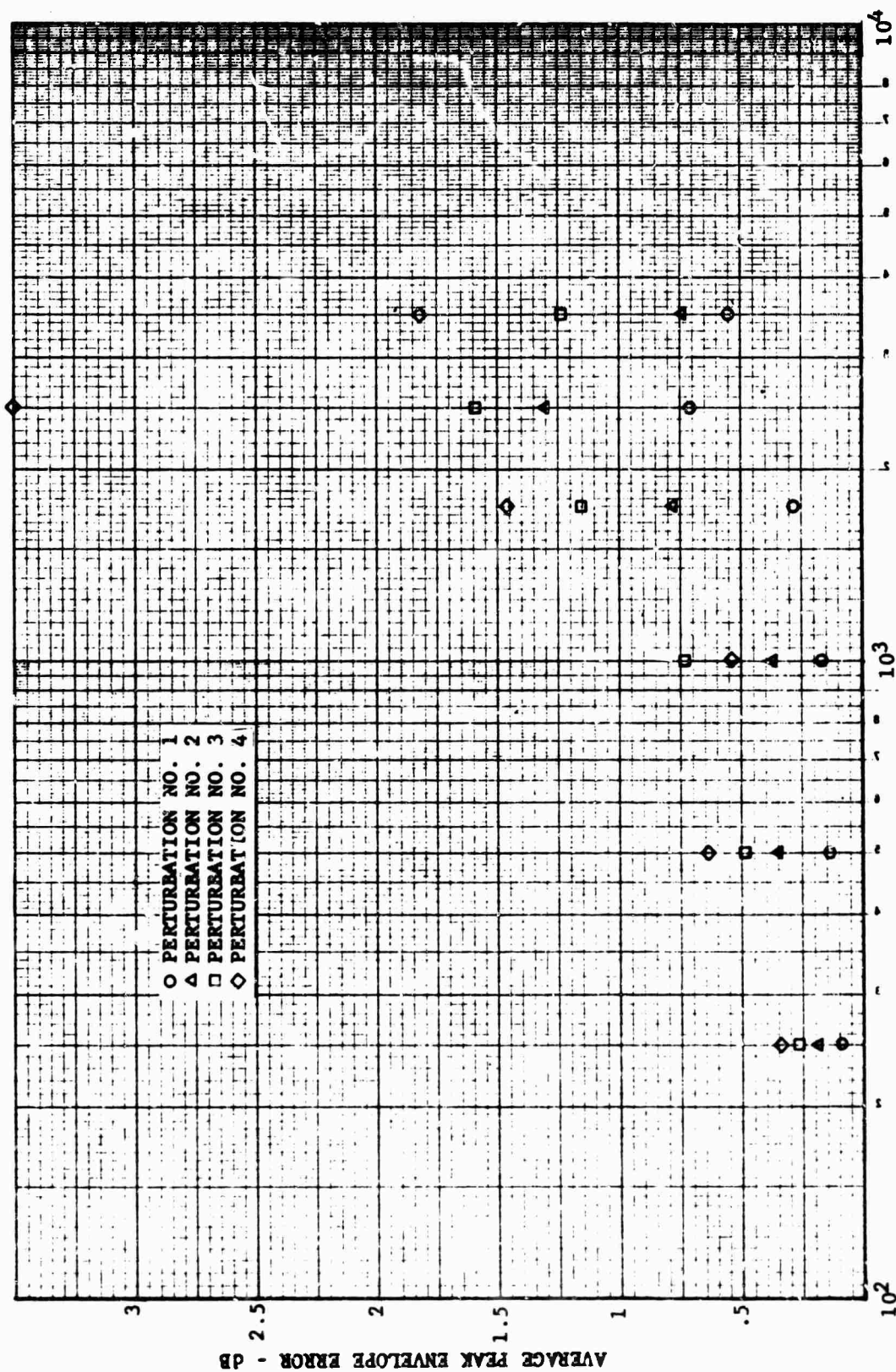


Fig. 1.1-18 PEAK ENVELOPE ERROR FOR TARGET 5

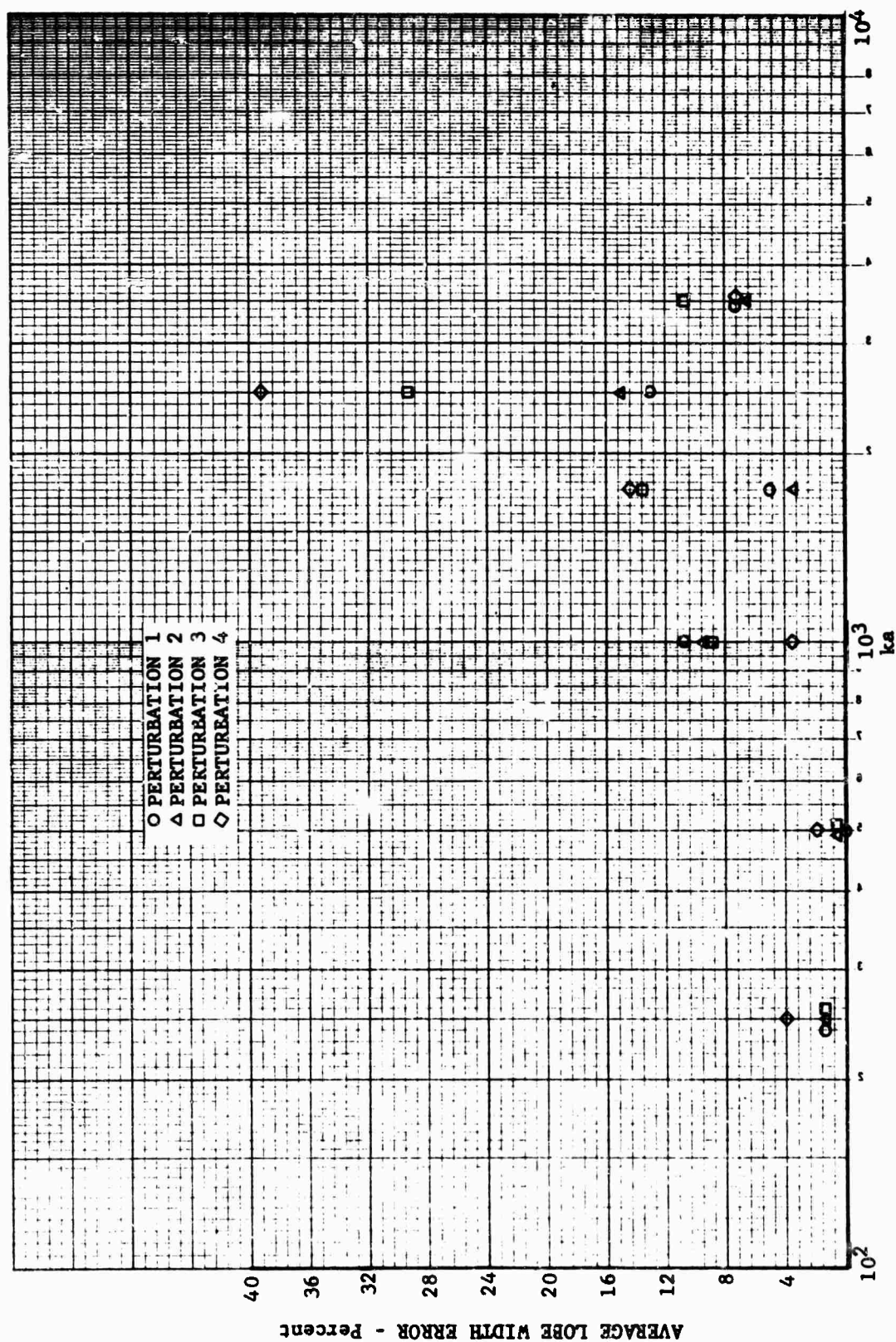


Fig. 1.1-19 LOBE WIDTH ERROR FOR TARGET 5

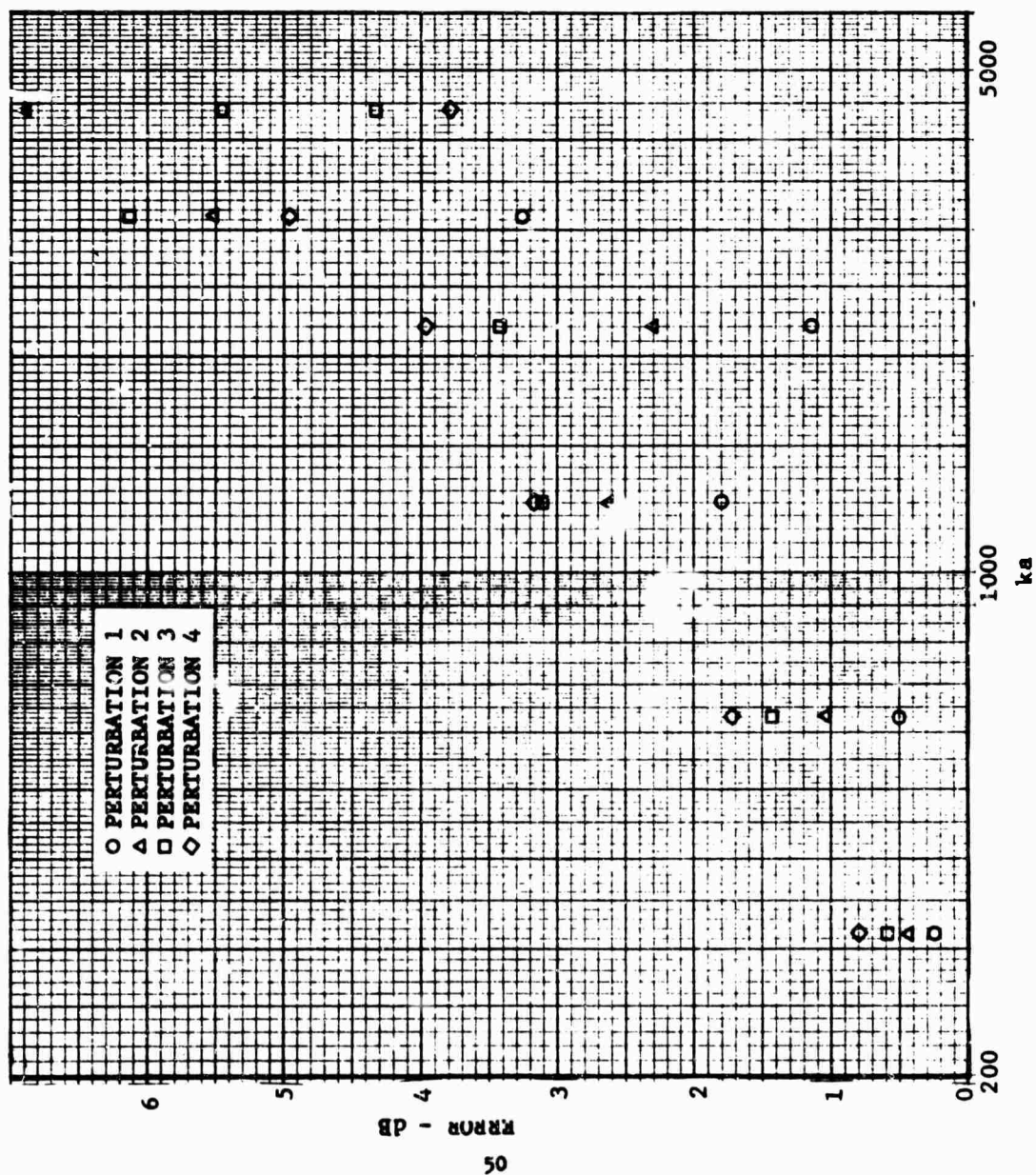


Fig. 1.1-20 CROSS SECTION ERROR FOR TARGET 6

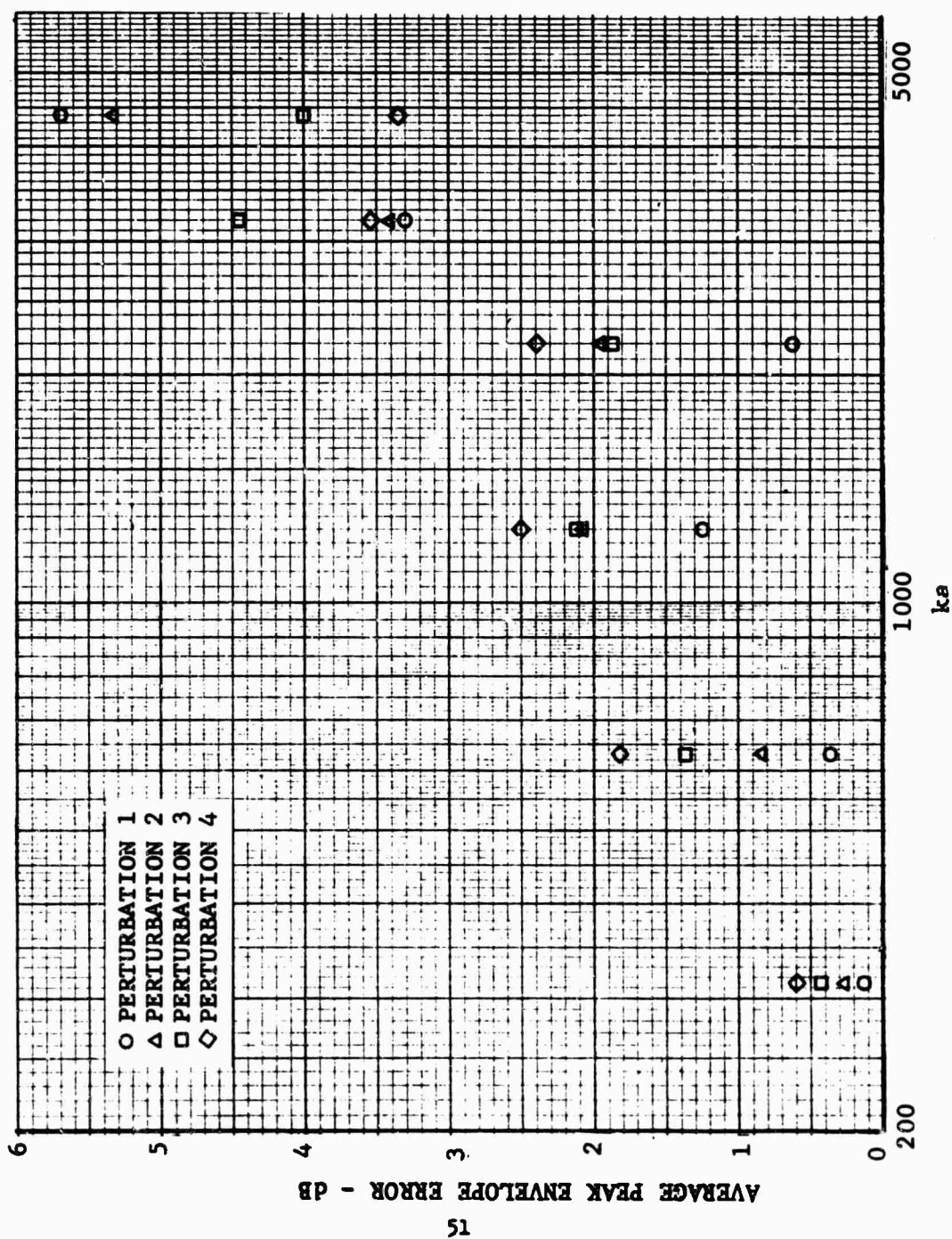


Fig. 1.1-21 PEAK ENVELOPE ERROR FOR TARGET 6

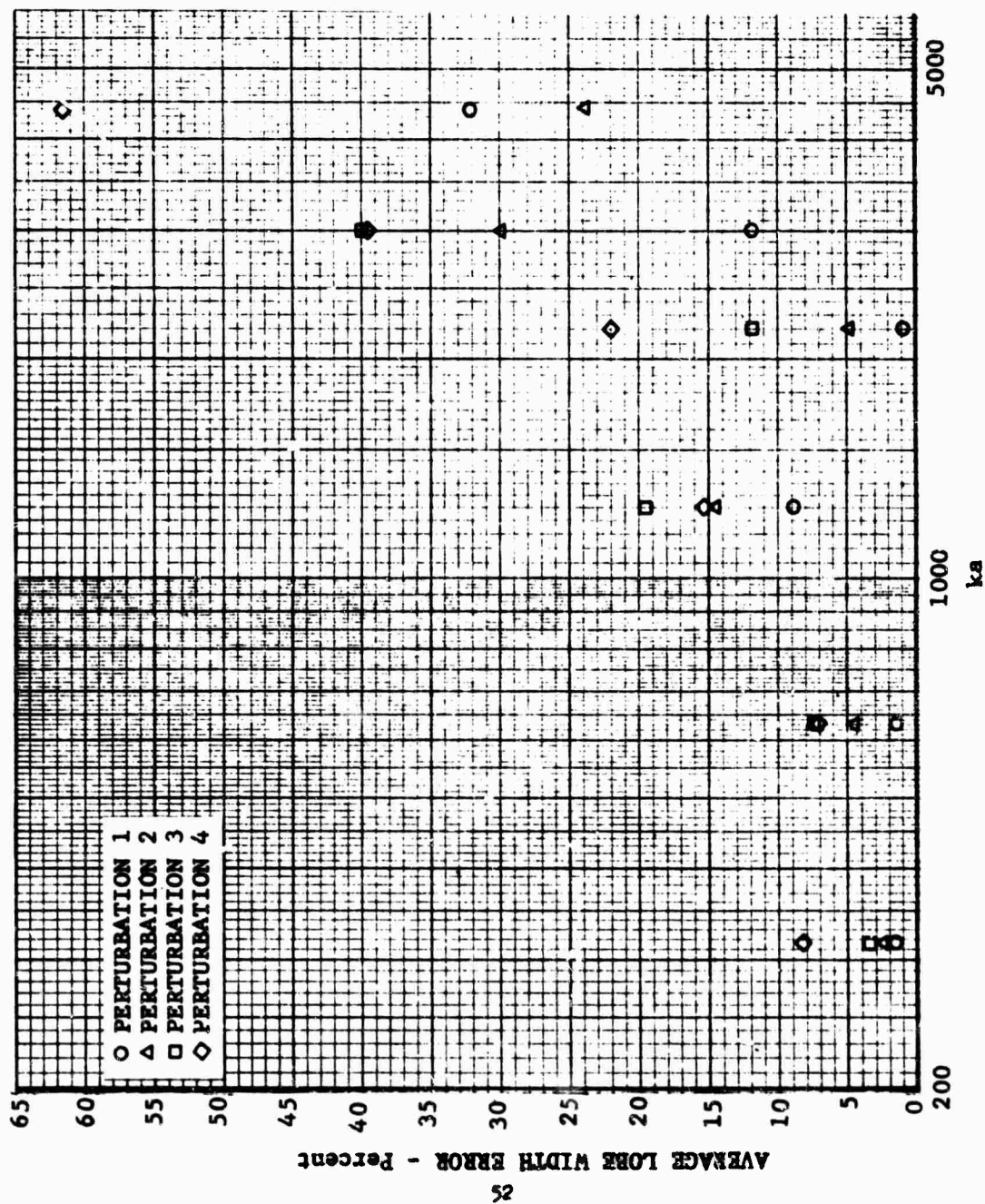


FIG. 1.1-22 LOBE WIDTH FOR TARGET 6

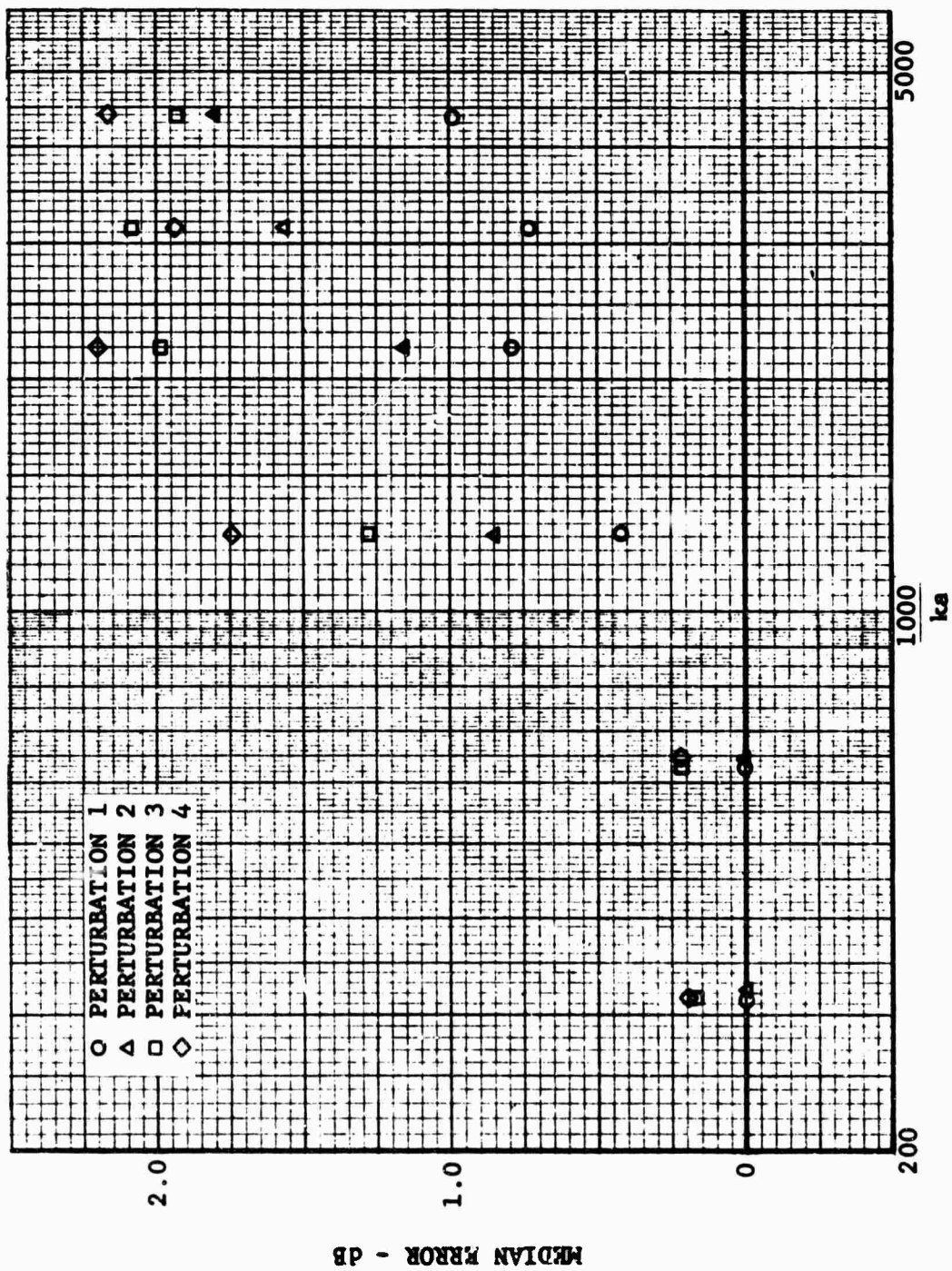


Fig. 1.1-23 CROSS SECTION ERROR FOR TARGET 7

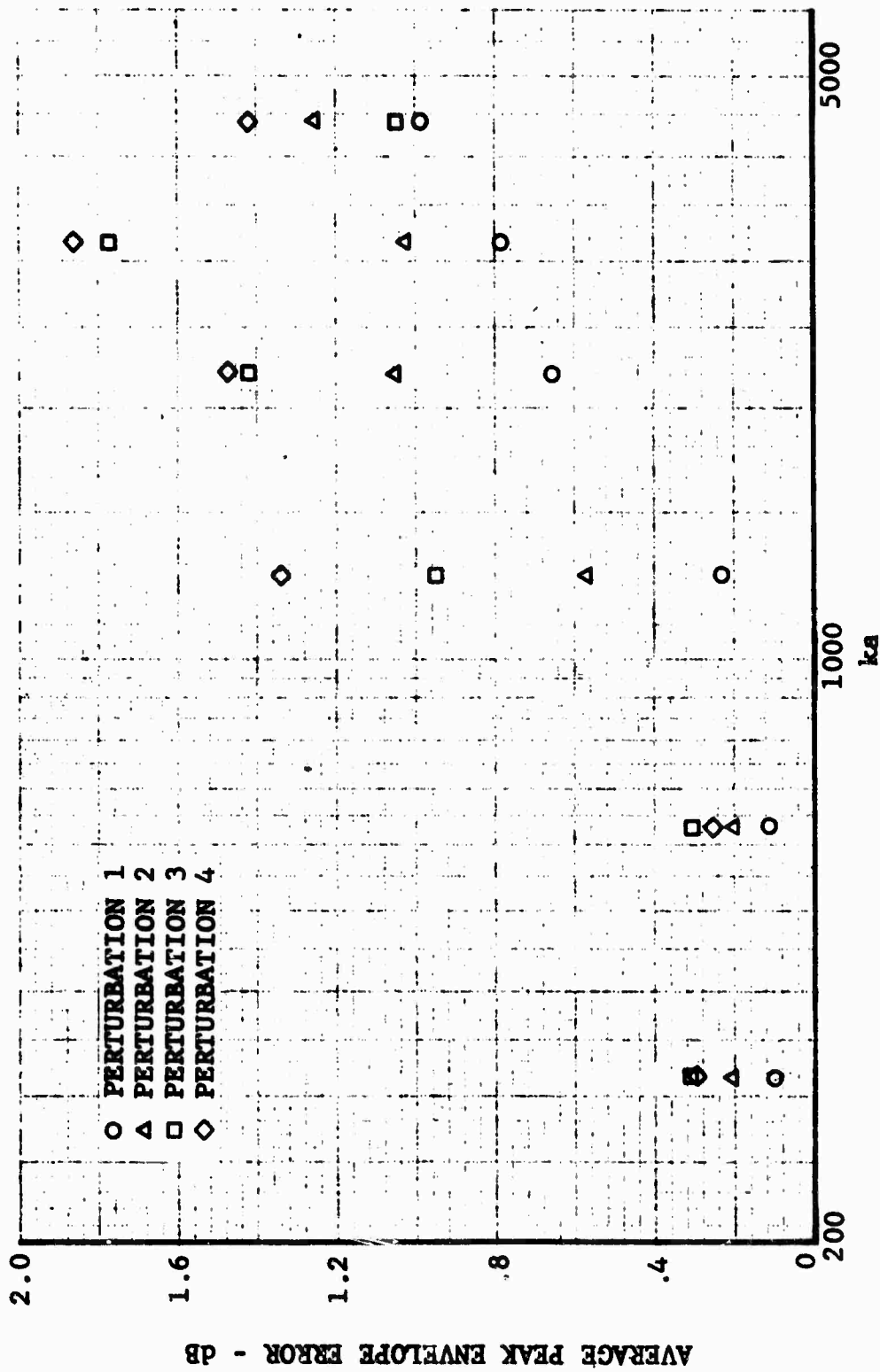


Fig. 1.1-24 PEAK ENVELOPE ERROR FOR TARGET 7

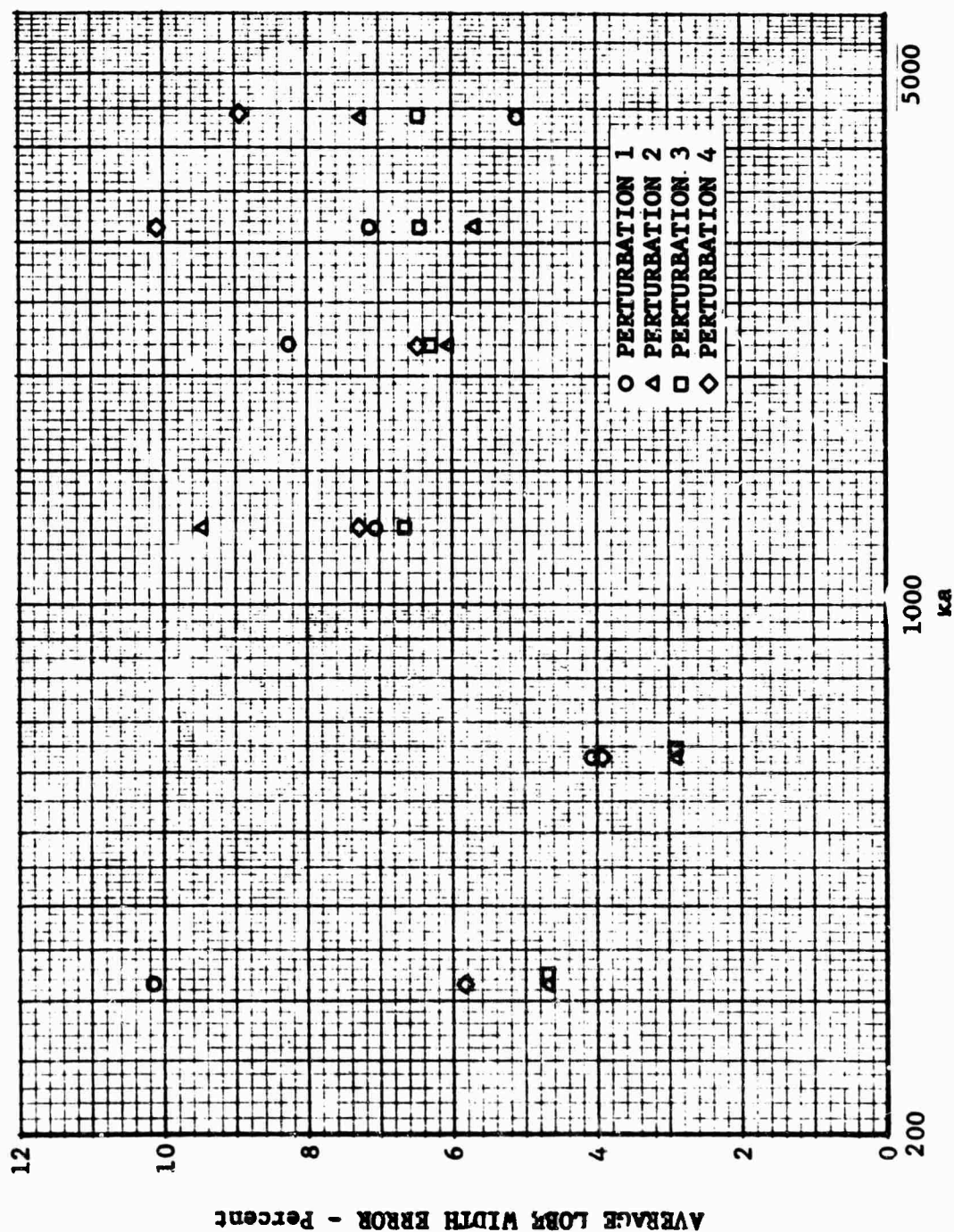


Fig. 1.1-25 LOBE WIDTH ERROR FOR TARGET 7

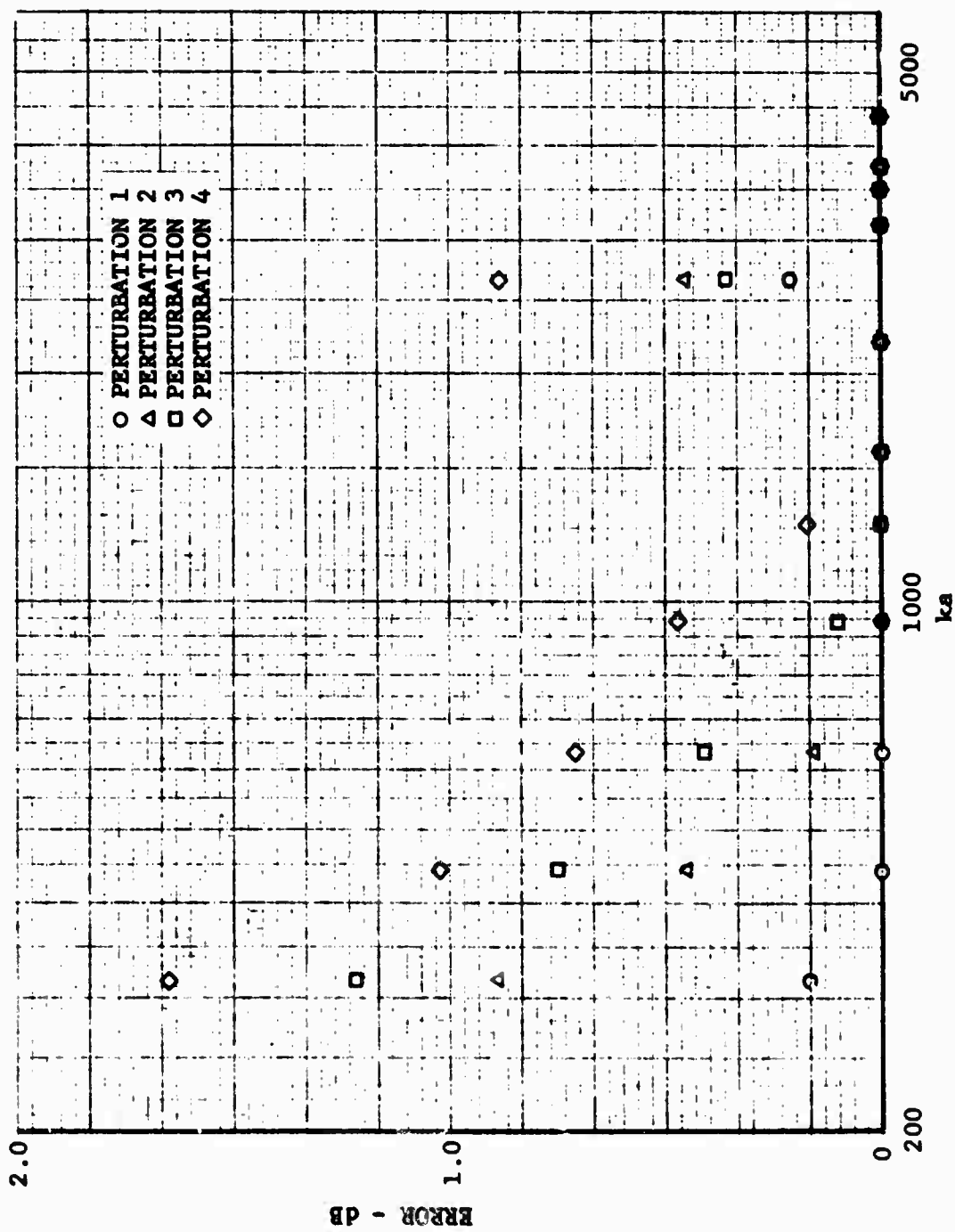


Fig. 1.1-26 CROSS SECTION ERROR FOR TARGET 8

Fig. 1.1-27 PEAK ENVELOPE ERROR FOR TARGET 8

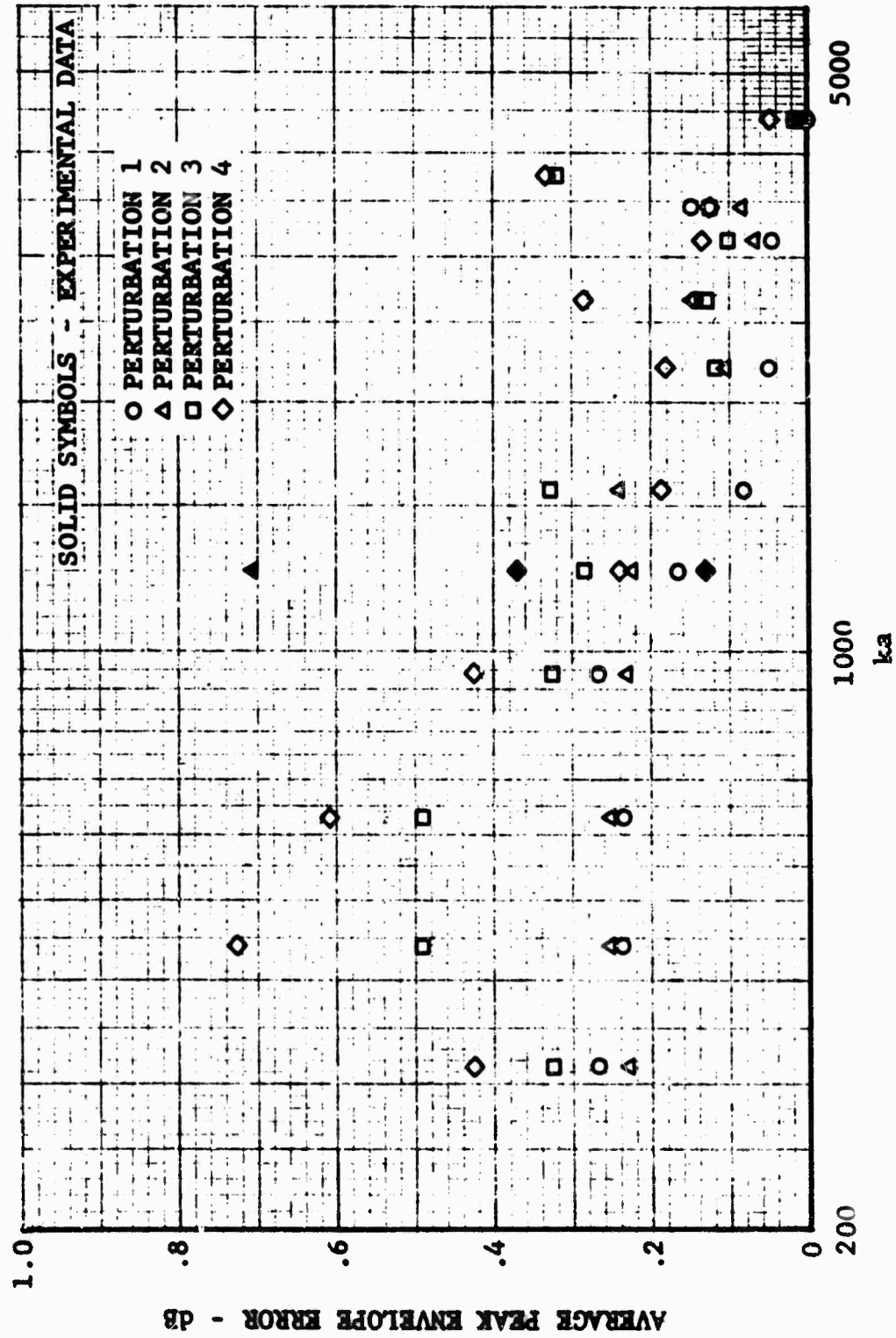


Fig. 1.1-27 PEAK ENVELOPE ERROR FOR TARGET 8

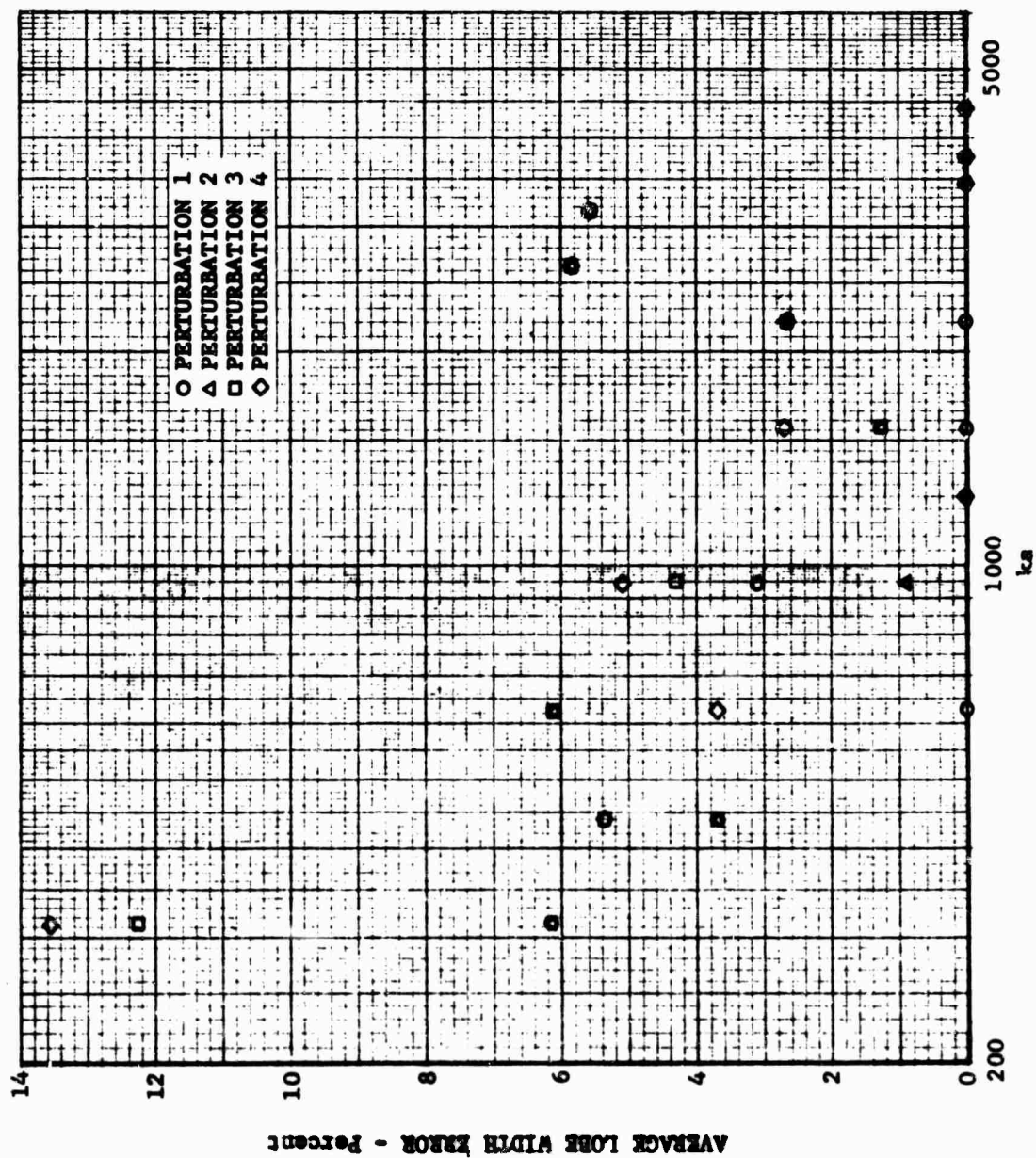


Fig. 1.1-28 LOBE WIDTH ERROR FOR TARGET 8

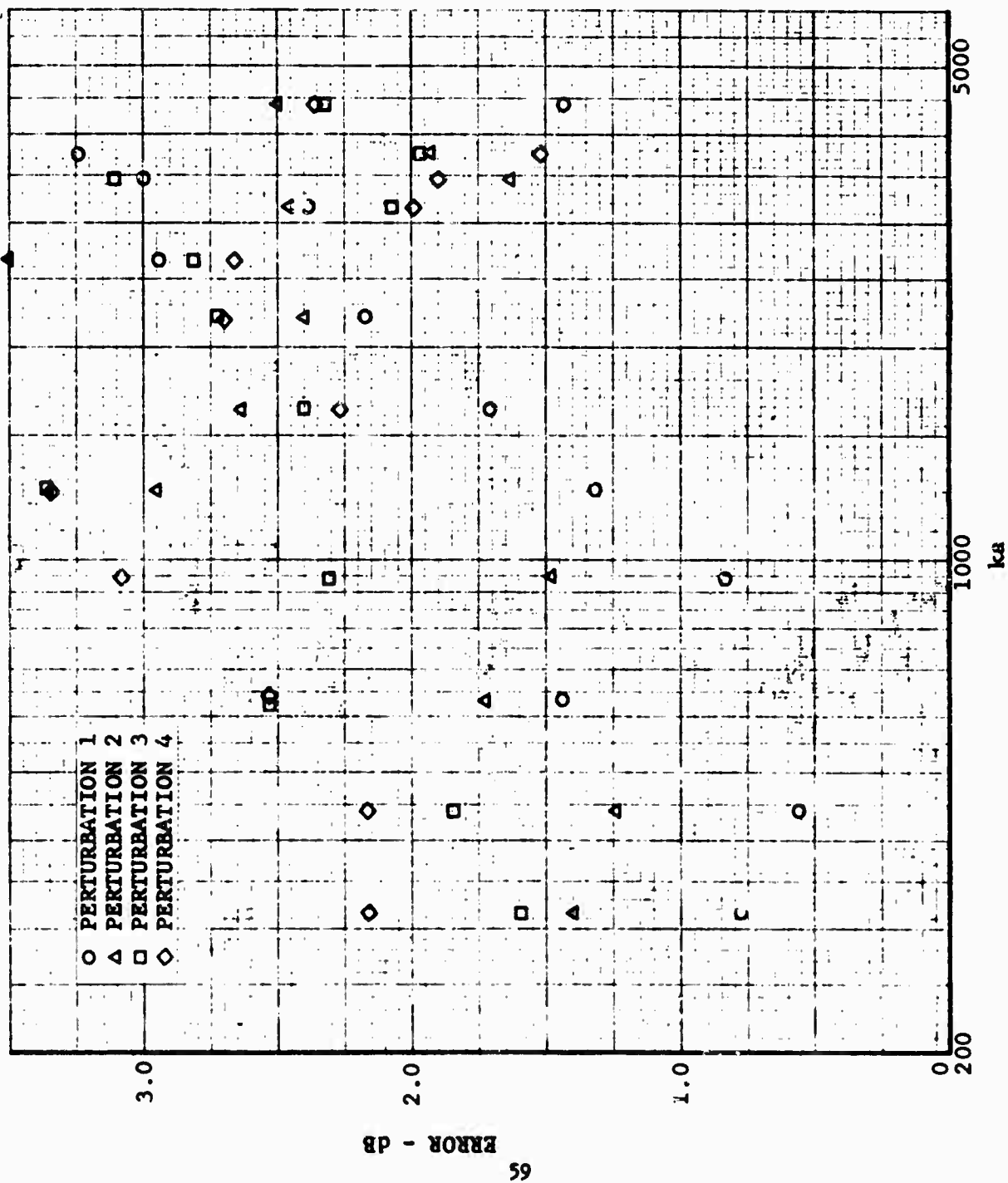


Fig. 1.1-29 CROSS SECTION ERROR FOR TARGET 9

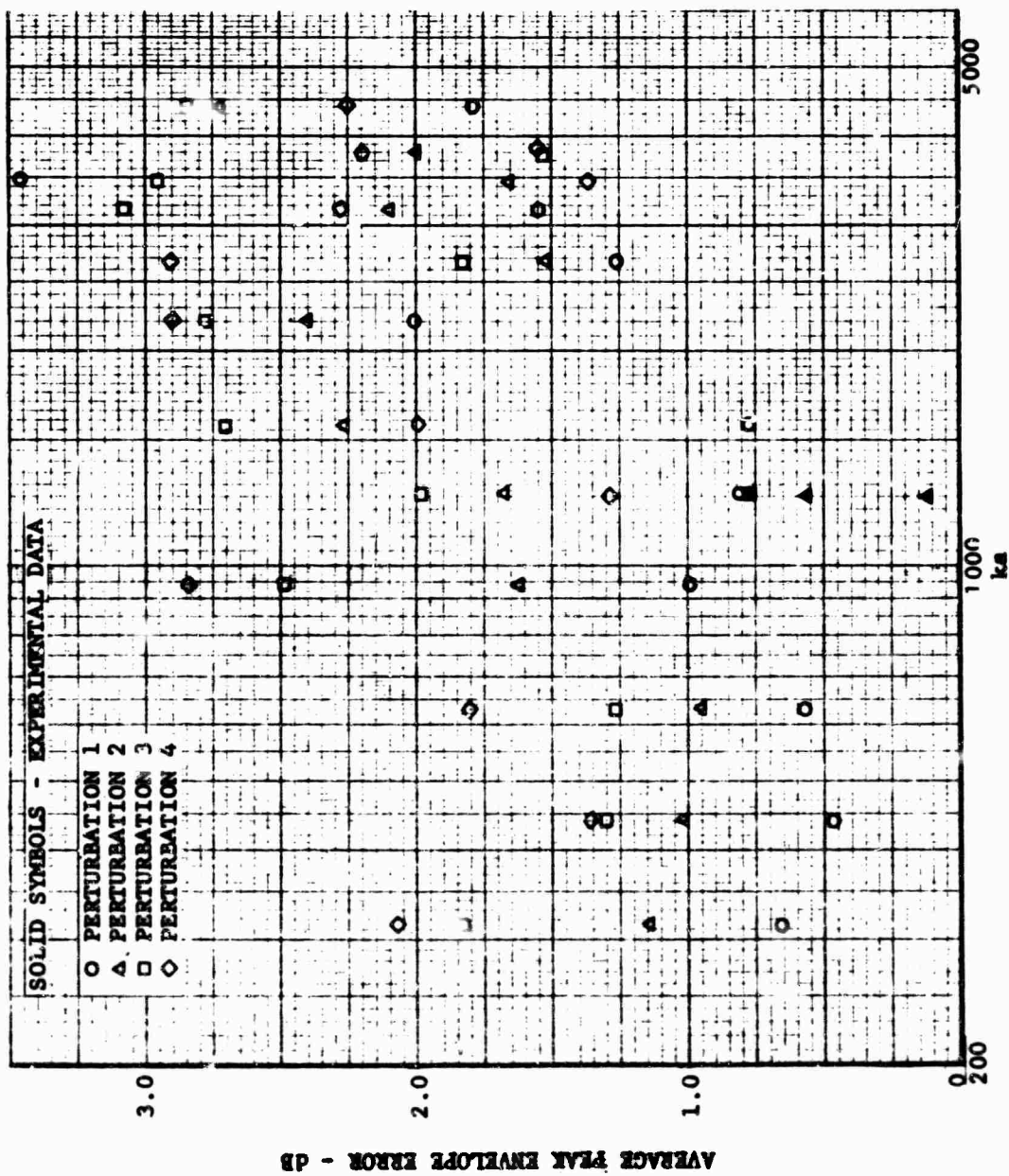


Fig. 1.1-30 PEAK ENVELOPE ERROR FOR TARGET 9

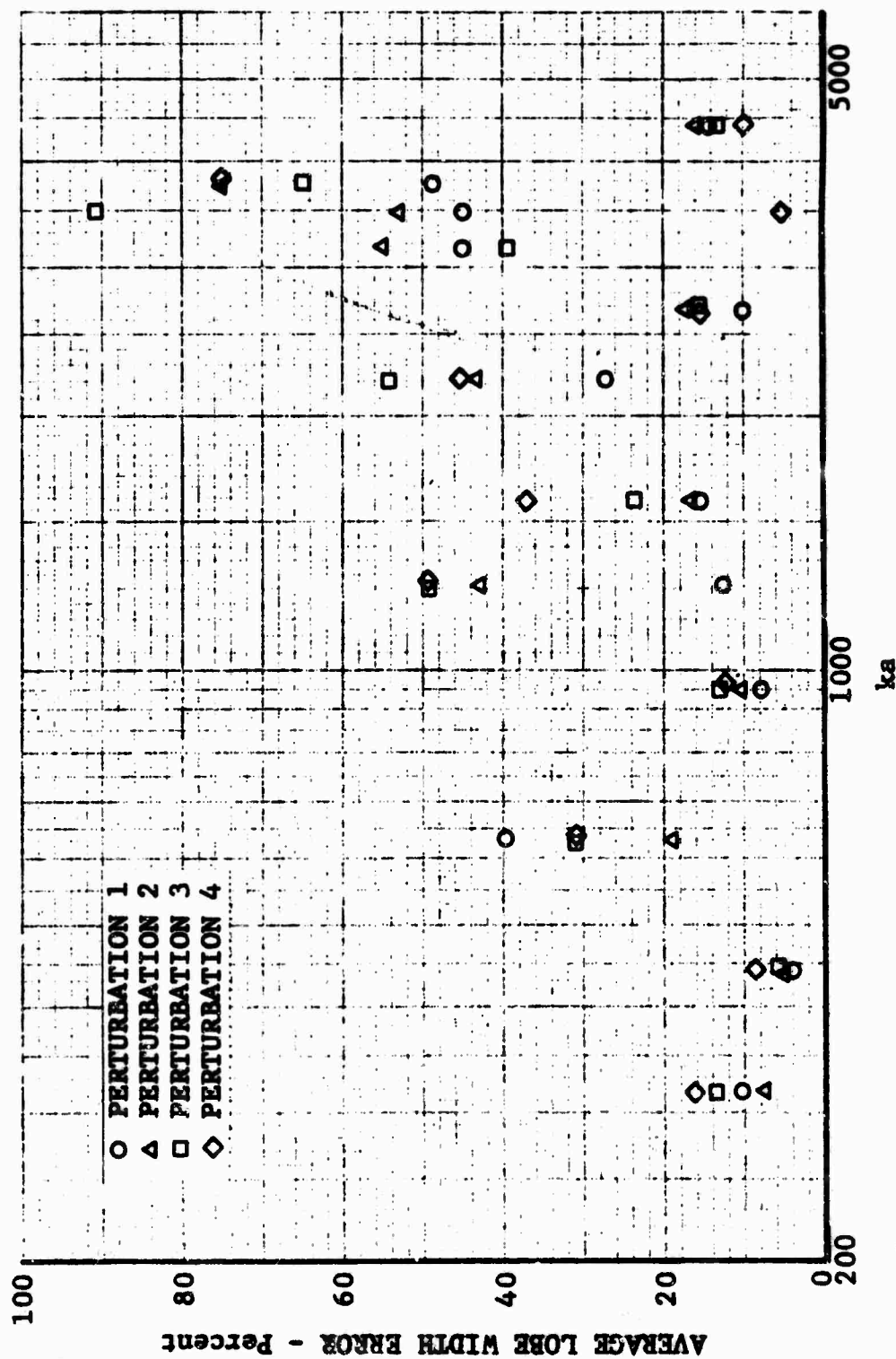


Fig. 1.1-31 LOBE WIDTH ERROR FOR TARGET 9

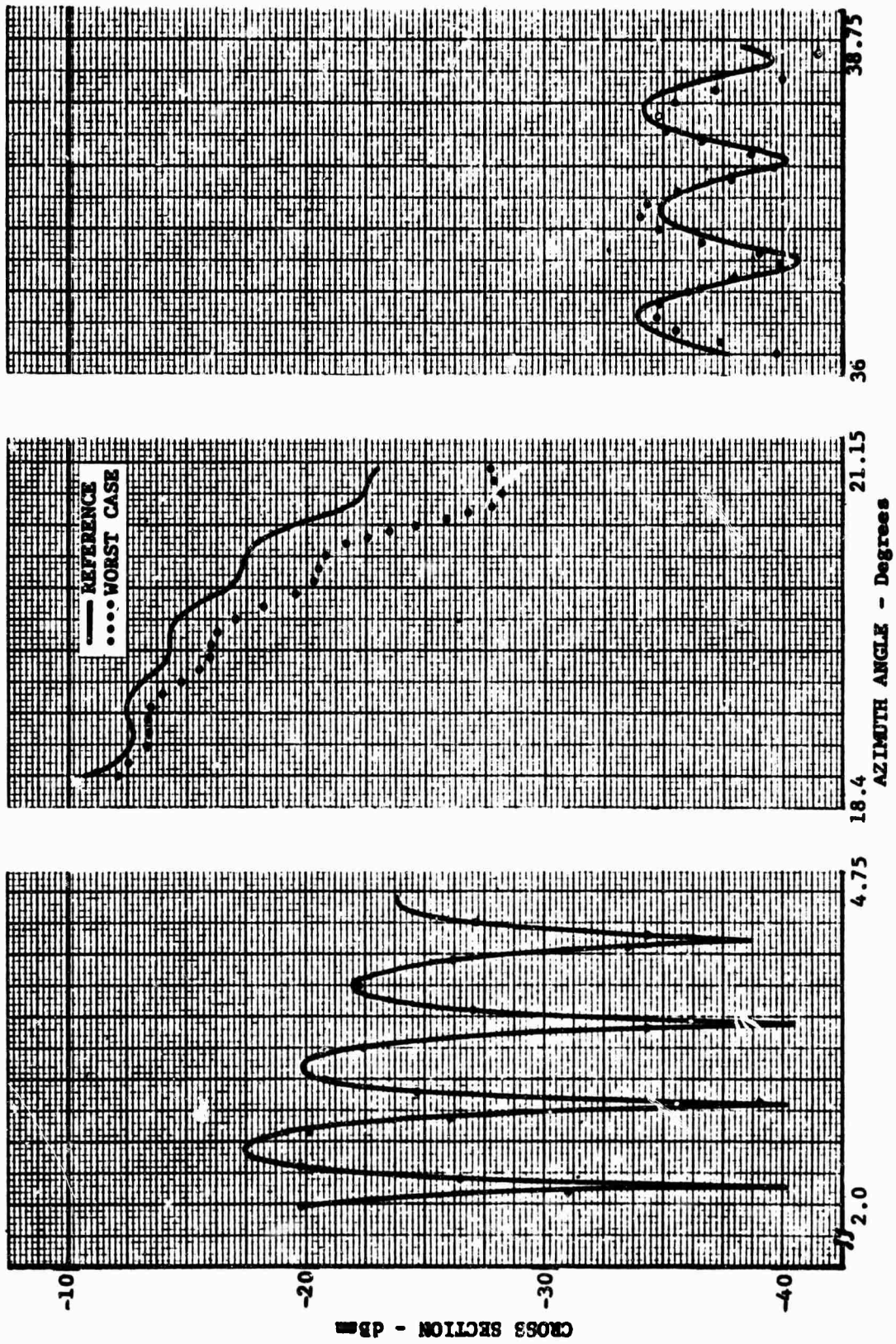


Fig. 1.1-32 CROSS SECTION OF TARGET 1 ($ka = 314$)

K&E **RESEARCH & DESIGN CO.**
10 N. O. HICKORY **MINN. 55117**
10 N. O. N. HICKORY **961253**

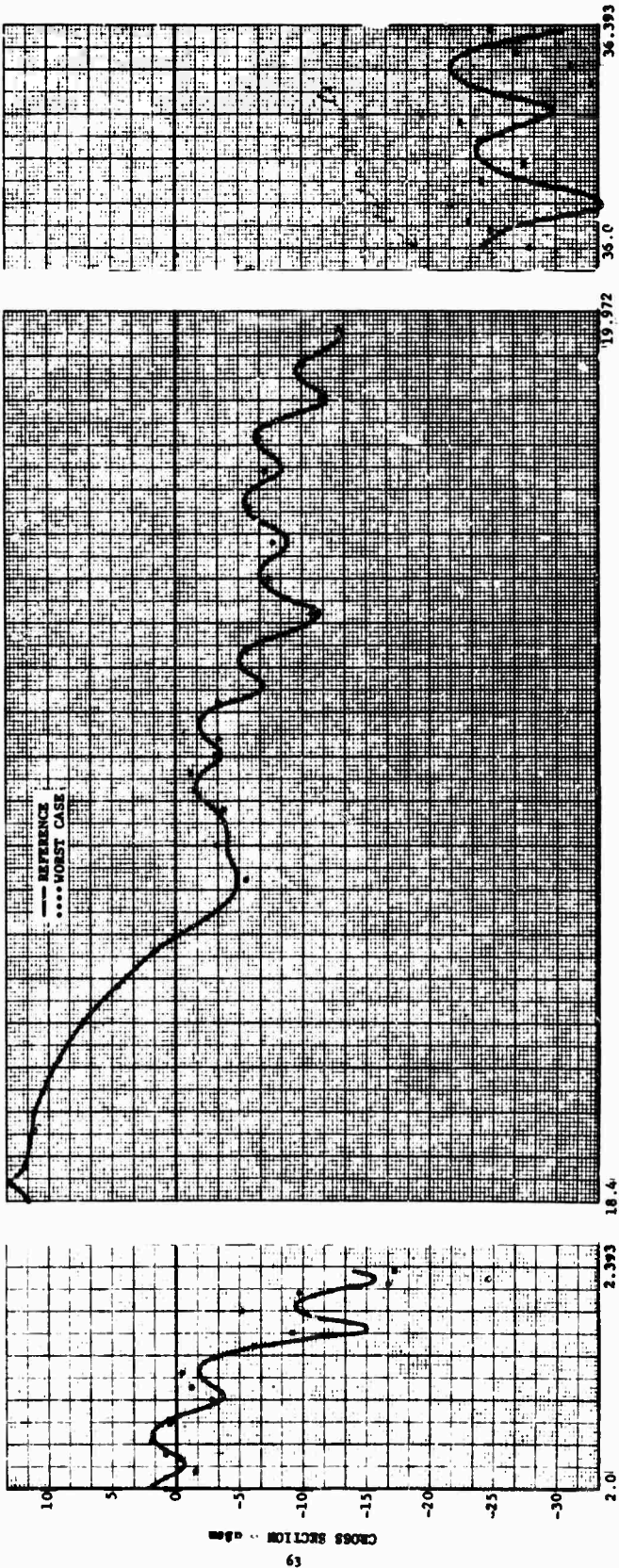
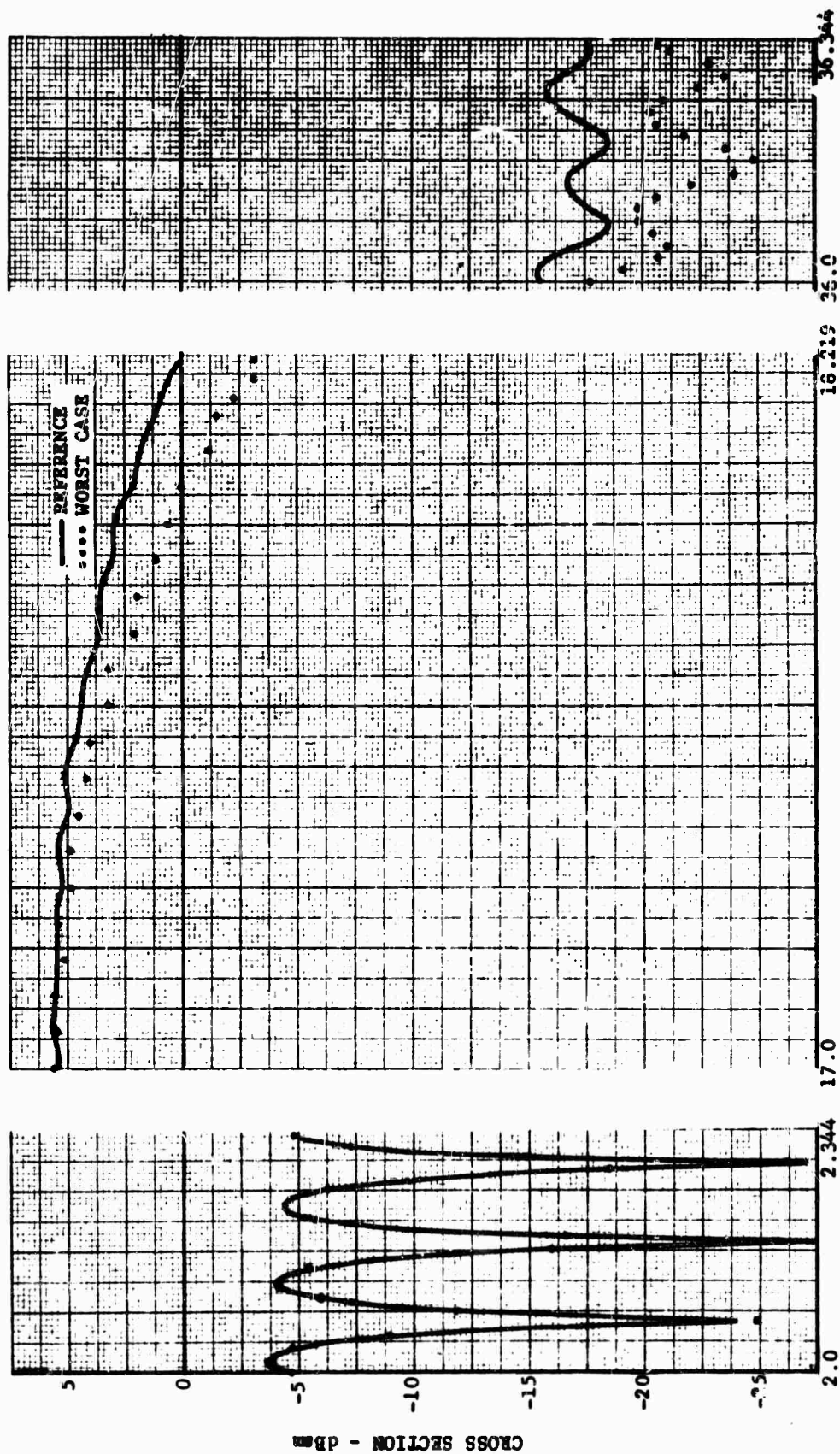


Fig. 1.1-33 CROSS SECTION OF TARGET 2 ($k_a = 2198$)



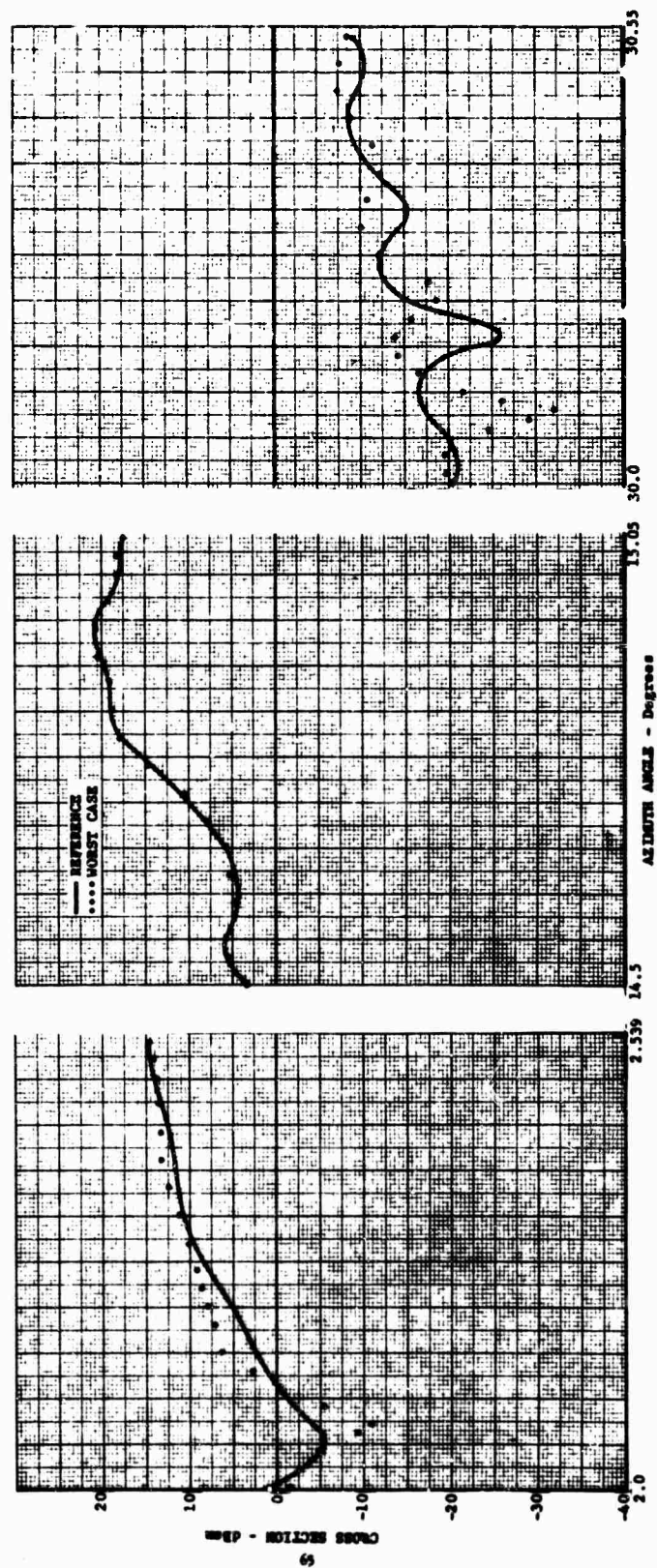


FIG. 1.1-35 CROSS SECTION OF TARGET 4 (1a - 2198)

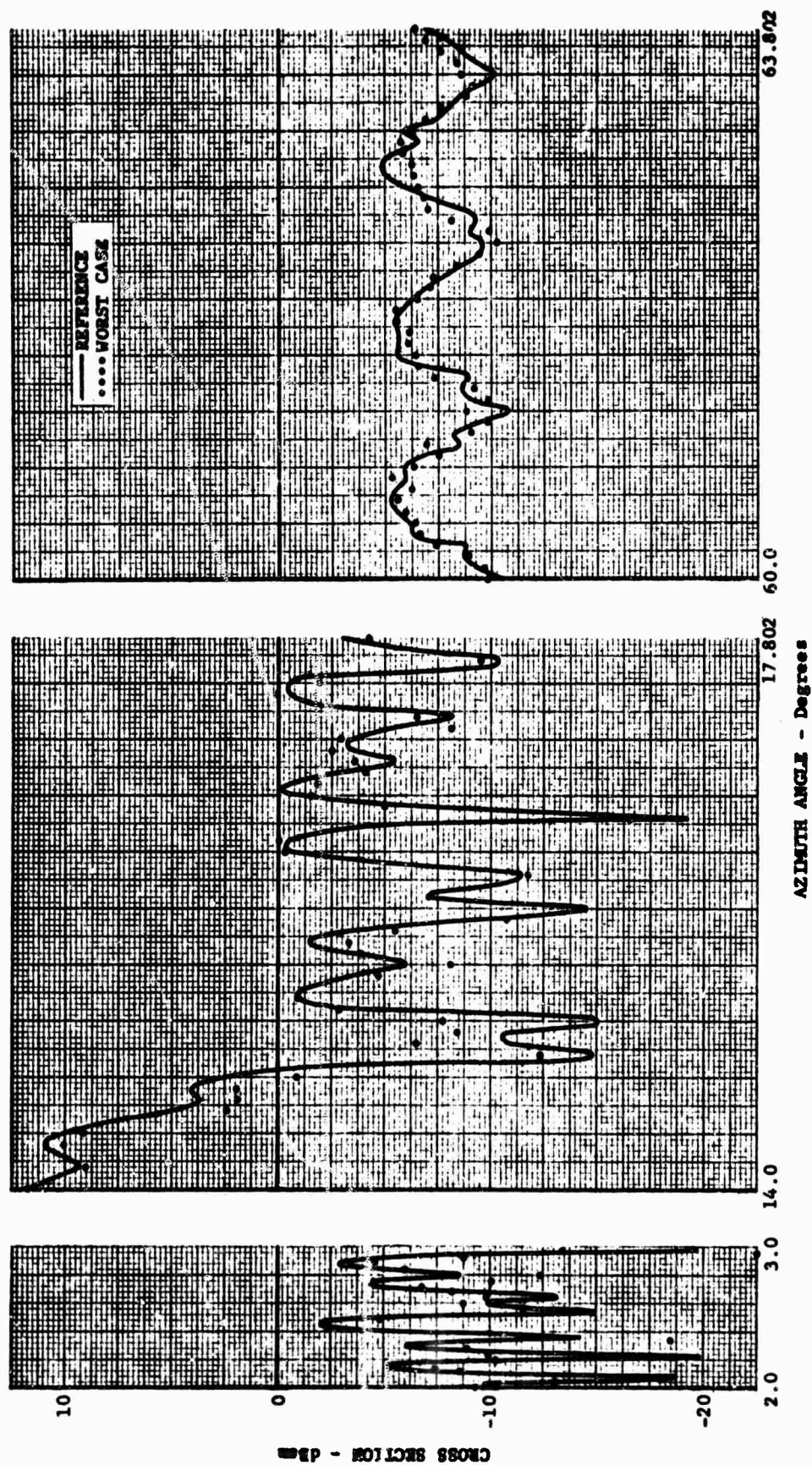


FIG. 1.1-36 CROSS SECTION OF TARGET 5 ($ka = 1760$)

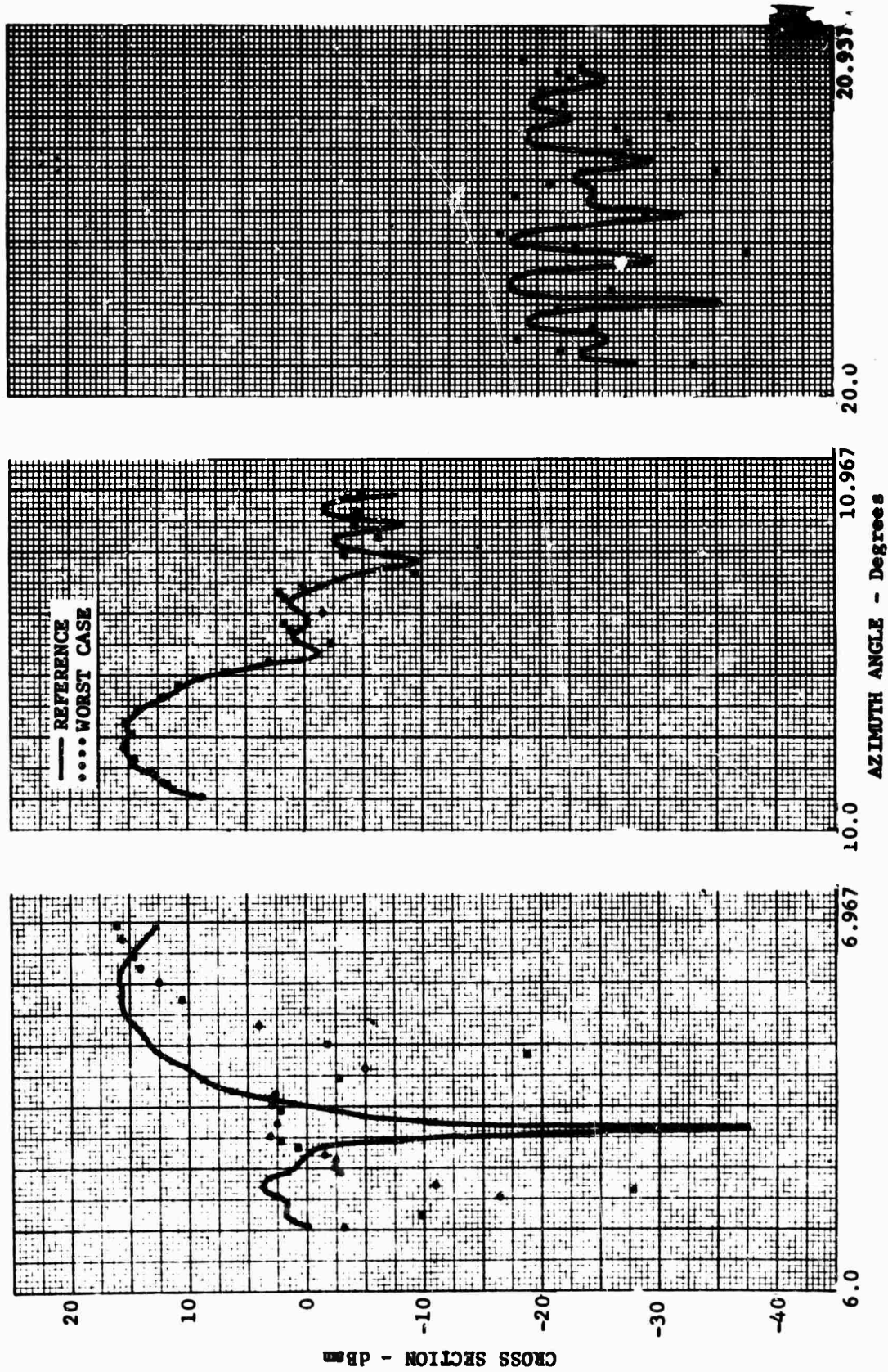


Fig. 1.1-37 CROSS SECTION OF TARGET 6

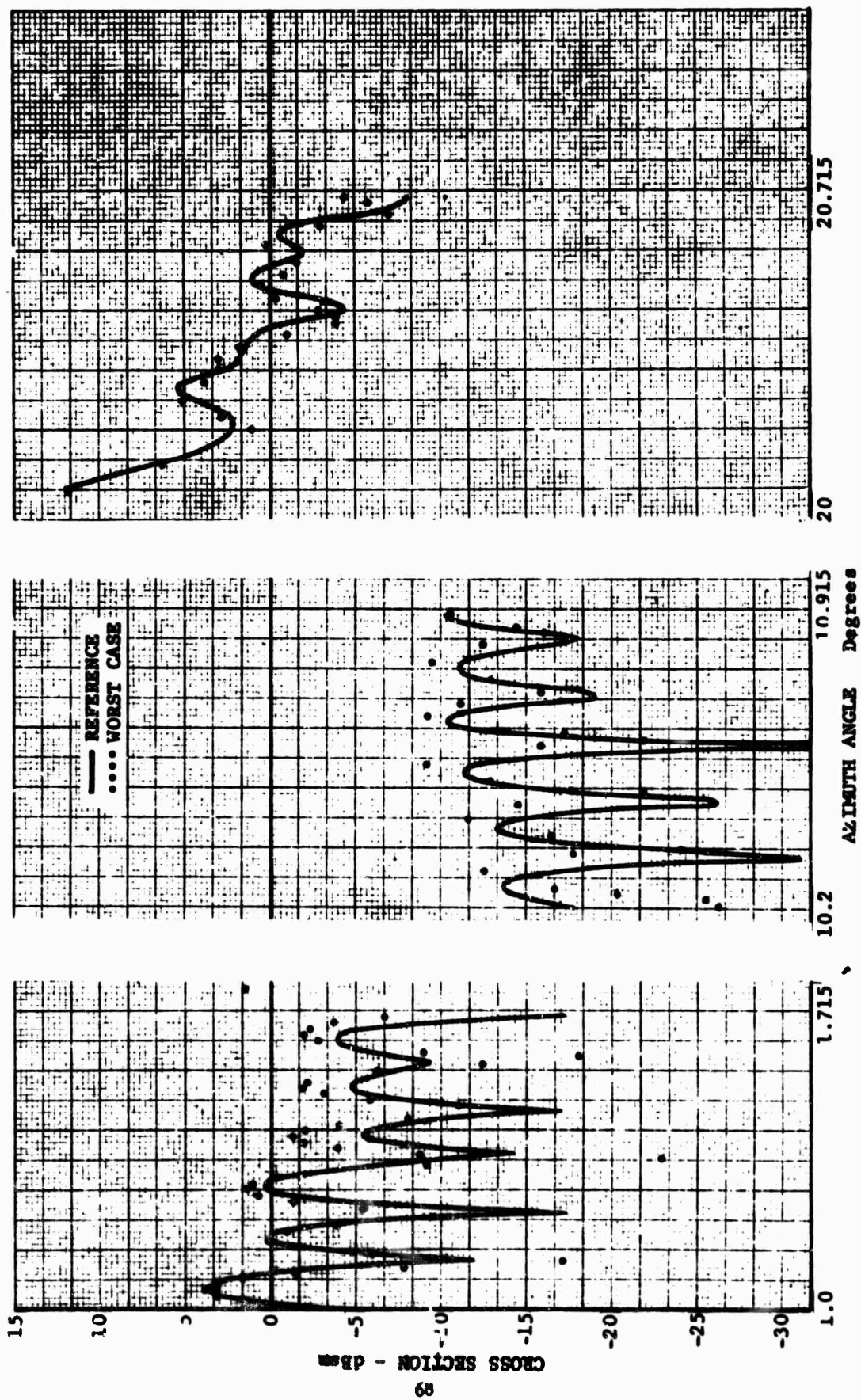


Fig. 1.1-38 CROSS SECTION OF TARGET 7 ($k_a = 2198$)

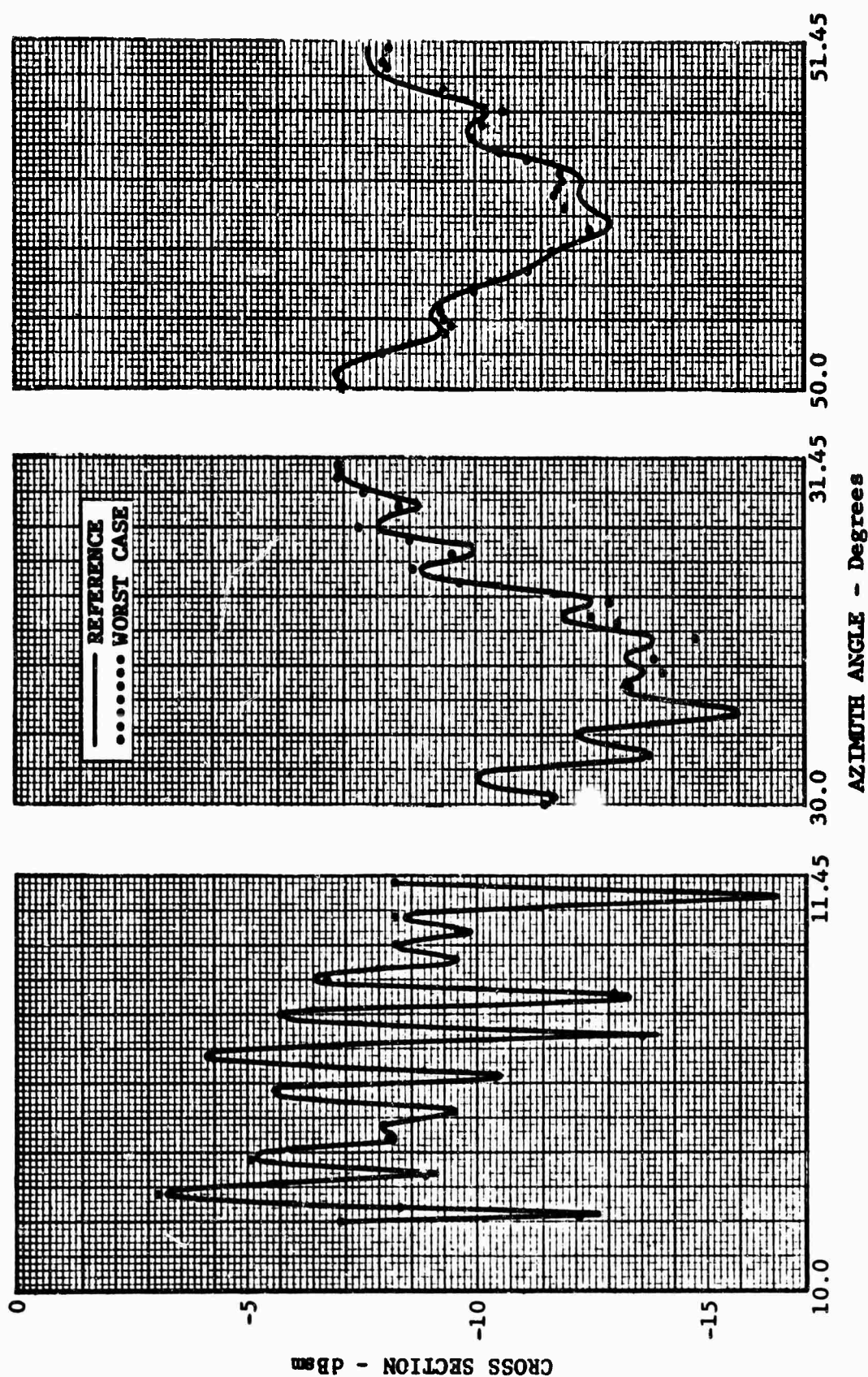


Fig. 1.1-39 CROSS SECTION OF TARGET 8 ($k_a = 2198$)

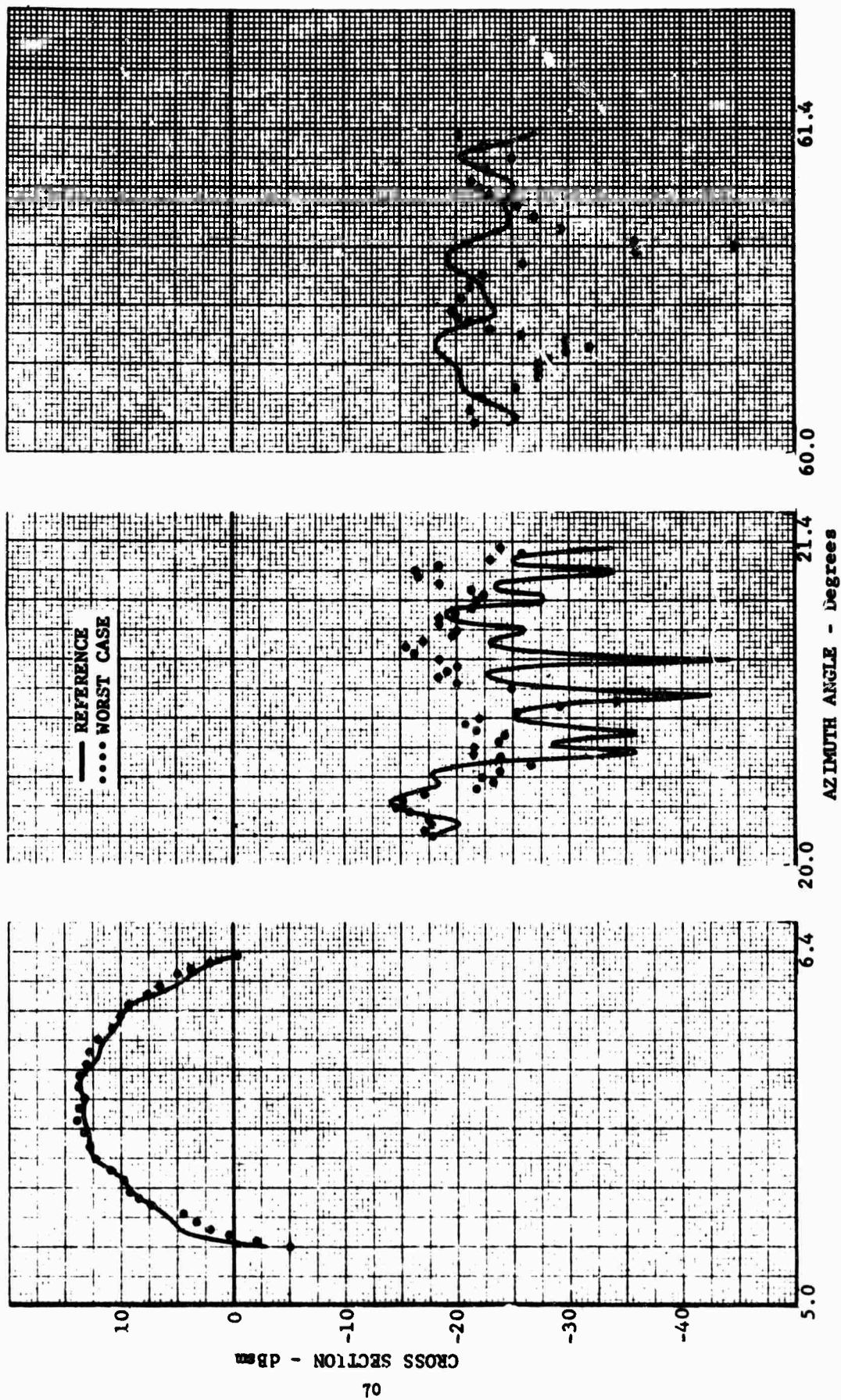
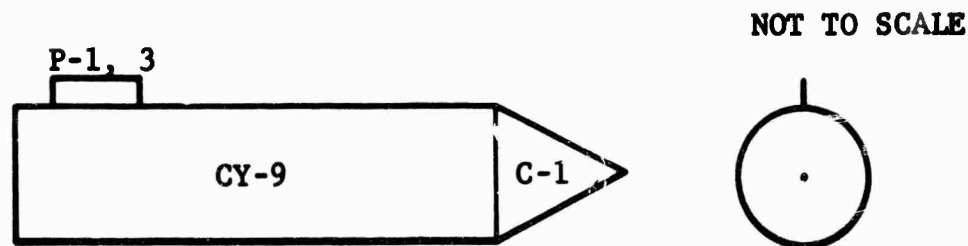
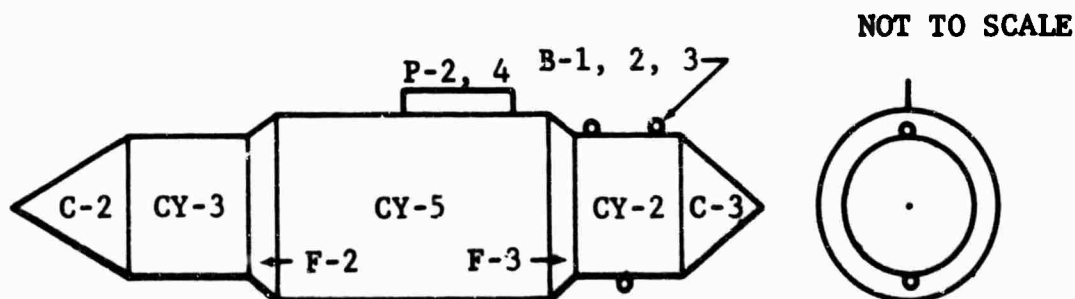


Fig. 1.1-40 CROSS SECTION OF TARGET 9 ($k_a = 2198$)



(a) CONE CYLINDER CONFIGURATION (TARGET 2A)

COMPONENT	LENGTH (Inch)	MAX DIA (Inch)	MIN DIA (Inch)	HEIGHT (Inch)
C-1	11.78	6.320	0	-
C-2	15.814	6.320	0	-
C-3	2.030	6.320	0	-
CY-2	8.317	6.320	-	-
CY-3	10.513	6.320	-	-
CY-5	17.260	7.500	-	-
CY-9	49.487	6.320	-	-
F-2	2.200	7.500	6.320	-
F-3	3.358	7.500	6.320	0.735
P-1	4.12	-	-	0.735
P-2	8.635	-	-	0.204
P-3	4.53	-	-	1.5
P-4	13.60	-	-	.3715
B-1	-	0.112	-	-
B-2	-	0.159	-	-
B-3	-	0.255	-	-



(b) TYPICAL AEROSPACE VEHICLE (TARGET 9A)

Fig. 1.1-41 TARGET CONFIGURATIONS

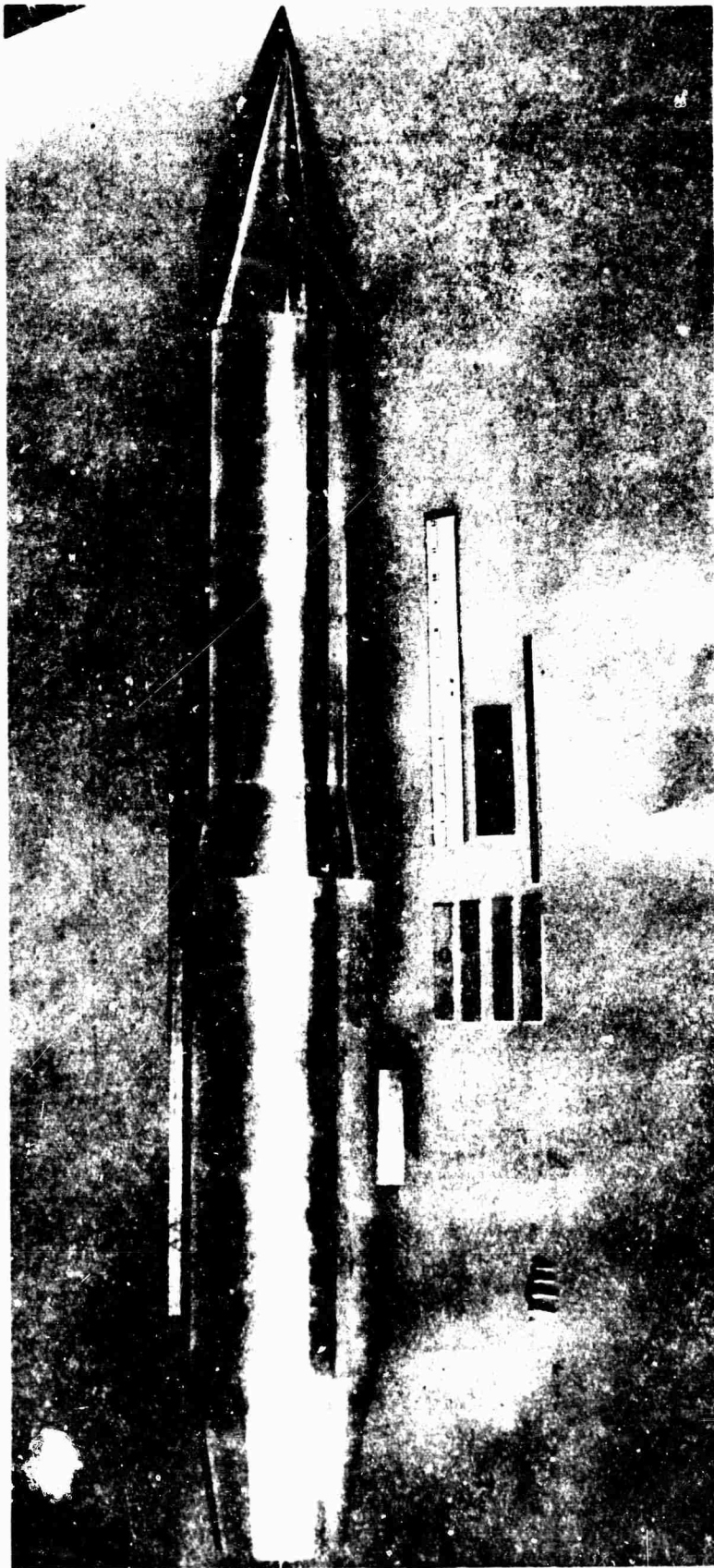


Fig. 1.1-42 TYPICAL AEROSPACE VEHICLE MOCKUP

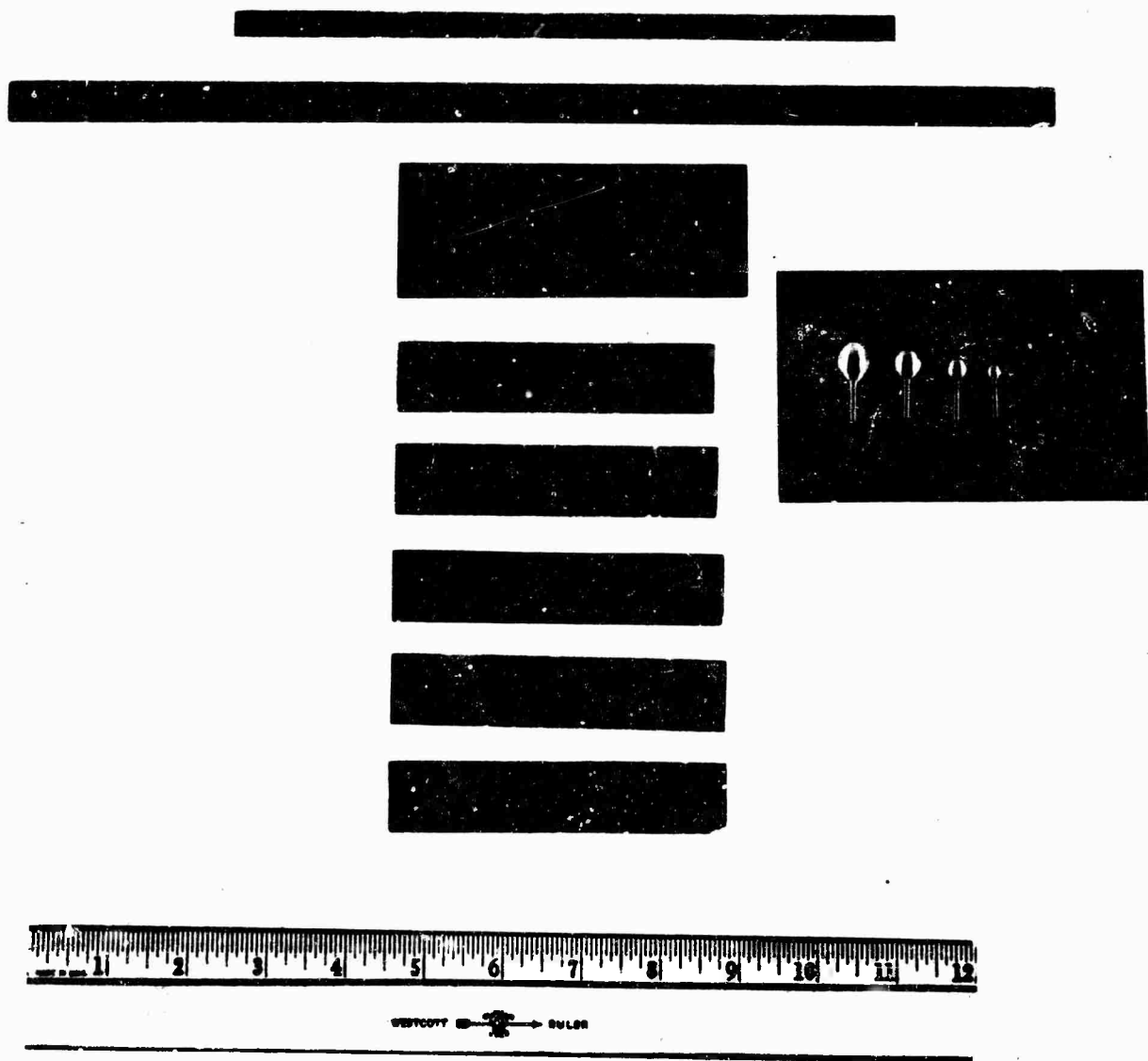
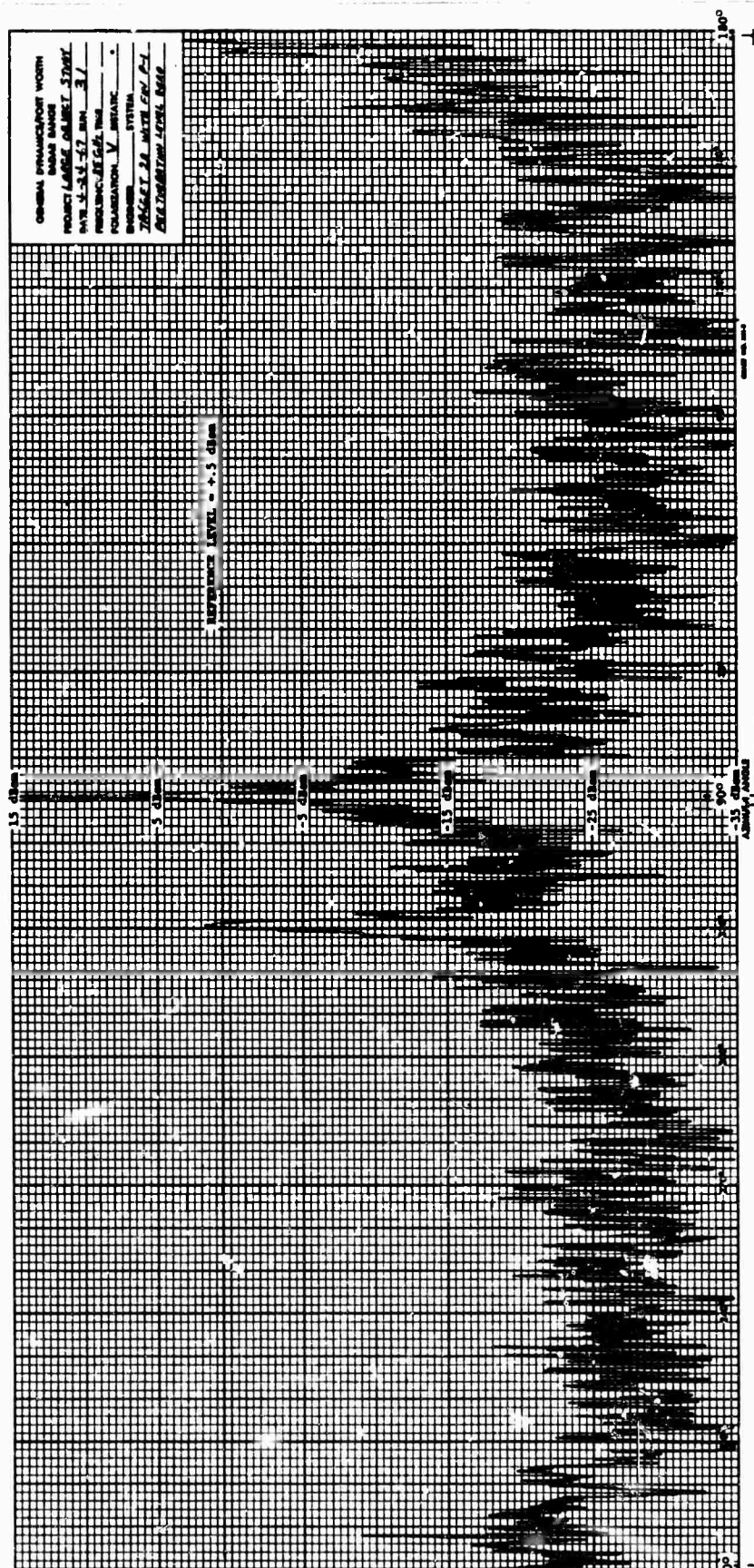


Fig. 1.1-43 TYPICAL TARGET APPENDAGES



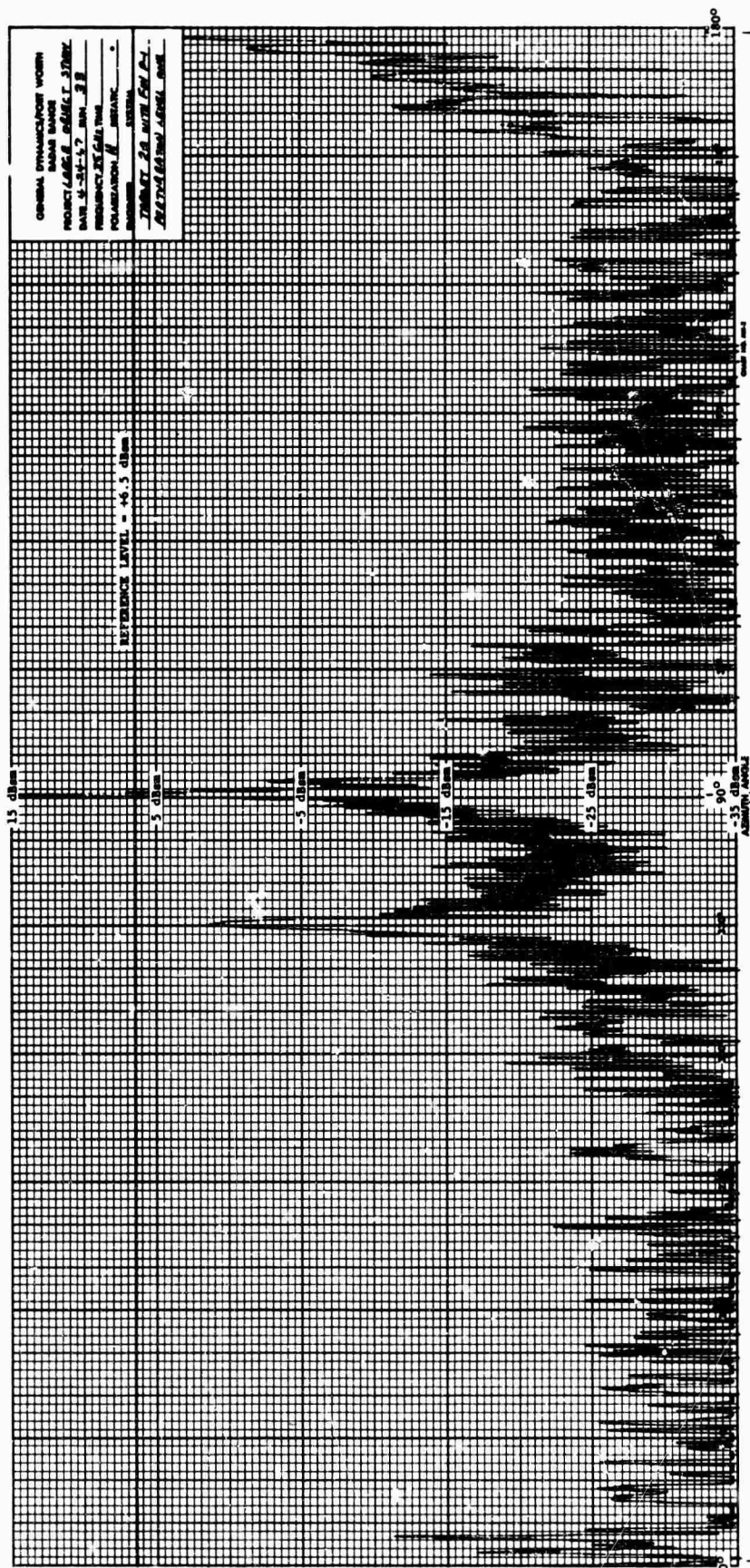


Fig. 1.1-45 EXPERIMENTAL DATA ON TARGET 2A, PERTURBATION LEVEL 1, FIN P-1

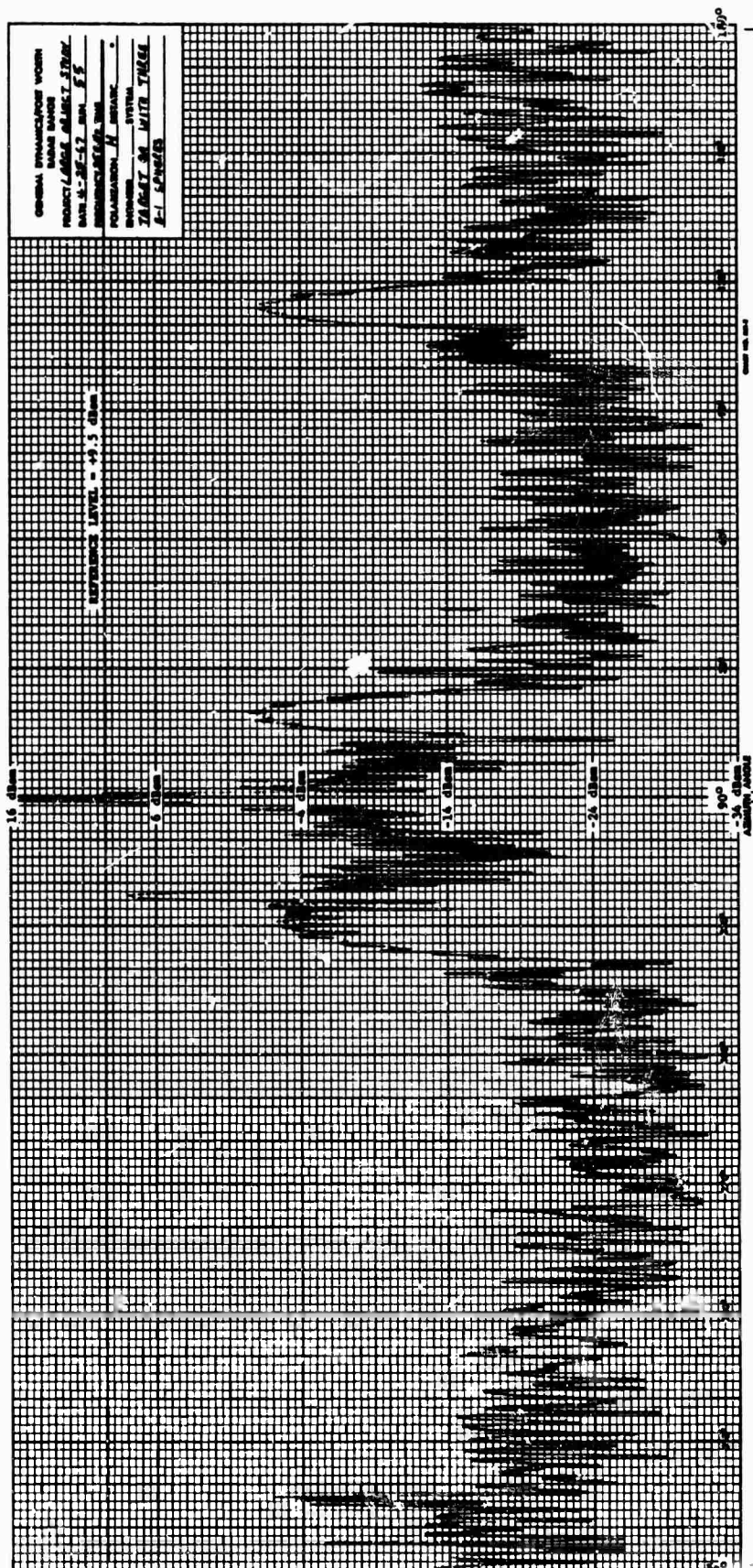


Fig. 1.1-46 EXPERIMENTAL DATA ON TARGET 9A, PERTURBATION LEVEL 0 (SPHERES B-1)

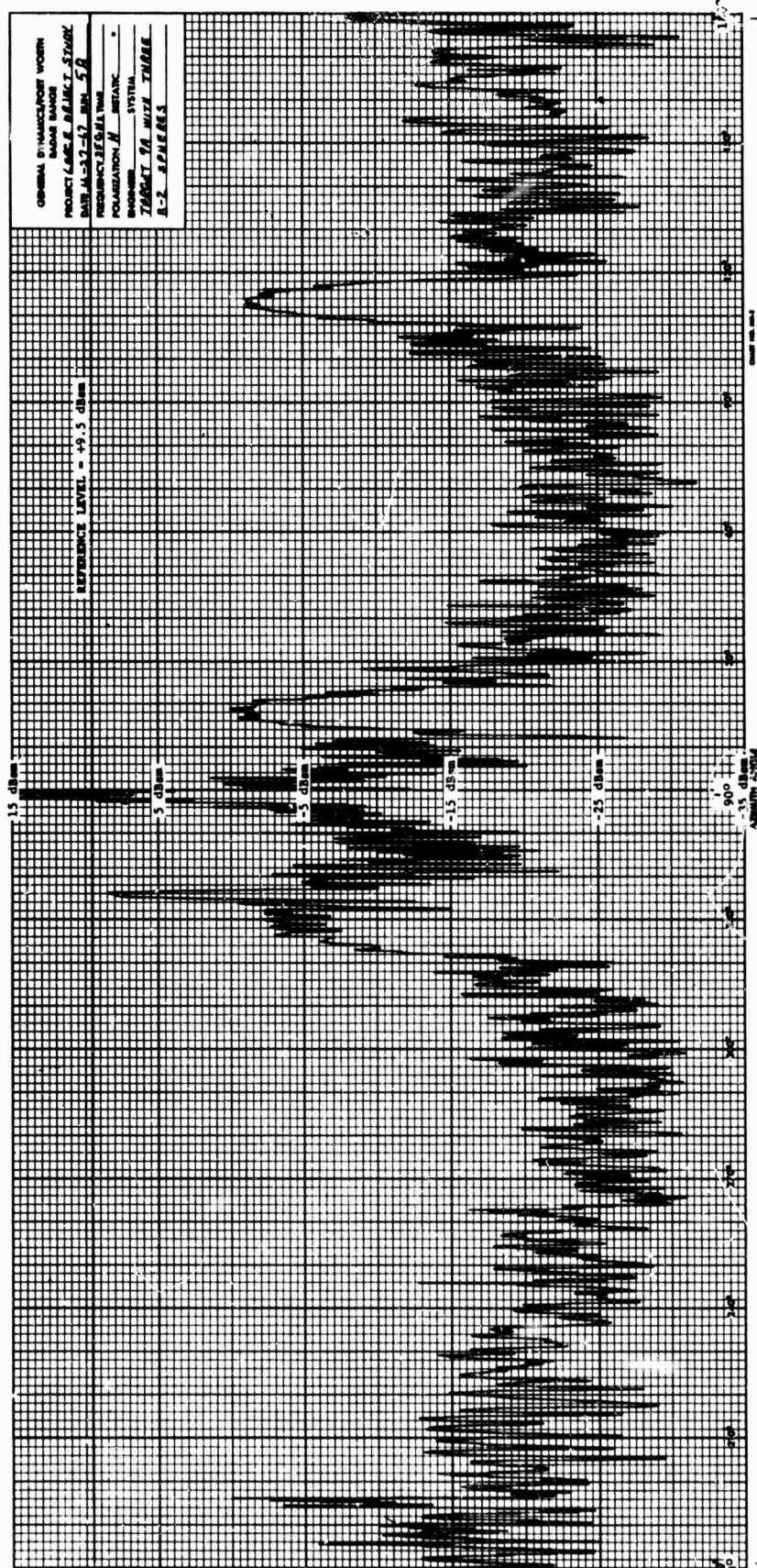


Fig. 1.1-47 EXPERIMENTAL DATA ON TARGET 9A, PERTURBATION LEVEL 2 (SPHERES B-2)

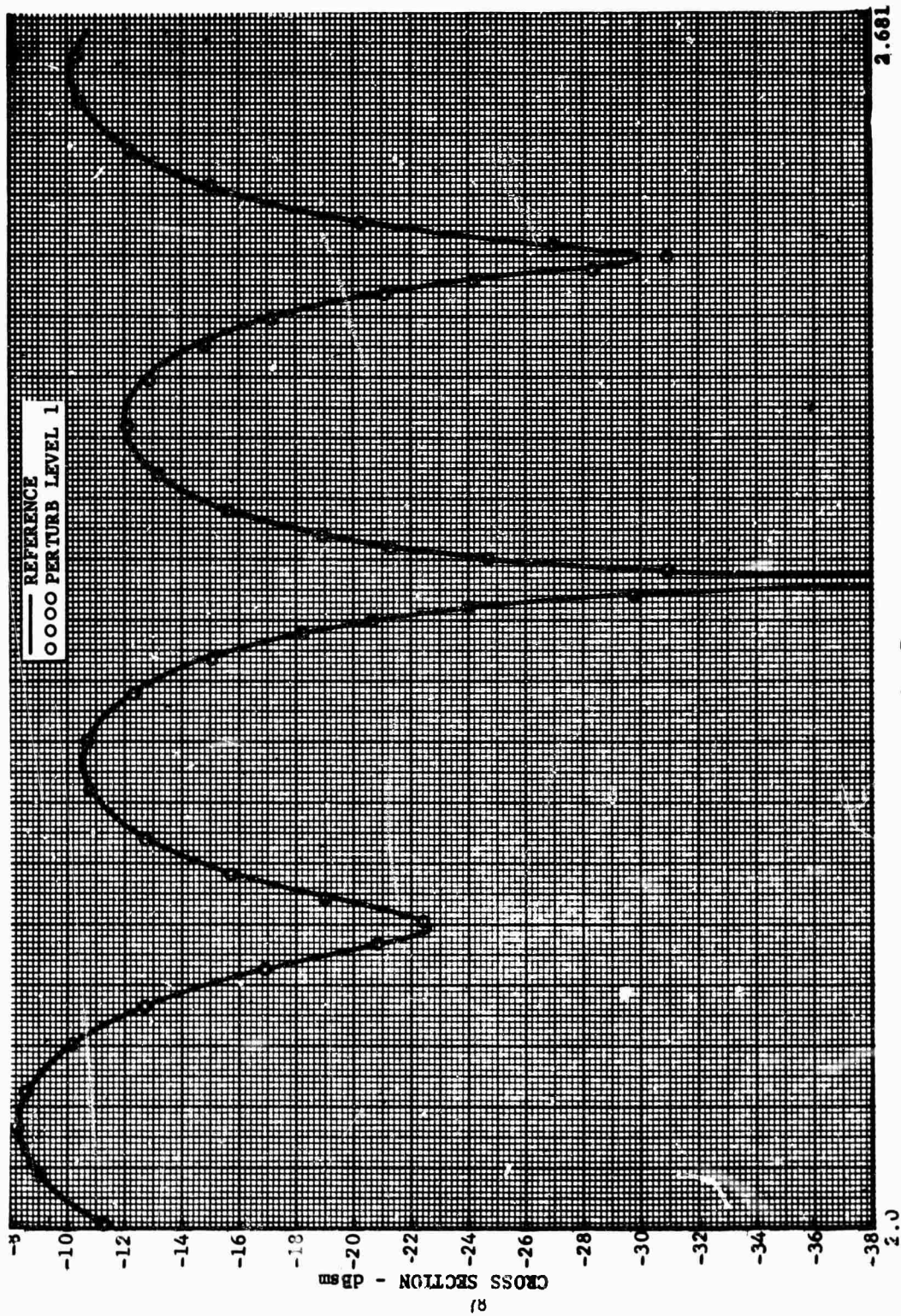


Fig. 1.1-48 CONE-CYLINDER RADAR CROSS SECTION DATA
(NEAR 2-DEGREES)

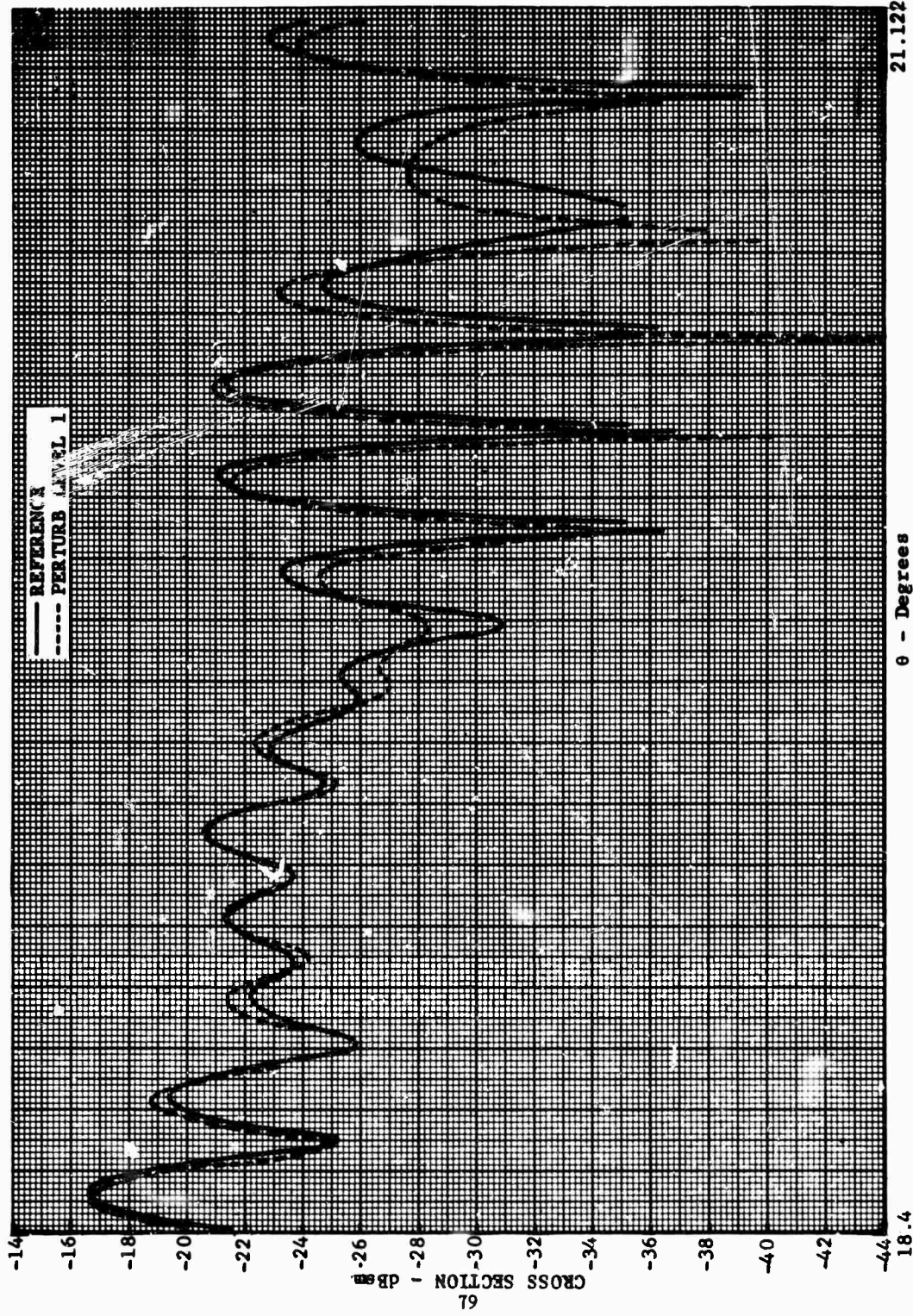


Fig. 1.1-49 CO-E-CYLINDER RADAR CROSS SECTION DATA (NEAR 18-DEGREES)

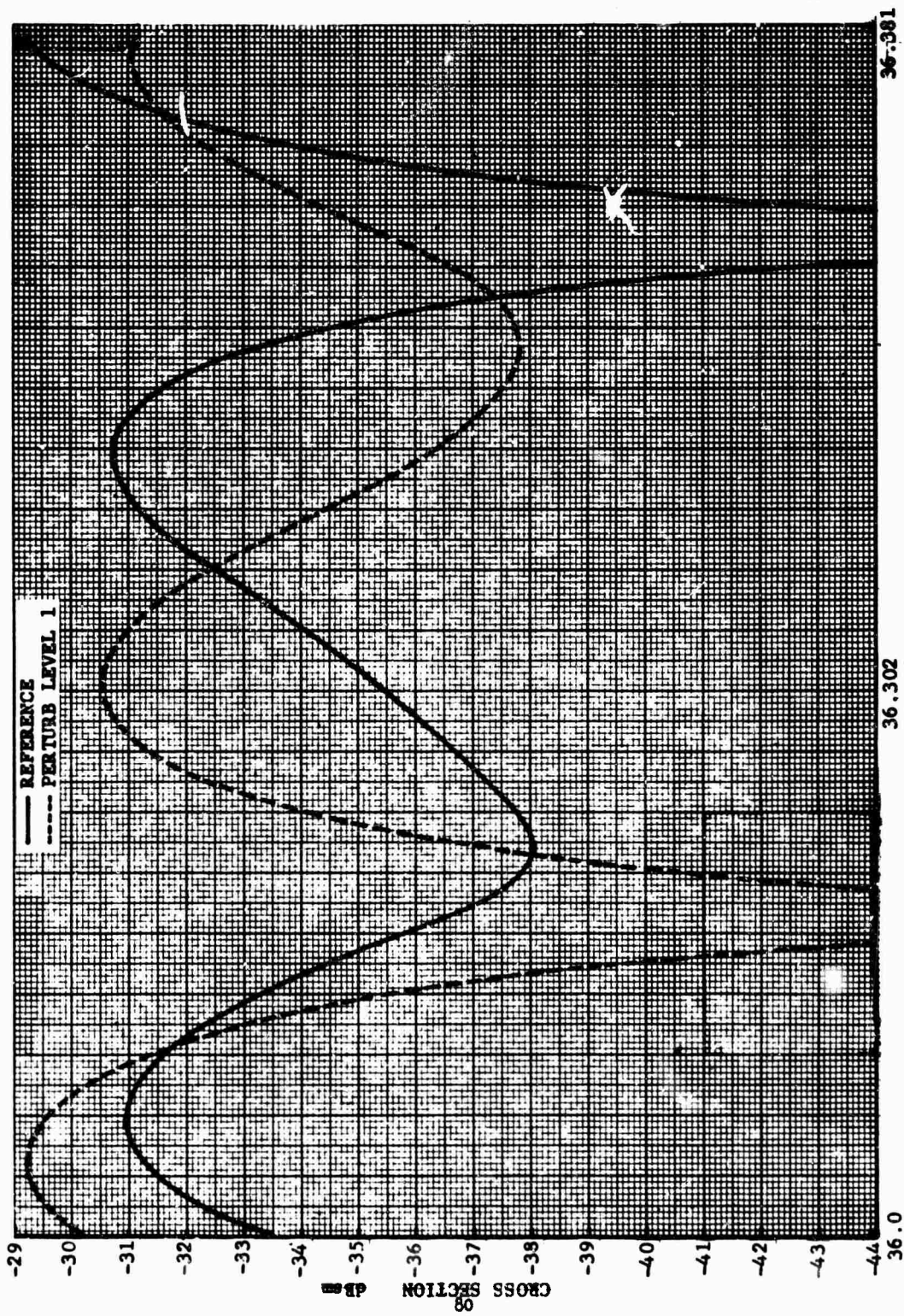


Fig. 1.1-50 CONE-CYLINDER RADAR CROSS SECTION DATA
(NEAR 36-DEGREES)

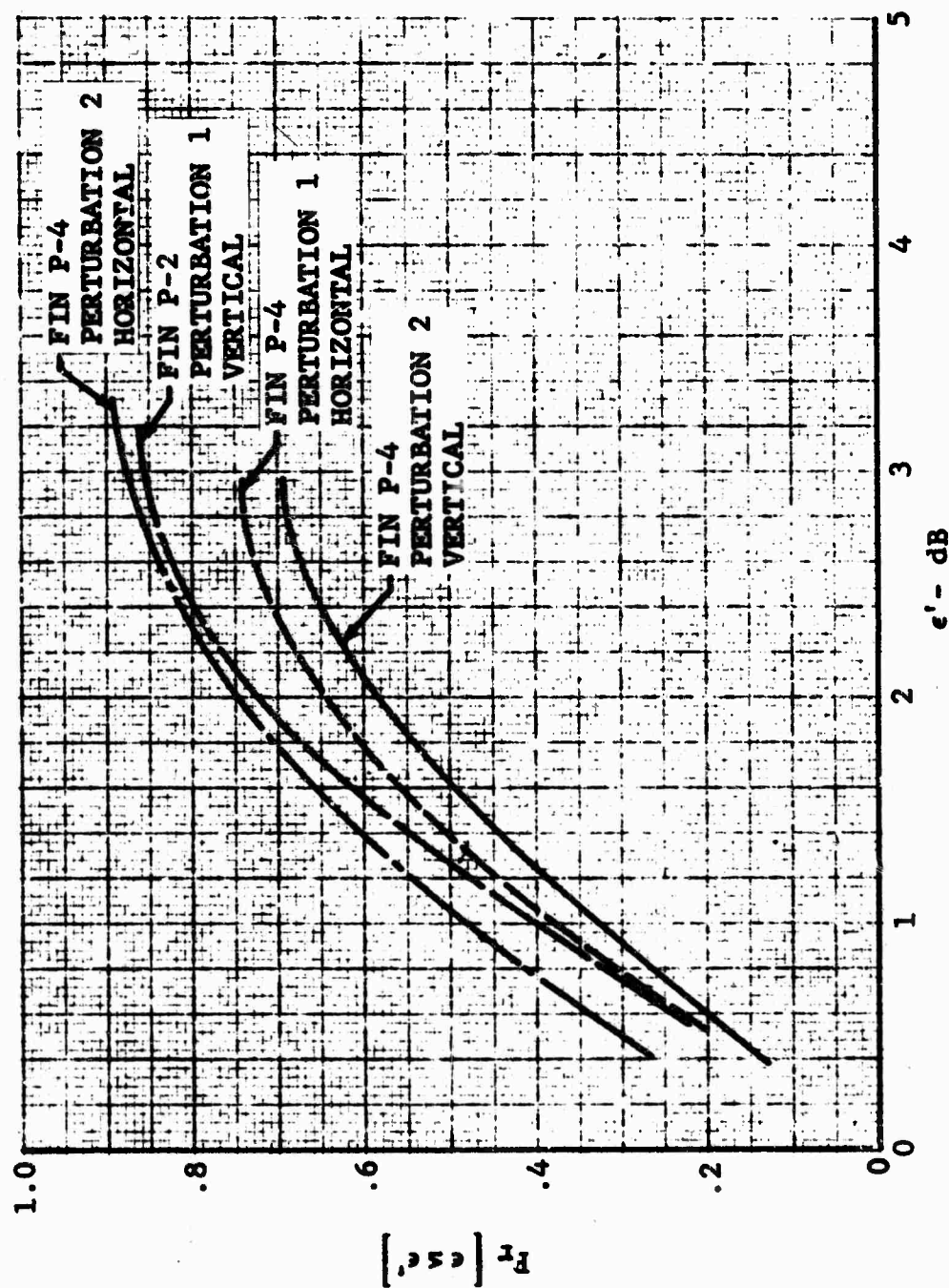


Fig. 1.1-51 ERROR DISTRIBUTIONS ON TARGET 2A WITH FIN PERTURBATIONS

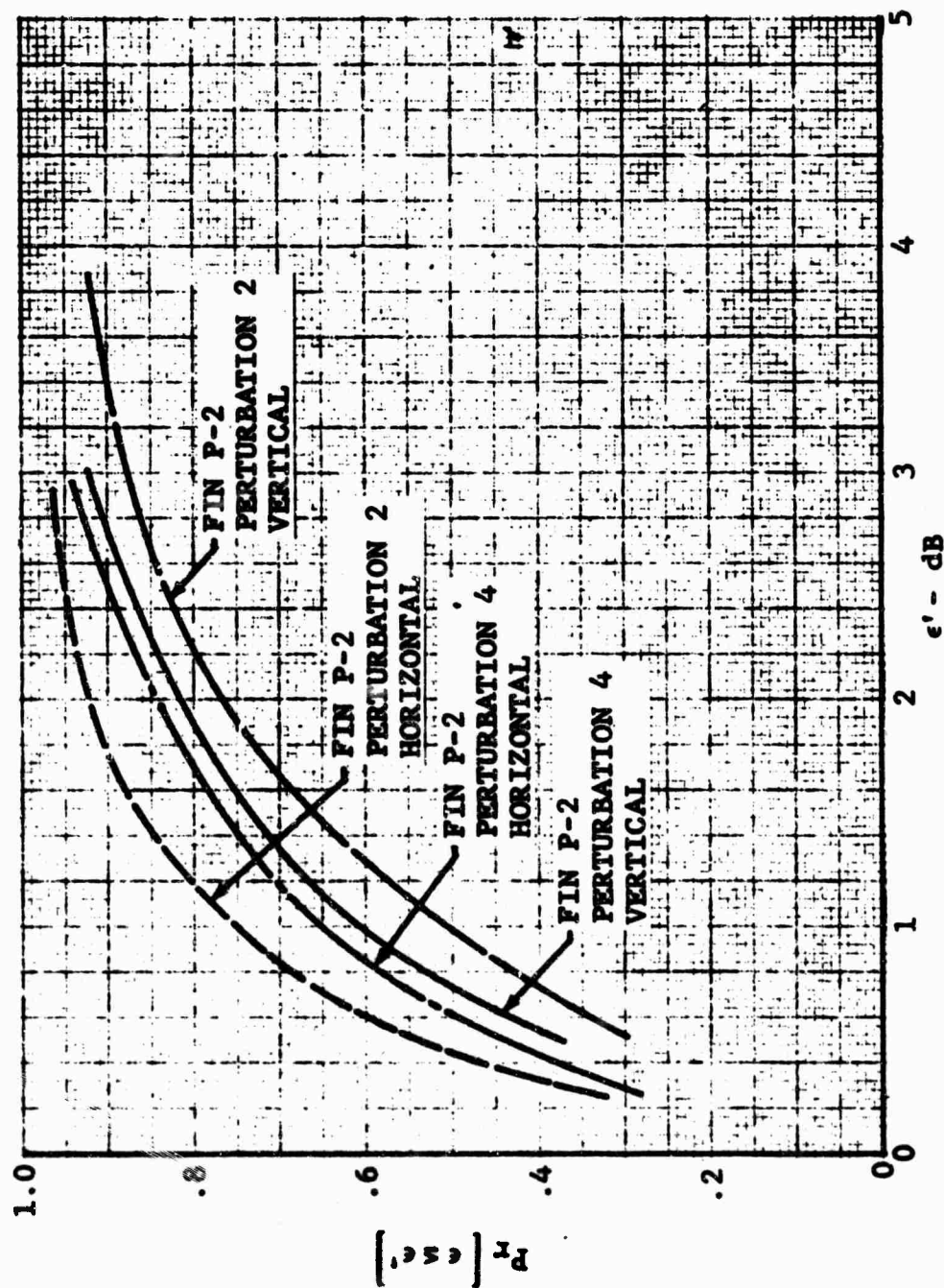


Fig. 1.1-52 ERROR DISTRIBUTIONS ON TARGET 8A WITH FIN PERTURBATIONS

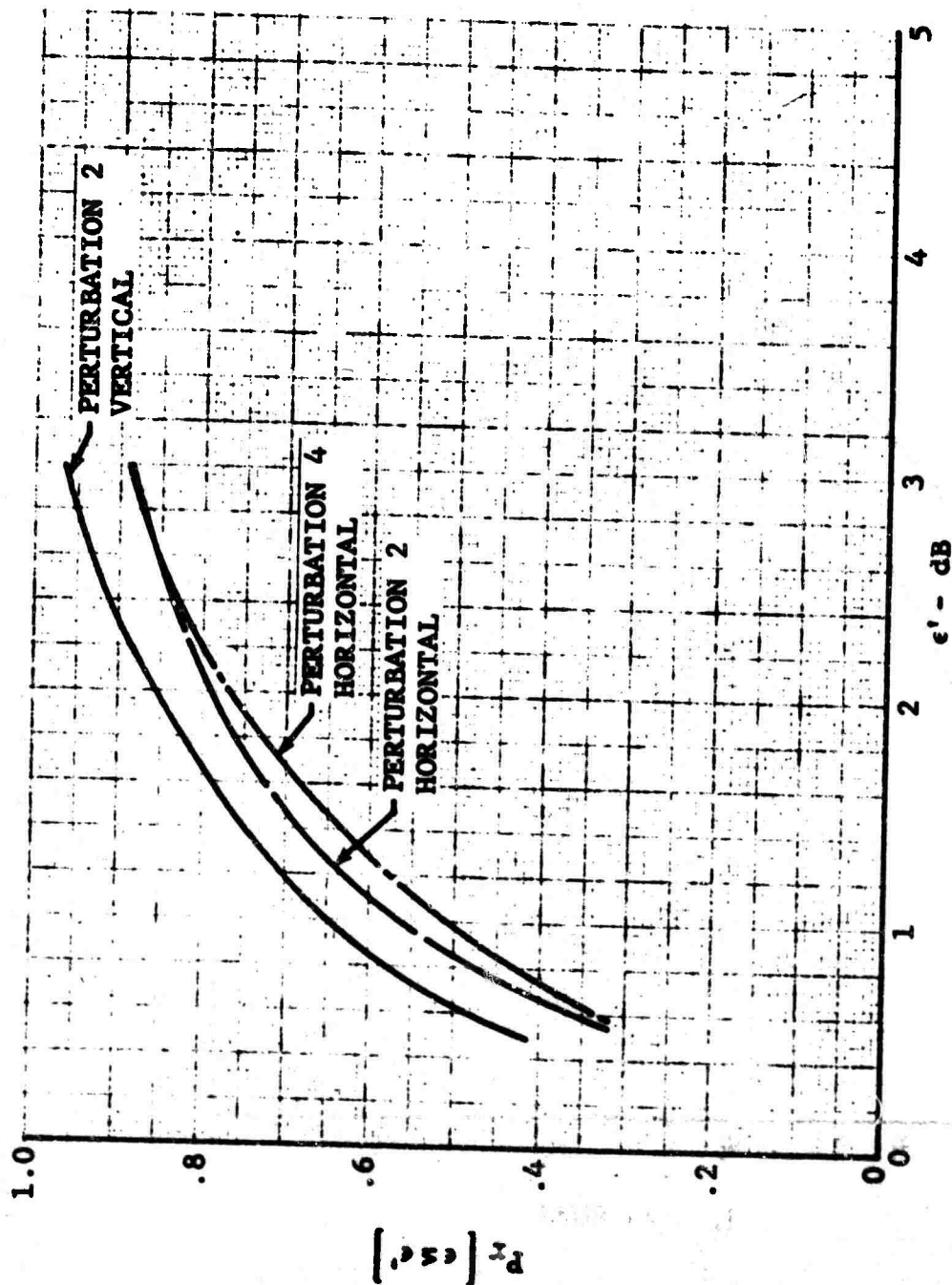


Fig. 1.1-53 ERROR DISTRIBUTIONS OR TARGET 9A WITH SPHERE PERTURBATIONS

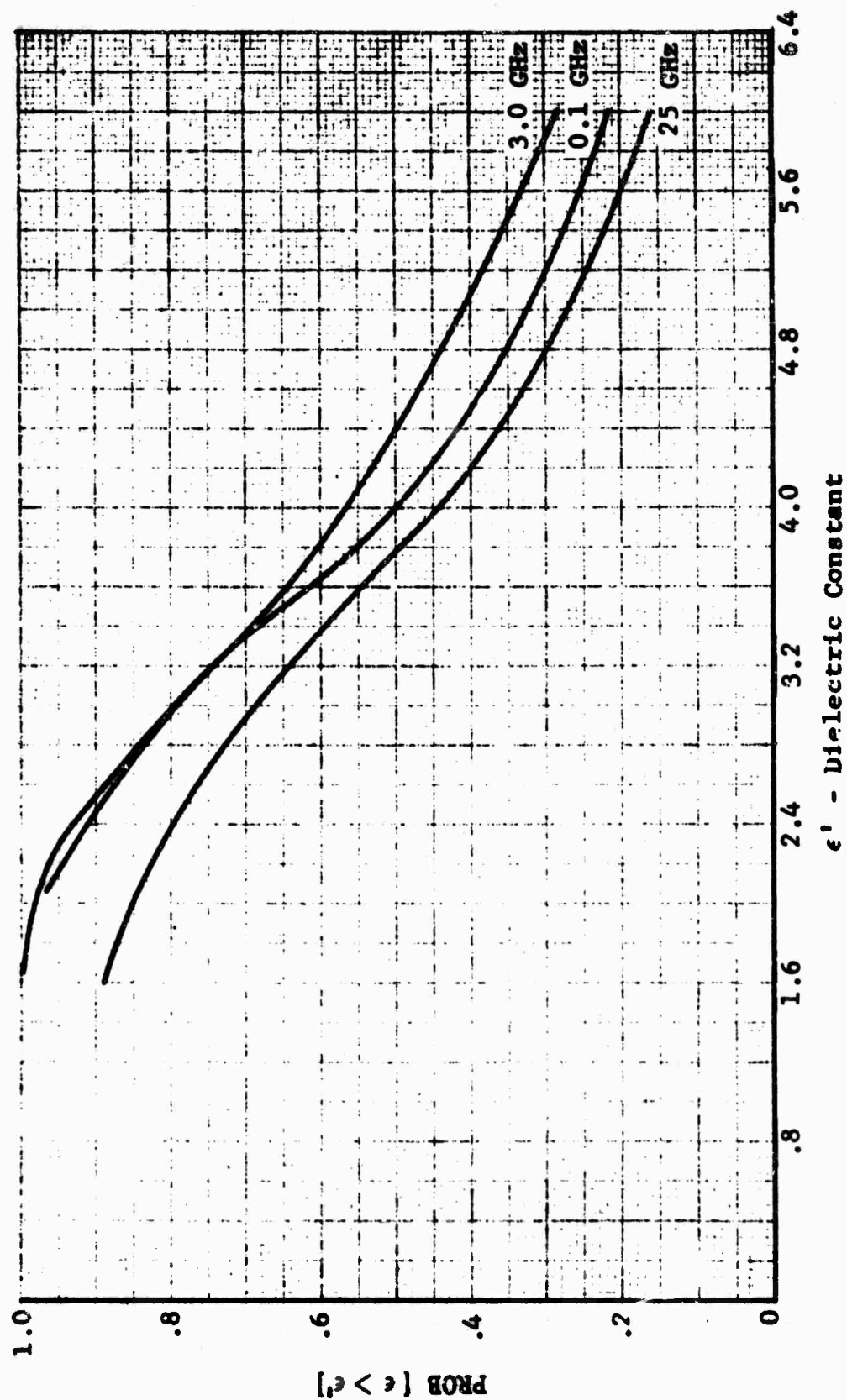


Fig. 1.1-54 CUMULATIVE PROBABILITY DENSITY ON MATERIAL DIELECTRIC CONSTANT

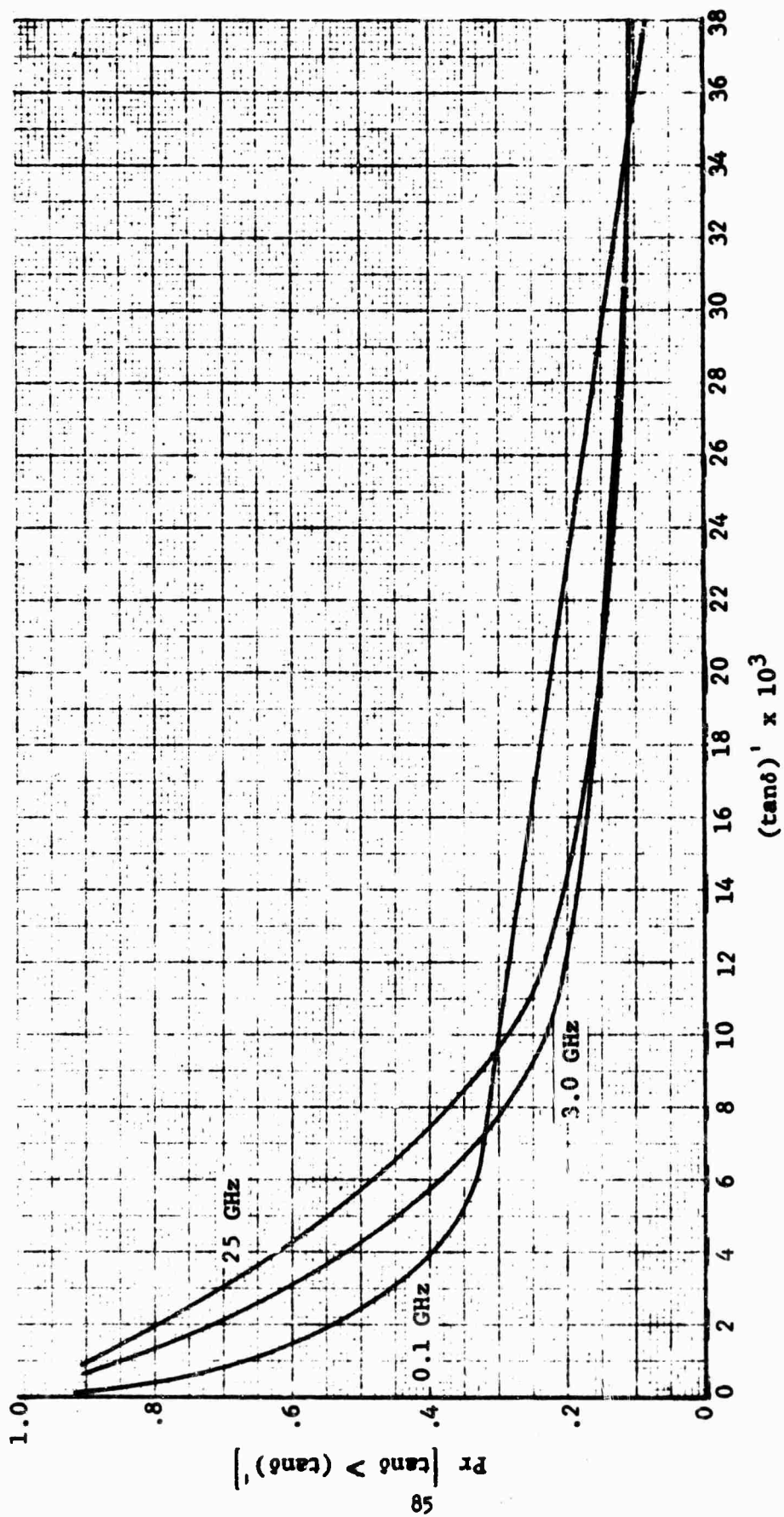


Fig. 1.1-55 CUMULATIVE PROBABILITY DENSITY ON LOSS TANGENT

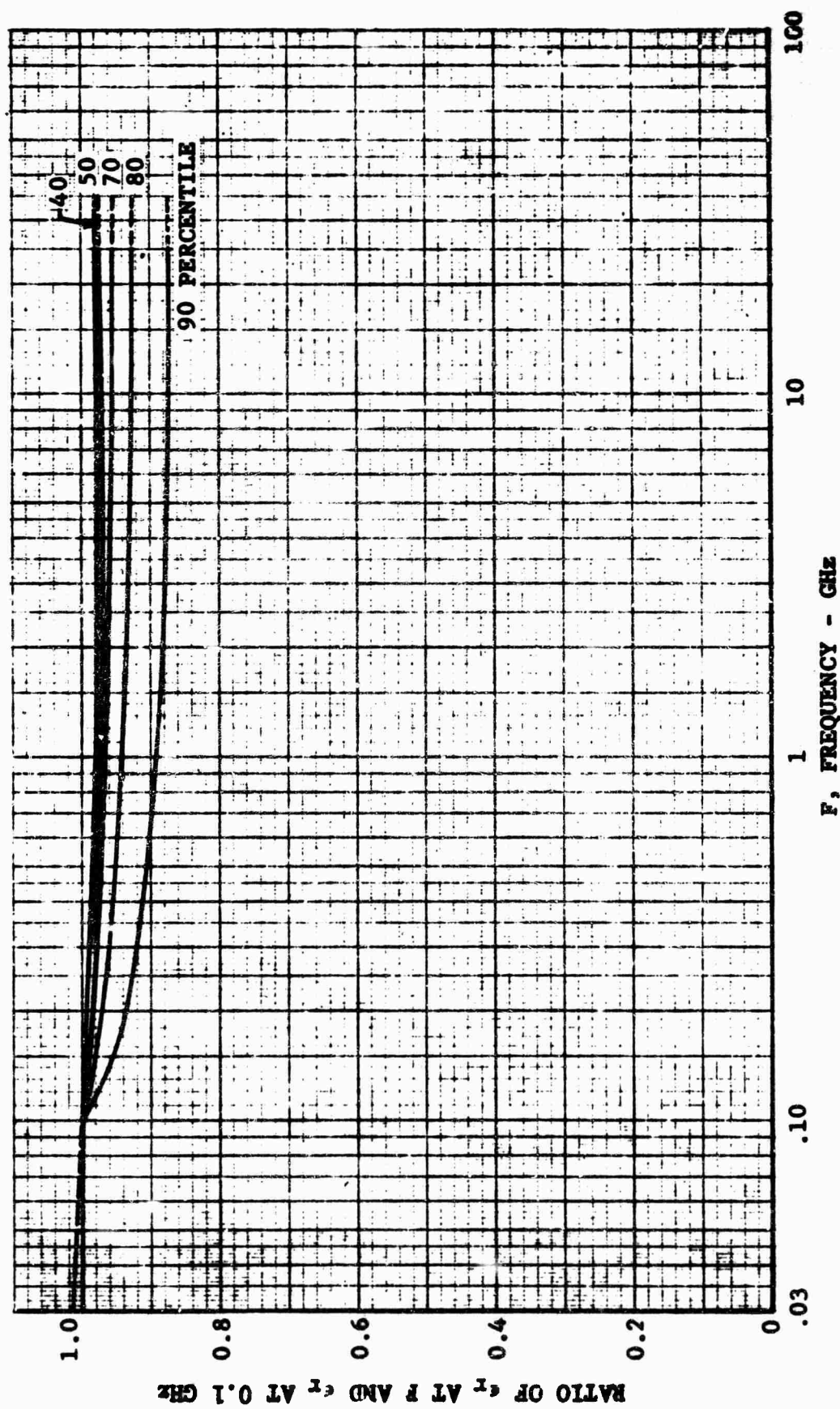


FIG. 1.1-56 FREQUENCY DEPENDENCE OF DIELECTRIC CONSTANT

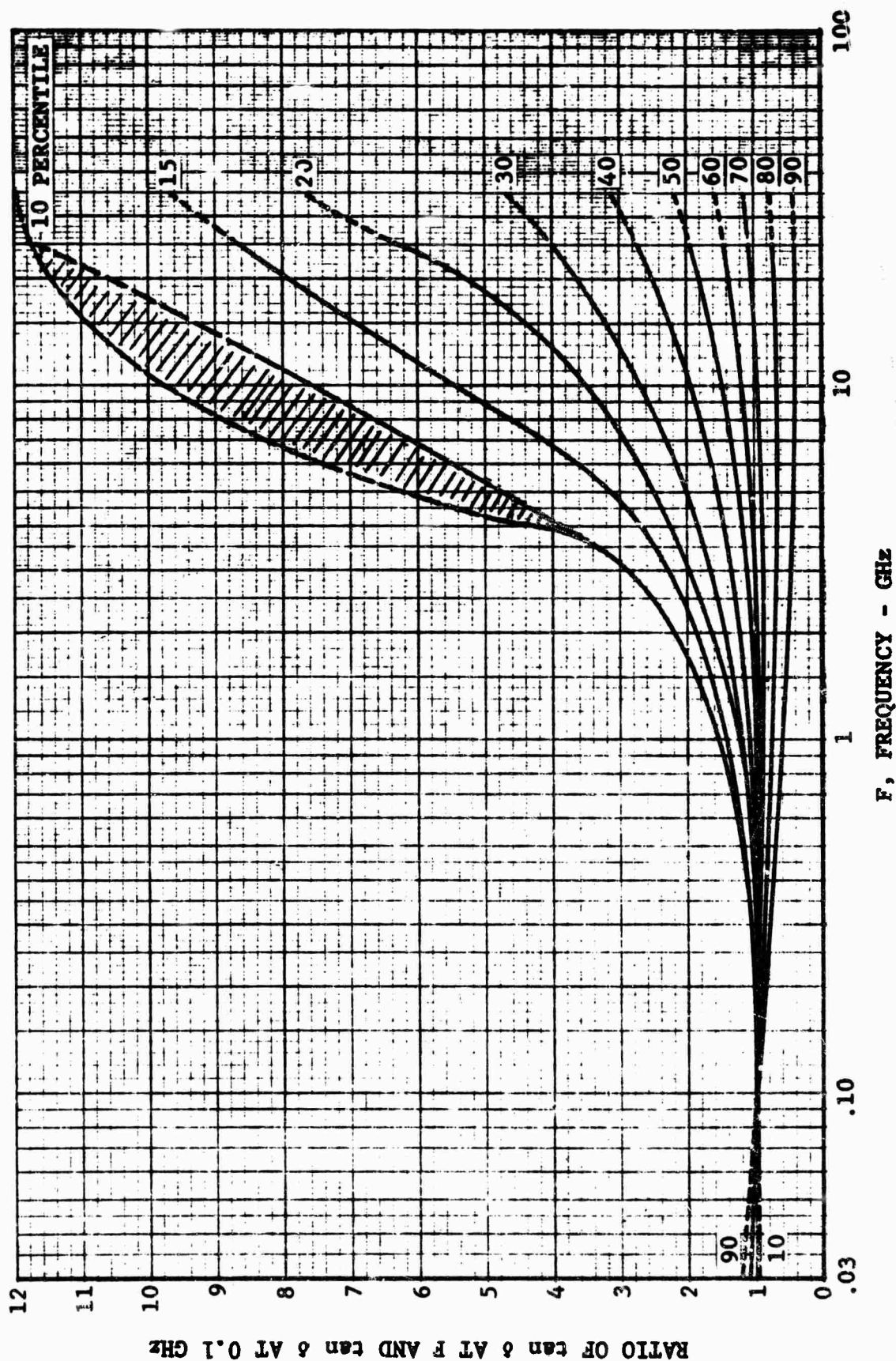


Fig. 1.1-57 FREQUENCY DEPENDENCE OF LOSS TANGENT

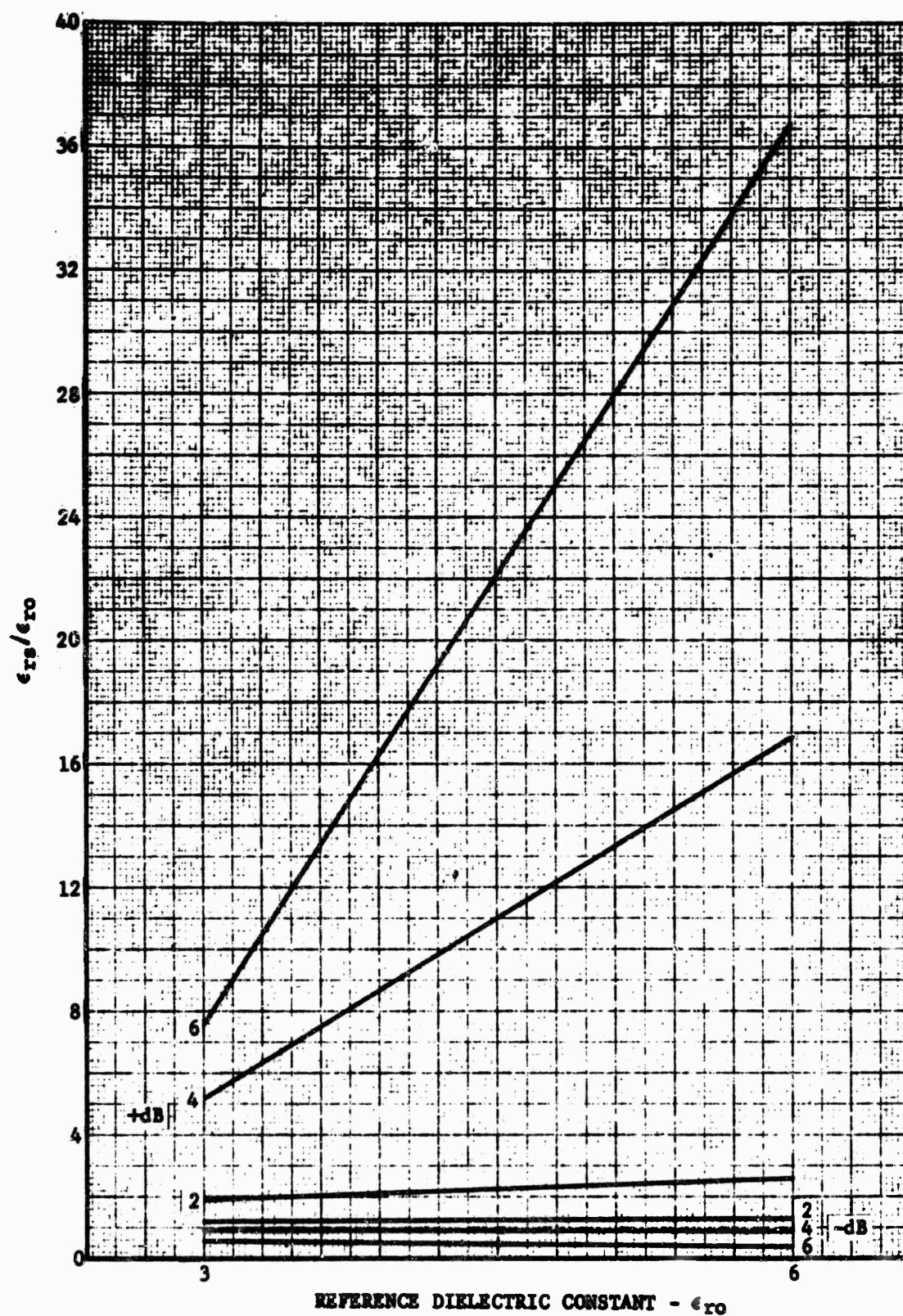


Fig. 1.1-58 DIELECTRIC SCALING COEFFICIENT ERROR

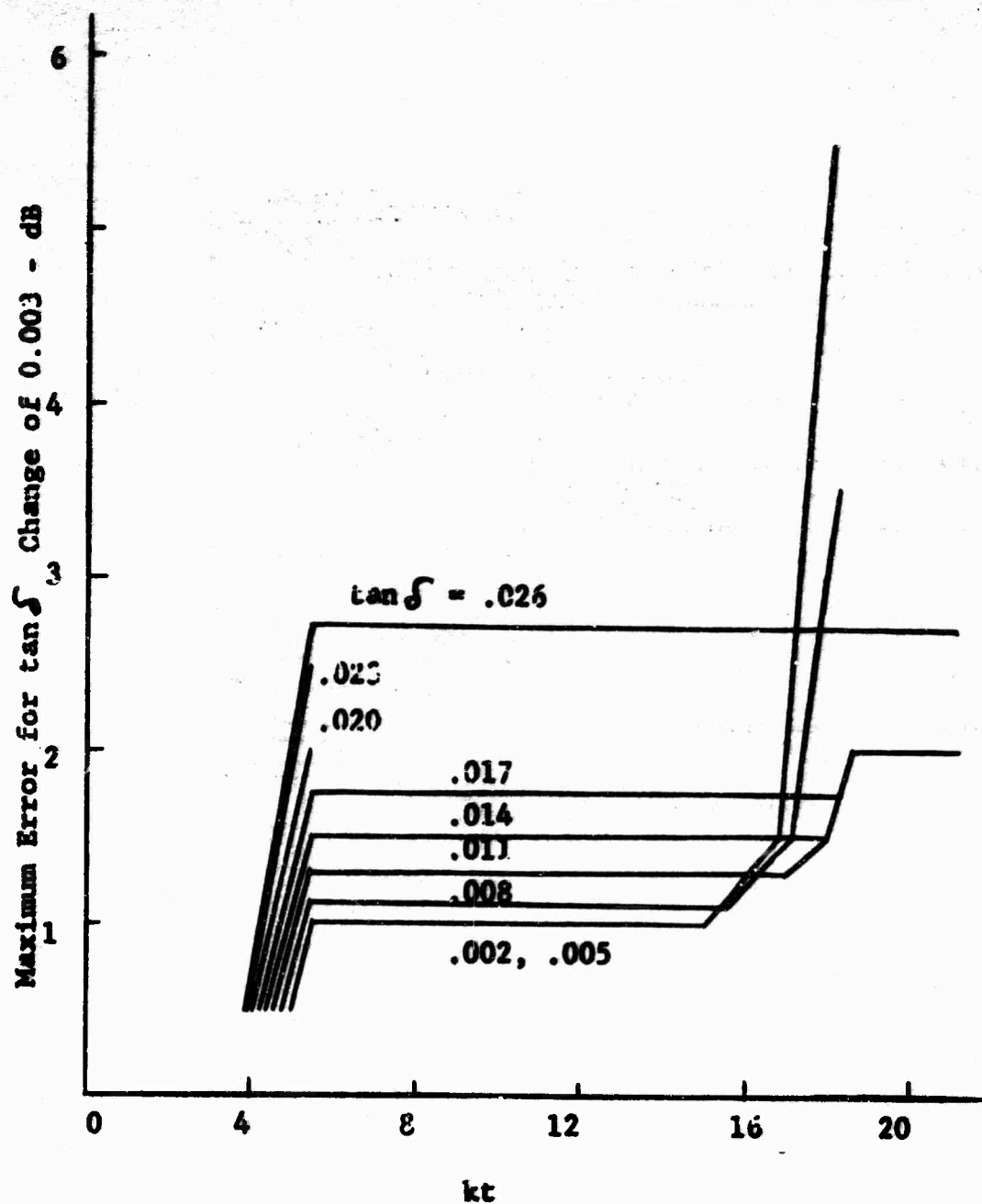


Fig. 1.1-59 EFFECT OF $\tan \delta$ ON DIELECTRIC SPHERE SCALING

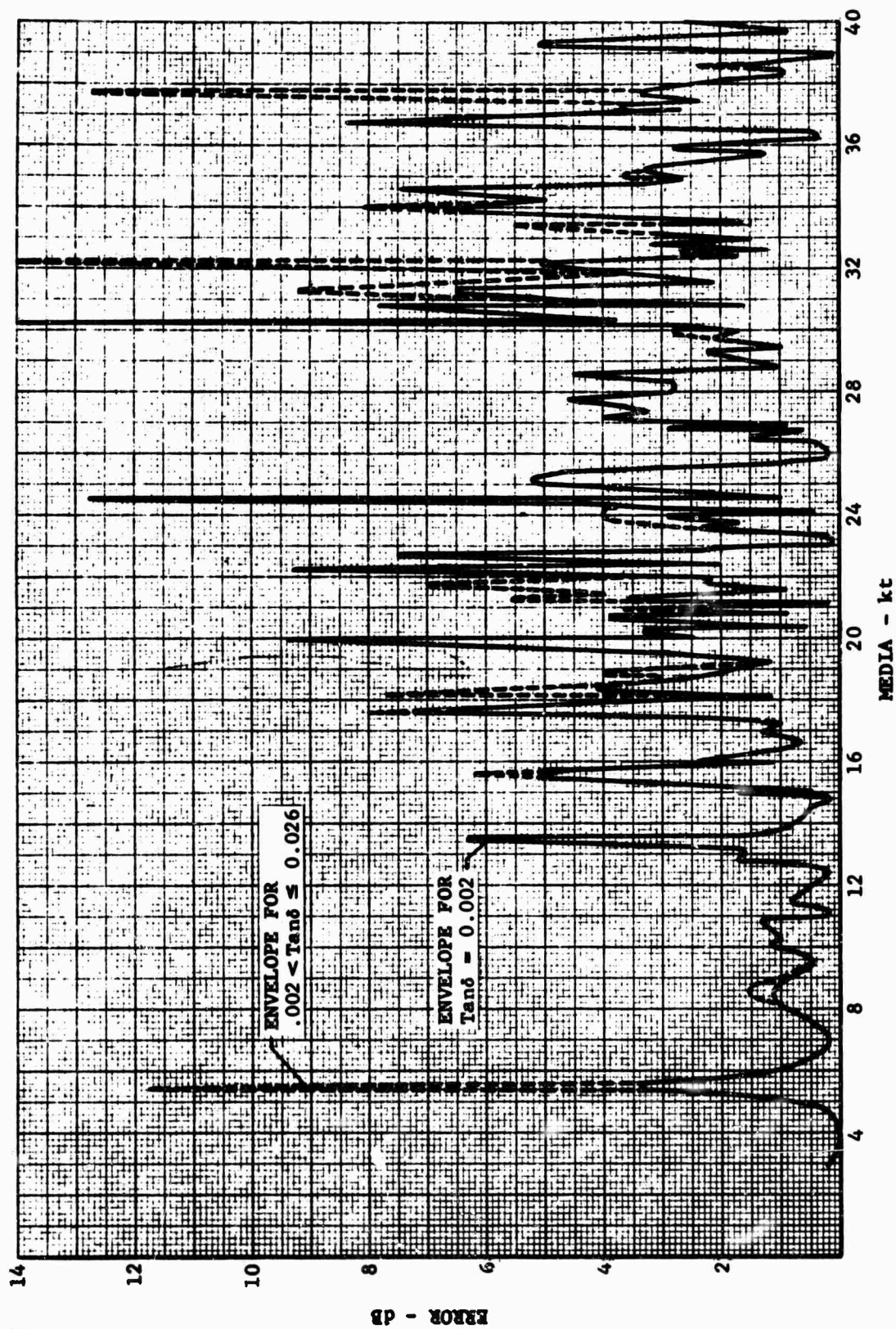


FIG. 1.1-60 EFFECT OF DIELECTRIC CONSTANT ON
DIELECTRIC SPHERE SCALING

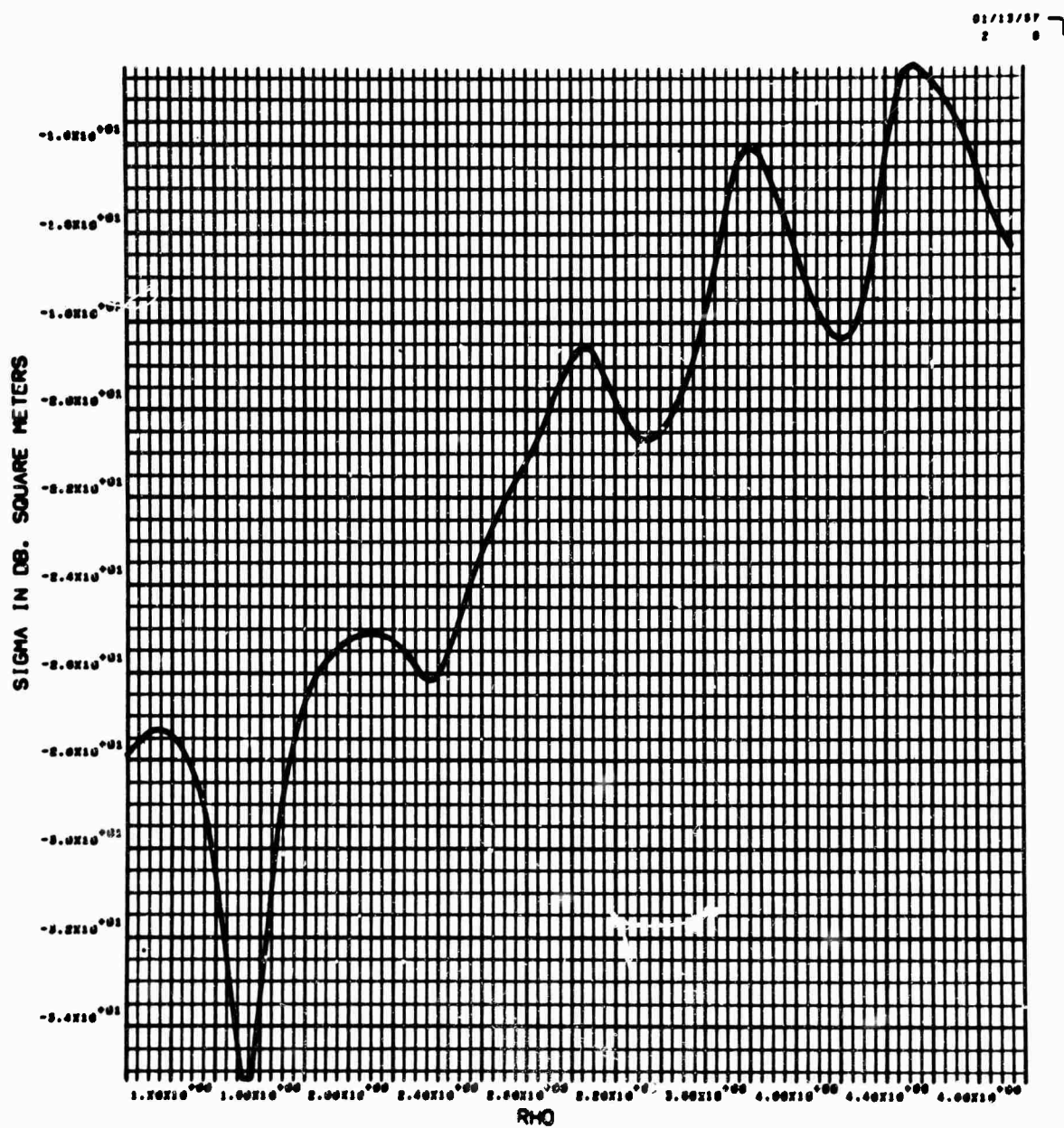


Fig. 1.1-61 DIELECTRIC SPHERE CROSS SECTION FOR
 $\tan \delta = .002$ (Small kt)

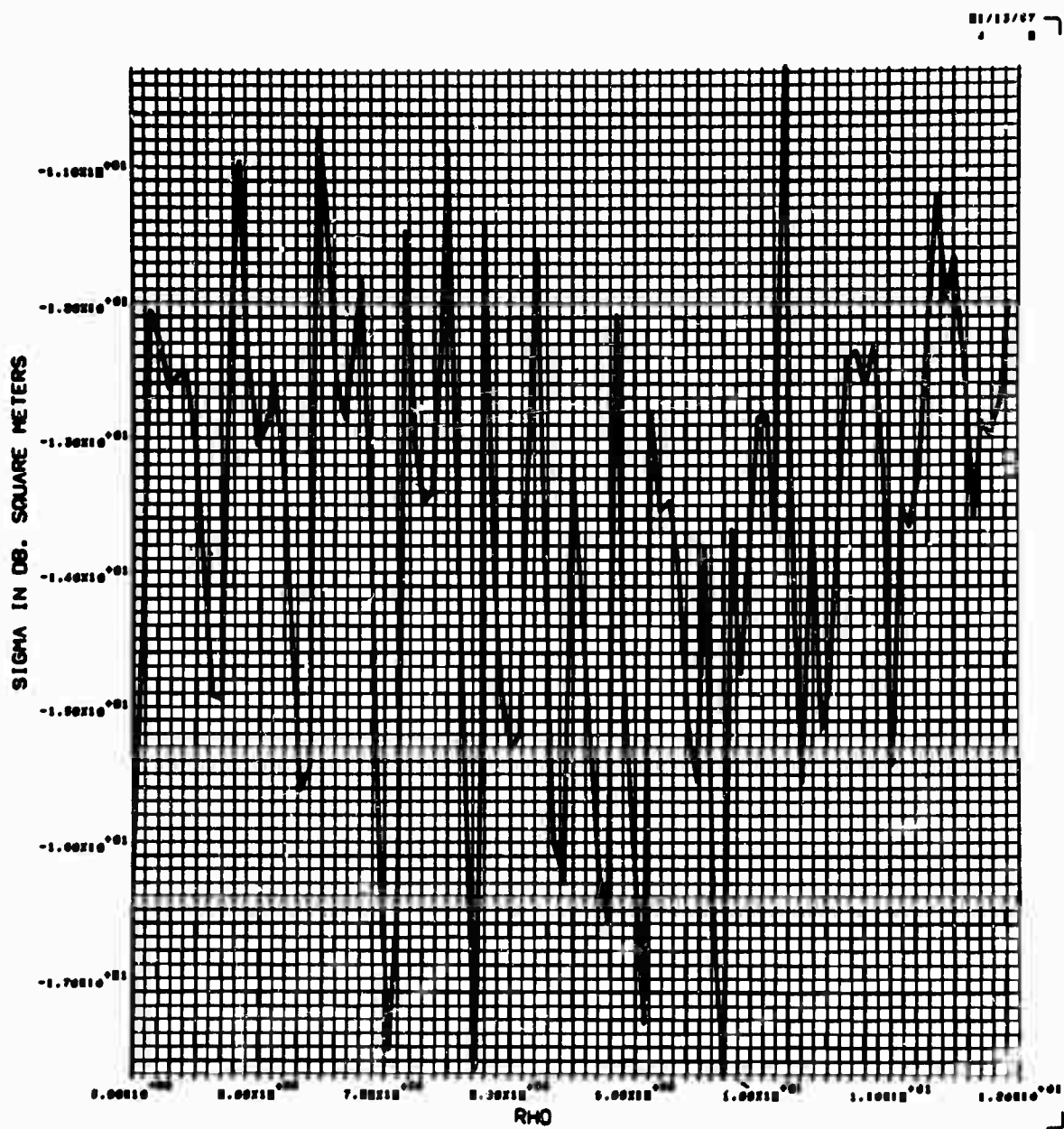


Fig. 1.1-62 DIELECTRIC SPHERE CROSS SECTION FOR
 $\tan \delta = .002$ (Large kt)

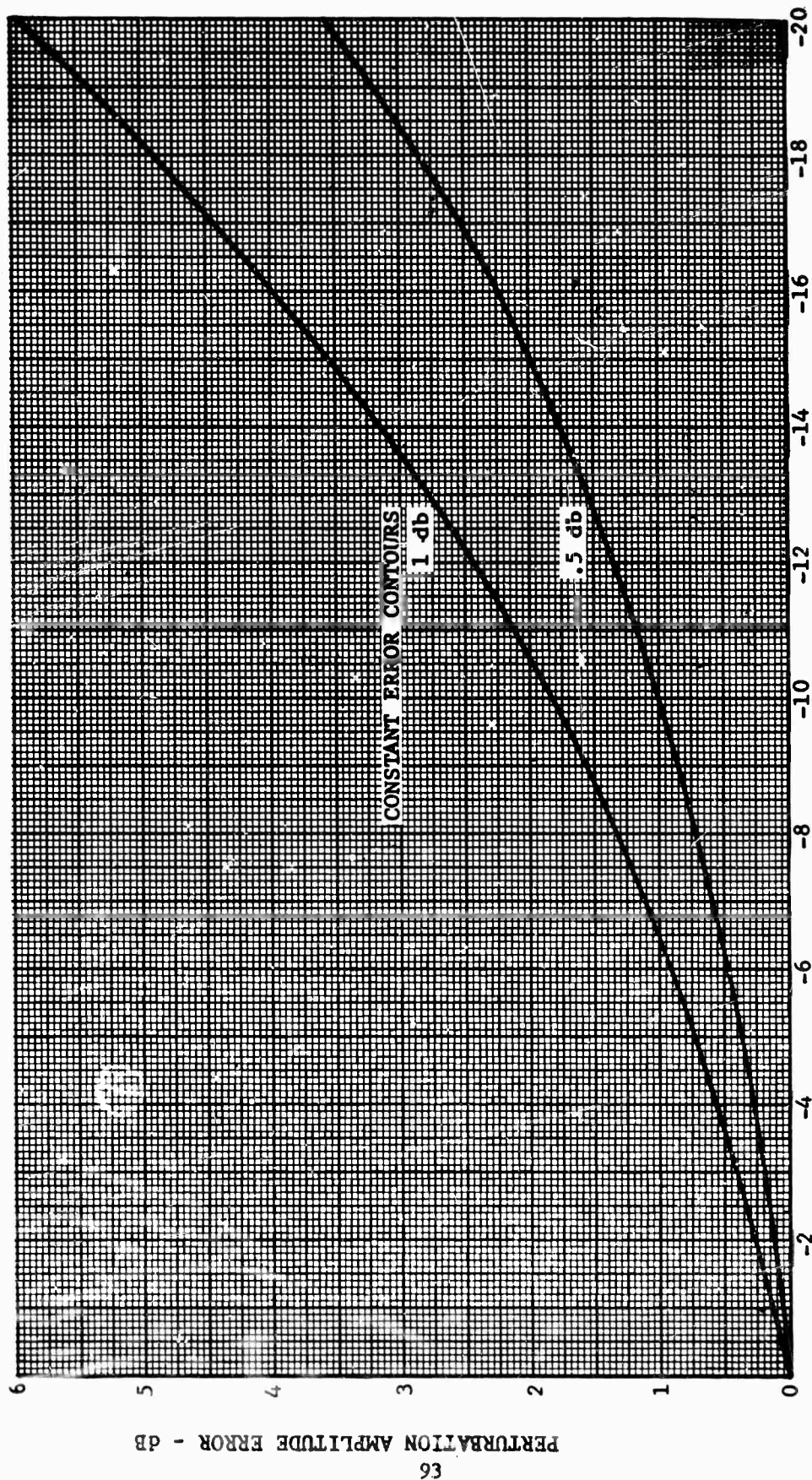


Fig. 1.1-63 PERTURBATION CROSS SECTION ERROR EFFECT

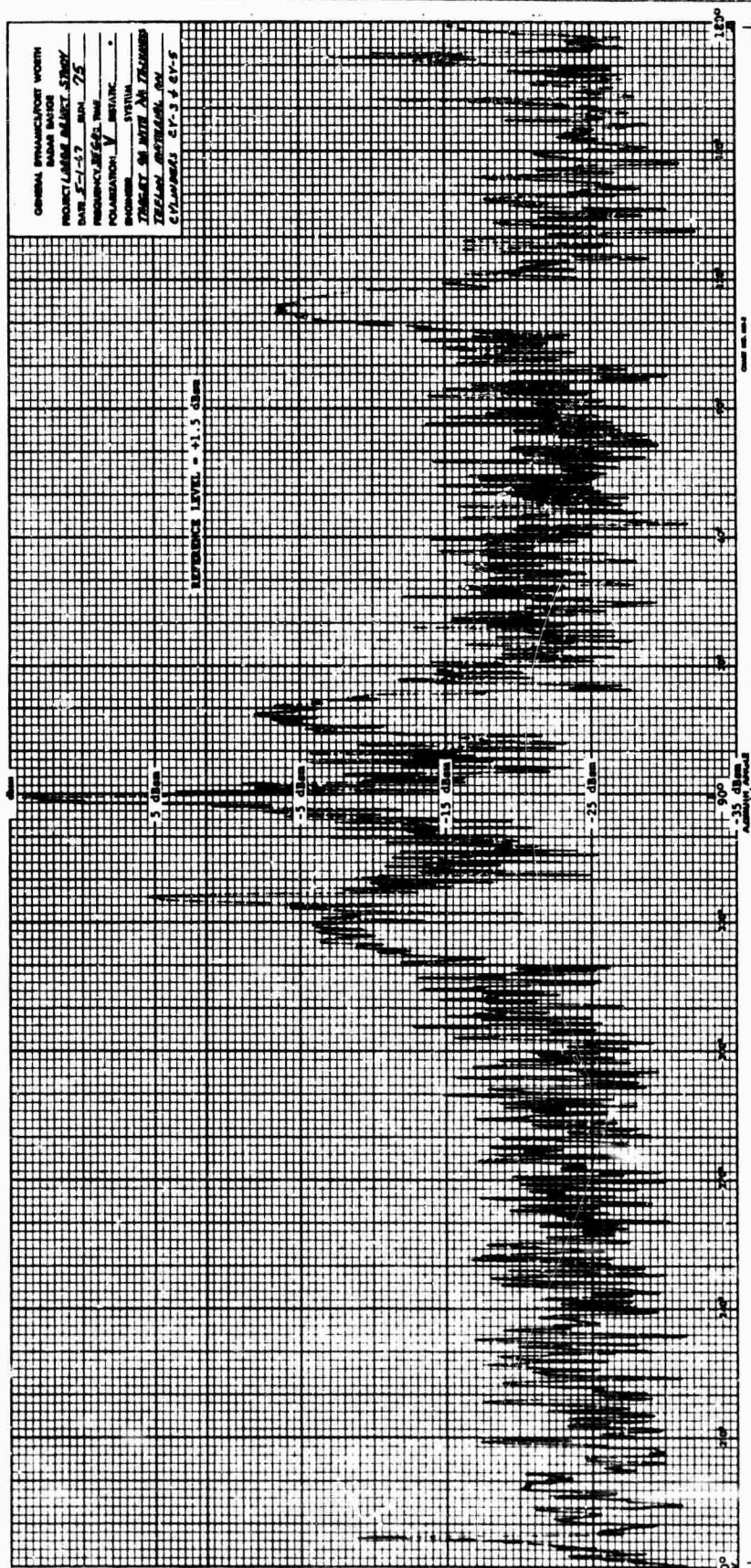


Fig. 1.1-64 DIELECTRIC COMPONENT TARGET DATA (1/4 THICKNESS TEFLON MATERIAL)

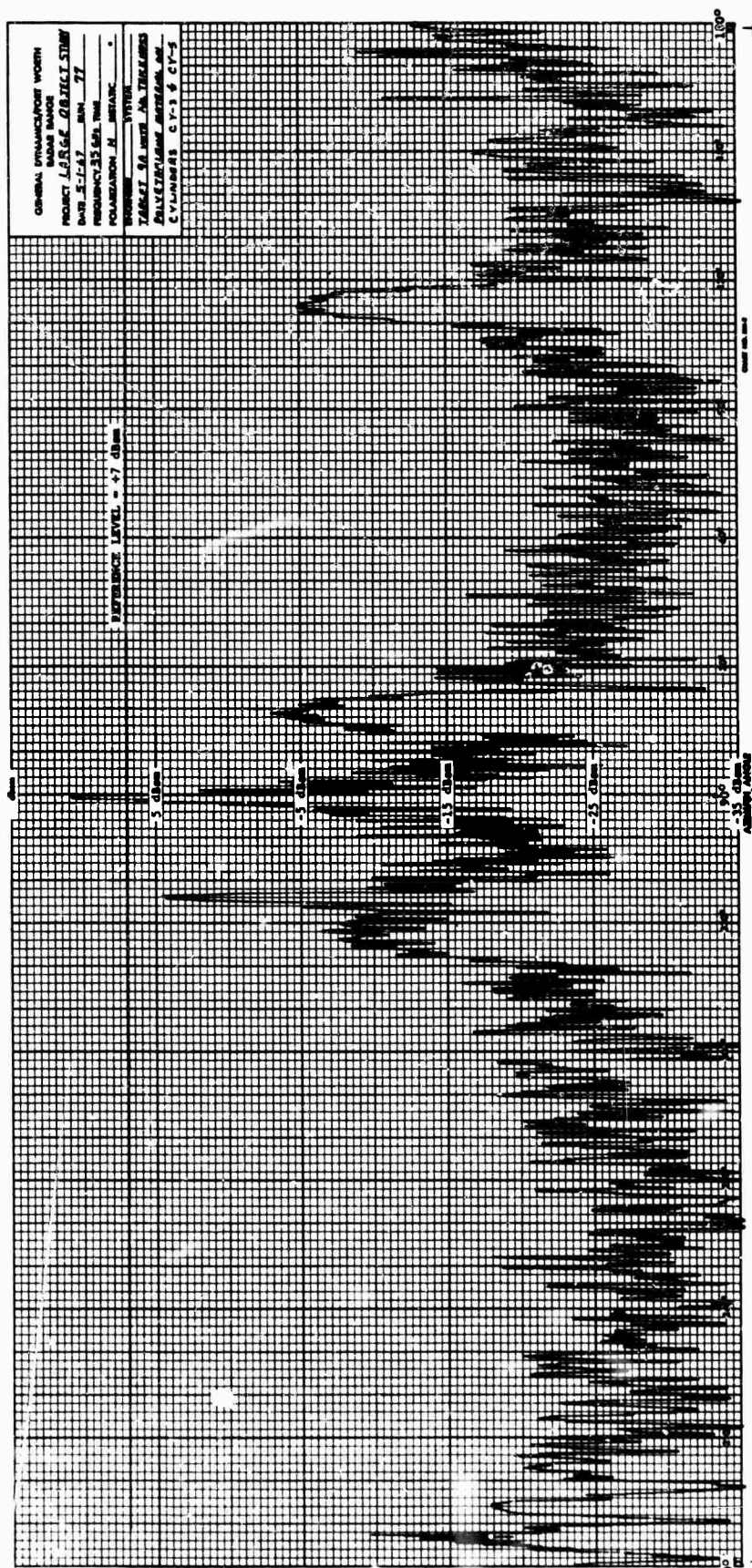


Fig. 1.1-65 DIELECTRIC COMPONENT TARGET DATA ($\lambda/4$ THICKNESS POLYETHYLENE MATERIAL)

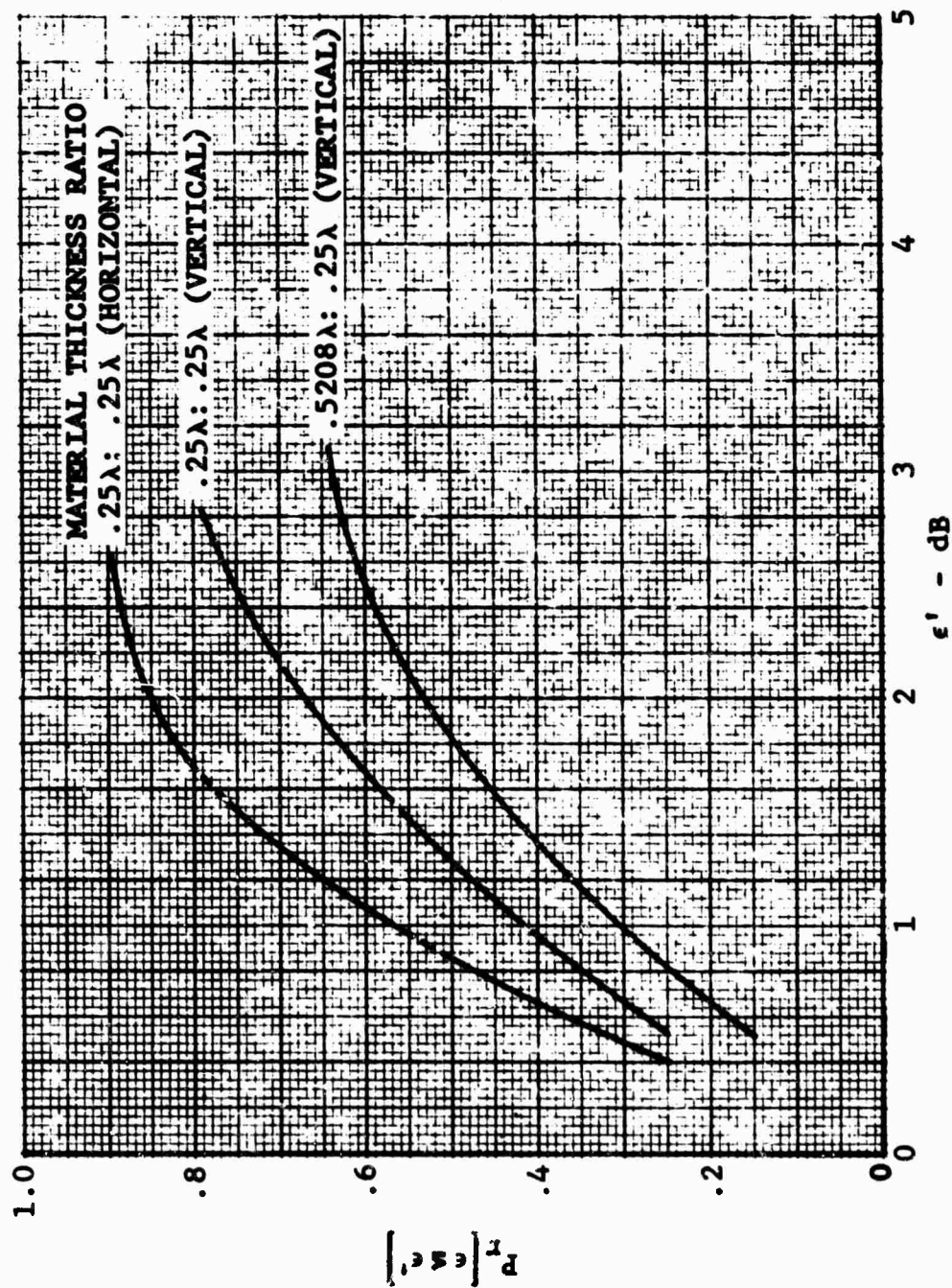


Fig. 1.1-66 CUMULATIVE DENSITY ON DIELECTRIC SCALING
ERROR (K_a -BAND, 35 GHz)

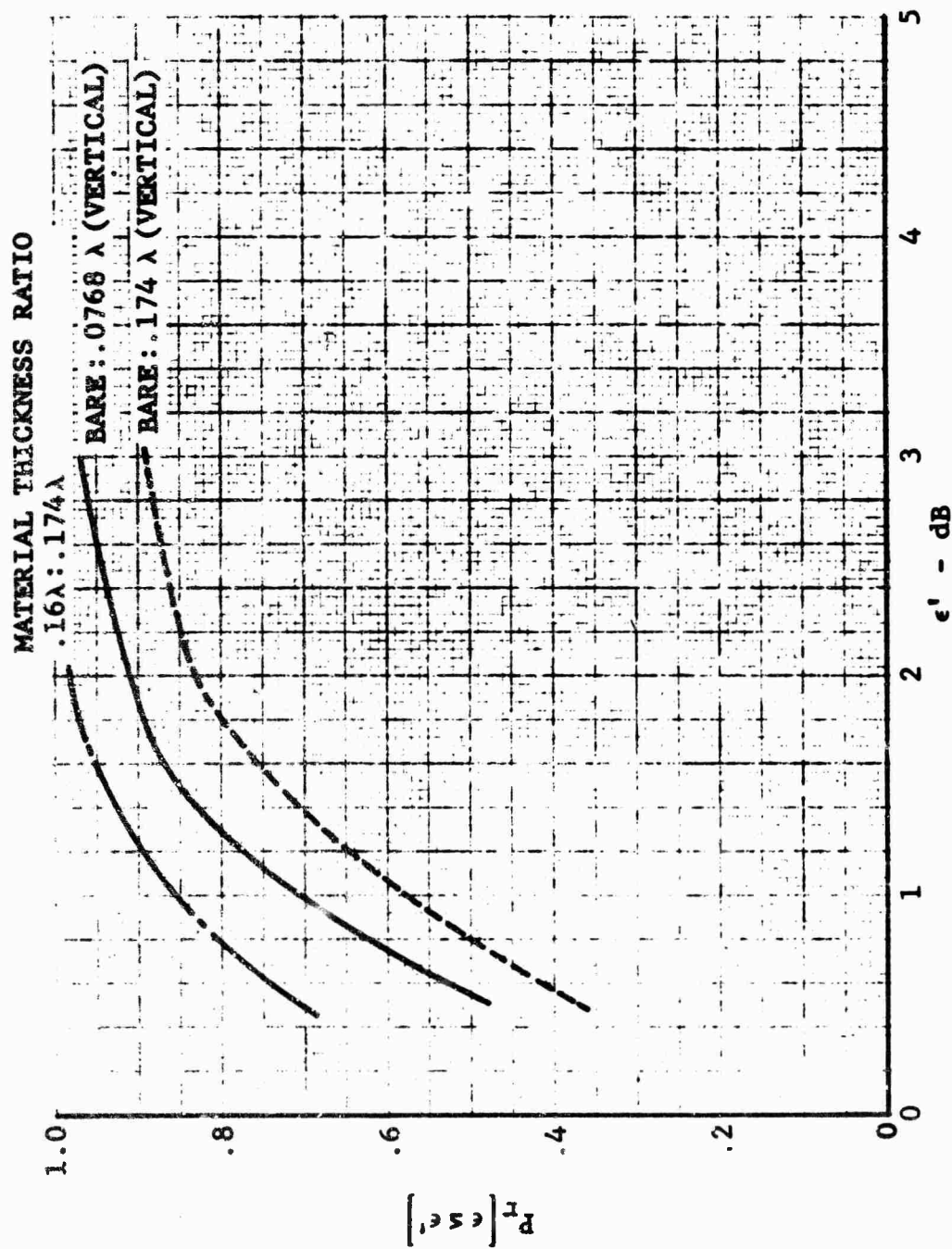


Fig. 1.1-67 CUMULATIVE DENSITY ON DIELECTRIC SCALING
ERROR (X-BAND, 10.75 GHz)

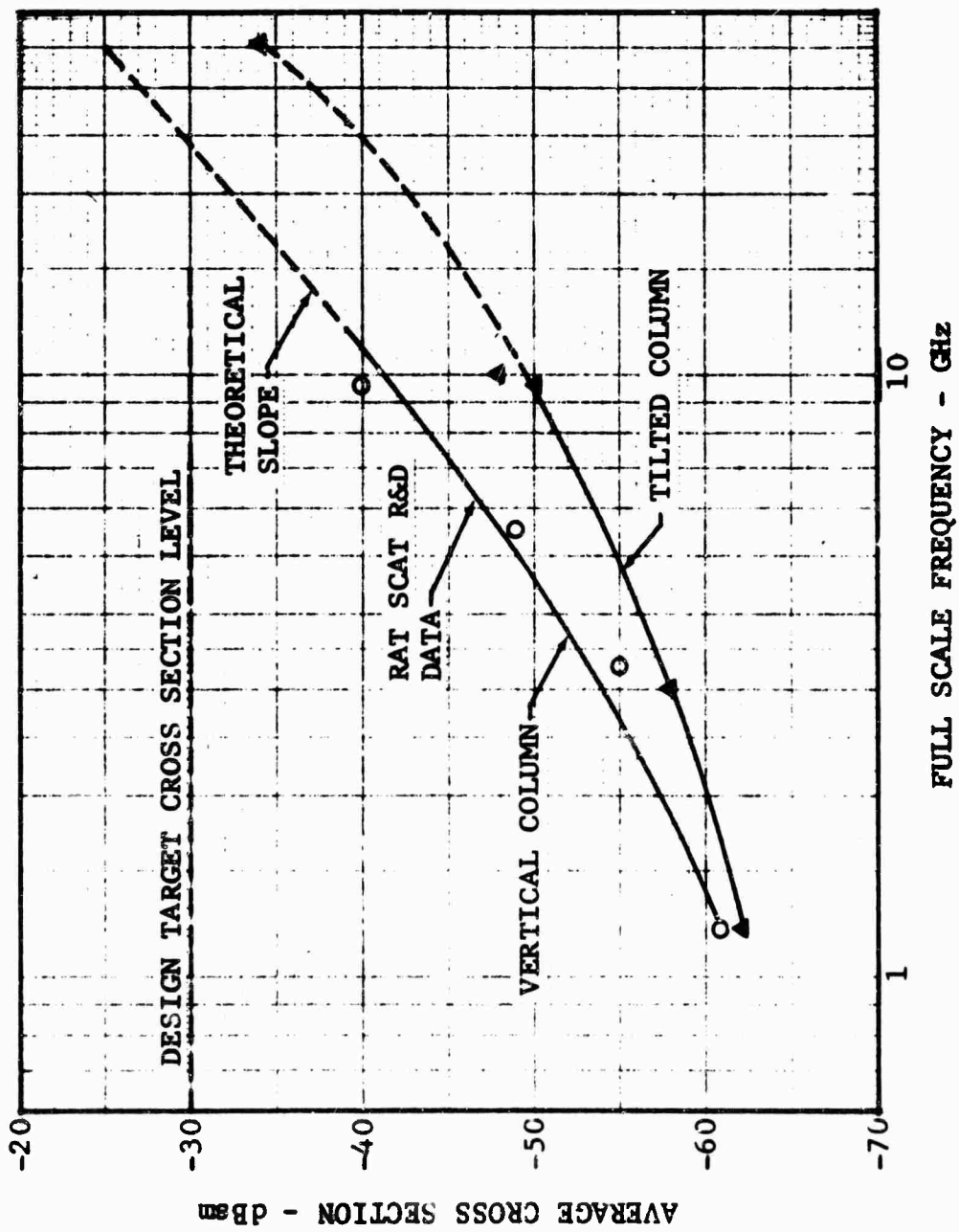
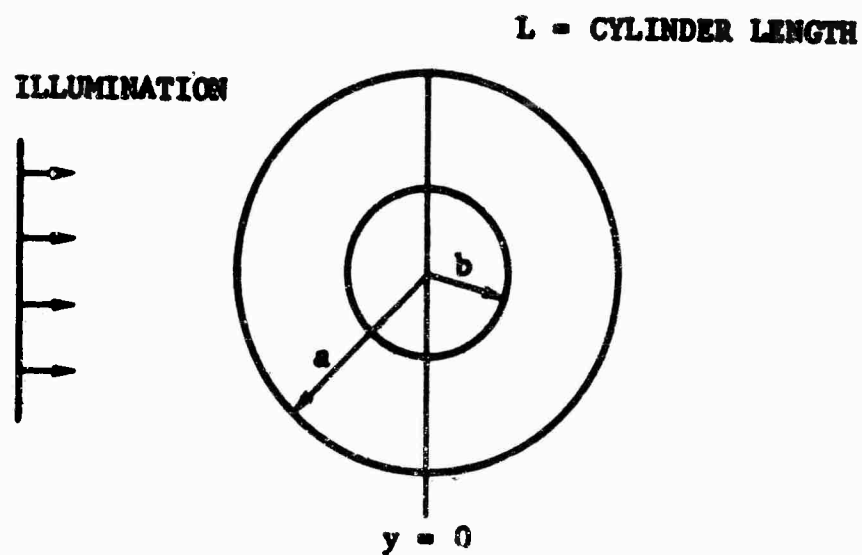


Fig. 1.1-68 FREQUENCY DEPENDENCE OF STYROFOAM COLUMN CROSS SECTION



**Fig. 1.1-69 HOLLOW TARGET SUPPORT
COLUMN GEOMETRY**

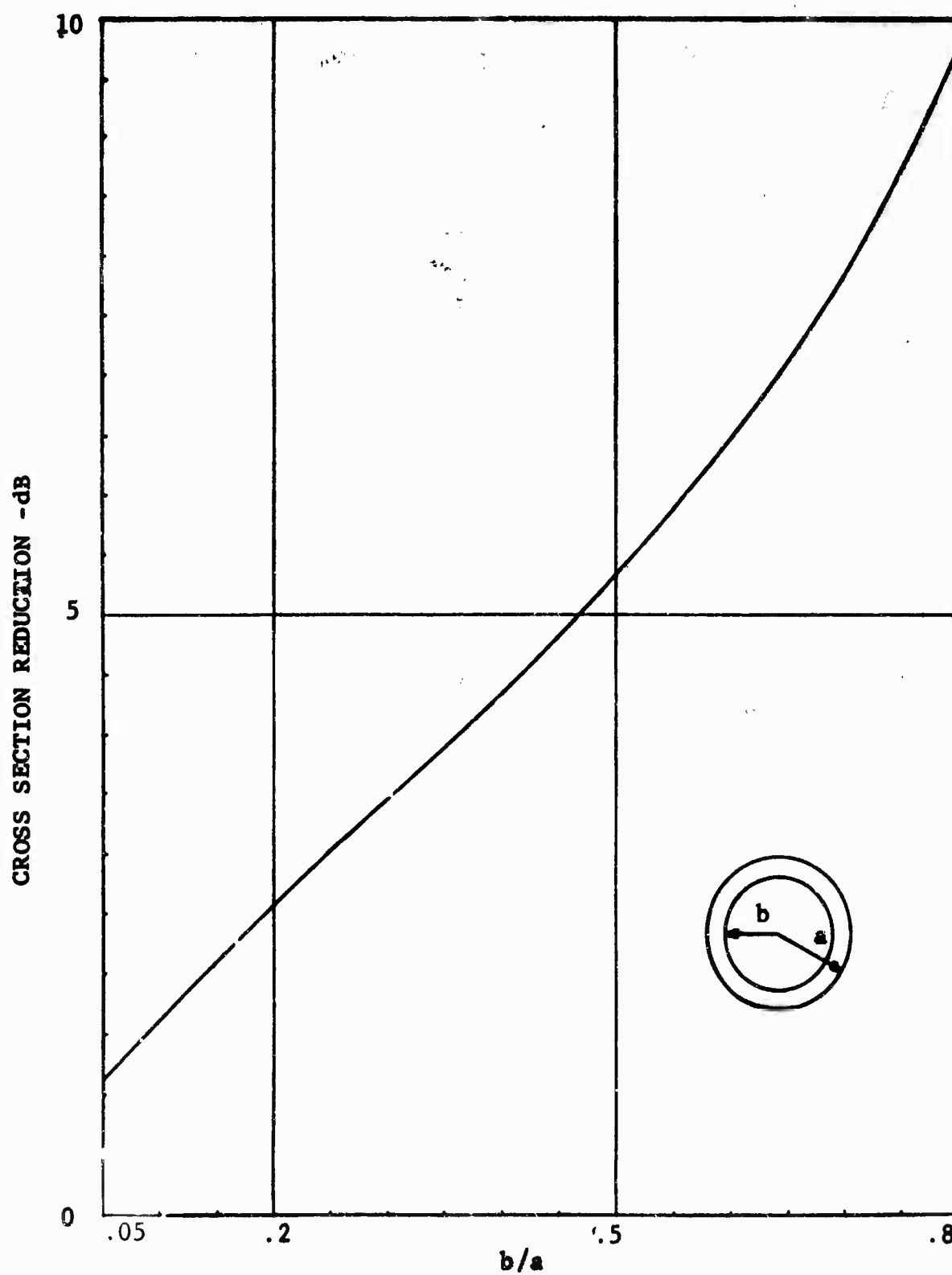


Fig. 1.1-70 HOLLOW STYROFOAM COLUMN CROSS SECTION REDUCTION

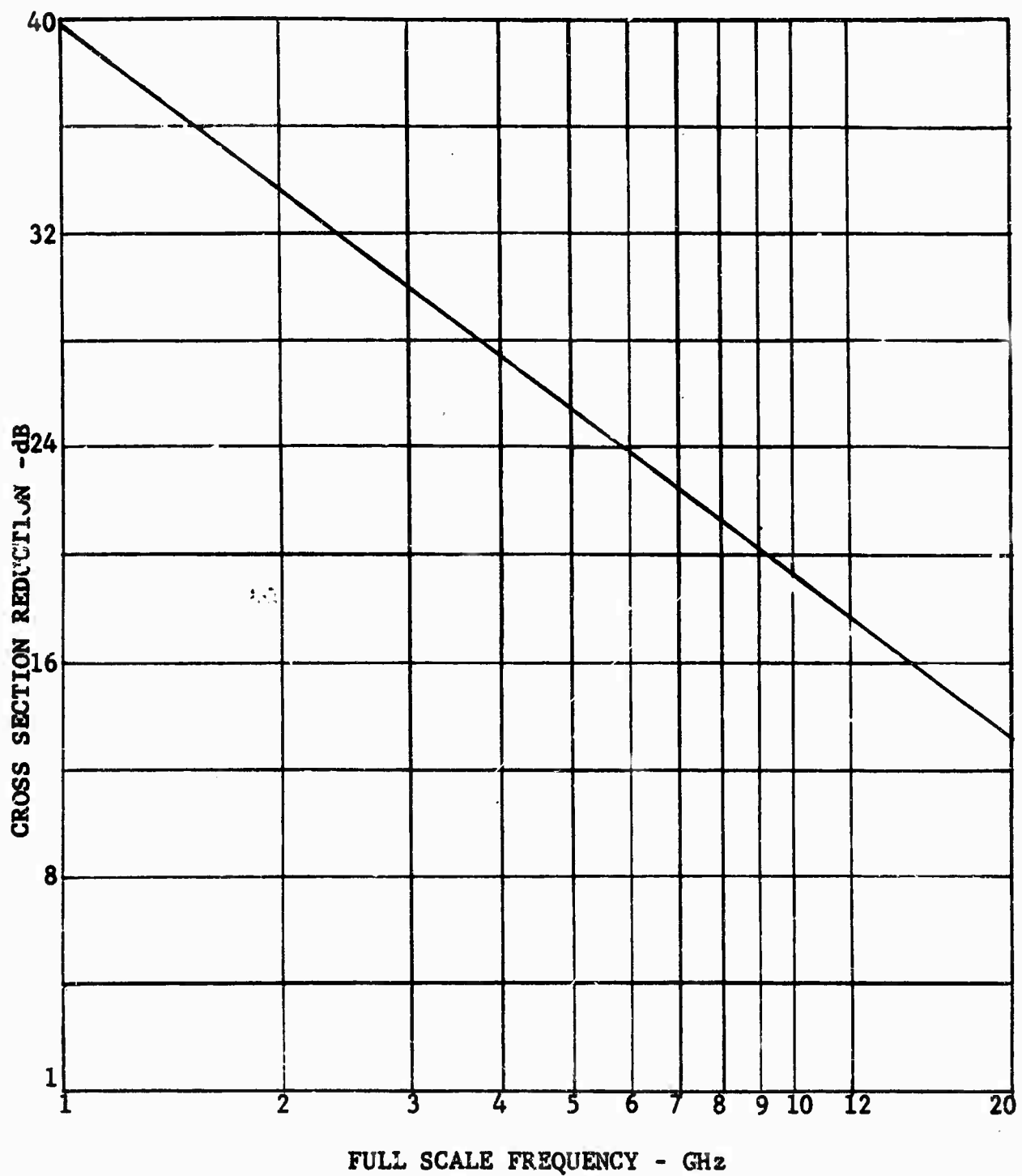


Fig. 1.1-71 COLUMN CROSS SECTION
REDUCTION REQUIREMENTS
FOR 35-GHz SCALING

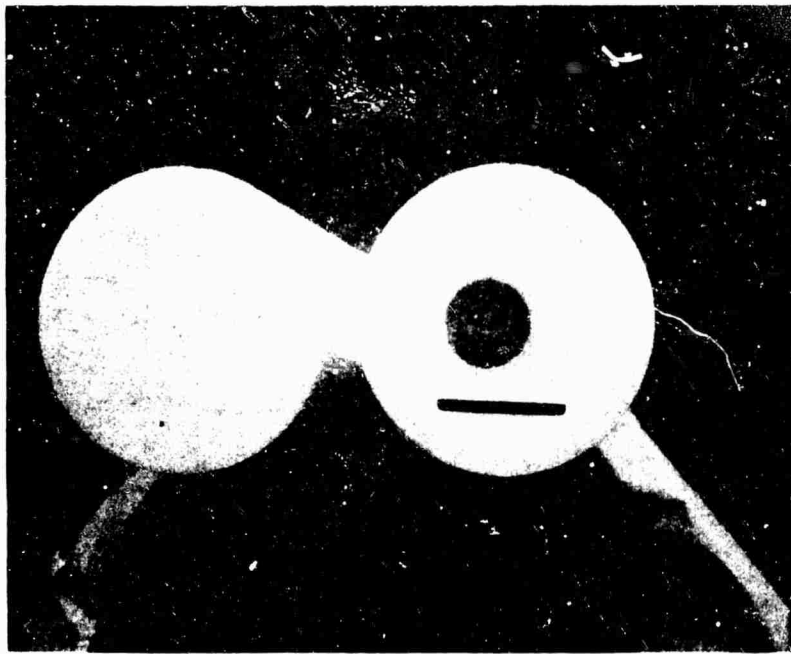
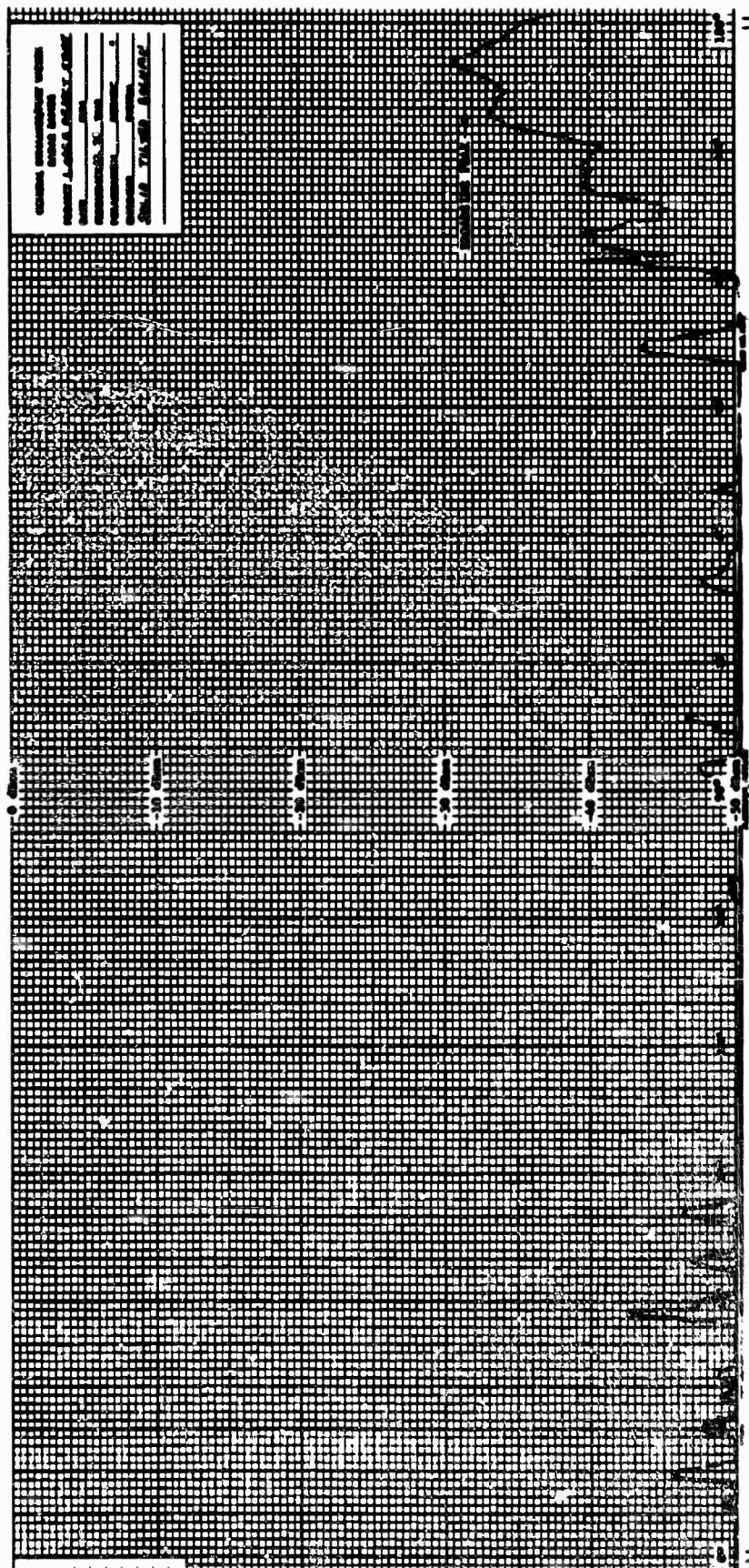


Fig. 1.1-72 TARGET SUPPORT COLUMNS



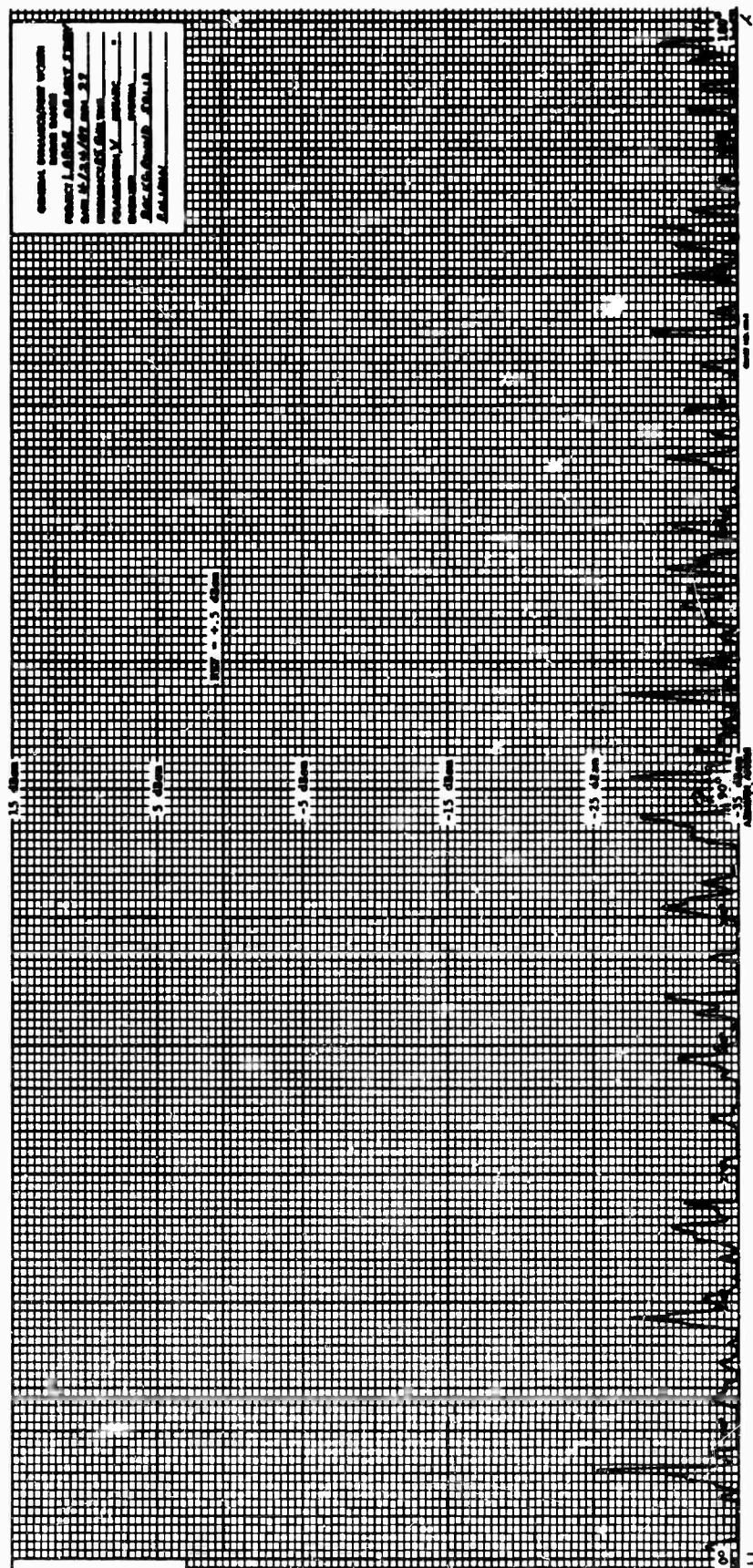


Fig. 1.1-74 TILTED STYROFOAM COLUMN DATA (Ka-BAND)

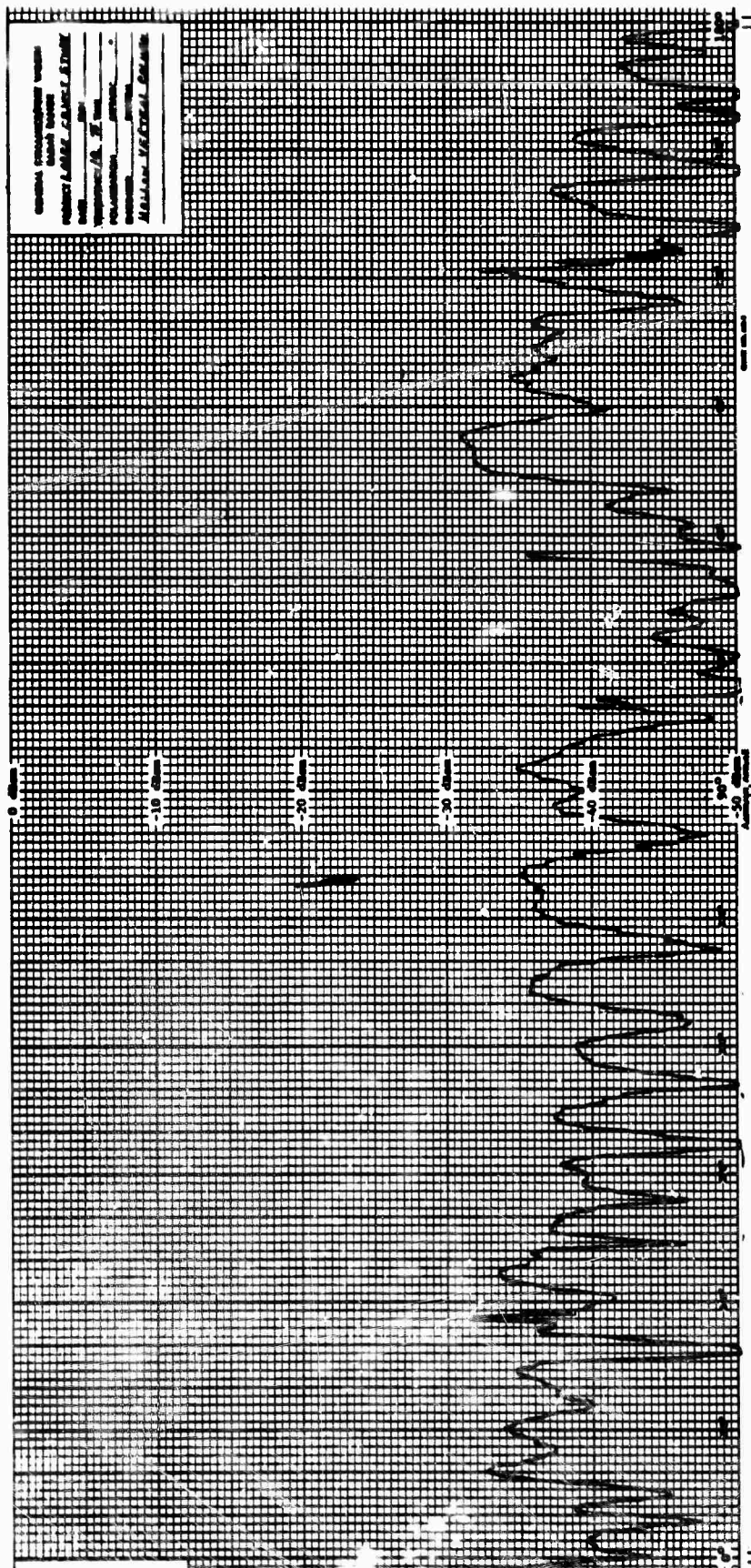


Fig. 1.1-75 VERTICAL, HOLLOW STYROFOAM COLUMN DATA (X-BAND)

1.2 Long Range and High Power

1.2.1 General

The long-range and high-power method of large object measurement is the most straightforward approach in that the procedures and all aspects of radar cross section measurement are identical to those presently used at RAT SCAT. The most significant deviations from the present RAT SCAT range geometry are the excessive range lengths required to meet the $2D^2/\lambda$ criterion (> 16 miles) and the antenna heights required under the normal ground plane range conditions. The latter geometry requirement is invariant to the measurement frequency under the condition of $R = 2D^2/\lambda$. Under these conditions and the case of a target length of 60 feet, the required product of antenna and target height is 1800 square feet. Thus, for a typical large target height of 12 feet, an antenna height of 150 feet is required ideally, however, lower antenna heights are practical. The large range lengths required for complete coverage of the target length-frequency spectrum of interest impose severe sensitivity requirements relative to the present RAT SCAT capability; a maximum of 37-dB improvement is required. Other significant features of the long-range and high-power method, which will be used extensively in the measurement of large objects, include the target design cross section level and the target support cross section levels. Details associated with this large object measurement method are treated in the following paragraphs.

1.2.2 Design Cross Section Level for Large Targets

The design cross section level is a necessary parameter in the specification of equipment sensitivity requirements. This parameter has been established at -30 dBsm on the basis of the theoretical and experimental data presented in Figure 1.2-1. These data points represent ± 5 -degree cross section averages. The minimum average shown is a level of -18 dBsm so that a negative excursion of 7 dB can be allowed before the system noise level begins to introduce an error in excess of 1 dB in the target data. An examination of the RAT SCAT and Fort Worth Division large target data indicates that the -30 dBsm level will be adequate 96 percent of the time over a typical 360-degree azimuth angle.

It is evident that the cross section values shown in the figure are essentially independent of frequency. The theoretical cross section data was obtained from the scaling study (target configurations used in the scaling study have been previously shown in Figure 1.1-2). The computations are plotted in Figures 1.2-2 through 1.2-10 to illustrate the nature of the large object cross section as a function of target type and the ka value. These data were obtained by averaging the cross section over at least 40 aspect angle values. The double value points represent values obtained in low cross section regions of target aspect angle (e.g., near-nose-on in the case of a cone cylinder) and maximum cross section regions.

Table 1.2-1 contains a list of characteristics of the targets examined. An analysis of these data suggests that there is no correlation between the target physical characteristics and the radar cross section maximum and minimum values. The data is ordered in terms of decreasing ka (where $k = 2\pi/\lambda$ and a is maximum target length).

1.2.3 Sensitivity Requirements

The sensitivity requirements for large object measurements are shown in Figures 1.2-11 and 2.3-4. These data are based on sensitivity measurements made at the RAT SCAT site (these data reflect the use of the largest antennas applicable to each frequency band). The data in Figure 1.2-11 are presented in terms of the sensitivity required and the present RAT SCAT capability as a function of target length and frequency. These data indicate that the improvement maximum required is 37 dB. An examination of the data in Figure 1.2-11 indicates that this level of improvement corresponds to a level 77 dBW in terms of the factor $PG^2/(B)(NF)$ where P is the transmitted power, G is the antenna gain, B is the receiver bandwidth, and NF is the receiver noise figure. This factor was selected because of the approach used in the improvement of equipment capability (refer to paragraph 1.2.6). In addition, these data illustrate the clear choice of using mobile range operation over fixed range operation.

Table 1.2-1 LARGE TARGET CROSS SECTION CHARACTERISTICS

Frequency (GHz)	kL	Axial Ratio	± 5° Average Cross Section (dBsm)				Weight (Pounds)
			Vertical Max	Polarization Min	Horizontal Max	Polarization Min	
11.5	3970	13.8	11.5	-3	13	-8.5	1500
11.5	2164	6.7	8	-11.5	7	-7	5800
9.6	1982	13.2	12	-11	13.5	-6.5	2500
9.13	1608	7.5	17	0	17	-9.5	800
10.125	1430	25					700
11.0	1313	3.8			18	-3	875
6.5	1212	6.7	7.5	-13	13	-8.5	5800
5.02	1042	13.2	11.5	-9.5	14.5	-8	2500
8.0	955	3.8			14	-2	875
* 9.6	724	4.8	-10.5	-30.5	-11	-28.5	1000
9.6	722	5.1	21.5	-6			2000
3.2	664	13.2	11.5	-5.5			2500
1.8	621	13.8	12.5	-13.5	16	-11.5	1500
5.6	422	5.1	19	-7			2000
* 5.5	415	4.8	-9	-26	-8	-28.5	1000
1.8	399	6.7	12	-14.5	14	-8	5800
2.5	393	25			15.5	-4.6	700
1.3	270	13.2	15.5	-4	16	-1	2500
* 3.02	228	4.8	+5	-18.5		-13	1000
3.0	226	5.1	27.5	-6.5	8.5		2000
* Low cross section design.							

The validity of extrapolating the short-range-length (2500-foot) RAT SCAT system gain data to the longer-range-lengths (30,000 feet or greater) required was obtained from an examination of long-range-length field-probe data measured at ranges of 10, 20, 30 and 40 thousand feet. The normal field probe contour was obtained; consequently, it may be safely assumed that the coherent reflection mechanism which provides the gain inherent in ground plane range utilization can be relied upon at the higher frequencies. In addition, verification of the proper system gain was made by comparing the peak amplitude of the field probe data from one range length to the next. An example of the data obtained at a frequency of 12 gigahertz and a range length of 20,000 and 30,000 feet is shown in Figure 1.2-12; in these measurements, data obtained using horizontal and vertical polarization were essentially the same. The contour of the terrain in the area used for obtaining field probe data is shown in Figure 1.2-13. This area was approximately about a straight line in the north west direction from the RAT SCAT operation building (see map subsequently presented in paragraph 3.3.2.). At each range length the correlation between the field probe data and theoretical results (including effects of earth curvature and refraction) is adequate to indicate that the desired field probe could be obtained through normal adjustment of the range geometry parameters. Adjustment of the peak amplitude height of the field probe data was limited by the present RAT SCAT antenna height limitation.

1.2.4 Antenna Height Effects

As previously indicated, the ideal antenna height in the case of a 60-foot target at a range of $2D^2/\lambda$ is given by $1800/h_t$ where h_t is the target height. The required antenna height would be about 150 feet, a dimension which is undesirable from the standpoint of operational problems and cost. In the case of a 12.5-foot target height and a 60-foot target in which the $2D^2/\lambda$ range criterion is satisfied, an antenna height of 140 feet is required if the center of the target is to coincide with the peak of the antenna beam. If the beam can be raised by decreasing the antenna height without significantly degrading the measurement accuracy, a substantial decrease in the cost and operational problems would result. During this program, the feasibility and practicality of making measurements at reduced antenna heights was investigated on the basis of theoretical and experimental data.

The theoretical investigation was that of computing the expected error which would be incurred if a horizontal cylinder were measured with the beam center at a height more than the ideal. In addition to the results obtained from this effort, results are also presented for the case of a vertical cylinder and a dumbbell type of target under these same conditions since measurement of these latter types of targets could possibly result in a requirement for a much more stringent height criterion. However, these latter targets are not considered to be representative of the type of scatterer to be encountered as the elliptic cylinder model, but since results obtained from the elliptic cylinder model indicated that very little error will be encountered if target heights even one half of the ideal are used, error data for the other types of models were also derived.

Figure 1.2-14 contains error data obtained by using the near-field error model developed for use in the analytical correction investigation (refer to Appendix B). Error data was computed for the case of a right circular cylinder and an elliptical cylinder whose major-to-minor axis ratio was 50 and vertical dimension was eight feet. Computations were made with the target at the center of the beam, and the model was then lowered to a position of one half the ideal height. On the basis of the error data shown, the error to be expected in this latter case (relative to the ideal) even for the relatively flat cylinder with 30 percent antenna reduction is less than 0.5 dB. That the error caused by vertical field curvature is relatively small for the size of the targets used in this study (up to eight feet in diameter) is not surprising when it is noted that the primary contribution comes from a small region about the specular point (first Fresnel zone). Since the calibration device in the model was also placed in this region and the field curvature over the first Fresnel zone is quite small, small errors are encountered even though the curvature over the total diameter is large.

In contrast to the model used to obtain the data in Figure 1.2-14, is the planar model or vertical cylinder model developed during the original RAT SCAT range evaluation and reported in Reference 3. The errors obtained by using that model can be found from the equation

$$E = 20 \log \left| \frac{1 - \frac{h}{\pi D} \left(\sin \pi \left[1 + \frac{D-2\alpha}{2h} \right] - \sin \pi \left[1 - \frac{D+2\alpha}{2h} \right] \right)}{\sin^2 \frac{\pi}{2} \left[1 - \frac{\alpha}{h} \right] \left(1 + \frac{2h}{D} \sin \frac{\pi D}{2h} \right)} \right| \quad (1.2-1)$$

where

h = ideal target center height

D = target vertical dimension

α = distance below ideal target height center.

In Figure 1.2-15, the error obtained by using the expression in Equation 1.2-1 is presented in graphic form for the case of a 4-, 6-, and 8-foot vertical target dimension as a function of percent of decrease in target height relative to the ideal. By comparing the data in Figures 1.2-14 and 1.2-15, it is evident that, when the vertical cylinder model is used, the errors to be expected because of antenna height reduction are initially of the same order as those found for the elliptical cylinder but they start to increase significantly as the antenna height is decreased more than 30 percent of the ideal. However, the reason for the small errors in the latter error model is quite different than that for the first. In the second type of model, the small errors are incurred because the effect of the field curvature at the lowest target position is such that the same order of magnitude of error is obtained as the error calculated for the center of the beam. In other words, although the error at the center of the beam pattern for the 8-foot target is approximately 2 dB, it likewise is approximately 2 dB when it is measured at one half of the ideal target height. Although this same situation was encountered in the case of the elliptical cylinder, the error at the center of the beam was also small because of the specular type of scattering discussed earlier.

A third type of model was used to investigate the effect of reduced antenna heights; this was a dumbbell type of target representative of targets for which a significant contribution to the signature is due to isolated scatterers separated in the vertical plane. The relative error expression (relative to the error in the center of the beam) for this type target is given in Equation 1.2-2 (the targets have been placed 90 degrees out of phase):

$$E = 10 \text{ Log } \left| \frac{\cos^4 \frac{\pi}{4h} (2\alpha + D) + \beta \cos^4 \frac{\pi}{4h} (2\alpha - D)}{\cos^4 \frac{\pi\alpha}{2h} \cos^4 \frac{\pi D}{4h} (1 + \beta)} \right| \quad (1.1-2)$$

where

D = vertical dimension between scattering centers

h = ideal target height

α = distance of target center below ideal height

β = ratio of cross section of scatterer above target center to that of scatterer below target center.

Figure 1.2-16 contains data which was obtained by using Equation 1.2-2, a target vertical dimension of 8 feet, and a column height of 10 feet. When the data shown in Figure 1.2-16 is compared with the 8-foot data in the other two near-field error-model figures, it is evident that this later model produces the severest degradation as the antenna height is lowered. However, even in this "worst-case" model, a decrease in antenna height of 20 percent results in degradation in measurement accuracy of less than 1 dB. In view of the fact that the target center is 14 feet for the case of the target used to compute the data shown, then an antenna height of no more than 100 feet rather than 130 feet would be required on a theoretical basis even for the worst-case target of 60 feet in length. Also, if the target center was placed at 12.5 feet rather than 10 feet, an antenna height of 87 feet could be used rather than 140 feet.

On the basis of the theoretical results, a reduction in antenna height to a maximum of 100 feet will allow large objects of interest to be measured with acceptable degradation in the data. This observation was not totally supported by the experimental results.

A series of tests was used to provide data for validation of the theoretical results obtained on the effects of introducing a field gradient across the target, in the vertical

plane, as a result of reducing the antenna heights. The specified tests were designed to obtain data on a reduction of antenna heights in excess of 30 percent over a wide range of target configurations. The targets consist of a right circular cylinder, 49 inches in length, and the two basic target configurations previously illustrated in Figure 1.1-41. Since the data were obtained on scaled targets, the gradient across the target was simulated. The conditions defined for these tests included a vertical plane gradient of 0, 3, 4.5, and 6 μf to approximate the conditions corresponding to the gradient resulting from antenna height reductions of 0, 20, 30, and 40 percent in the case of a full-scale target 8 feet in extent in the vertical plane. Error data was obtained by a direct comparison of the data obtained at a given field gradient and that obtained at essentially no field gradient. A total of 18 experiments were conducted.

The approximate field gradients were established by operating the system at large antenna heights. Under these circumstances, the field gradient across the calibration target (commonly a 6- to 24-inch diameter sphere) was excessive relative to that which will be encountered in normal, full-scale operation. This condition introduced a calibration problem which will not be significant in the full-scale case in normal operation, because the target and calibration sphere position became critical in the process of attempting to serially reproduce the position of several targets. Because of the effects described above, the data reduction process was conducted by use of a "best fit" process, i.e., in comparing data runs at different heights, a bias was imposed to minimize the extraordinary calibration error effects. The results of this process are presented in Figures 1.2-17 through 20. The three target configurations were (1) right circular cylinder, (2) target 2A with Fin P-1, and (3) target 9A with Fin P-3 and P-4; the target configuration dimensions are shown in Figure 1.1-41. In each case, the cumulative error was obtained by comparing the data from measurements at position 0 (no field gradient) with the results obtained at the lower antenna heights. The data in Figure 1.2-17 is a summary of the 1 σ (standard deviation) points from Figure 1.2-18 through 1.2-20. Typical experimental scattering diagram data are illustrated in Figures 1.2-21 and 22. A listing of the calibration bias imposed on each of the data runs is presented in Table 1.2-2.

Table 1.2-2 CALIBRATION DATA ADJUSTMENTS

Target	Percent Antenna Height Reduction		
	20%	30%	40%
	Position 2	Position 3	Position 4
Cylinder	-1.8 dB	-3, -3.5 dB	1.5, -3 dB
Target 2A	0, 1.5 dB	-1, 1.5 dB	-1, -1 dB
Target 9A	1, 6.5 dB	-.5, 0 dB	0, 2.75 dB

An examination of the data results indicates that the cylinder measurements closely approximate the theoretical results when considered on the basis of the calibration problem discussed above. However, the results obtained by using the complex target, indicate that the error levels to be expected are significantly higher. This observation appears realistic in that a significant scatterer (e.g. a fin) at the extreme of the target radius will not be properly illuminated because of the field gradients. On the basis of these results and the fact that no severe differential in cost is introduced by the selection of a 150 foot relative to 100 foot tower, the implementation of a 150 foot tower seems appropriate.

1.2.5 Target Support Requirements

The problem of target support requirements is common to all of the measurement methods under consideration although it becomes severer as the frequency is increased, i.e., there is a severe limitation in the scaling method (refer to paragraph 1.1.6). The present capability in this area at RAT SCAT is illustrated in Figure 1.2-23. These data represent the cross section level of polyfoam tripods with a weight-bearing capacity of 5,000 pounds. Previous studies (References 2 and 4) have shown that the use of polyfoam in target support systems is optimum for targets of any significant size. In addition, the aspect of controlling target orientation involves, at the least, the use of a semirigid support configuration (refer to paragraph 1.2.6.4).

The commonly accepted criterion for an acceptable level of support cross section is 20 dB below the target cross section level of interest. This criterion is based on a maximum error level of 1 dB introduced by the coherent scatter from the support system. On this basis, the data illustrated in Figure 1.2-23 indicate that the cross section level to be expected is not adequate for large object measurements over the full dynamic range expected because a support cross section level of -50 dBsm is required to accommodate a -30 dBsm target level.

In many cases, a combination of approaches must be used to obtain a satisfactory margin between the target and the support system levels. The effort required is dependent on the level of error as a function of the radar cross section level of the target, which is acceptable to the individual customer.

The first means of reducing the support system cross section is that of minimizing target weight. This process may be extended to defining a measurement program requirement that certain classes of targets be received on site as shells of the target configuration with hard points specified for mounting purposes. If this approach is used, the volume of polyfoam required to support the target can be reduced; consequently, the amount of support material in the radar beam is also reduced. Thus, a reduction in weight should be possible to the point of limiting the target support configuration to two tripod configurations. In the worst case, measurement at 12 gigahertz, the maximum improvement required is about 26 dB.

One means of further increasing the target-to-support system cross section margin is to insure that the fabrication of the support system is carefully accomplished and that the vertical plane field pattern is optimized. Careful fabrication of the support system includes minimizing the volume of material through accurate structural design and minimizing joints and other potential discontinuities. The vertical plane field probe can be used to reduce the effective radar cross section of the support system. The most significant aspect of this feature is that of insuring a good null in the vertical plane pattern near the ground. The combination of these two features, used to advantage, may be expected to reduce the cross section on the order of 10 dB. An approach investigated for use at VHF (Reference 5) is a real-time vector-subtraction process. The range geometry associated with the implementation of the technique is shown in Figure 1.2-24, and the implementation block diagram is shown in Figure 1.2-25. Measurements obtained by using this technique involve the provision

of 3 antennas, one slave antenna (receiver only) and the normal receiving and transmitting antenna arrangement. As illustrated in Figure 1.2-24, the slave antenna is placed at approximately twice the normal antenna height so that the signal appearing at the aperture is only a weak function of the signal scattered by the target. Under the assumption of adequate stability, the phase and amplitude of the slave antenna signal can be adjusted to minimize the sum of the two received signals (see Figure 1.2-25). The signal scattered by the target will unbalance the signal at the output of the summing network and therefore provide a measure of the radar cross section of the target only. It will be noted that use of this particular approach obviates the severe requirement for frequency stability common to many cancellation techniques.

In addition to the data available at VHF, preliminary tests were conducted at C- and X-band to obtain a measure of the effectiveness of using this approach at the higher frequencies. The results, as expected, indicate that the equipment setup problems were severe at the higher frequencies. Because of the inadequacy of the equipment setup (the antenna in particular), the two radar antennas do not "see" the same target. This problem is severer at high frequencies because of the more pronounced angular aspect sensitivity of the target support system.

The test results indicate that a background signal reduction in excesses of 8, and 4 dB can be expected at C-, and X-Band, respectively, using a pulse length of 0.2 microseconds. Since the primary interest in this program is the high frequency region, the test results do not appear to warrant any further consideration relative to support system reduction.

Another form of vector subtraction has been successfully demonstrated at RAT SCAT in Band 4 (1 to 2 gigahertz). This process involves a two-step process similar to the noise subtraction process previously discussed except that both signals are coherent and phase measurements, as well as amplitude measurements must be used (Reference 6). The required process is defined by use of the equation

$$\sigma_t = \left(\sqrt{\sigma_{t+c}} e^{i\phi_{t+c}} - \sqrt{\sigma_c} e^{i\phi_c} \right)^2 \quad (1.2-3)$$

where σ represent radar cross section, ϕ represents phase, and the t and c subscripts denote target and column, respectively. The use of this process involves the implementation of a phase

measurement capability. The only other significant item of required equipment is a relatively simple computer; the RAT SCAT equipment complement includes a PB-250 which is adequate for this purpose when a 0.1-degree azimuth increment is used. As presently implemented, the system operation includes serial measurement of a complete set of data over 360 degrees of azimuth angle with and without the target emplaced on the support system. A digital paper tape and analog output are available (essentially in real time) during the second data run.

The results obtained by using this system indicated a capability to achieve a 20-dB improvement in the signal-to-coherent noise ratio. It appears that a 15-dB improvement can be realized in X-band if the target can be mounted with proportionate rigidity and other stability aspects of phase measurement, such as frequency stability, can be maintained. The use of fiberglass target supports is recommended. On the basis of the above discussion, it appears that the target support system requirements can be provided a high percentage of the time to the degree required by the customer.

1.2.6 Equipment Requirements

The basic equipment components required in the long-range and high-power method are discussed below in terms of requirements and cost. Each of the items are of general interest but some do not influence the trade-off study and are therefore, not treated in detail. Area cost data on non-sensitive equipment items shown in Table 1.2-3 are discussed in the appropriate paragraphs below.

Table 1.2-3 RANGE CAPABILITY IMPROVEMENT COSTS

<u>Item</u>	<u>Order of Cost (1000 Dollars)</u>
Mobile Van Modification	5
100-Foot Antenna Tower - Fixed	14
150-Foot Antenna Tower - Fixed	15
100-Foot Antenna Tower - Mobile	55
150-Foot Antenna Tower - Mobile	60
8000-pound Rotator	62
50,000-Pound Rotator	300
Rotator Power Source	20
Phase Measurement Capability	
Band 5	21
Band 6 & 7	41

1.2.6.1 Sensitivity Improvements. The means of providing the maximum improvement in required sensitivity involves costly equipment items and therefore must be given detailed consideration. The approach taken in defining requirements for improved sensitivity was to define (1) the $PG^2/(B)(NF)$ factor required as a function of frequency, (2) the specific equipment improvements and the associated level of improvement, and (3) the cost, beginning with the low-cost approach; the improvement factor of $PG^2/(B)(NF)$, when P is the transmitted power, G is the antenna gain, B is the noise band width and NF is the system noise figure, was selected in order to provide convenient means of accounting for each of the significant means of sensitivity improvement. The specific approaches used in this analysis were:

1. Provision of narrow-band IF strip and use of a long-pulse length
2. Noise figure improvement
3. Provision for subtraction of incoherent noise
4. Provision of a capability for coherent integration
5. Provision of high-gain antennas
6. Provision of high-power transmitter tubes.

The improvement made possible by each of these items is summarized in Table 1.2-4. The improvement realizable from item 1 above is 9 dB, and dependent on frequency, a noise figure of 3 to 4 dB is readily available. The bandwidth reduction approach offers the most significant sensitivity improvement on a cost effectiveness basis since the cost is nominal and a single IF amplifier unit is applicable to all bands. Items 1 and 2 represent the low cost sensitivity improvement components. The more extensive additions and modifications for sensitivity improvement are discussed in the following paragraphs.

Table 1.2-4 EQUIPMENT SENSITIVITY IMPROVEMENT

Freq. (GHz)	Total Improvement Required (dB)	Low Cost Improvements			Antenna Gain (dB)		Noise Subtraction Gain Required	Power Req. with 48-dB Ant. Gain (kW)
		1-MHz BW (dB)	Coher. Intg. (dB)	NF (dB)	Present	Req.		
4	7	9	8					
5	21	9	8	3	38	38.5	1	
6	24	9	8	3	41	43	4	
7	27	9	8	3	41	44.5	7	
8	30	9	8	4	42	46.5	9	
9	32	9	8	4	40	45.5	11	
10	34	9	8	4	42	48.5**	13	1.3
11	35	9	8	4	42	49**	14	1.6
12	37	9	8	4	43	51**	16	4

*Based on utilization of largest applicable dish

**48.0 dB Limit Assumed

Provision of a means of incoherent noise subtraction is expected to produce a gain in excess of 10 dB in system sensitivity. This observation is based on the results of the experimental program conducted during this study and the study reported in Reference 7. This process is based on the relationship

$$\sigma_t = \sigma_{t+n} - \sigma_n \quad (1.2-4)$$

where σ denotes radar cross section in square meters and the t and n subscripts denote target and noise, respectively. This process can be simply implemented by recording the target-plus-noise signal and the noise signal and subsequently performing the operation defined in Equation 1.2-5. Data on this process is shown in Figures 1.2-26 and 1.2-27. The computed target cross section data are also shown in these figures. Although the low-level signals are not accurately recovered because of the variance associated with the noise, the improvement realized in the peaks is apparent, and the results indicate an effective signal-to-noise improvement of 8 dB. The accuracy of this simplified approach is severely limited by the fact that the time interval between the two sets of measured data is long with respect to the long-term noise periodicity. This source of inaccuracy can be greatly reduced through the use of the analog subsystem illustrated in Figure 1.2-28. Except for the logarithmic response, this system can be designed to operate in a manner identical to the Sigma Servo presently used at RAT SCAT. In operation, the gating circuits to the Sigma Servo will be identical to those presently used, but the Noise Subtraction Servo will be gated in the proper time relationship to the system noise level. The noise subtraction servo tracks the system noise level (smoothed over several pulses) and automatically corrects the Sigma Servo input to subtract the noise level.

Provision of coherent integration will produce a limited improvement because of the advanced characteristics of the RAT SCAT Sigma Servo which exhibits the properties of a nearly perfect post-detection integrator. Under these circumstances, a gain of $n^{0.8}$ (where n is the number of pulses integrated) can be realized over a wide range of conditions (Reference 8); however, because of the potential instability of the system in operation near the noise level, the normal set of results in a 5 to 10 dB deviation from incoherent integration optimum. This deviation is unnecessary if care is exercised in performing the adjustment. The theoretical maximum for the case of coherent integration is a gain of n. Thus the theoretical improvement in the RAT SCAT system sensitivity by use of coherent integration is given by $G_1 = 2 \log n$, dB

On the basis of the time element involved in the measurement of large targets, n has been selected to be about 50. When this value is used, G becomes 3.4 dB. However, consideration of normal degradation in the adjustment of the radar system and the results of tests conducted at the Fort Worth Division have resulted in the selection of the 8 dB improvement value and implementation of this integration technique is dependent on implementation of the basic phase measurement capability used at RAT SCAT in Band 4.

The improvement in antenna gain is based on the provision of antennas with a maximum practical gain of 48 dB and the maximum gain presently available at RAT SCAT.

Data on the required improvement is listed in Table 1.2-4 in a form convenient for use in the trade-off study subsequently discussed in subsection 2.5. It is based on measurement of a -30 dB_{SN}, 60-foot target. The listing includes the total improvement required, and the required antenna gain, power increase and noise subtraction improvements are specified in separate columns on the basis of the availability of the 1-megahertz bandwidth, coherent integration, and noise figure improvement.

Cost data associated with each of the improvement items are shown in the Table 1.2-5. An examination of these data indicates that the cost of improvement in sensitivity increases rapidly after a gain of about 12 dB. This gain will allow extension of the present RAT SCAT capability to the measurement of 60-foot targets in Band 5 (4 gigahertz) and 30-foot targets in Band 7 (12 gigahertz).

1.2.6.2 Antenna Configuration. On the basis of the trade-off results presented in subsection 2.4, the system sensitivity and other aspects associated with the present RAT SCAT dishes and feeds are adequate for use in large-object measurements. The analysis presented in paragraph 1.2.4 resulted in the conclusion that a 120-foot antenna target height would be adequate for the large object program. The requirement for a mobile operation capability imposes a requirement for a mobile antenna configuration. The height of the antenna towers obviously influences such cost and operational features as setup time and environmental problems.

Additional flexibility in RAT SCAT operation will be afforded by the provision of a fixed antenna tower at the present RAT SCAT operations building. This tower can be provided at a low cost, as shown in Table 1.2-3. The antenna tower configuration under consideration will be capable of supporting 16-foot dishes in a 50-knot wind. In addition, provision will be made for remotely adjusting the dish tilt angles.

Table 1.2-5 LONG RANGE AND HIGH POWER SENSITIVITY COST DATA

IF Strips (1-MHz Bandwidth, Usable for all Bands):

First Unit	\$ 1,500.
Spare	1,000.

Coherent Integration* (New AGC and Error Detector Drawer plus Phase Console Modifications):

\$ 6,000.

Noise Figure Improvement:

Low Noise Tubes, Band 5	\$ 3,500.
Band 6	3,500.
Band 7	3,500.
Packaging	2,000.

Noise Subtraction Servo Subsystem:

15,000.

High-Power TWT Transmitters:

5- to 20-kW TWT, Upper X-band	\$100,000.
Lower X-band	100,000.
10-to15-kW TWT, Upper C-band	100,000.
5- to 10-kW TWT, Lower C-band	100,000.
TWT Power Supply	30,000.
2- to 5-kW TWT, Upper X-band	20,000.
TWT Power Supply	15,000.

Antennas:

16-foot parabolas, 6 feeds, and development - Set of 2	\$ 60,000.
--	------------

*See Table 1.2-3 for costs of the required phase measurement capability.

1.2.6.3 Target Rotator Configuration. Although the selection of the target rotator configuration does not influence the trade-off study, a set of preliminary specifications has been defined in order to obtain area cost data. The most significant feature of the rotator is that of weight-bearing capability. On the basis of extrapolating the target weight data previously presented in Table 1.2-1, a 50,000-pound capability is required. Preliminary specifications are subsequently shown in Table 2.4-1; the area cost is \$300,000. It should be noted that a significant reduction in cost can be realized if a capability for tilting the target is not included. The rotator power source must necessarily be a remote unit in order to avoid the high costs of prime power lines over the long ranges required. However, control and signal lines must be provided from the rotator to the mobile van and the operations building.

1.2.6.4 Data Recording Subsystem. The data processing and recording system used for radar cross section measurements should be designed on the basis of target size or the ratio of target size to measurement frequency wavelength, D/λ in order to preserve the information content in the data to be gathered since the sample rate is dependent on the fineness of the lobe structure. This ratio is invariant in the several approaches considered in this study. Therefore the data recording investigation may be considered to be independent of the solutions of the near-field problem.

The minimum backscattered lobe width to be expected from a target may be approximated by

$$L.W. = \frac{\lambda}{2D}$$

where λ is the wavelength and D is the maximum dimension of the target. A 60-foot target measured at 12 gigahertz, which is the most severe case, exhibits a lobe width of approximately 0.04 degree. Consequently, there is an immediate problem in obtaining analog recordings at RAT SCAT at normal chart speed since the ink width on the recording is approximately 0.3 degree wide. Although the recorders are capable of advancing at a stepped-up rate of 6 to 1, which provides an ink width of approximately 0.05 degree, the present analog recorders are marginal in the worst case.

However, the basic problems are system response and digital recording. The response of the mechanical portions of the Sigma Servo used in the RAT SCAT system is approximately 150 dB per second. If the lobe width of the data to be recorded is 0.04 degree and its lobe amplitude, peak to null, is 20 dB (the amplitude would be greater than this if the full null depth were to be preserved),

the target must be rotated at a rate of one revolution per hour or slower. This rate of rotation allows the system to follow a target-return variation rate of 1,000 dB per degree which appears realistic for the case of 60-foot targets at X-band. The present RAT SCAT rotator minimum rotation rate is 12 to 15 minutes per revolution.

In sampling theory, it is stated that a sampling rate of 2 samples per cycle is necessary (not necessarily sufficient) to preserve data content. However, a sampling rate of 4 to 10 samples per cycle would actually be required to reconstruct a realistic analog of the cross section. Therefore, if the lobe width of a 60-foot target at X-band is 0.04 degree, a sampling interval for digital recording of 0.01 to 0.004 is required but an interval of 0.02 degree is more realistic. The minimum recording interval of the present RAT SCAT system is 0.1 degree.

The necessary digital sampling intervals and time per measurement are shown in Figure 1.2-29 as a function of target size and frequency for the most severe cases. As can be seen, the measurement time and sample rate are directly proportional to target size; therefore, by extrapolation of the present RAT SCAT capability for handling 12-foot targets to 60-foot targets, a rotation speed of one hour per revolution and a sampling interval of 0.02 are obtained to compare with the realistic values above.

In view of the extreme requirements imposed by the worst case examples cited above, it appears necessary to temper the selection of a data rate criterion by imposing a number of practical considerations of (1) the probability of encountering the worst case situation and (2) the actual utility of the fine-grain information content in the data associated with the worst case situation in terms of a simple extension of the present RAT SCAT capability.

Item 1 above can be examined in terms of the operational data subsequently presented in subsection 2.2. For example, the conditional probability of encountering a 30-foot or longer target, at 12 gigahertz and a requirement for a 6-gigahertz or greater measurement on a 60-foot target is 0.43 and 0.25, respectively. Both of these conditions impose a requirement for an angular sampling rate of 0.02 degree on the basis of the previous discussion. In addition, an examination of typical target scattering diagrams will reveal that, except for small amplitude variations superimposed on the coarse grain structure, the lobe width characteristics will seldom be significantly characterized by a worst-case lobe-width pattern. In addition, the target stability criterion imposed (e.g.,

apparent lack of constant rotation speed, which includes target motion on a semiflexible support) must be quite stringent to completely justify specification of a sampling rate of 0.02 degree. Thus it appears that a sampling interval of 0.02 degree will provide an adequate resolution for all frequency and target conditions except a configuration which closely resembles a 60-foot cylinder near broadside.

The problem of rotation speeds of the target is separable from the angular sampling rate problem if the recording system capability or response is adequate for handling the data rates under consideration. The RAT SCAT paper tape punch presently used for digital records and the mechanical sigma servo and a recorder presently used for analog records are not adequate. However, a prototype of an electronic sigma servo with a capability of 10,000 dB per second has been delivered to RAT SCAT. This unit and one of several off-the-shelf commercial recorders will provide more than adequate analog-recording capability. The digital subsystem presently under consideration for use at RAT SCAT will be adequate for this application (Subsection 3.2). The usable data rate in this system is in excess of 30 samples per second which can be interpreted to allow a target rotation period of less than 10 minutes at a sampling interval of 0.02 degree of azimuth angle. Consideration of the influence of target rotation speed on system sensitivity, in terms of the influence on the number of pulses integrated, will reveal that the effect is insignificant if the radar pulse repetition frequency is high (near 5,000 pulses per second). Although the \$250 cost per range hour may influence the target rotation rate, this time element is relatively insignificant when it is considered in terms of the overall cost involved in a typical measurement program, as illustrated by the operational models discussed in subsection 2.2.

1.2.7 Conclusions

The conclusions reached in the investigation of the long-range and high-power method, as a potentially cost effective means of large object radar cross section measurement, are delineated in the following paragraphs in terms of the factors of (1) adaptability to field operation, (2) accuracy, and (3) cost. Study results indicate that this measurement approach is a clear choice for the lower frequency measurements. As a result, a number of equipment features, such as rotator requirements and minimum range lengths, are necessary equipment items and do not influence the trade-off results. The trade-off results indicate that this method is most

cost effective except in the target length region between 30 and 60 feet in Band 7 (8 to 12 gigahertz), and 40 and 60 feet in Band 6 (4 to 8 gigahertz).

1.2.7.1 Adaptability to Field Operations. Inasmuch as this method of measurement exactly duplicates the present RAT SCAT operation except for a direct extension of the range length and sensitivity requirements, no problem exists in terms of the suitability of using this method at RAT SCAT.

1.2.7.2 Accuracy. The long-range and high-power method is based on duplicating the radar cross section measurement technique and procedures; therefore, no deviation from the present RAT SCAT accuracy levels is anticipated.

1.2.7.3 Cost. The most significant cost associated with implementation and operation in use of this technique can be found in Tables 1.2-3 and 1.2-5, and in the operational models subsequently presented in subsection 1.5. The direct costs associated with excessive range length and provision of control and signal lines and roadways represent the primary reason for limiting the use of the technique as a single solution to large object measurement. The equipment cost associated with implementation of this technique is presented in Table 1.2-6 on the basis of a coverage considered optimum for this technique. The required sensitivity can be achieved by incorporating the combinations of components shown. The choice of including coherent integration is based on a recommendation to provide a vector subtraction capability as a means of minimizing the target support problem. Provisions of this capability involves provision of a basic phase measurement capability which represents the most significant cost of providing coherent integration. Other significant costs associated with implementation of this method are those associated with the long range lengths required.

1.2.7.4 Other Considerations. Other considerations associated with the implementation of this method for full coverage of the target length-frequency spectrum include (1) the availability of adequate space at the White Sands Missile Range, (2) the limited practicality of setting up measurement equipments at ranges in excess of 16 miles, and (3) potentially high recurring costs associated with the operation and maintenance of the large number of sophisticated subsystems required to obtain the necessary equipment sensitivity.

Table 1.2-6 LONG-RANGE AND HIGH-POWER METHOD

EQUIPMENT REQUIREMENTS

		Area Cost (1000 Dollars)
Sensitivity Equipments	Coherent Integration(Bands 6&7)	6.0
	Phase Measurement Capability (Bands 6&7)	4.1
	RF Preamplifier (Bands 6&7)	9.0
	1 MHz IR Amplifier	2.5
	Noise Subtraction Equipment	15
	Antenna (Band 7)	20
Facility Equipments	Gantry	50
	Rotator & Azimuth Encoder	300
	Mobile Van Modifications	5
	Roadway and Cables	216
	Generator	20
	Mobile Antenna Tower	60

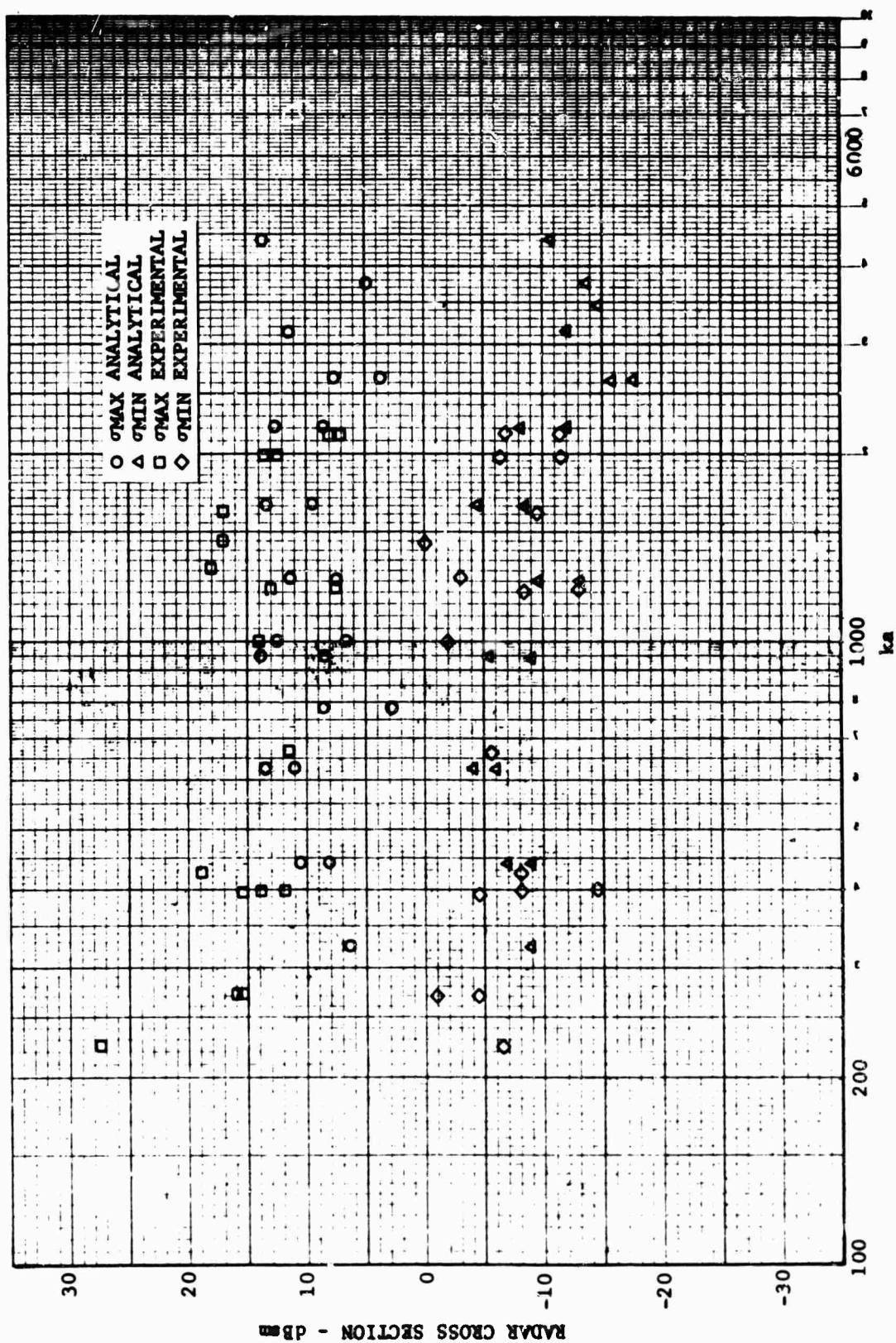


Fig. 1.2-1 AVERAGE CROSS SECTION FOR REPRESENTATIVE LARGE TARGETS

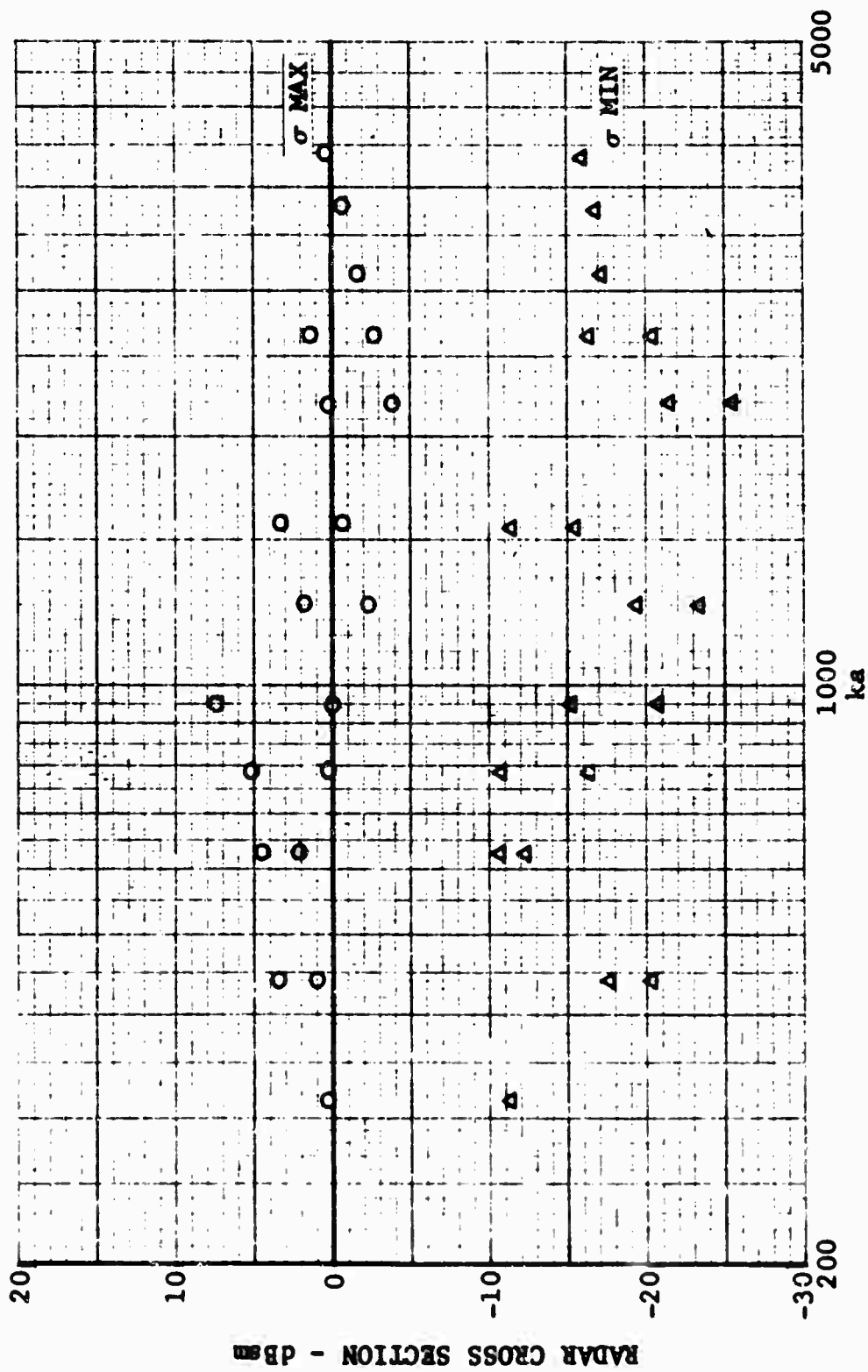


FIG. 1.2-2 CROSS SECTION OF TARGET 1

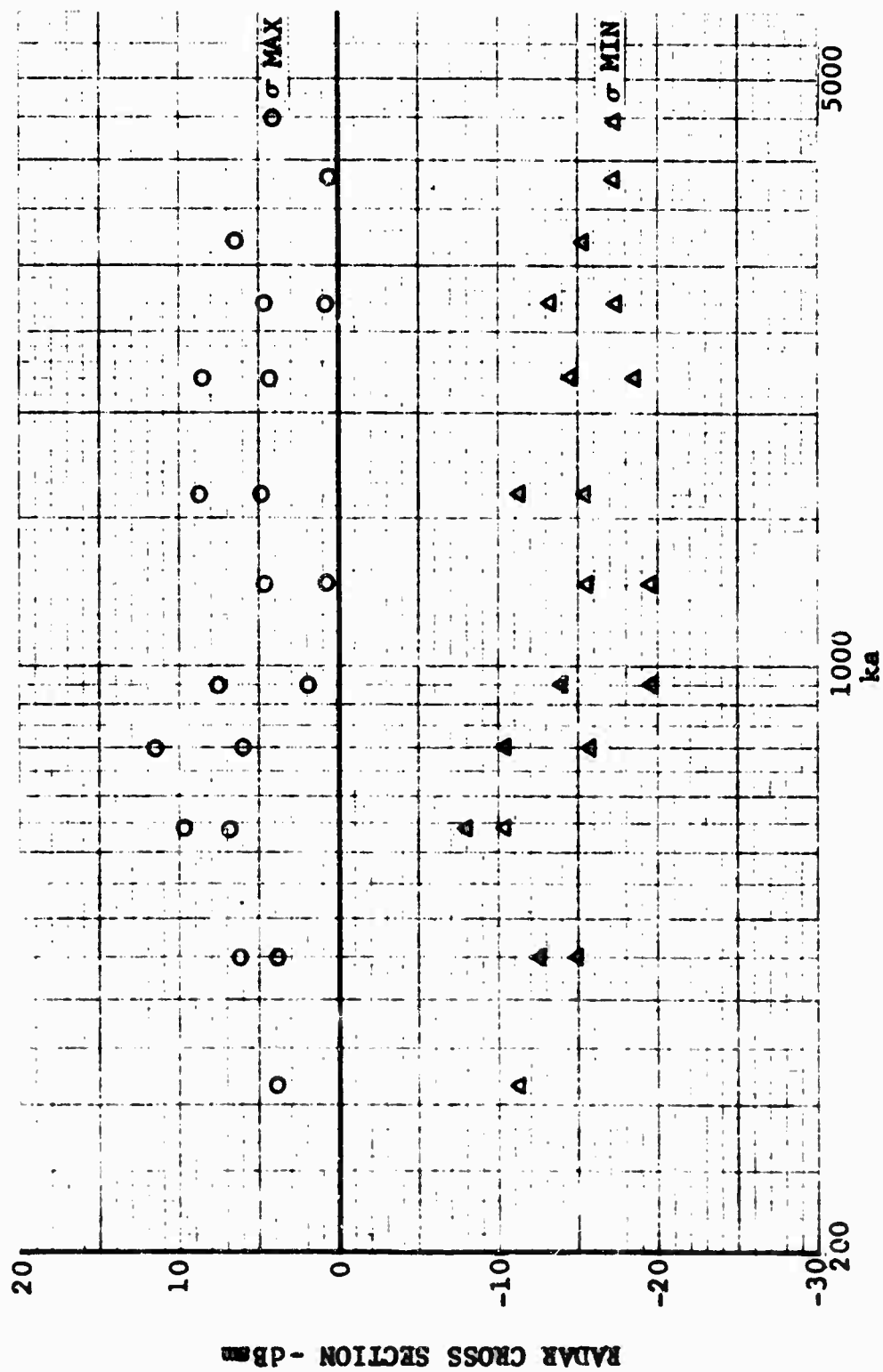


Fig. 1.2-3 CROSS SECTION OF TARGET 2

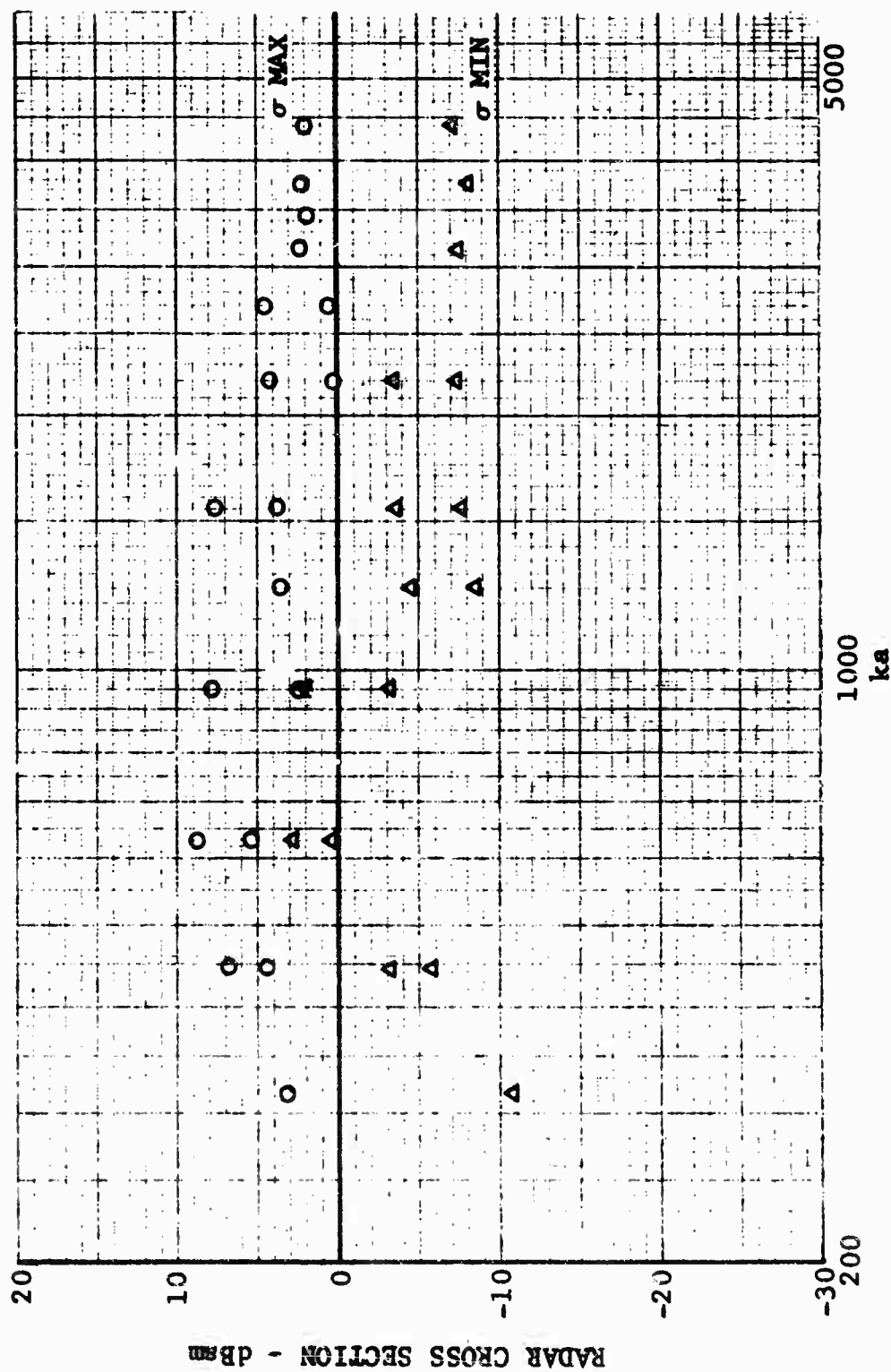


FIG. 1.2-4 CROSS SECTION OF TARGET 3

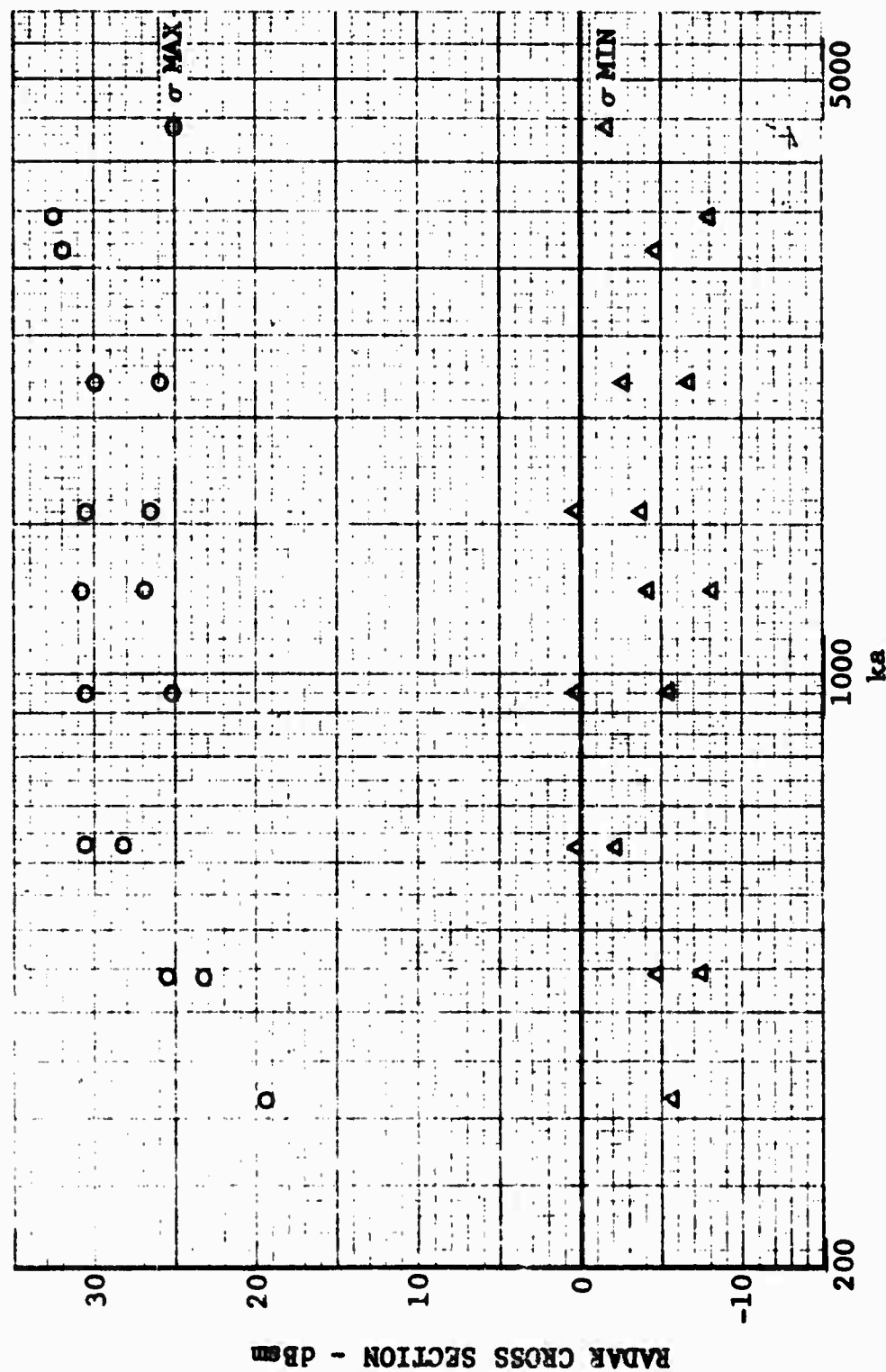


Fig. 1.2-5 CROSS SECTION OF TARGET 4

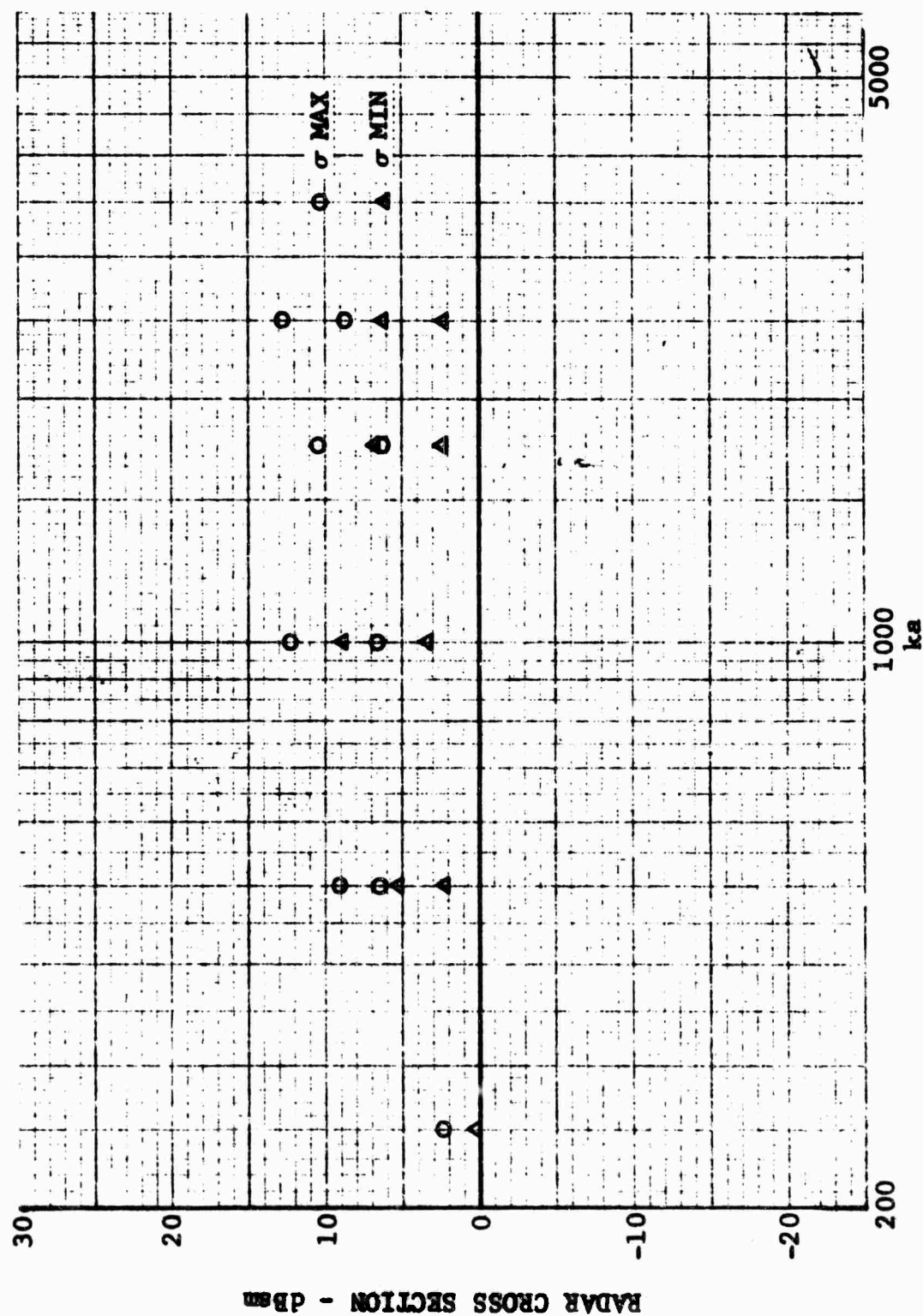


Fig. 1.2-6 CROSS SECTION OF TARGET 5

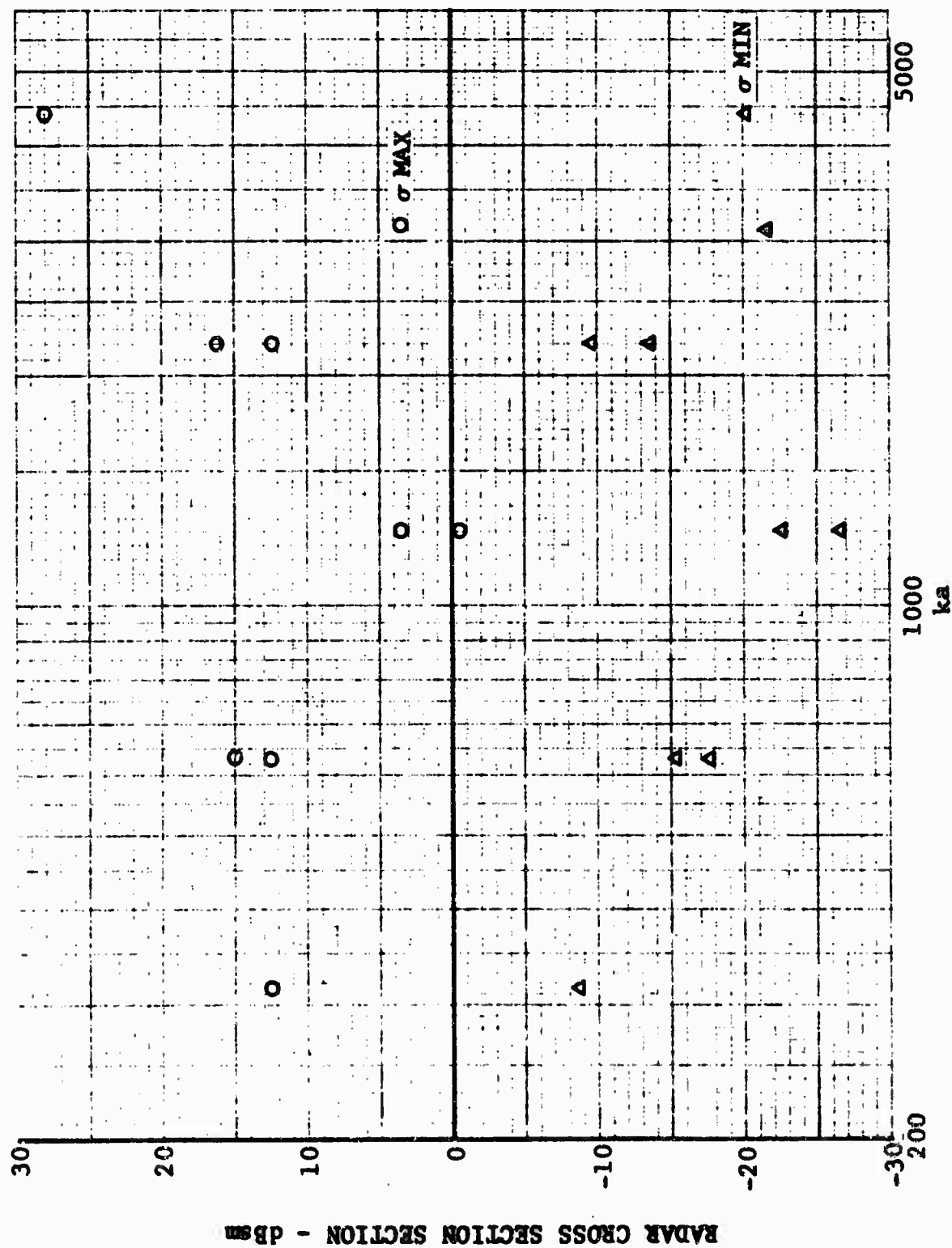


Fig. 1.2-7 CROSS SECTION OF TARGET 6

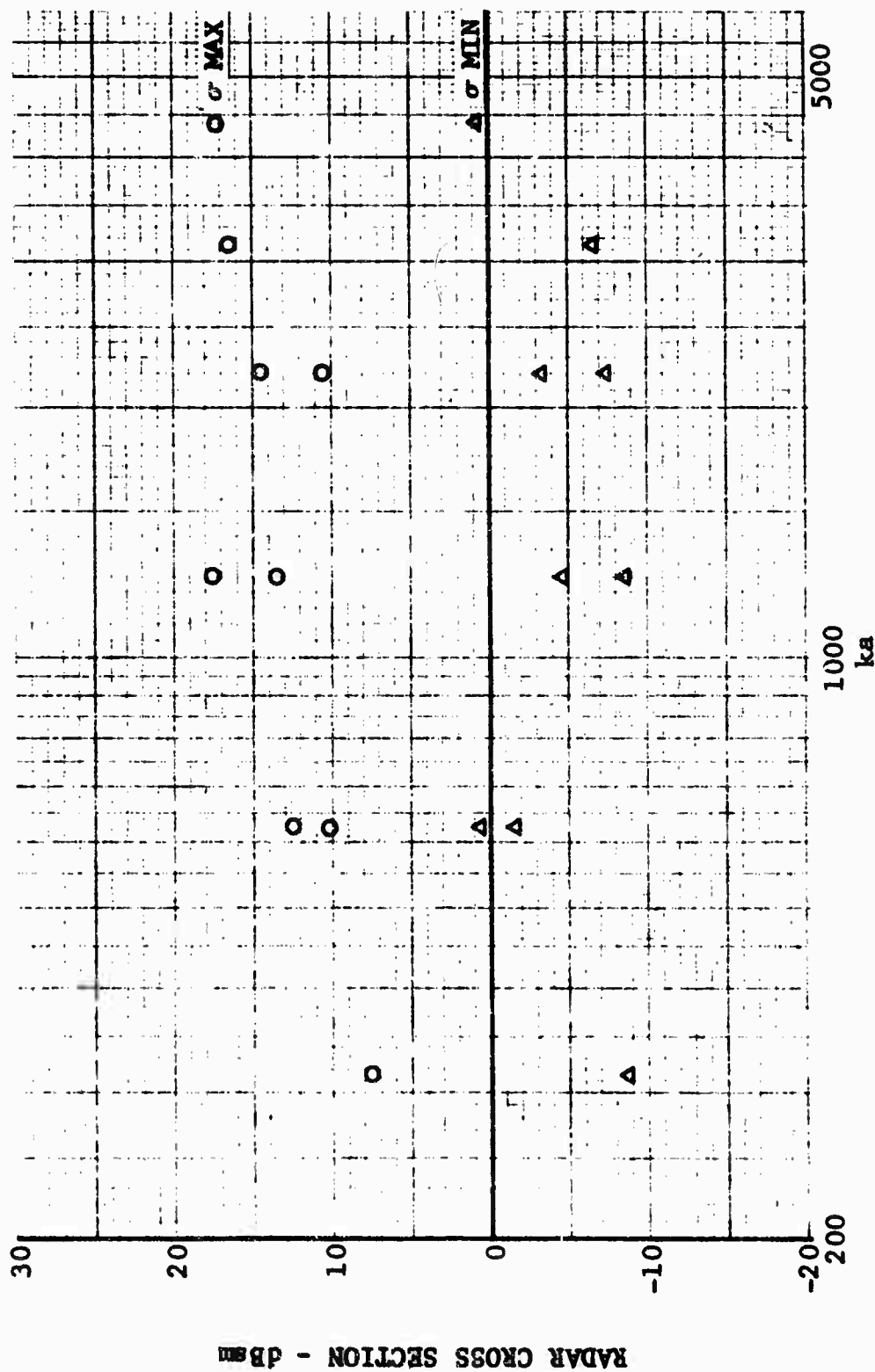


Fig. 1.2-8 CROSS SECTION OF TARGET 7

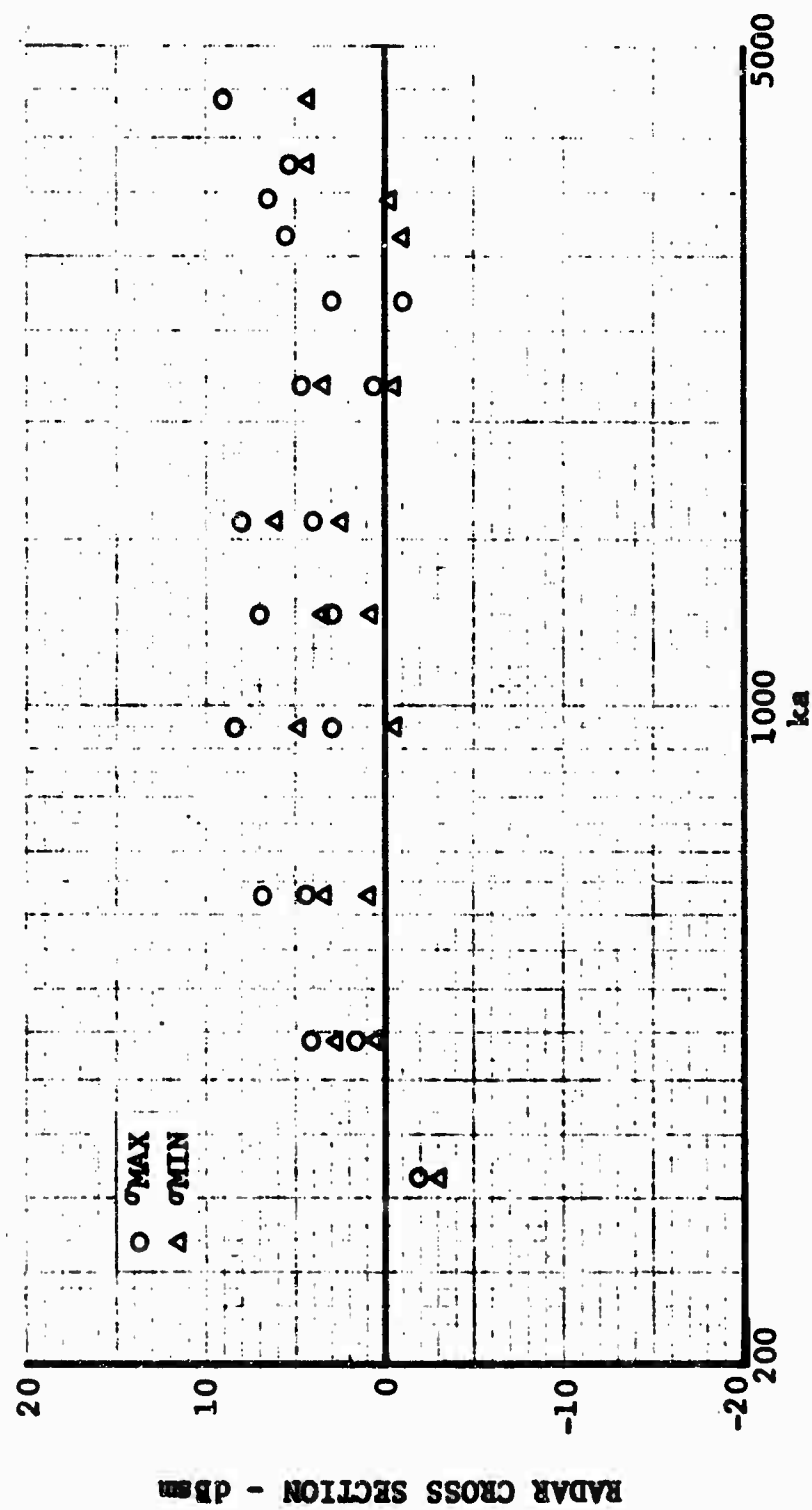


Fig. 1.2-9 CROSS SECTION OF TARGET 8

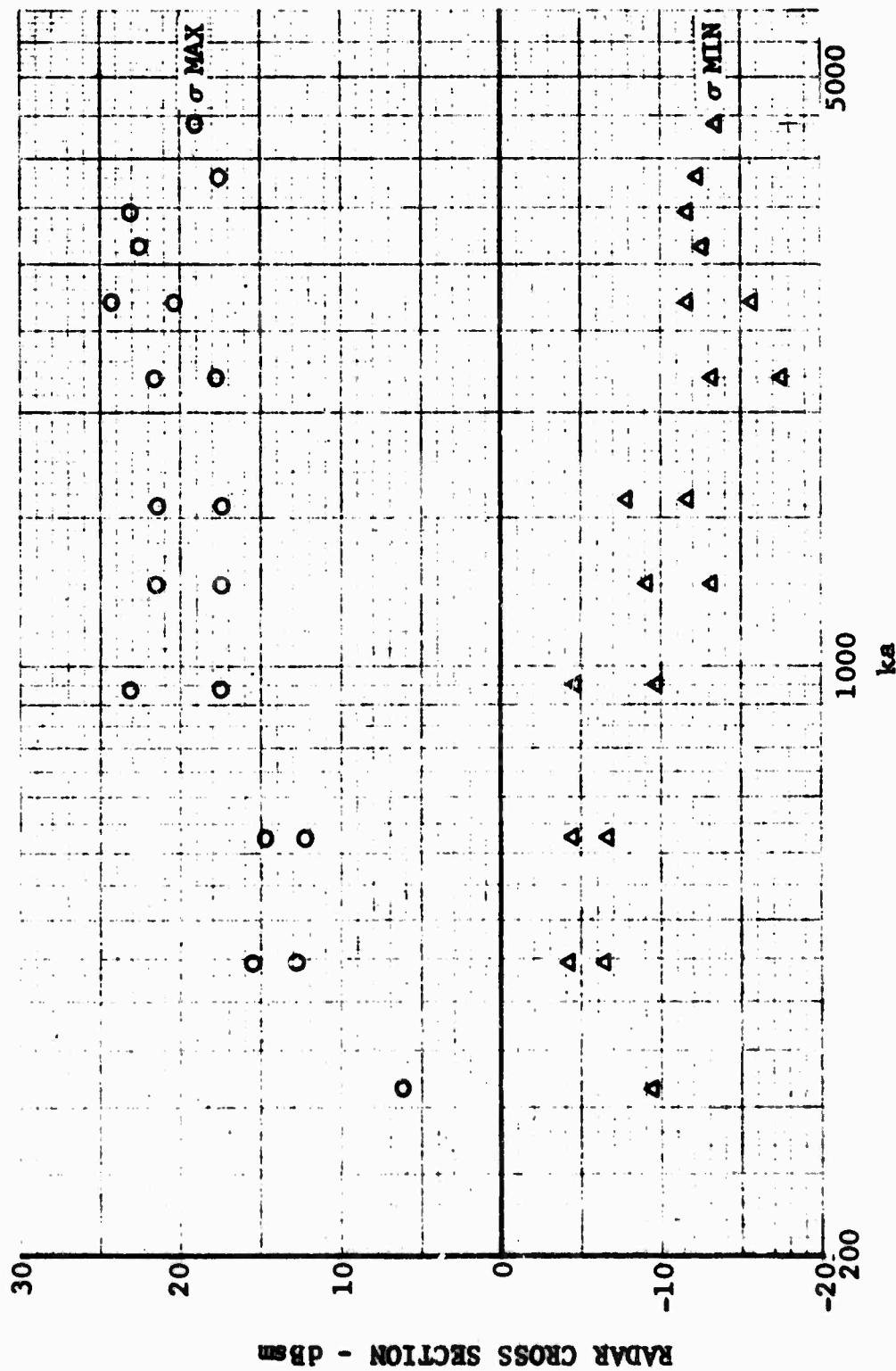


Fig. 1.2-10 CROSS SECTION OF TARGET 9

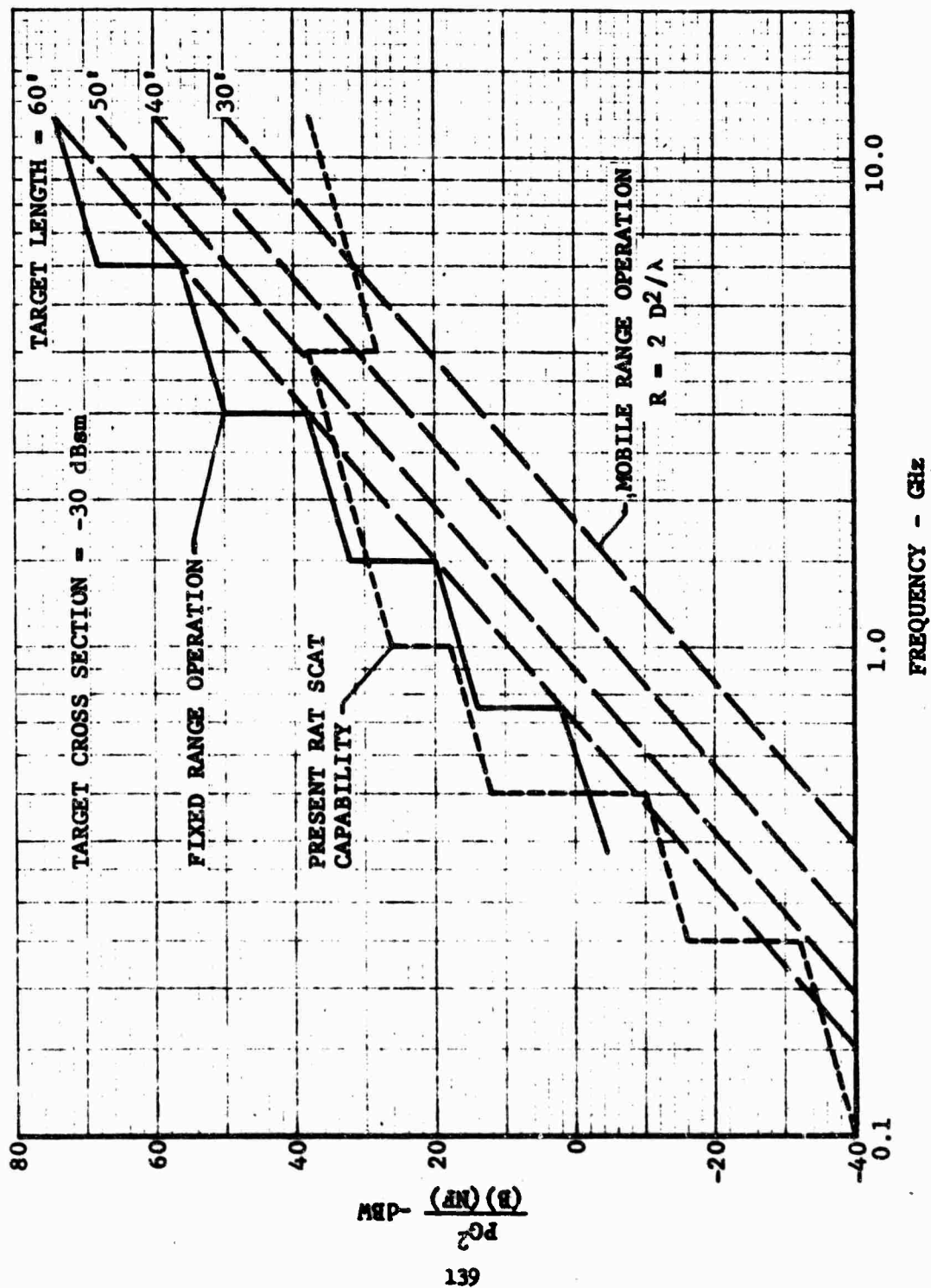


Fig. 1.2-11 LONG RANGE AND HIGH POWER SENSITIVITY REQUIREMENTS

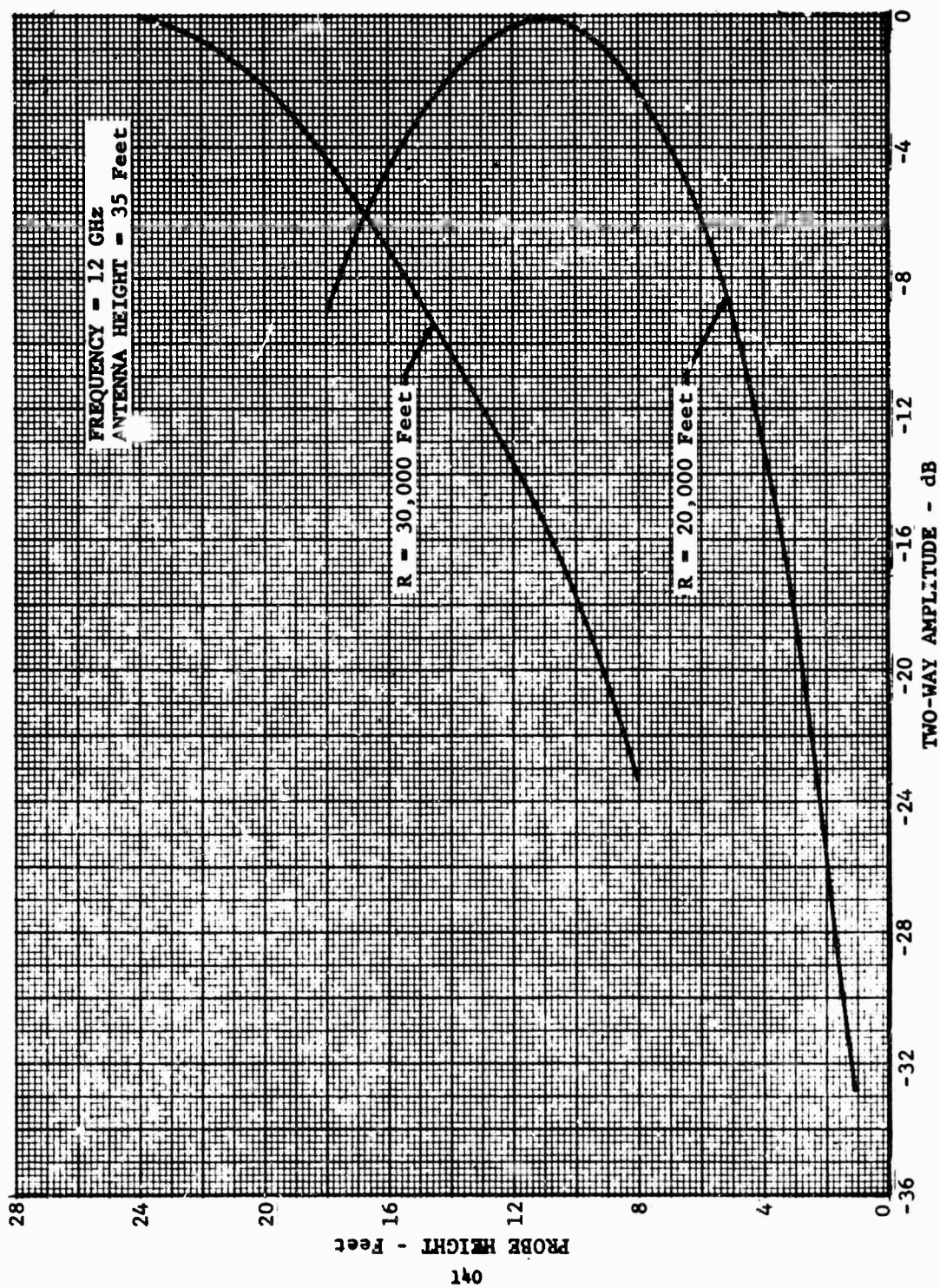


Fig. 1.2-12 VERTICAL PLANE FIELD PROBE

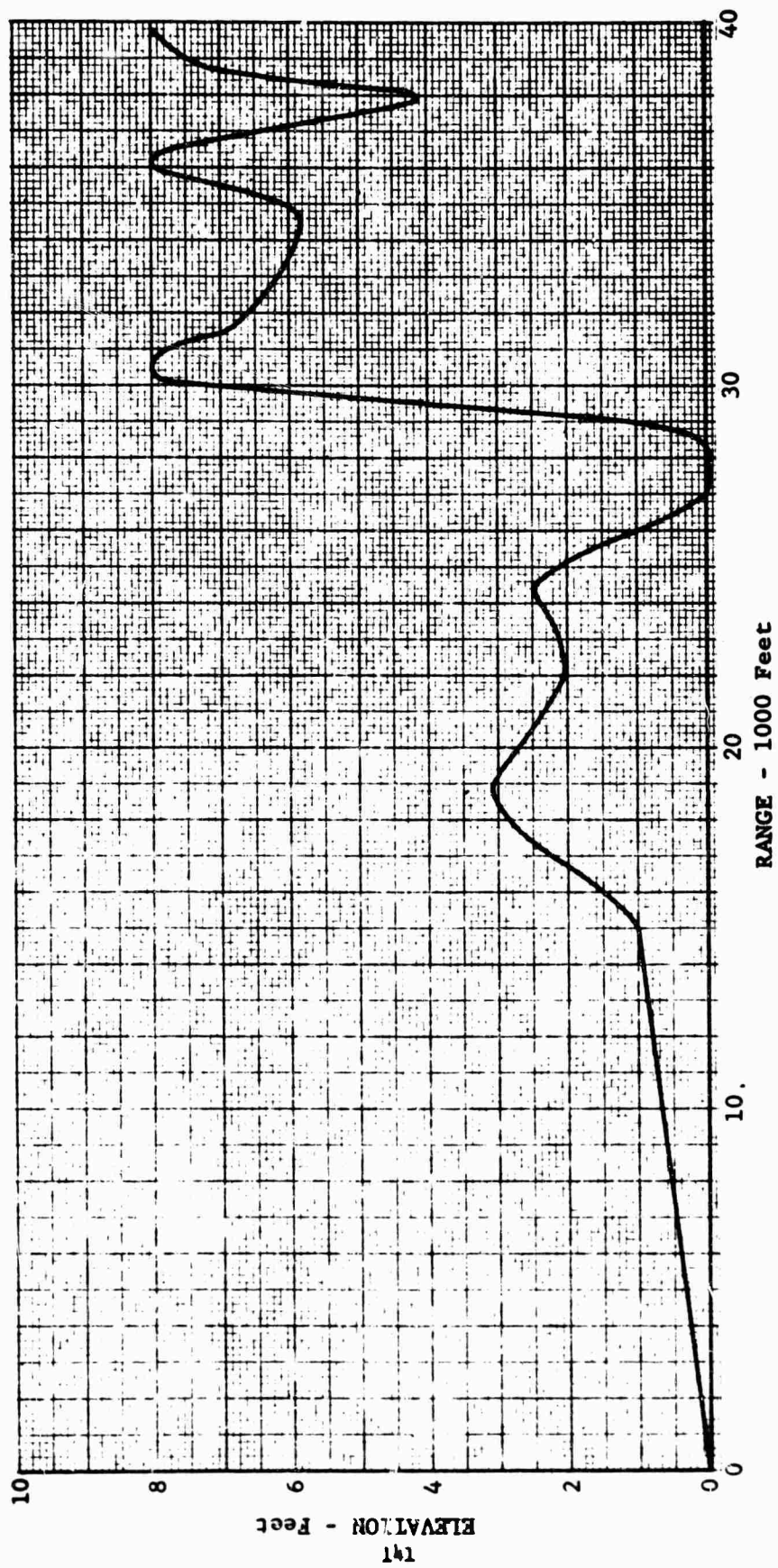


FIG. 1.2-13 TERRAIN ELEVATION CONTOUR

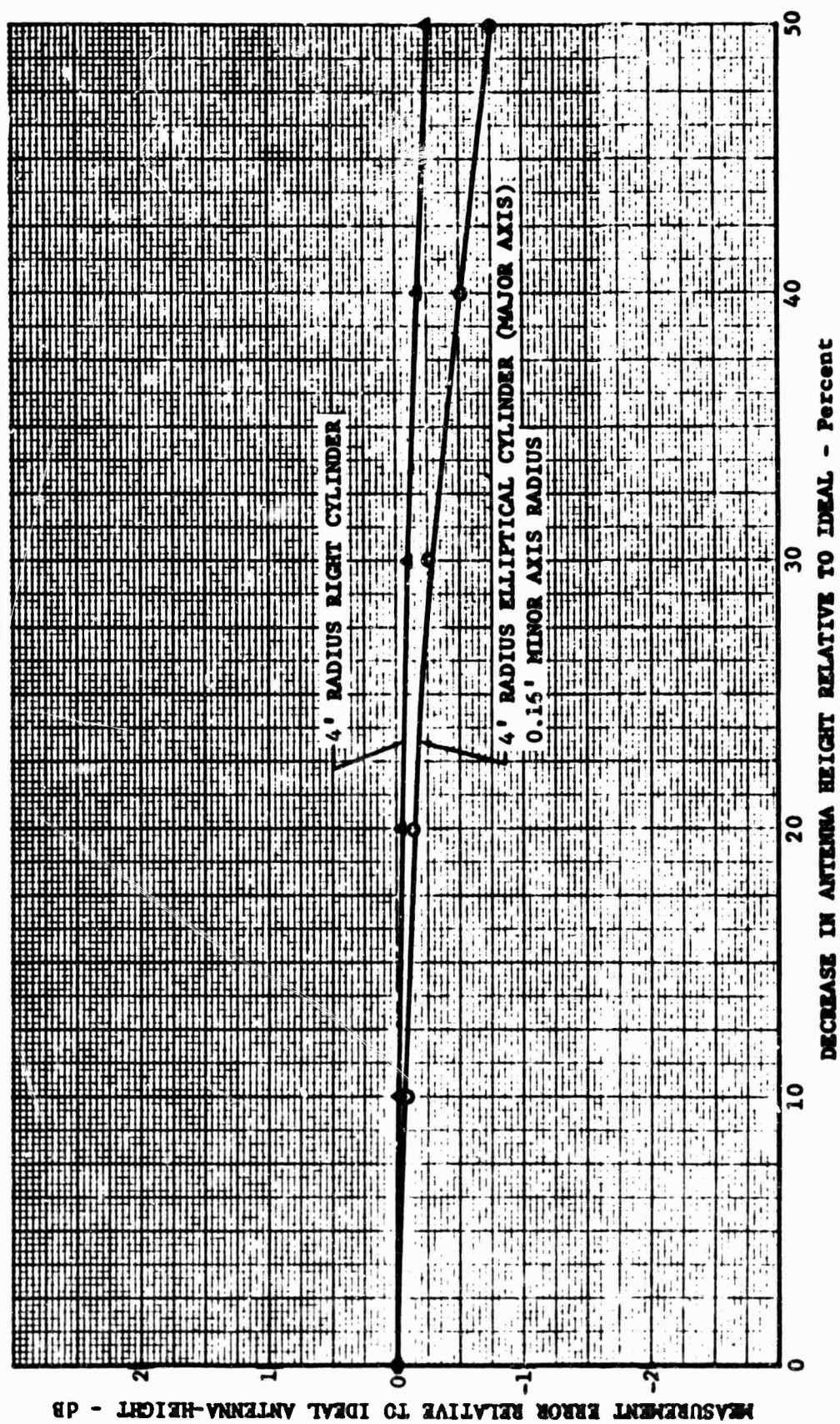


Fig. 1.2-14 VERTICAL PLANE NEAR FIELD ERROR
(HORIZONTAL CYLINDER MODEL)

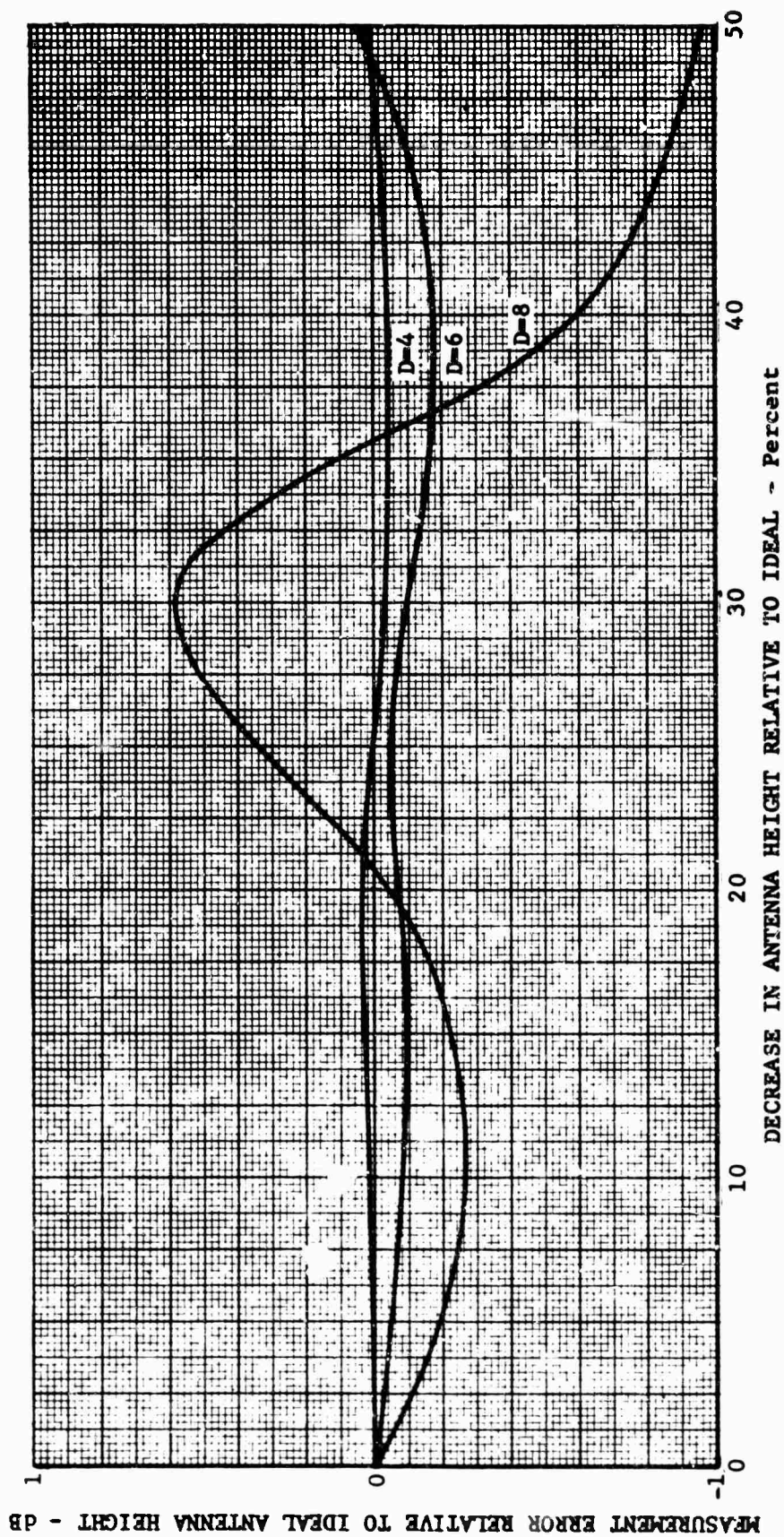


Fig. 1.2-15 VERTICAL PLANE NEAR FIELD ERROR
(VERTICAL CYLINDER MODEL)

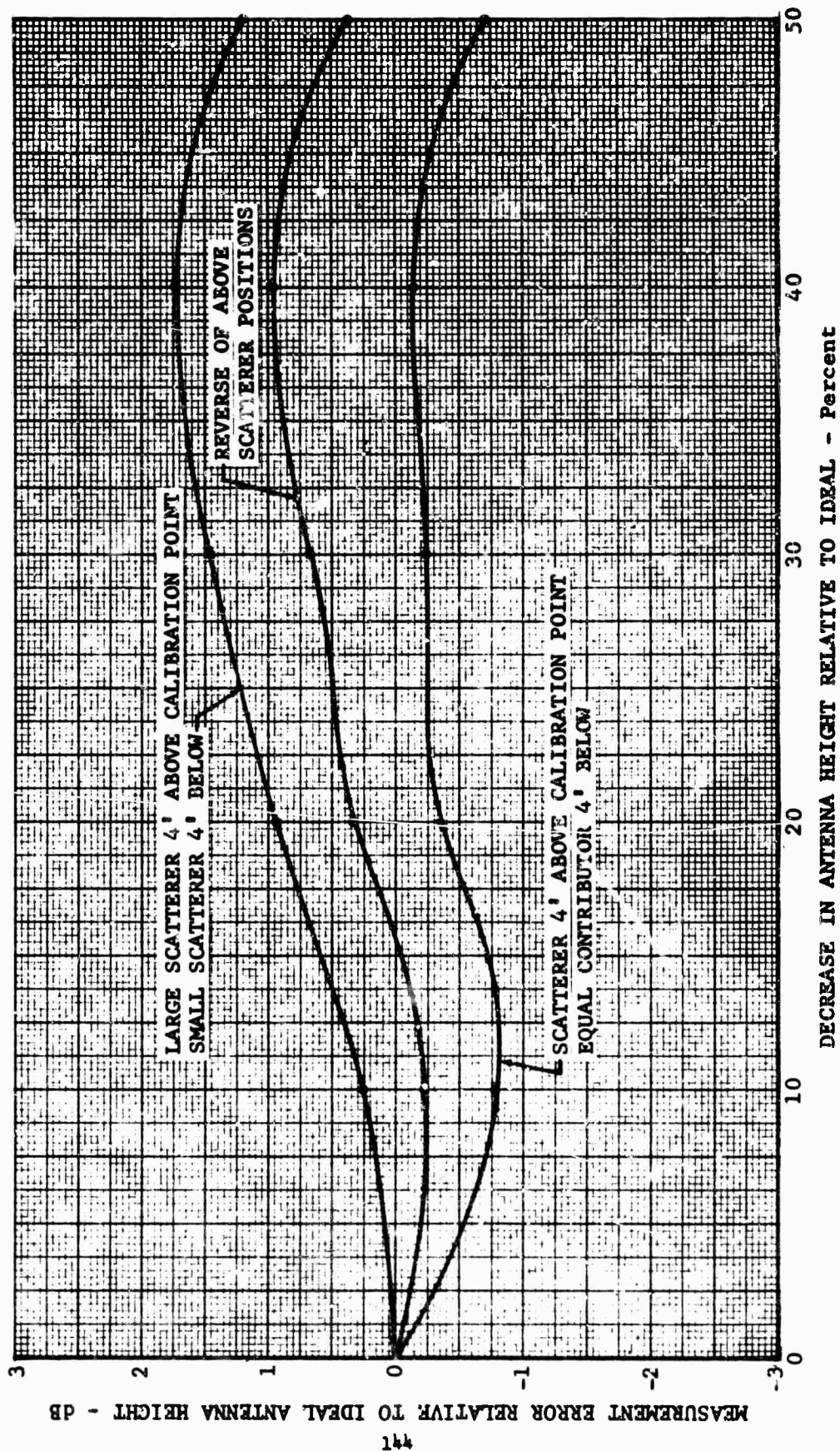


Fig. 1.2-16 VERTICAL PLANE NEAR FIELD ERROR
(TWO SCATTERER MODEL)

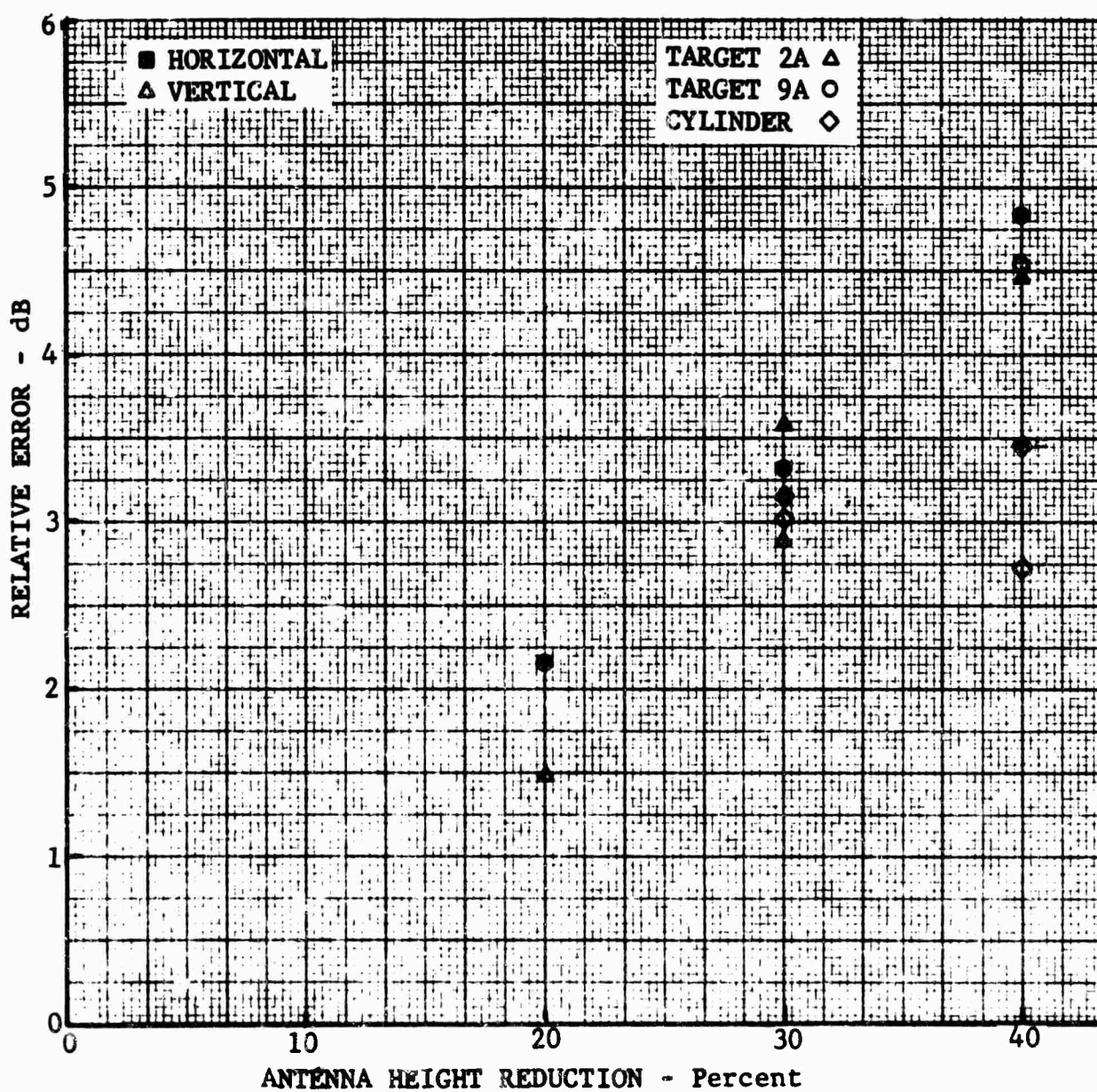


Fig. 1.2-17 ANTENNA HEIGHT REDUCTION ERROR LEVELS

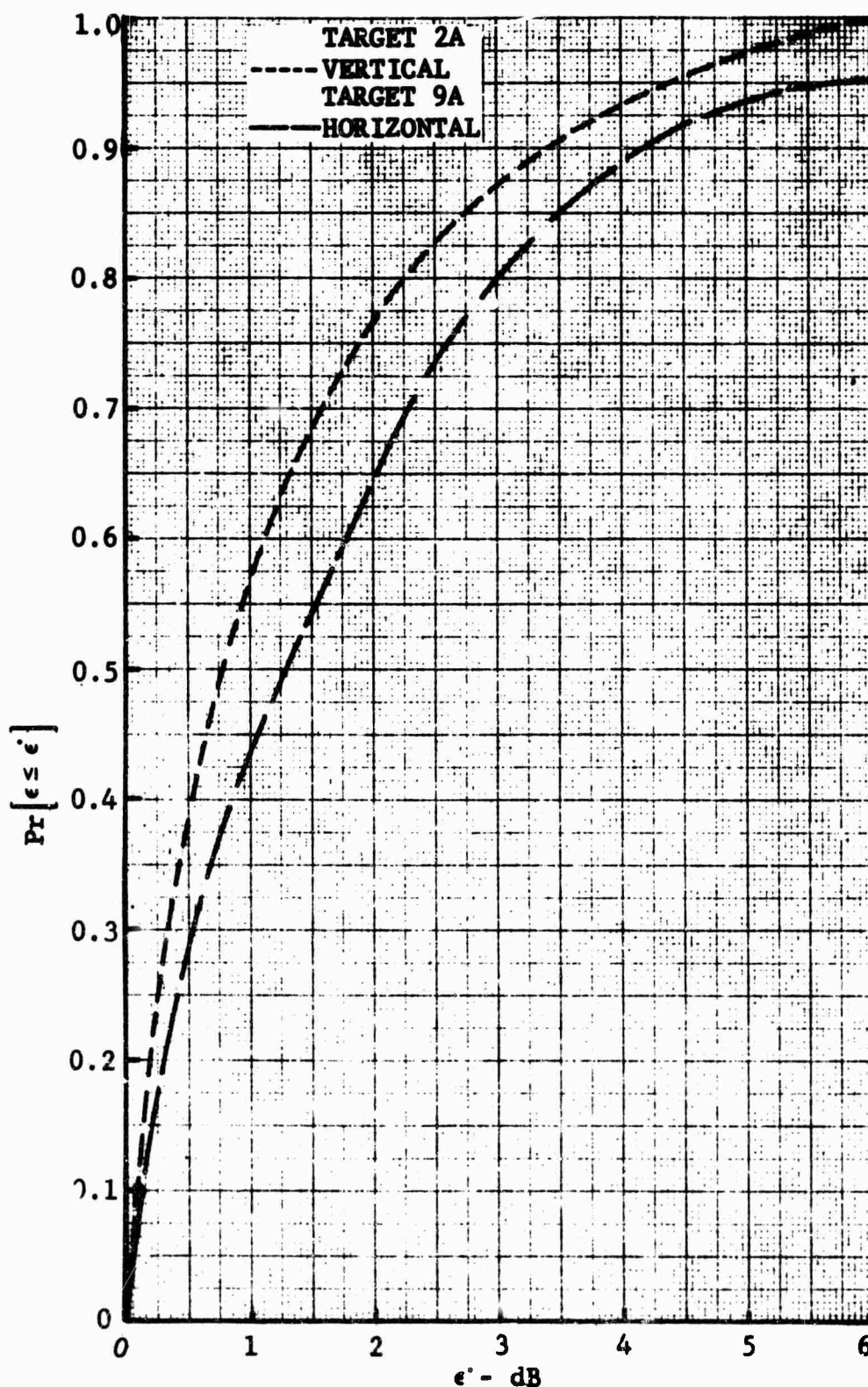


Fig. 1.2-18 CUMULATIVE ERROR DENSITY WITH 20 PERCENT ANTENNA HEIGHT REDUCTION

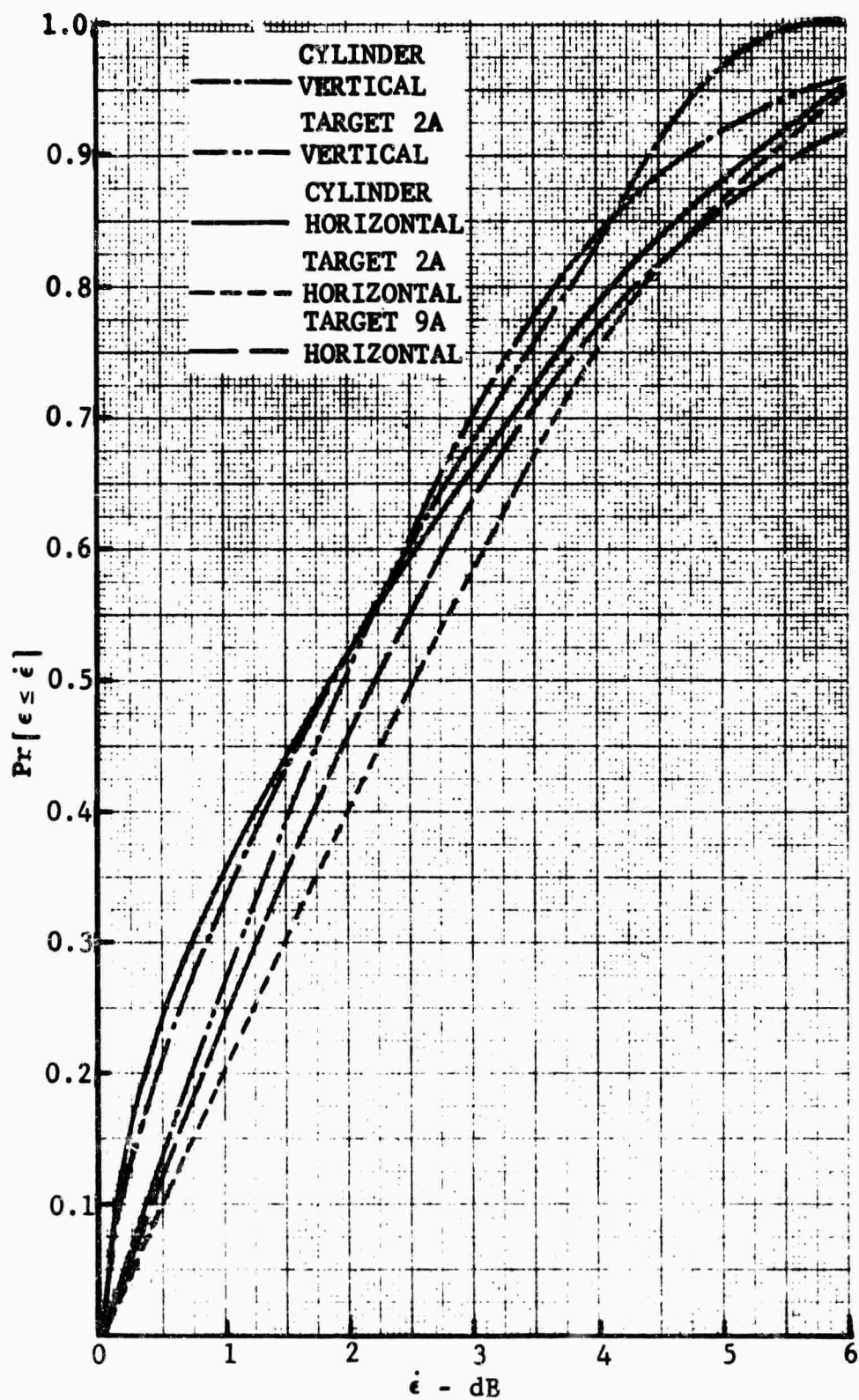


Fig. 1.2-19 CUMULATIVE ERROR DENSITY WITH 30 PERCENT ANTENNA HEIGHT REDUCTION

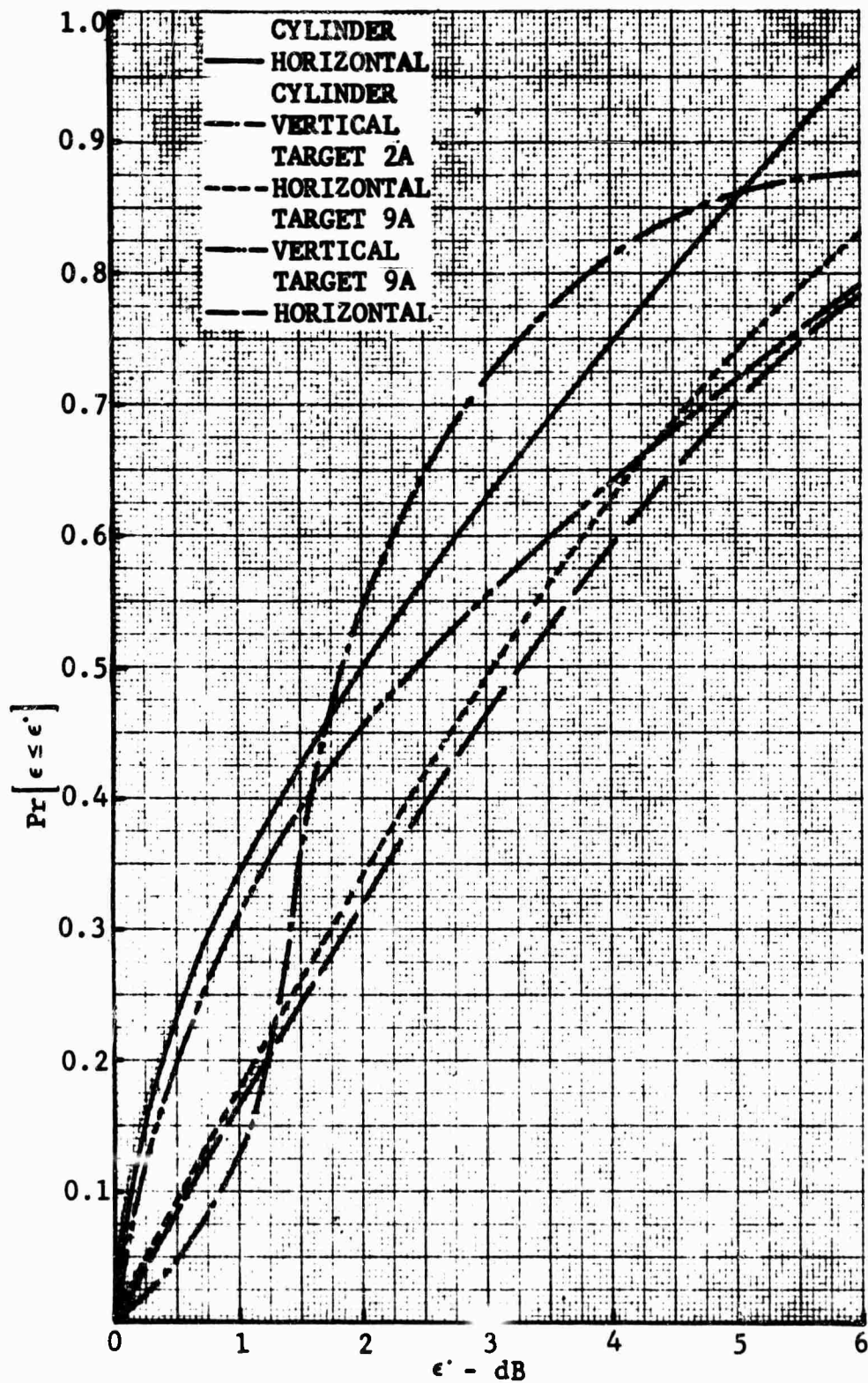


Fig. 1.2-20 CUMULATIVE ERROR DENSITY WITH 40 PERCENT ANTENNA HEIGHT REDUCTION

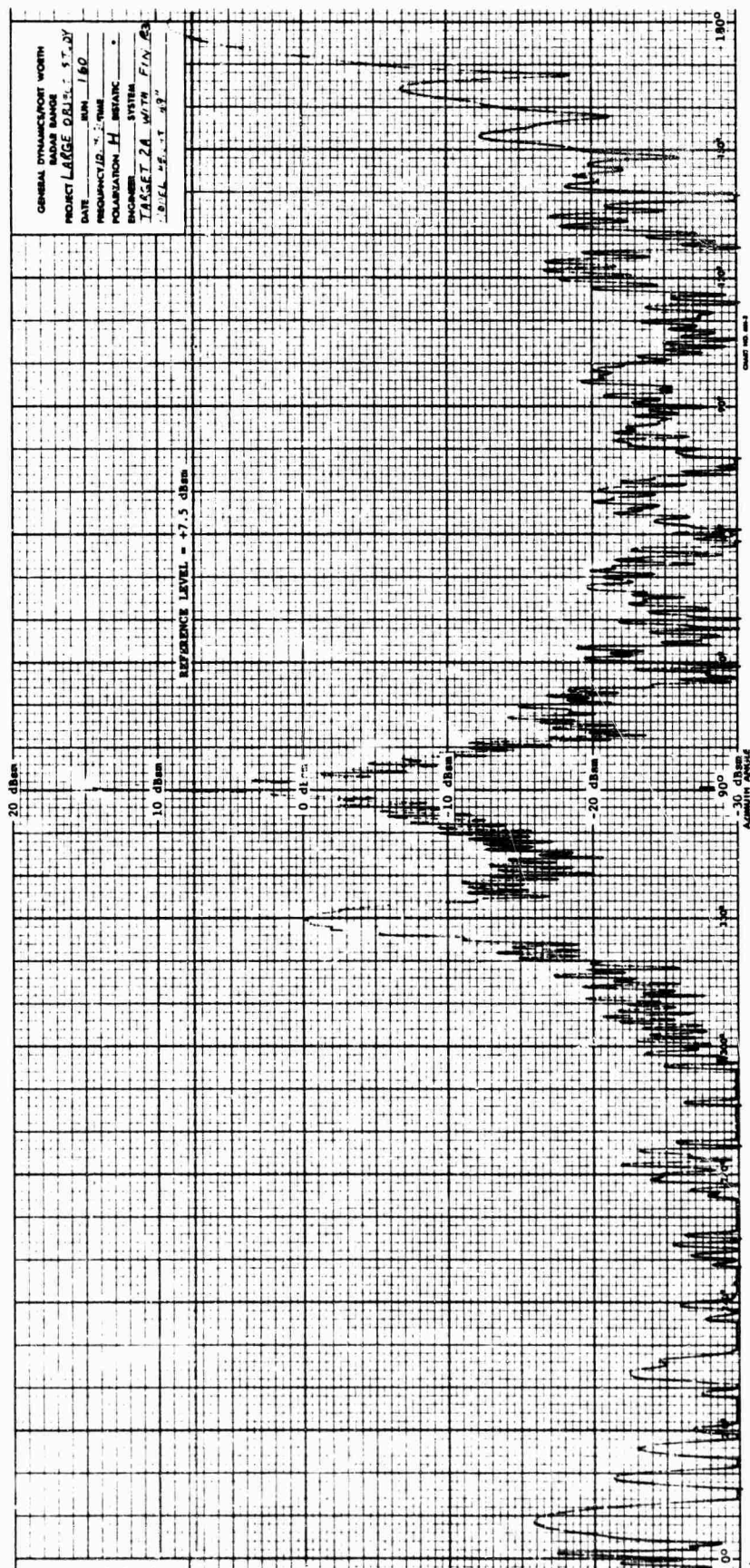


Fig. 1.2-21 VERTICAL PLANE GRADIENT EXPERIMENTAL DATA
(IDEAL ANTENNA HEIGHT)

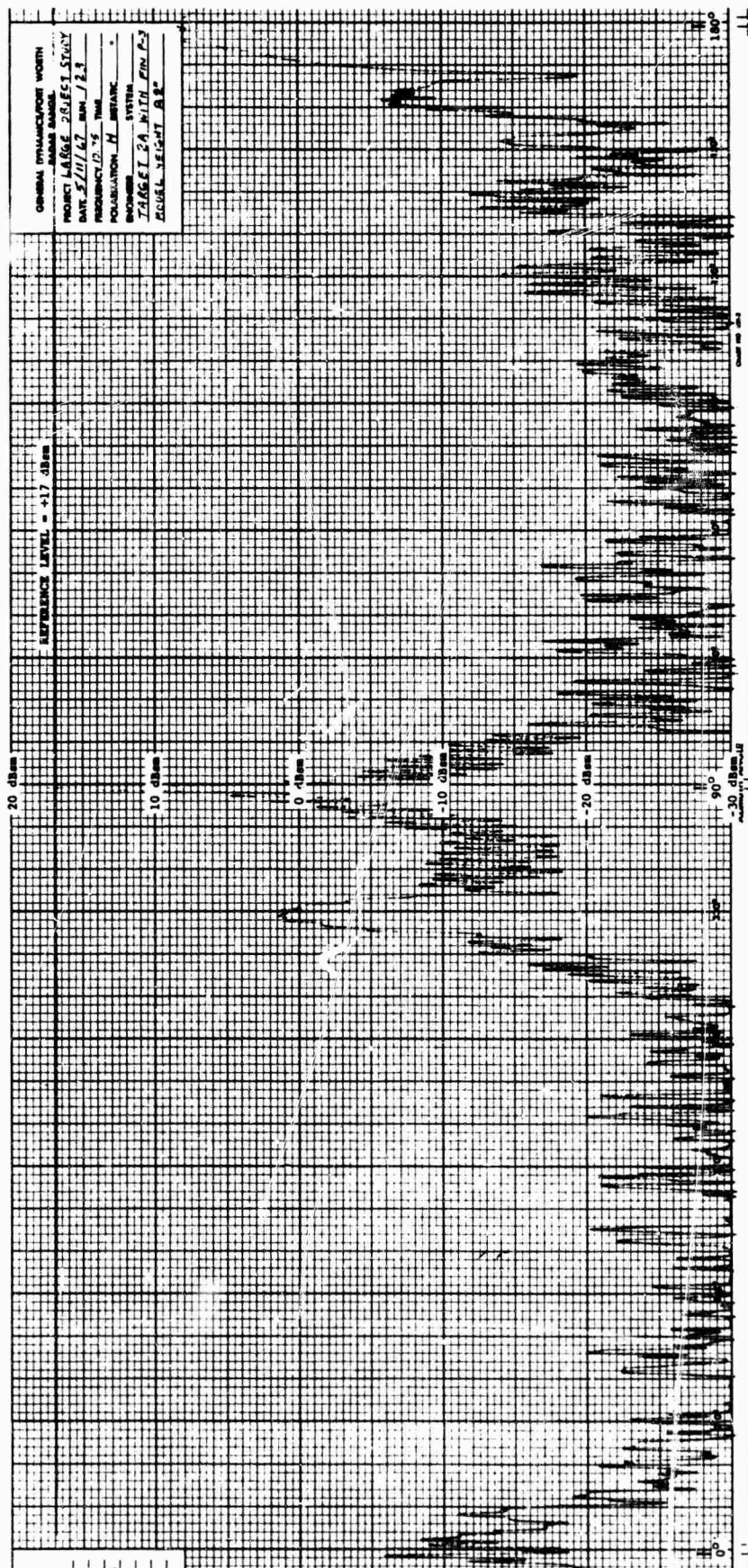


Fig. 1.2-22 VERTICAL PLANE GRADIENT EXPERIMENTAL DATA
(30 PERCENT ANTENNA HEIGHT REDUCTION)

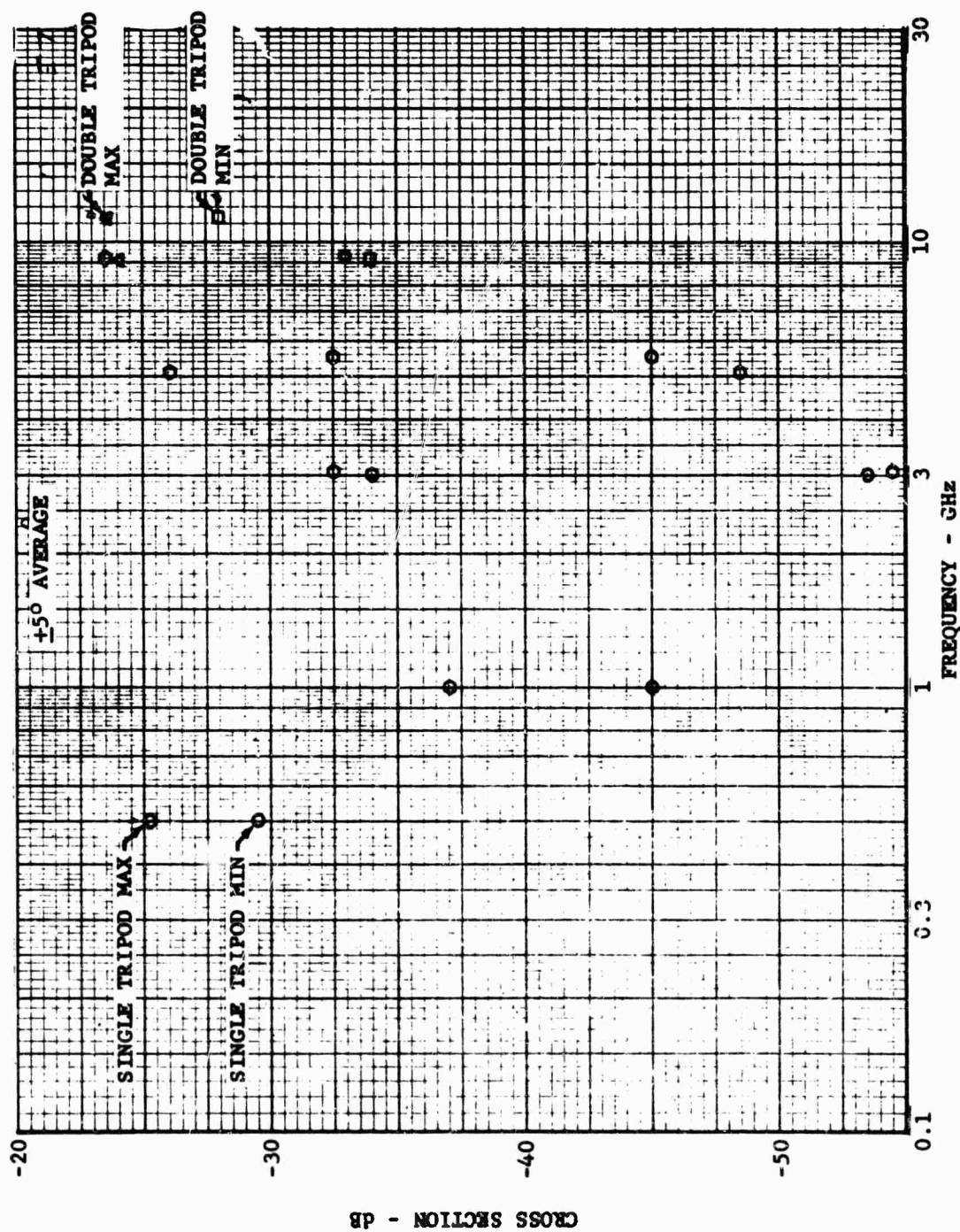


Fig. 1.2-23 LARGE TARGET STYROFOAM SUPPORT CROSS SECTION DATA

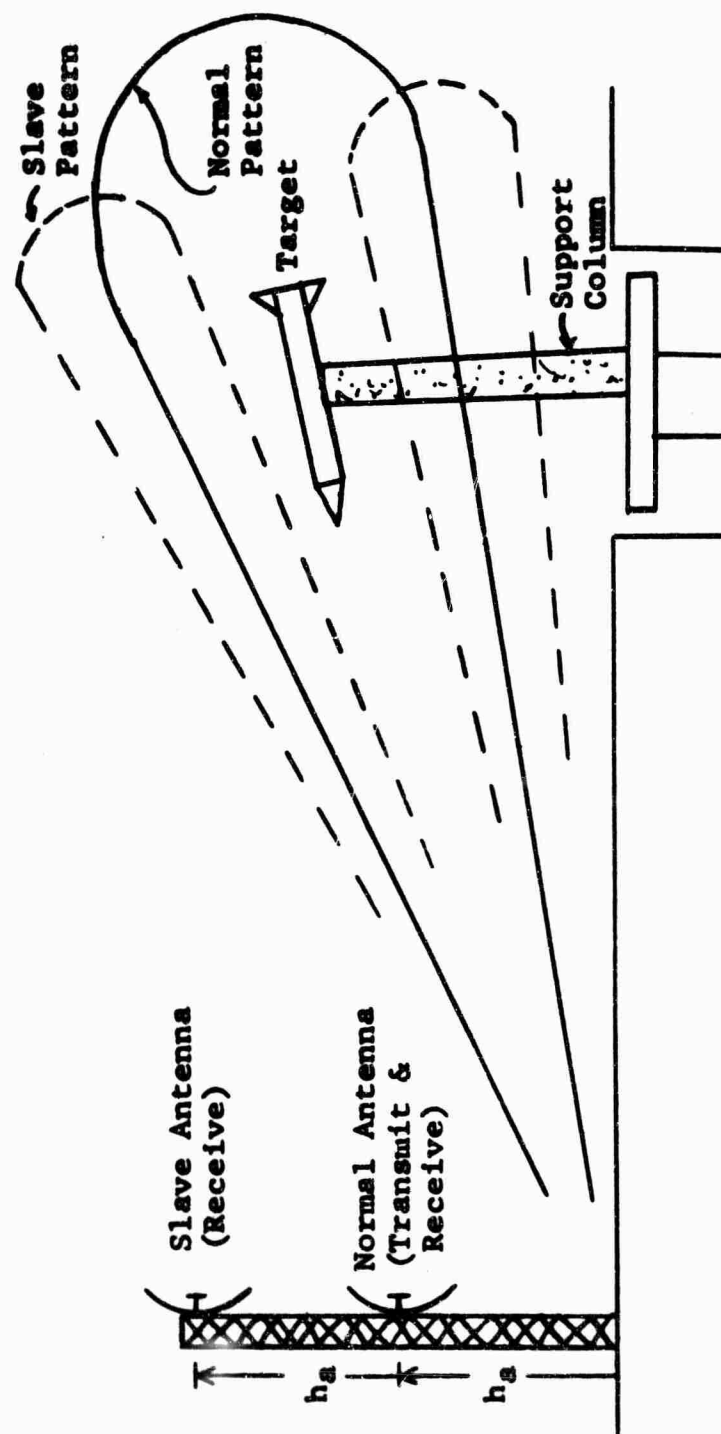


Fig. 1.2-24 REAL TIME VECTOR SUBTRACTION RANGE GEOMETRY

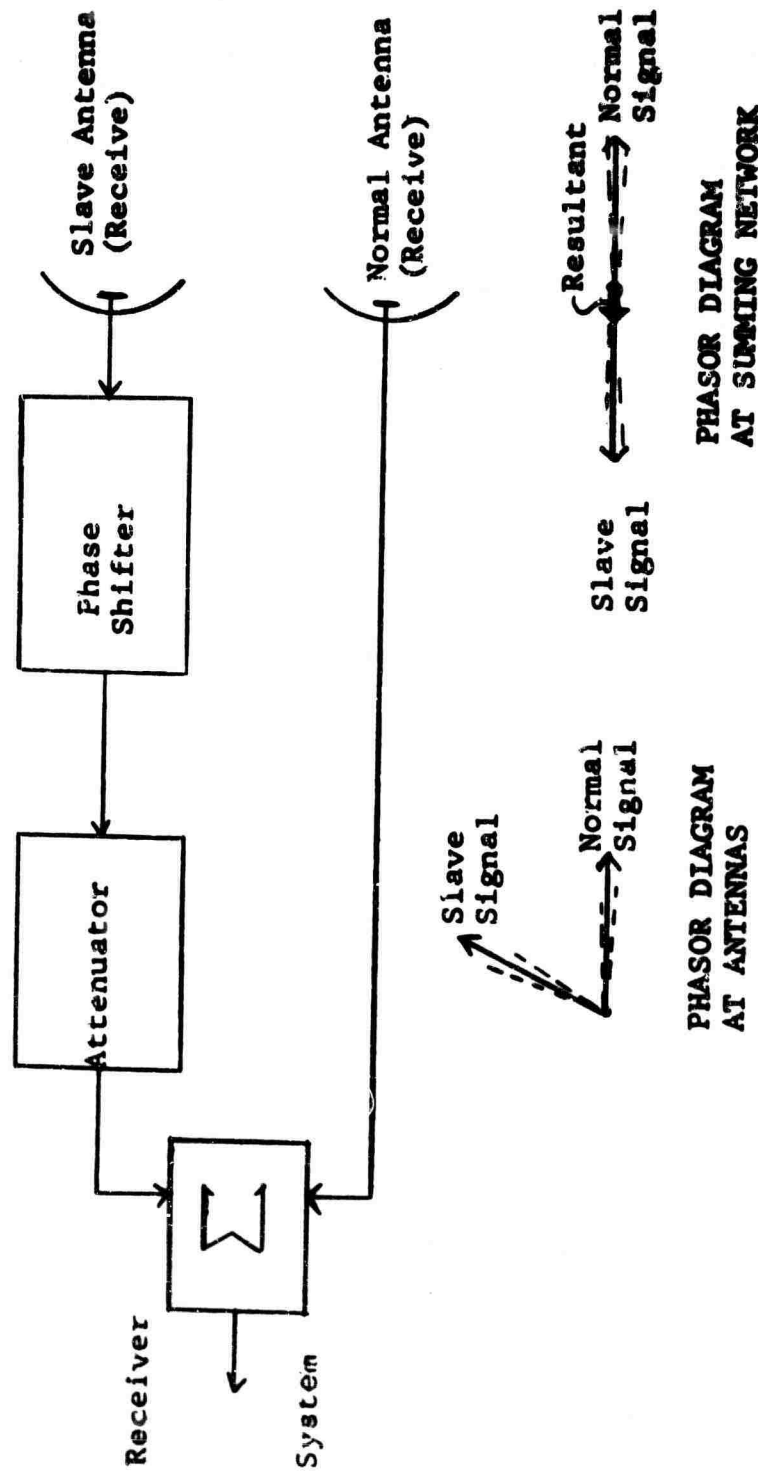


Fig. 1.1.2-25 REAL TIME VECTOR SUBTRACTION BLOCK DIAGRAM

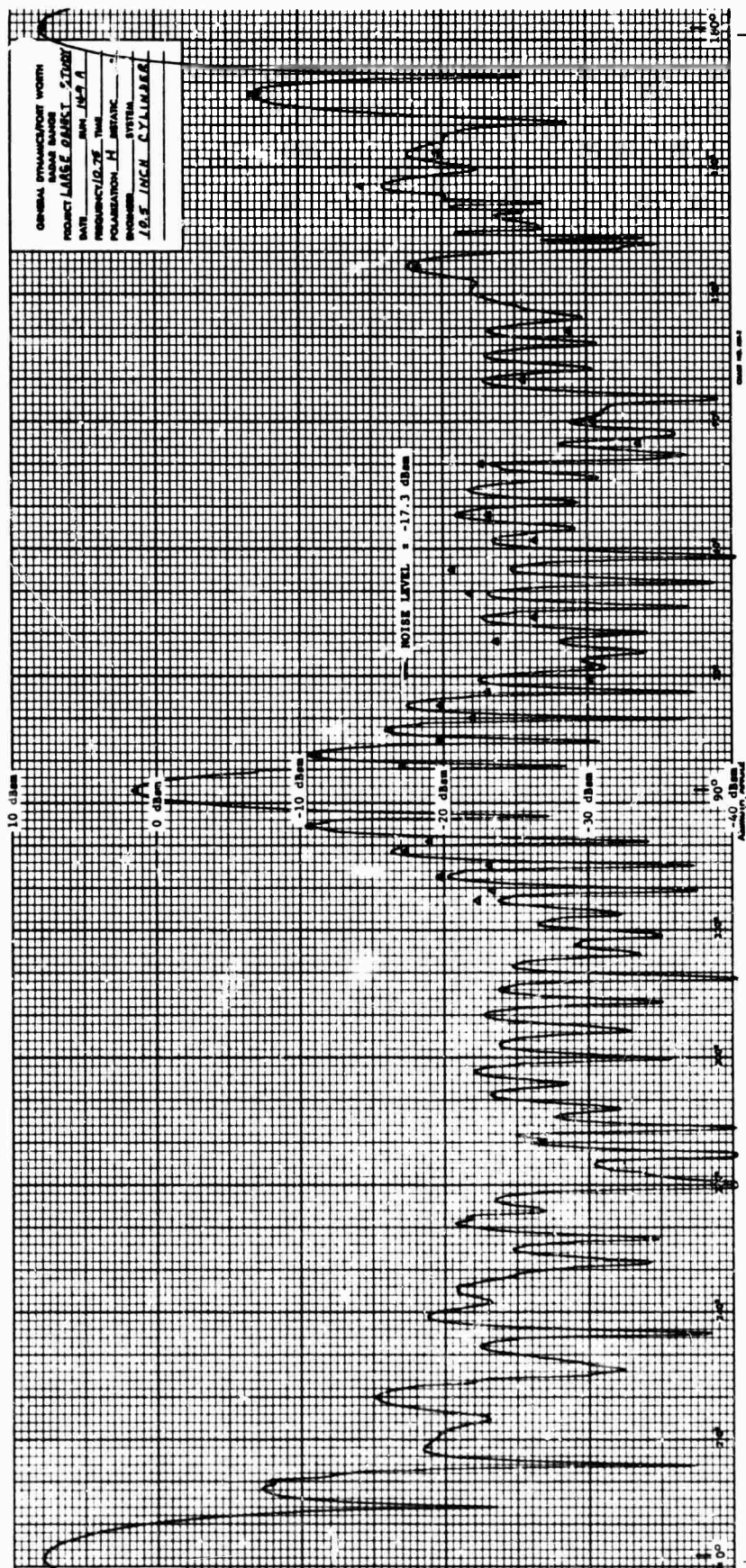


Fig. 1.2-26 TARGET CROSS SECTION DATA FOR NOISE SUBTRACTION

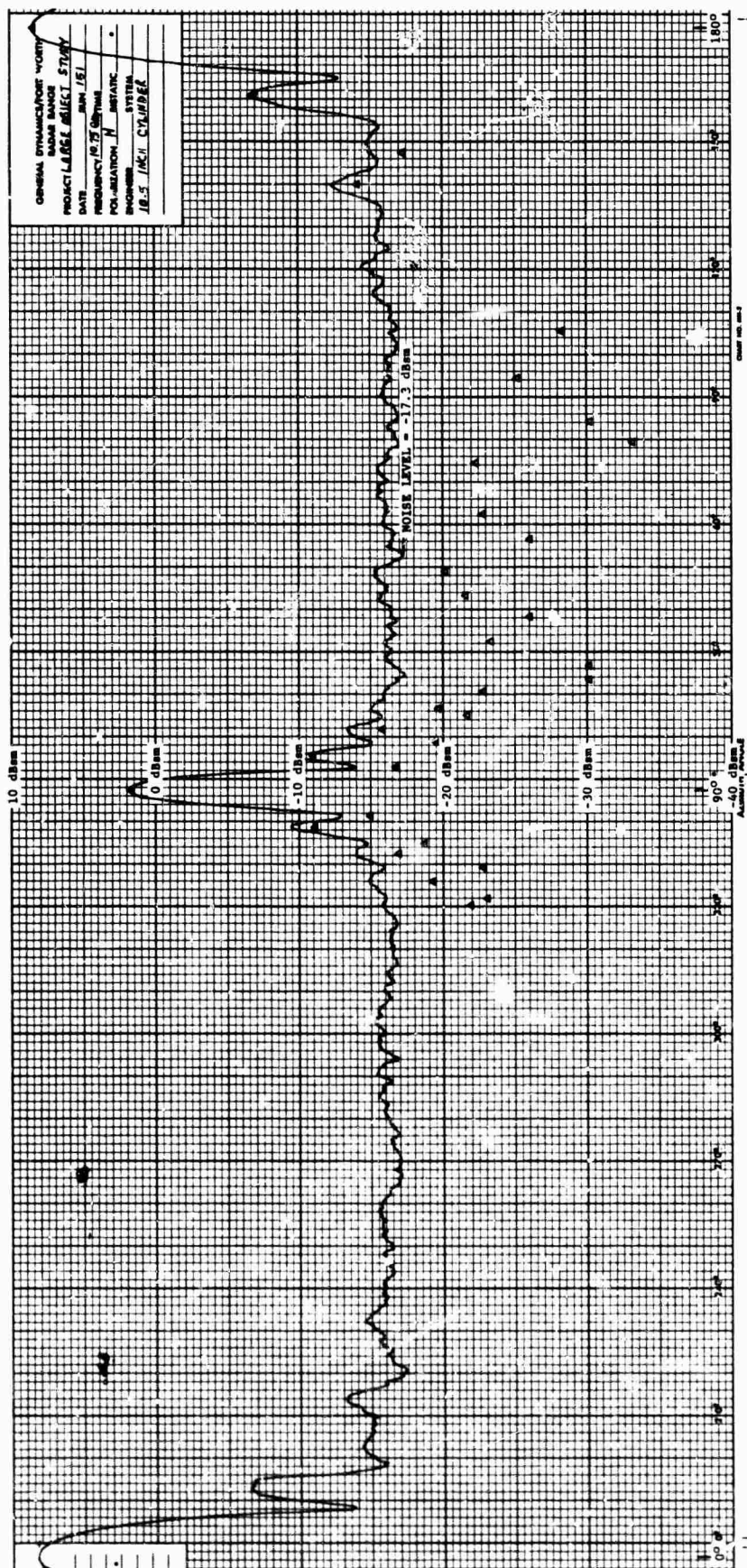


FIG. 1.2-27 TARGET-PLUS NOISE DATA FOR NOISE SUBTRACTION

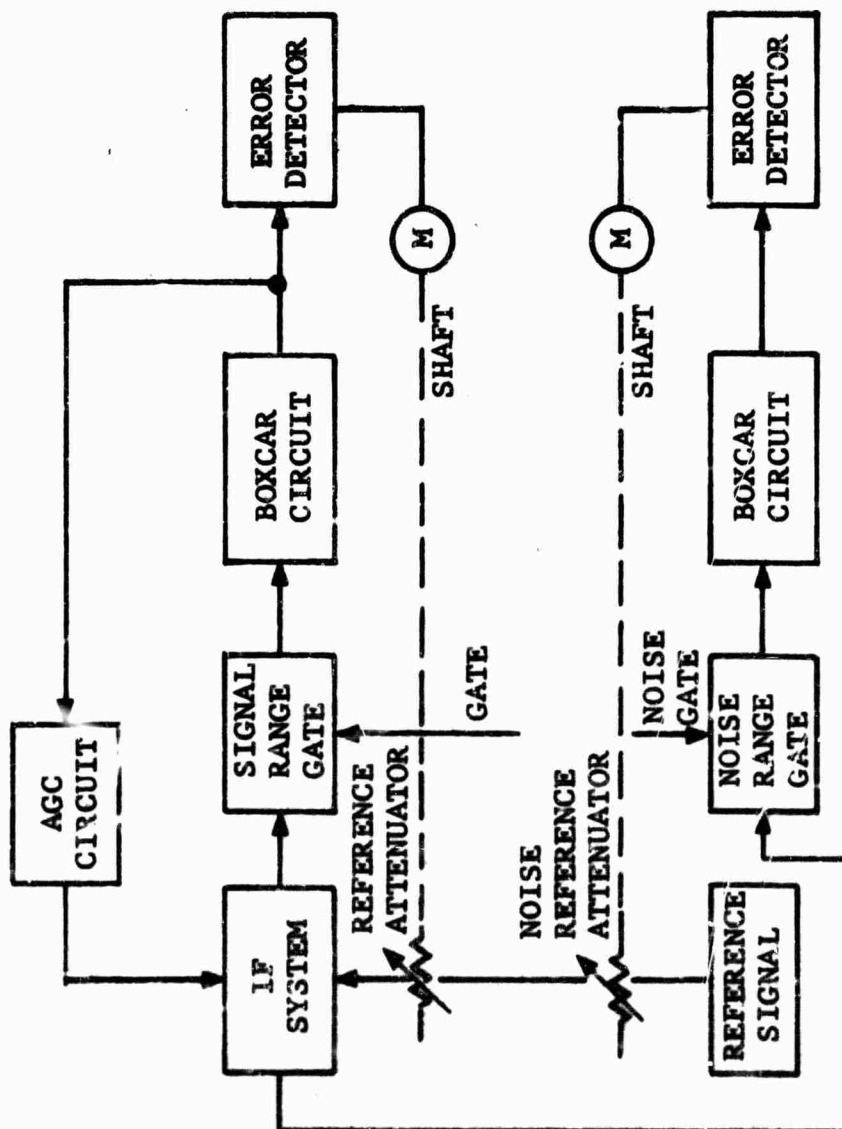


Fig. 1.2-28 ANALOG NOISE SUBTRACTION BLOCK DIAGRAM

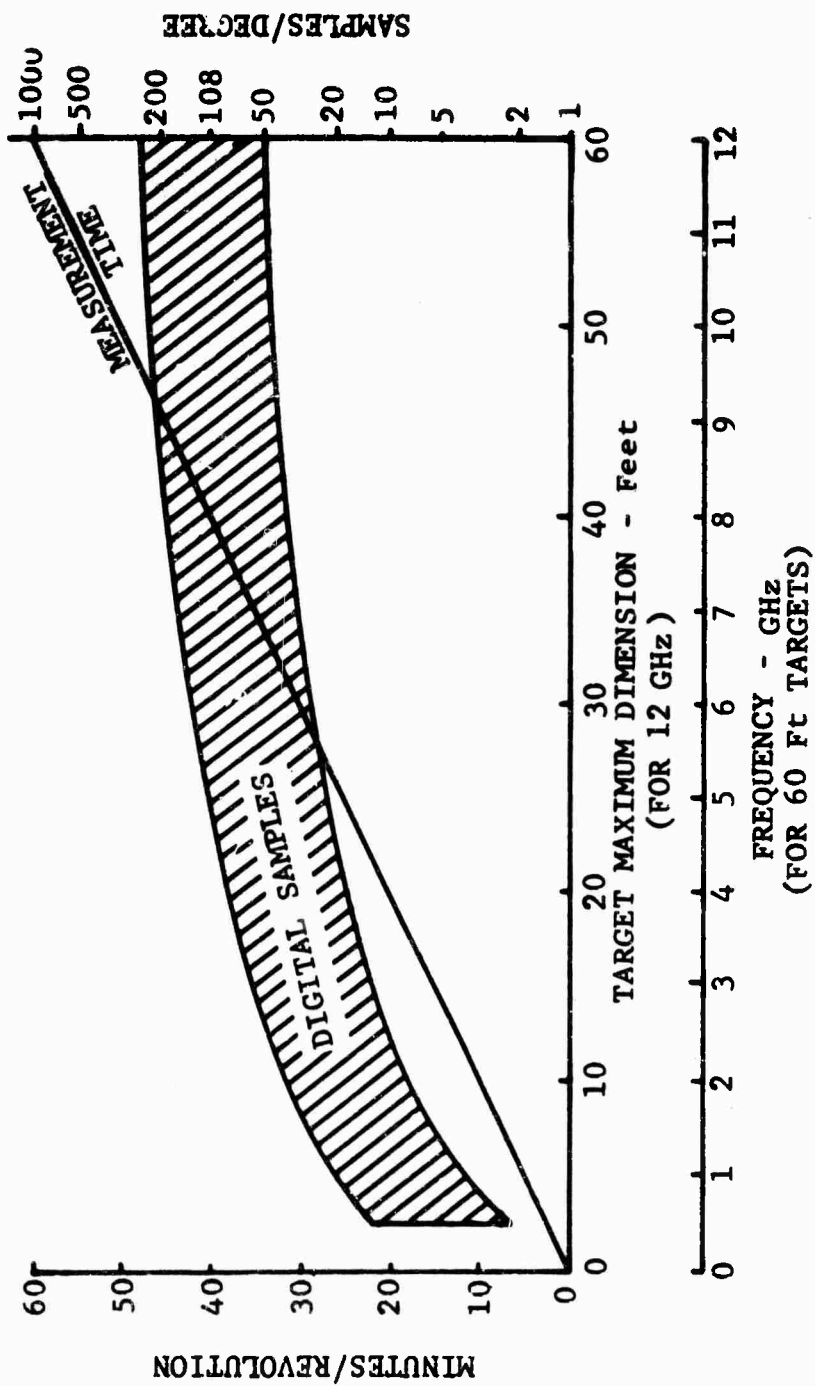


Fig. 1.2-29 DATA RATE AND INTERVAL

1.3 Antenna Far-Field Simulation

1.3.1 General

The approach to providing a technique for the measurement of large targets by antenna far-field simulation is based on the use of a polyfoam lens between the antenna system and the target in order to improve the field pattern in the vicinity of the target (Reference 9 and 10). The primary requirement associated with the technique is that of providing a horizontal plane phase gradient equivalent to that encountered in the case of a range length of $2D^2/\lambda$. The primary features of interest are (1) correction efficacy, (2) lens backscatter levels, (3) lens tolerance requirements, and (4) operational features. These items and other are discussed in the following paragraphs.

This approach to the measurement of large objects proved to be the most cost effective in Band 6 (4 to 8 gigahertz) in the case of target lengths from 40 to 60 feet, and in Band 7 (8 to 12 gigahertz) in the case of targets 30 to 60 feet in length. The primary advantages lies in the reduction of range length and associated costs. The primary disadvantage is that of the lens set up time.

1.3.2 Basic Design

The design of the dielectric lens is established on the basis of the provision of an adequately small phase gradient in the vicinity of the target. The design of the dielectric lens is based on ray tracing, rather than on the complex and intractable boundary value problem, and the results obtained in practice indicate that this design approach is accurate (References 9 and 10). The size of the lens is a function of the antenna system used and the design target size since the rays from the antenna which intercept the target must pass through the lens. This situation can be easily met in the horizontal plane, but some consideration of additional parameters is required in the case of the vertical plane on a ground plane range. These requirements are discussed in paragraph 1.3.4 under physical properties.

The common lens design is contingent on placing the target in close proximity to the lens and on placing the lens a suitable distance from the antenna so that a spherical wave front appears at the lens. This latter approximation is generally good and more than adequate in the case of the geometry envisioned for RAT SCAT operations. The lens design commonly provides for complete correction of the phase front at the target, in addition to collimation. In view of the size of targets in this study and the corresponding operational problems encountered with a lens of comparable size, an examination of means of achieving adequate phase correction without complete collimation of the field at an exit plane of the lens is indicated. In addition, consideration should be given to the effects of a particular design on the backscatter level of the lens.

The effect of utilizing the lens can be described on the basis of Huygens principle as follows. The antenna is considered a point source so that the wave front incident on the lens is spherical. The lens corrects the phase and direction of the incident wave rays to produce an essentially collimated plane wave at the target. On the basis of Huygens principle, each incremental unit of surface acts as a point source and upon excitation by the incident wave will produce a spherical wave. An analysis of the resultant of these waves in the vicinity of the target will show that the well-known near-field pattern is obtained. However, on the basis of the model described, the resultant at the antenna is not influenced by near-field effects because only one ray path from each surface "source" will arrive at the receiving antenna. Thus, while the illumination of the lens via the target will be characterized by the normal near-field pattern, the overall result of the lens correction, except for lens anomalies, will be the far-field pattern of the target at the antenna.

The basic design selected for the lens consists of a two sided convex surface (see Figure 1.3-1) with a surface function. This basic design is selected instead of a single surface because of the following advantages:

1. More flexibility in design
2. Reduced radar cross section
3. Reduced weight
4. Reduced wind loading.

All of these advantages accrue as a result of eliminating the plane exit surface.

As previously indicated, the primary features of interest in the effects of the lens are those of phase correction and the additional consideration that a degree of collimation is desired. The limited degree of collimation required enhances the utility of a lens; e.g., at $2 D^2/\lambda$ a one-way phase variation of 22.5° appears at the target extremes.

The rigorous requirements for lens surface contours of this type are more complicated than those for the single-surface lens since refraction occurs at two surfaces. However, accurate approximations are available for reducing the analytical problems. The parameters of the analysis can be limited to those associated with the angles θ , τ , and ρ and the appropriate path length. (Figure 1.3-1). By the use of Snell's law, the equation governing the antenna side surface is given by

$$\frac{1}{R} \frac{dR}{d\theta} = \frac{n \sin(\theta - \tau)}{n \cos(\theta - \tau) - 1} \quad (1.3-1)$$

After integration, by using the special case of τ as a constant and imposing the boundary condition, $R = R_0 - T$ when $\theta = \tau = 0$,

$$R = \frac{(R_0 - T) (n \cos \tau - 1)}{n \cos (\theta - \tau) - 1} \quad (1.3-2)$$

For the case of $\tau = 0$, Equation 1.3-2 becomes the expression for the single curved surface lens (Reference 9) which is presently being used at the Fort Worth Division range (Reference 10).

In the case of the double curved surface lens, it is necessary to make τ a function of θ in order to achieve the proper results, in terms of a requirement for collimation or a requirement for a given wave divergence at the exit of the

lens. In this case, it is convenient to write Equation 1.3-1 as

$$\frac{1}{R} \frac{dR}{d\theta} = \frac{n \sin [\theta(1-a)]}{n \cos [\theta(1-a)] - 1} \quad (1.3-3)$$

where τ has been replaced by $a\theta$.

The general solution of Equation 1.3-3 is given by

$$\ln R = \frac{-1}{(1-a)} \ln \left\{ n \cos [\theta(1-a)] \right\} + \text{const.} \quad (1.3-4)$$

Given the geometrical boundary condition, $R = R_0 - T$ when $\theta = 0$.

$$\ln \frac{R}{R_0 - T} = \frac{1}{1-a} \ln \frac{n-1}{n \cos [\theta(1-a)] - 1} \quad (1.3-5)$$

and since $R_0 - T \approx R$ and $\theta(1-a)$ is small, Equation 1.3-5 can be accurately approximated by

$$R = \frac{(R_0 - T)}{(1-a)} \frac{n-1}{n \cos [\theta(1-a)] - 1} \quad (1.3-6)$$

The selection of the value of a will determine the degree of collimation and phase correction exhibited by the lens. A higher order of the τ dependence on θ can be selected, but a satisfactory power density uniformity can be realized in the simple relationship selected. The most reasonable practical approach appears to be that of providing the same curvature on both lens surfaces but additional flexibility can be obtained by providing a different function on the two sides. From the geometry of the lens shown in Figure 1.3-1, the exit angle is obtained by using Snell's law through the relationship,

$$\rho \approx n\tau - (n-1)(\pi/2 + \theta) \quad (1.3-7)$$

where the approximation is based on $n \sin \gamma \approx \sin n\gamma$, which is valid over a much wider region than $n \sin \gamma \approx n\gamma$. Also, ϕ is given by $\tan^{-1}(dx/dy)$ at the position of interest.

The remaining condition requiring consideration is that of the phase correction introduced by the lens. As shown in the geometry of Figure 1.3-1, the condition for phase correction at the plane $y = T'$ is given by

$$R + n\Delta + (T + T' - y)\sec\phi = R_0 + T' + T(2n - 1) \quad (1.3-8)$$

where the x and y correspond to points on the exit surface.

On the basis of the foregoing equation, the properties of the lens can be defined to an arbitrarily high accuracy, but in order to examine the properties of the lens by using equations in closed and more tractable form, it is convenient to simplify these equations through the use of approximations. The approximations used in this context are considered valid in the range of geometries under consideration in the large-object study and are based on (1) placing the lens at a reasonable range, expected to be much greater than 2000 feet, and (2) the choice of a lens material whose refractive index is near one. The significance of the range in this case is a result of the angle of incidence of the energy from the antenna; the worst-case range cited above for a 60-foot target will result in a ray divergence of only 0.03 radian. In addition, it will be evident that, in practical cases, the lens thickness will be much less than the range length.

On the basis of these approximations, Equation 1.3-6 can be reduced to the convenient form in rectangular coordinates

$$x^2 = 2(n - 1) [y^2 + R_0y - T^2 + R_0T]/(1 - a), \quad -T \leq y \leq 0 \quad (1.3-9)$$

and, by using a symmetrical lens configuration, to the form

$$x^2 = 2(n - 1) [y^2 - R_0y - T^2 + R_0T]/(1 - a), \quad 0 \leq y \leq T \quad (1.3-10)$$

It can be seen that the form of the single surface collimating lens results if $a = 0$. (References 9 and 10). It can also be seen that the lens thickness is given by

$$T = \frac{D^2(1 - a)}{8 R_0(n - 1)} \quad (1.3-11)$$

Under the conditions of long range length cited above, it is apparent that the lens will not exhibit much curvature and that an approximately linear relationship will exist between the ray incidence angle at the lens surface, inside the lens, and at the lens exit surface so that a correction of approximately $\theta/2$ can be expected at each surface in the case of a collimating lens. In this case, $a \approx 0.5$ and the overall lens thickness, given by $2T$, will be approximately equal to that of the single curved surface lens. However, a significant reduction in mass will be realized because of the reduction of the material along the edge of the lens.

Equations 1.3-7, 1.3-9, and 1.3-10 can be used to obtain an accurate estimate of the lens properties relative to the basic design parameter a . The divergence of the exit rays, from Equation 1.3-7, can be written

$$\rho \approx \left[\frac{(n + 1)a - 1}{R_0} \right] (x) \quad (1.3-12)$$

where the angular approximation

$$\theta = x/R_0$$

has been used. In addition, it is assumed that the angles θ , ρ , and τ are small and no appreciable change in the angle occurs between the point a ray enters and leaves the lens. Similarly, it is evident that the divergence pattern represented by Equation 1.3-12 is equivalent to a range length of

$$R = \frac{R_0}{(n + 1)a - 1} \approx \frac{R_0}{2a - 1} \quad (1.3-13)$$

It can be seen from this equation that, when $a \approx 0.5$ (or $\gamma \approx 0.5 \theta$), the range approaches infinity, the condition previously suggested on an intuitive basis. Given this result, it is necessary to define the phase shift correction introduced by the lens in the vicinity of the exit surface of the lens in order to predict the phase pattern at the target. By using Equation 1.3-8, the phase ϕ of the wave at $y = T$ is given by

$$\phi/k_0 = R - R_0 - y(2n - 1) - 2T(n - 1) \quad (1.3-14)$$

where the y term defines the point at which a ray enters the lens (i.e., $-T \leq y \leq 0$) and, under the assumptions discussed above, Δ has been replaced by $-2y$. Since

$$R \approx R_0 + y + \frac{x^2}{2(R_0 + y)}$$

and

$$y \approx \frac{x^2(1 - a)}{2(n - 1)R_0} - T$$

from Equation 1.3-9, Equation 1.3-14 becomes

$$\frac{\phi}{k_0} = \frac{x^2}{2R_0} (2a - 1) \quad (1.3-15)$$

which is the common form for quadratic phase variation at a range of $R = R_0/(2a - 1)$.

Thus the effect of the lens is that of producing a wave front equivalent to a range of $R_0/(2a - 1)$ relative to the divergence pattern and the phase shift near the exit of the lens. The effective range to the target can be written $R_0/(2a - 1) + T'$, and this effective range can be equated to $2D^2/\lambda$ in the case of a particular target and frequency to obtain the required value of a .

The value of a is illustrated in Figure 1.3-2 for the case of a number of conditions based on obtaining a $2D^2/\lambda$ for a selected target length at 12 gigahertz. An examination of these data indicates that a small change in the value of a has a pronounced effect on the pattern produced by the lens, or conversely, a large degree of flexibility in the use of a given lens can be obtained by the simple expedient of varying the measurement range configuration. Other parameters of interest in the design of a dielectric lens include size, weight, and radar backscatter.

1.3.3 Radar Cross Section

The radar cross section of the lens can be a significant feature in terms of a source of an extraneous signal which can introduce coherent interference. If the strength of this extraneous signal, relative to the target signal, is excessive, an error in the target signal measurement will result. The relative signal level between the lens backscatter and the target backscatter is effectively dependent on (1) the cross section levels of the two scatterers, (2) the relative range to each scatterer and (3) the isolation capability of the radar system. The isolation feature of primary interest is that of range gating the target.

Successive approximations were used to demonstrate that the maximum lens cross section level (X-band) is on the order of 50 dBsm, a value which indicates that the equipment isolation must be on the order of 90 dB. The evaluation of the isolation capability of the appropriate equipment is not amenable to theoretical analysis and therefore was accomplished on the basis of data obtained from the experimental measurements.

Data obtained at RAT SCAT indicated that two signal levels in essentially adjacent range bins (500 foot separation) will not interact to a measurable degree when the relative signal strength between the two signals is in excess of 80 dB. This situation was simulated at the RAT SCAT site by providing a closed loop (antennas bypassed) 1-microsecond signal followed by 1-microsecond signal with an amplitude of 80 dB below the first. These signal levels essentially encompassed the receiver

saturation level and noise levels which is a worst case situation. It is, therefore, concluded that the recovery time of the RAT SCAT system is such that no isolation problem would exist.

No approach to lens design has revealed a method of providing broadband radar cross section reduction.

1.3.4 Lens Physical Properties

The primary physical properties of interest in the use and design of the lens are the size and weight. A significant influence of these features is the choice of the dielectric constant of the material although this choice is not critical for reasonable values thereof. The dielectric constant of the material is approximately proportional to the material density, and the volume under a given range condition is approximately inversely proportional to the dielectric constant because of the increased thickness required. From the viewpoint of structural strength, including susceptibility to accidental damage, the density of the material should be about 3 pounds per cubic foot. This value will result in a refractive index in the vicinity of 1.05 which is a practical value from the viewpoint of other lens properties; in addition, in this range such properties as weight, radar cross section, and construction tolerances are not critical in terms of the value selected. From the viewpoint of fabrication problems, a material whose density is in this vicinity is readily machinable and there is no severe handling problem.

Representative data on the weight and thickness expected can be found in Figures 1.3-3 through 1.3-5. There is no severe problem in selecting a manageable design from the viewpoint of weight and size although handling requirements will be similar to those for a large target. The data shown in these figures are based on the analysis presented in paragraph 1.3.2. In Figure 1.3-3, the lens width is displayed as a function of the antenna-to-lens and lens-to-target ranges. The lens width requirement is based on the geometrical relationship given by

$$W = \frac{R_0 D}{R_0 + T'} \quad (1.3-16)$$

where W is lens width, R_0 is the lens to antenna range length, T' is the lens-to-target range length, and D is the target length.

In Figure 1.3-4, the lens thickness is illustrated as a function of the same range parameters. On the basis of a density of 3 pounds per cubic foot, the weight of the lens resulting from the choice of various parameters is shown in Figure 1.3-5. It can be seen from these data that there is no critical region in the physical design parameters of the dielectric lens and that a reasonable size and weight can be realized.

A significant aspect of the use of the lens configuration of interest is that of wind loading. This feature will limit the operational utility and requires the use of a shelter when not in use. The problem is not considered to be severe because (1) the utilization rate is expected to be low, (2) quiet wind periods are common and (3) the prevalent wind direction under the anticipated range geometry is in a direction such that the primary wind loading is along the longitudinal axis of the lens. An estimate of wind loading magnitude is shown in the case of broadside and end-on wind loading in Figure 1.3-6. These data are based on an equation (Reference 11) of the wind force

$$W = CqA \quad (1.3-17)$$

where

V = wind velocity in miles per hour

$p = 0.002378 \text{ lb sec}^2/\text{ft}^4$

A = the effective area

C = shape factor

$q = 0.002558 V^2$

This worst case situation of a 63 by 10 foot lens (refer to Figure 1.3-6) was computed by using coefficient of 1.5 and 0.5 for the broadside and end-on cases which appear to be somewhat excessive in this case. The computed dates indicates that the end on loading will not introduce severe problems over a wide range of wind velocity, but the broadside case is clearly excessive. The mounting and guy line arrangement expected to be used with the lens (refer to subsection 3.3) and the quiet wind periods in the RAT SCAT area are expected to allow a reasonable lens utilization rate.

Since the size of the lens is dependent on the target-lens separation, it is necessary to consider the electrical effects of this separation. In Figure 1.3-7, a set of contours is presented which represent the amplitude variation in the near field of a uniformly illuminated aperture (Reference 12). These data are shown in terms of the contours normal and parallel to the axis of the aperture and are also normalized in aperture widths. The effective aperture of interest in the lens application is the horizontal plane lobe width - range length product in the lens vicinity. This beam width can be approximated by $1.6 \lambda / d$ where d is the antenna dish diameter. In the worst case of a 21,000 foot range length (refer to paragraph 1.3.6) and a 6 foot antenna at X-Band, the effective aperture width is 470 feet. In terms of the worst case target length of 60 feet, the region of interest is in 0.13 apertures normal and parallel to the axis of the effective aperture. The data in Figure 1.3-7 indicates that the region of these dimensions, where the amplitude gradients are insignificant, will exist over a wide region along the axis of the lens. In terms of the amplitude levels, losses appear to become excessive at a distance of greater than 1.4 apertures (660 feet). Thus it appears that no problem will arise from field gradients in the near field region in this application. This region is compatible with the system recovery time requirements of a lens-target separation of about 600 feet (refer to paragraph 1.3.3). On the basis of the above discussion, the recommended target lens separation is 600 feet. It is of interest to note that excessive phase variations appear at a distance along the aperture axis at about 2 apertures (Reference 12).

Tests using the Fort Worth Division Dielectric lens have demonstrated the correction of a basic lens (Reference 10). An example of the phase correction efficiency of the subject lens is presented in Figure 1.3-8. These data are indicative of the extreme correction available using a dielectric lens.

Restrictions on the utilization of the range of lens physical properties described above include the accuracies required in construction tolerances (paragraph 1.3.5) and the requirements for lens height which result from the generation of the typical groundplane range field pattern in the vertical plane.

The lens height limitation can be examined on the basis of the geometry in Figure 1.3-9. A limitation is imposed only when the antenna height (h_a) is greater than the target height (h_t). From this figure, it can be seen that in the case of a total range length of $R_0 + T'$ and a target radius of a , the upper (h_2) and lower (h_1) bounds of the lens can be expressed in terms of the geometry to obtain

$$h_2 - h_1 = 2a + \lambda T' / (2h_t) \quad (1.3-18)$$

It can be seen that the lens height is independent of target height except through the familiar relation $h_{\text{ant}} = \lambda(R_0 + T')/4$. The data shown in Figure 1.3-9 are based on the use of Equation 1.3-7, a target radius of 4 feet, a target height of 12 feet, and selected values of T' . A range geometry feature of interest in interpreting the data in Figure 1.3-10 and the trade-off study is shown in Figure 1.3-11. In this figure, the minimum operating frequency available for the case of a selected fixed range is shown in terms of a family of curves based on selected values of the product of the antenna height and the target height. On the basis of the target to lens separation required using the aperture model and height model, it is necessary to obviate any further consideration of reducing the width of the lens by increasing the lens to target separation.

1.3.5 Lens Tolerance Requirements

The requirement for mechanical accuracy in the fabrication of a dielectric lens is expected to be a significant parameter in the initial cost of such a lens. A number of criteria can be used to form a practical basis for establishing the lens tolerance requirements. The primary feature of interest in the use of a lens is the phase illumination pattern in the vicinity of the target since the low loss and short-path length through the lens introduce negligible amplitude variation. It will be seen that the requirements for construction tolerance are severe as the refraction index of the lens materials is increased and that the distance separating the lens from the target can influence the tolerance limitation.

The model selected for evaluation the requirements for lens accuracy is based on a prediction of the backscatter from a target with an infinite radius of curvature (e.g., flat plate or cylinder) and a regular deviation of the lens surface from the

true value. The regular surface variation, i.e., the lens thickness variation, was selected to be represented by a circular function to produce the form

$$T(x) = A \sin(Bx) \quad (1.3-19)$$

where the A is the peak amplitude variation and the B represents the periodicity of the variation.

When Huygen's principle is applied, the error resulting from the phase illumination pattern is given by

$$E = \frac{1}{L^2} \left| \int_{-\frac{L}{2}}^{\frac{L}{2}} e^{i2kAT(n-1)x} dx \right|^2 \quad (1.3-20)$$

where L is the length of the line scatterer and x is measured along L. Equation 1.3-20 can be evaluated by means of the substitution,

$\theta = Bx$, to obtain

$$E = \frac{1}{L^2} \left[\frac{1}{B} \int_0^\pi 2 \cos [2kA(n-1) \cos \theta] d\theta + \frac{1}{B} \int_0^{(m-1)\pi} 2 \cos [2kA(n-1) \cos \theta] d\theta \right]^2 \quad (1.3-21)$$

where B is interpreted as $BL = 2M\pi$. This interpretation can be made without loss of generality if B is large enough to produce a large number of periods of the phase distribution over the length L. Then,

$$E = \frac{1}{L^2} \left[\frac{m}{LB} \int_0^\pi 2 \cos [2kA(n-1) \cos \theta] d\theta \right]^2 \quad (1.3-22)$$

or

$$E = \left| J_0 \left[2 k A (n - 1) \right] \right|^2 \quad (1.3-23)$$

where J_0 is the zero order Bessel function. In anticipation of the requirement for a small value of the J_0 argument in order to maintain small errors, Equation 1.3-23 can be accurately approximated by

$$E = \left[1 - k^2 A^2 (n - 1)^2 + 2 k^4 A^4 (n - 1)^4 \right]^2 \quad (1.3-24)$$

The evaluation of this expression is shown in Figure 1.3-12 in terms of the error introduced by a construction tolerance relative to $(n - 1)/\lambda$. This result is not sensitive to the analytical form selected for the fabrication variation. It can also be seen that the accuracy requirements are reduced by reducing the refractive index.

The foregoing analysis is based on placing the target in close proximity to the lens in that no consideration is given to the phase gradient introduced by a deviation of the waves from the usual path and the corresponding phase lag caused by increased path length. It is therefore necessary to consider a criterion based on variation in the slope of the lens surface in terms of the target-to-lens separation. If, as previously supposed, the surface variation is reasonably regular and small in effect, then the phase variation in the vicinity of the target resulting from slope variation is expected to be regular and produce an error of the same form. Because of the expected surface forming conditions and the range of target-to-lens distance of interest, this effect is not expected to be significant. However, a criterion can be established on the basis of the foregoing analysis by considering the path length error required to produce the same amount of phase shift encountered as a result of the variation in the path length through the lens.

On the basis of the geometrical considerations illustrated in Figure 1.3-13, the path length error R resulting from a deviation in the path direction is given by

$$\Delta R = \rho - T' \approx \frac{T'}{2} \sin^2 \alpha$$

where T' is the separation between the target and the lens and α is the ray path deviation. In the case of interest, the correct slope of the surface and the slope error (β) are small, and on this basis $\sin \gamma \approx \sin (n\beta)$ so that

$$\Delta R \approx \frac{T'}{2} \sin^2 [\beta(n - 1)] \quad (1.3-25)$$

The resulting maximum phase deviation is comparable to the variation resulting from the use of Equation 1.3-19 when

$$A = \frac{T'}{2} \sin^2 [\beta(n - 1)] \quad (1.3-26)$$

In Figure 1.3-14, the parameter A , representing the peak variation in the lens surface, is related to the equivalent slope variation for selected values of T' and for the case of $n = 1.05$. These data, along with those in Figure 1.3-12, can be used to define the desired slope limitation in the cases where a requirement for a large T' exists.

Another approach to the specification of lens tolerances is based on the requirements for phase measurement accuracy. In this case, the resultant requirements for lens tolerance are sensitive to the type of analytical model selected. In the analysis leading to Equation 1.3-24, it is clear that no phase measurement error will result although the amplitude measurement error can become excessive. However, in the case wherein a point scatterer is used for a reference, the maximum phase error is given by

$$\Delta \phi_{\max} = 2 kA \quad (1.3-27)$$

which is a severe restriction at high frequency in the range of phase accuracy commonly required. Of course, if use were made of the model described above for lens surface variation, the average phase error would be zero, and the rms error would

be 2 kA. Use of a model which contains a large number of contributing scatterers will also tend to reduce the net phase error, as in the case of the infinite radius of curvature target. This case appears to be the most appropriate to the large-object study; consequently, the lens tolerance requirements will be based on Equation 1.3-24 where the worst case will be taken to be the amplitude error resulting from the use of a target with an infinite radius of curvature.

The practicality of the lens-fabrication tolerance described above has been established through discussions with potential manufacturing firms and the fact that the design of the lens presently in use at the Fort Worth Division was based on a form of Equation 1.3-27 to produce a phase error of 2 degrees rms.

1.3.6 Equipment Requirements

The basic equipment components required in the antenna far field simulation method and similar to those required in one long range and high power approach except for the addition of the dielectric lens. The equipment description present in paragraph 1.2.6 is applicable to the individual items required except that the total sensitivity requirement is reduced by the use of this method.

The required components are presented in Table 1.3-1 along with cost information. These requirements are treated in more detail in the subsection 3.2.

Table 1.3-1 ANTENNA FAR FIELD SIMULATION
METHOD EQUIPMENTS *

Equipment	Area (1000 Dollars)
Dielectric lens	30
Lens Shelter	10
1 MHz Bandwidth IF	2.5
Band 6,7 - Phase Measurement	41
Band 6,7 - Coherent Integration	8.5
Band 7 - Low noise preamplifier	4.5
Roads and Signal Cables	72

*Facility equipments presented in Table 1.2-6 are applicable.

1.3.7 Conclusions

The conclusions reached in the investigation of the antenna far field simulation method as a potentially cost effective means of large object radar cross section measurements are delineated below in terms of the factors of (1) adaptability to field operations, (2) accuracy, and (3) cost.

The overall study results (subsection 2.5) indicate that this measurement approach is the most cost effective in the target length region between 30 and 60 feet in Band 7 (8 to 12 gigahertz, and 40 to 60 feet in Band 6 (4 to 8 gigahertz). As a result, detailed information associated with this method are presented in the recommendations section (Section 3).

1.3.7.1 Adaptability to Field Operations. The use of this technique duplicates the present RAT SCAT operation procedures except for the operations associated with the use of a dielectric lens. The incorporation of the lens introduces operational features such as additional set up time and potential problems in inclement weather. However, the study results indicate that these problems will be minimal inasmuch as sufficient time under good weather conditions is available and the emplacement of the lens introduces only a small additional cost because of increased measurement program range time.

1.3.7.2 Accuracy. The study results and the results obtained in other programs indicate that a lens design can be provided which will introduce negligible error (i.e., less than 0.5 dB. This factor, when weighed against the errors of potentially severe problem areas associated with other methods was the basic reason for selecting this technique for use in the large D^2/λ region.

1.3.7.3 Cost. The primary cost associated with implementation of this method are those associated with providing the required measurement sensitivity, the dielectric lens and the additional set up time required using the lens.

Other significant costs include roadway and signal and control cable cost which total \$2.5 per foot and are applicable over a range of length of 28,800 feet.

Details associated with the costs of implementing this method are presented in the recommendation section of this report (Section 3).

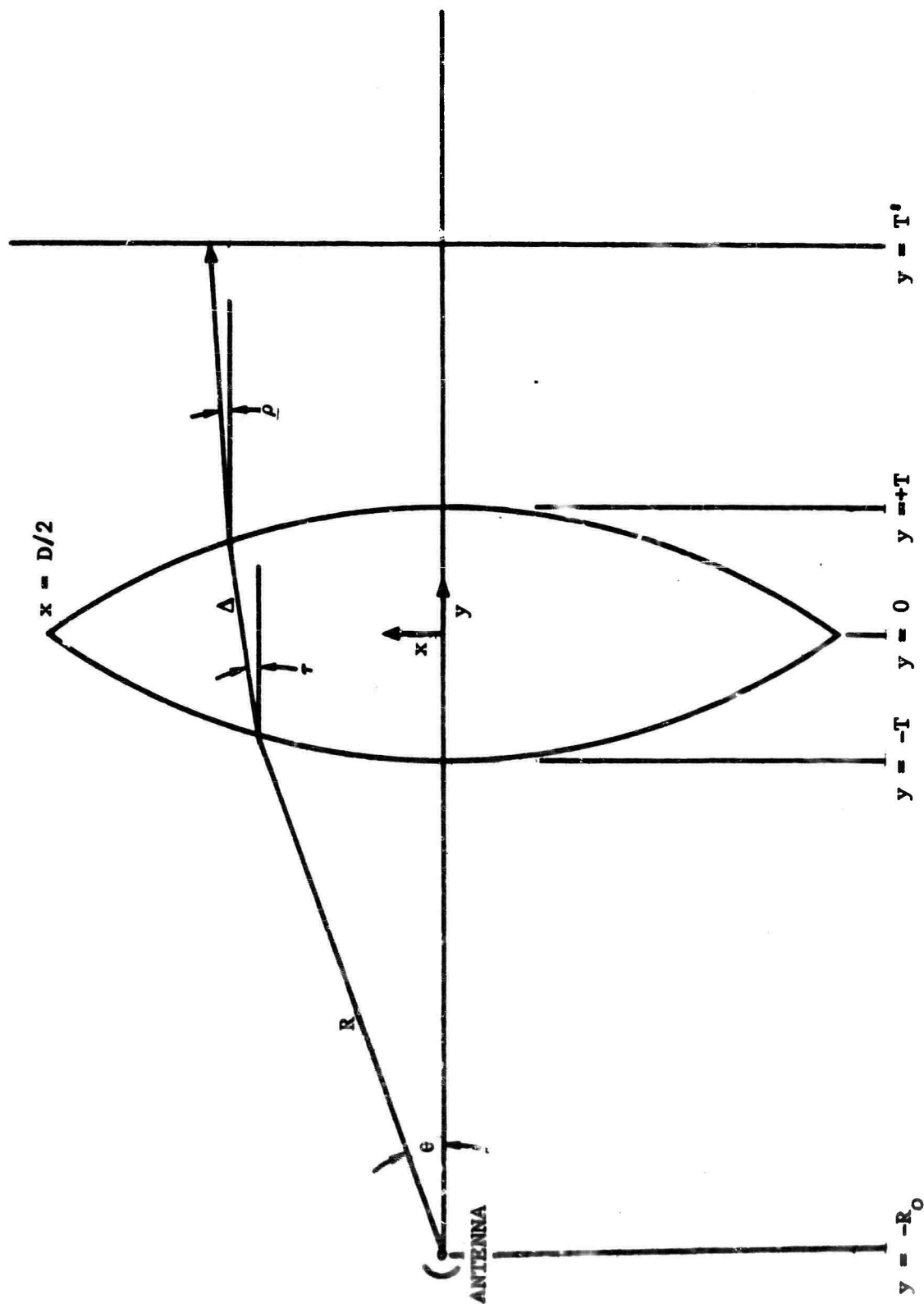


Fig. 1.3-1 DIELECTRIC LENS GEOMETRY

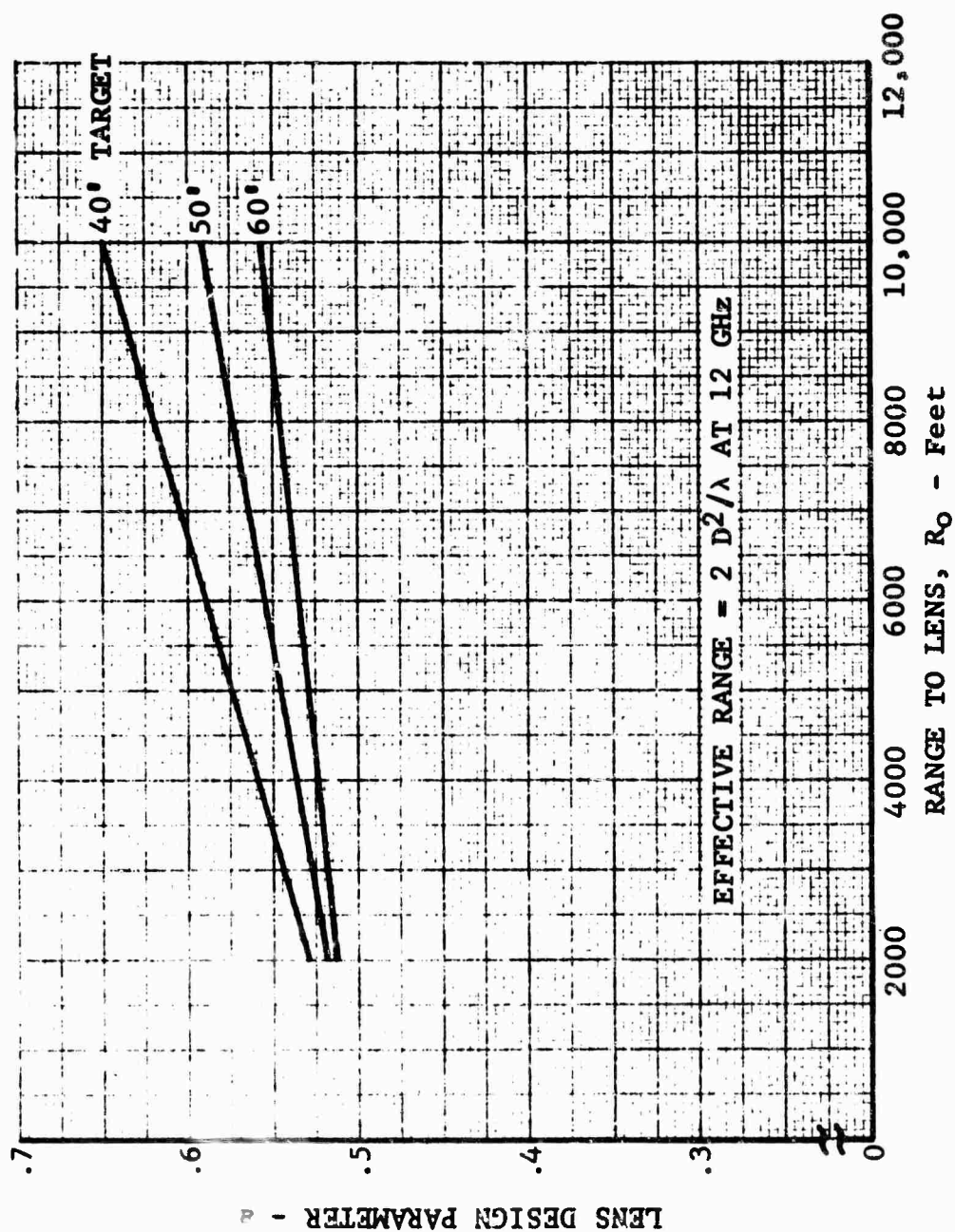


FIG. 1.3-2 DIELECTRIC LENS DESIGN PARAMETER

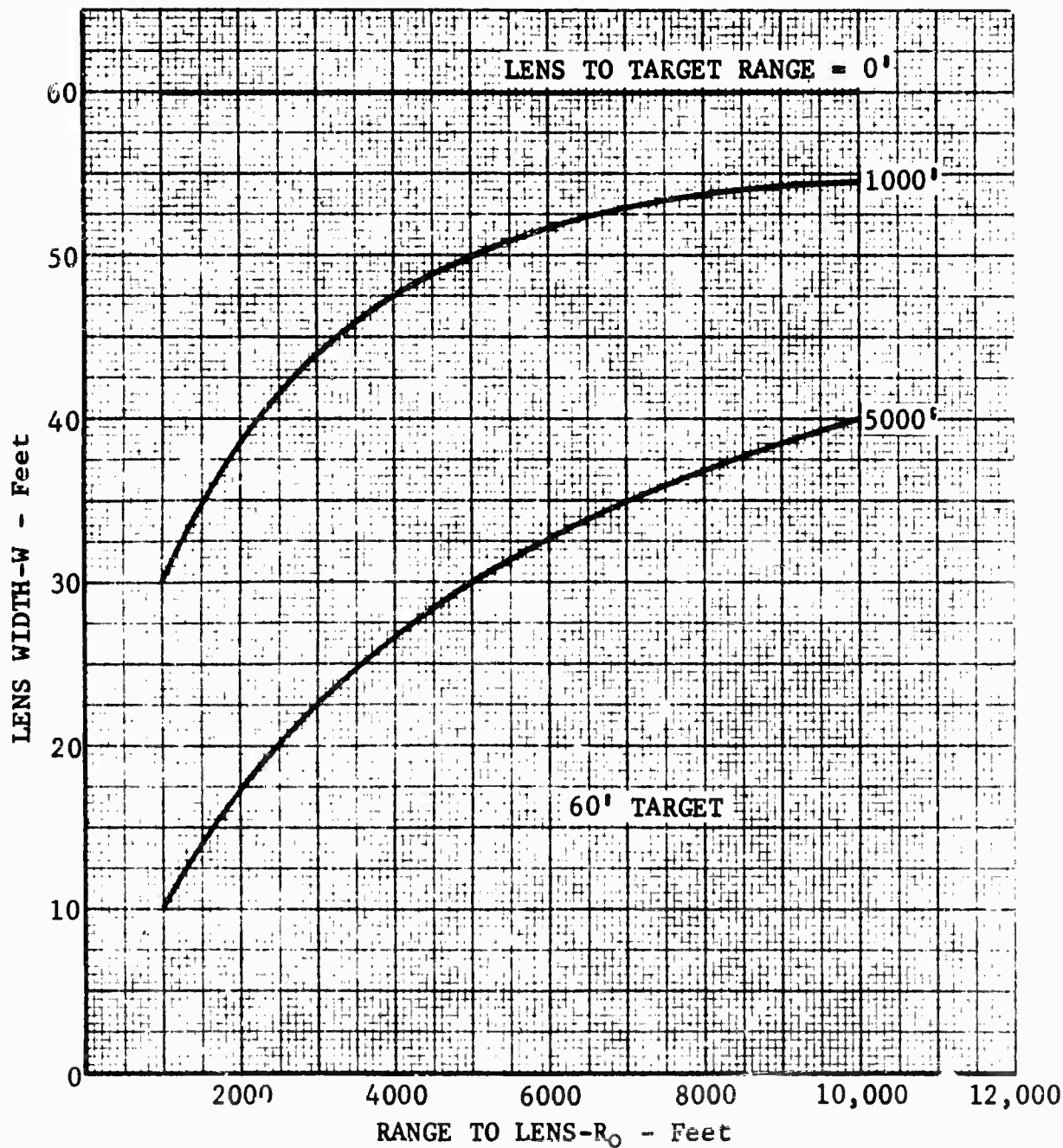


Fig. 1.3-3 LENS WIDTH REQUIREMENTS

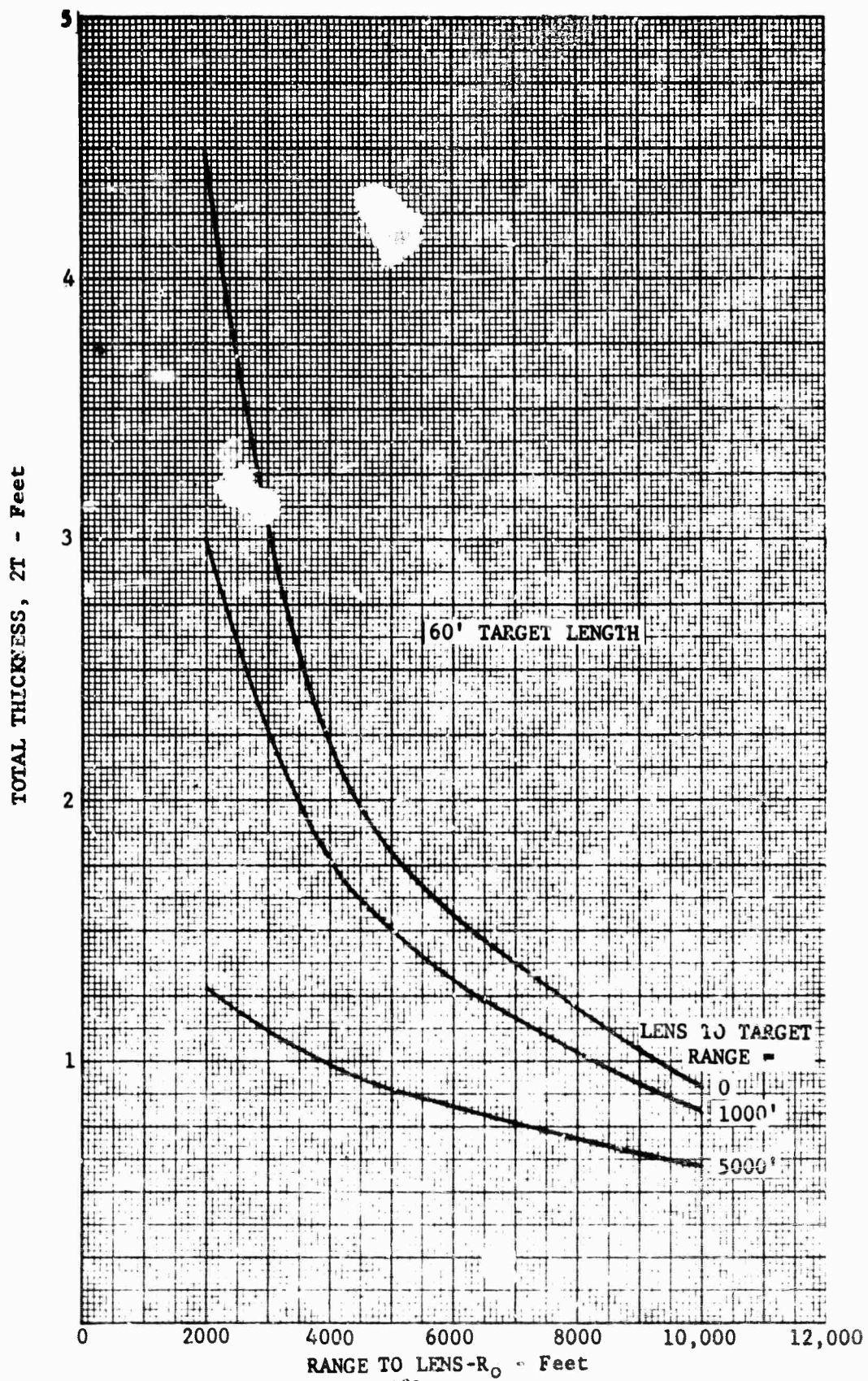


Fig. 1.3-4 ¹⁸⁰ LENS THICKNESS REQUIREMENTS

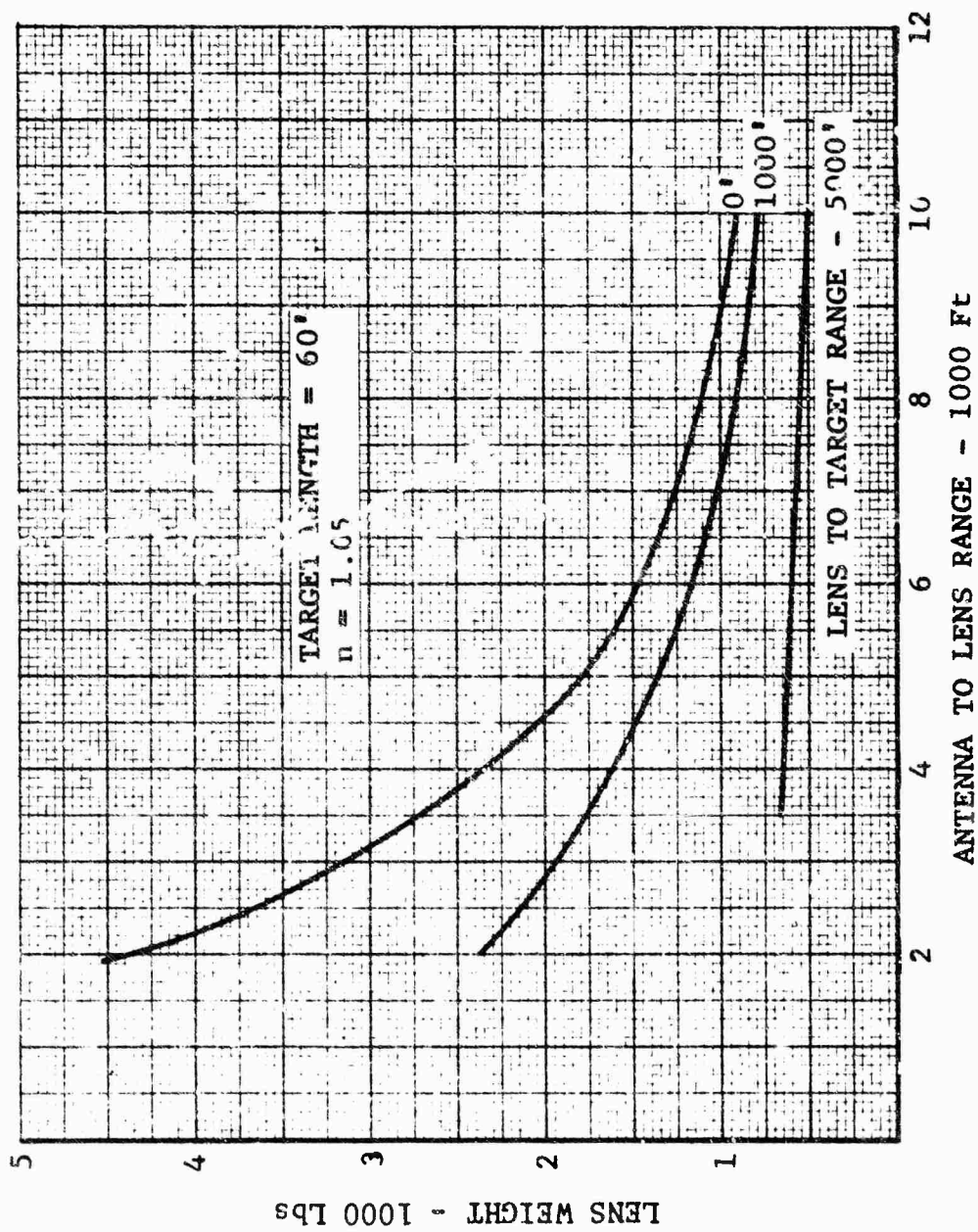


Fig. 1.3-5 WEIGHT OF DIELECTRIC LENS

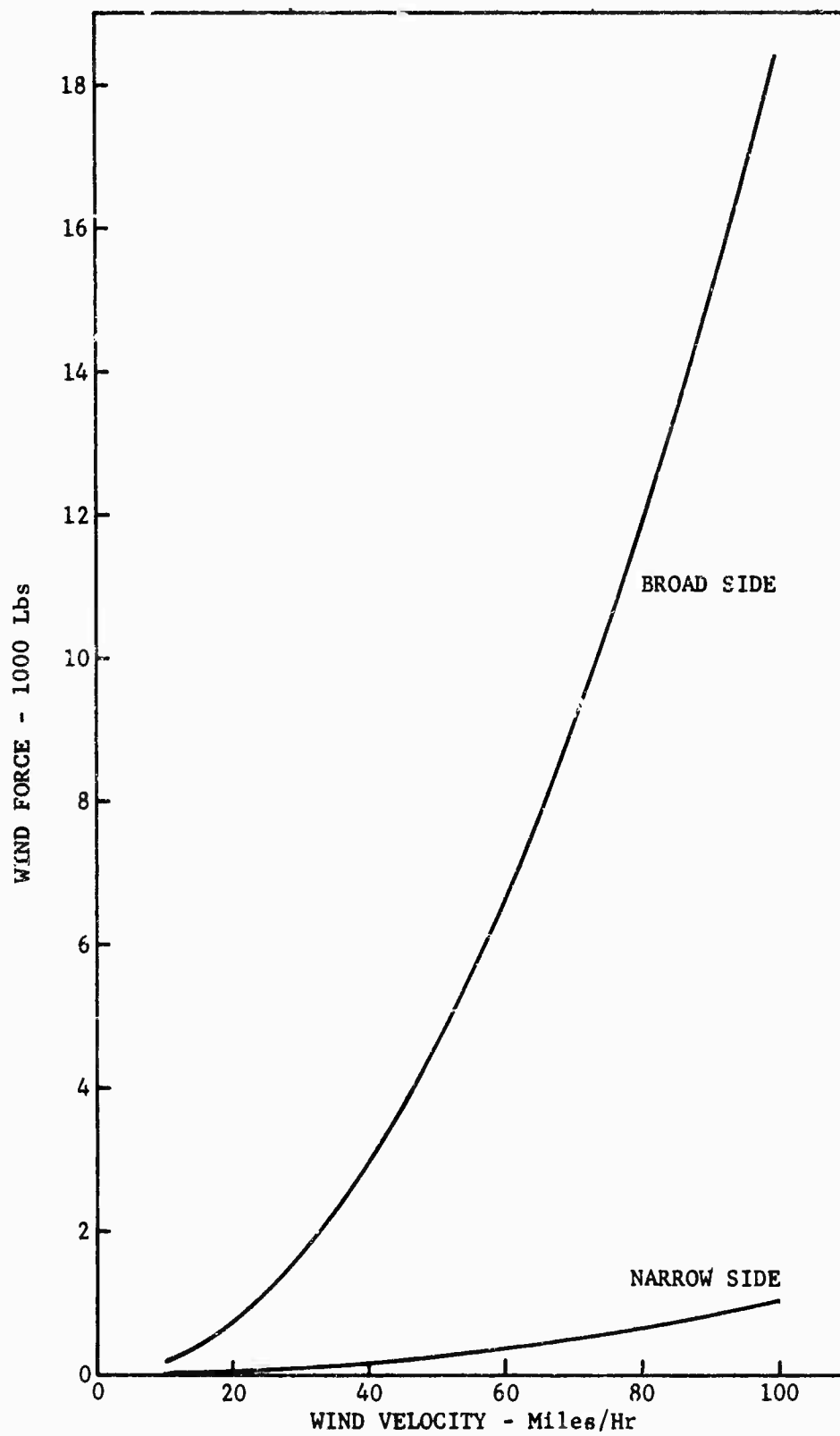
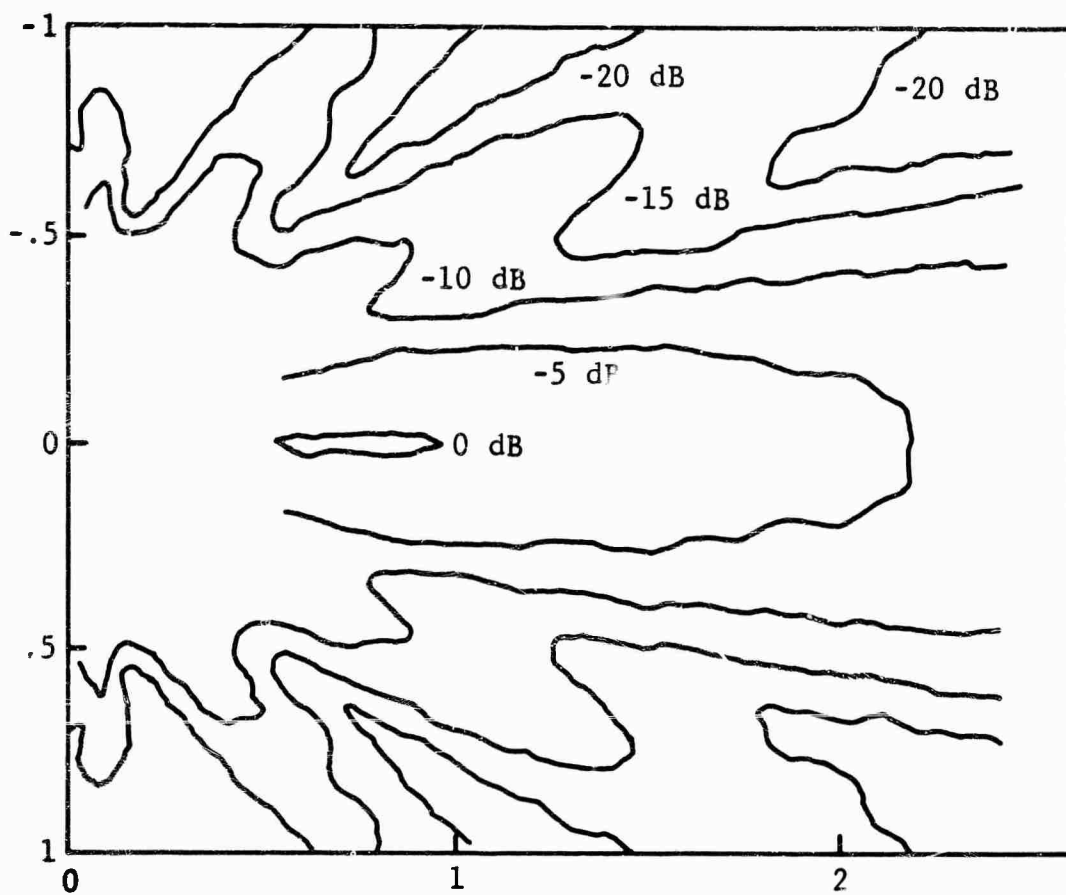


Fig. 1.3-6 LENS WIND LOADING

DISTANCE NORMAL TO APERTURE AXIS - Aperture Widths



DISTANCE ALONG APERTURE AXIS - Aperture Widths

Fig. 1.3-7 NEAR FIELD APERTURE PATTERN

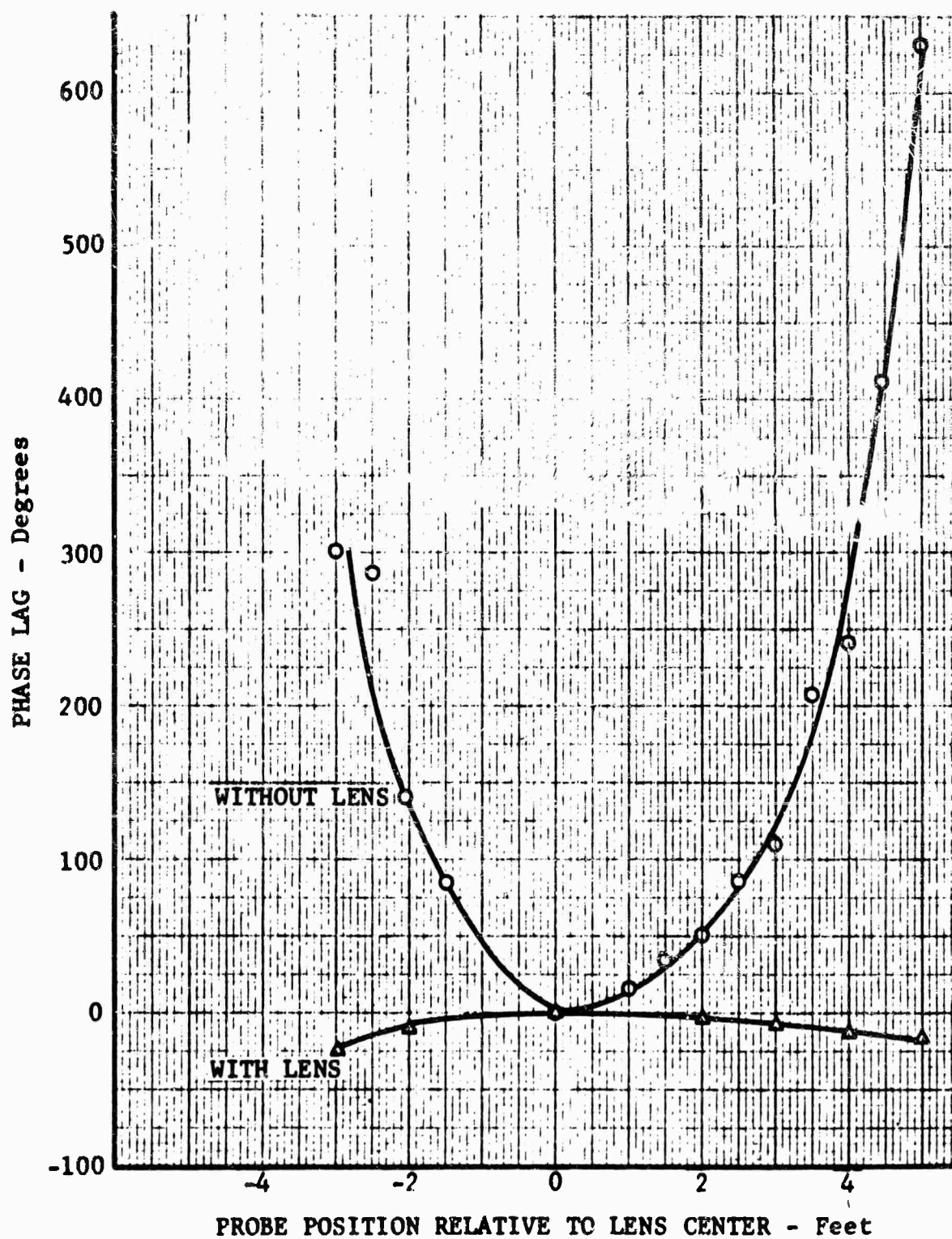


Fig. 1.3-8 DIELECTRIC LENS PHASE CONTOUR CORRECTION

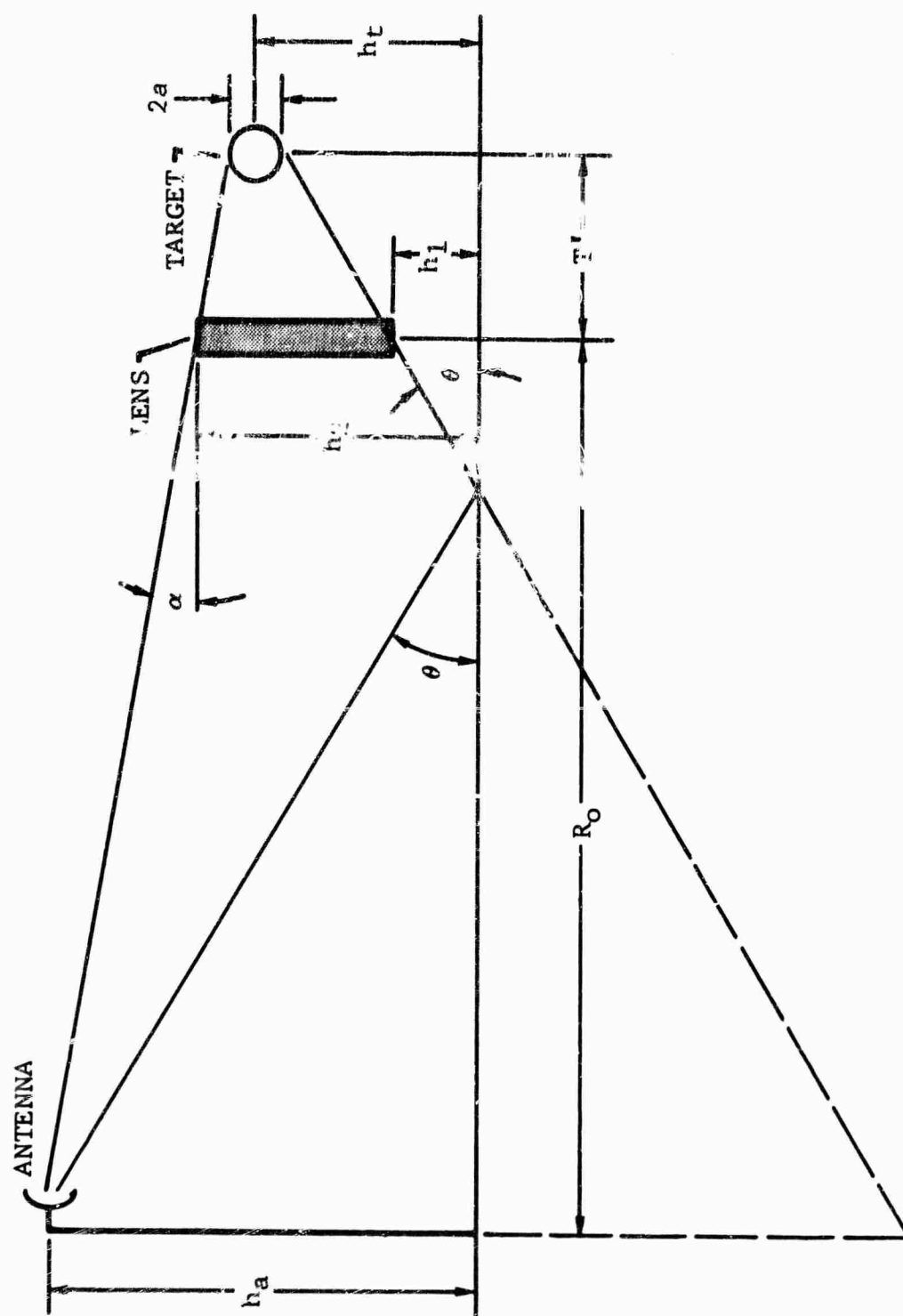


FIG. 1.3-9 RANGE GEOMETRY USING LENS

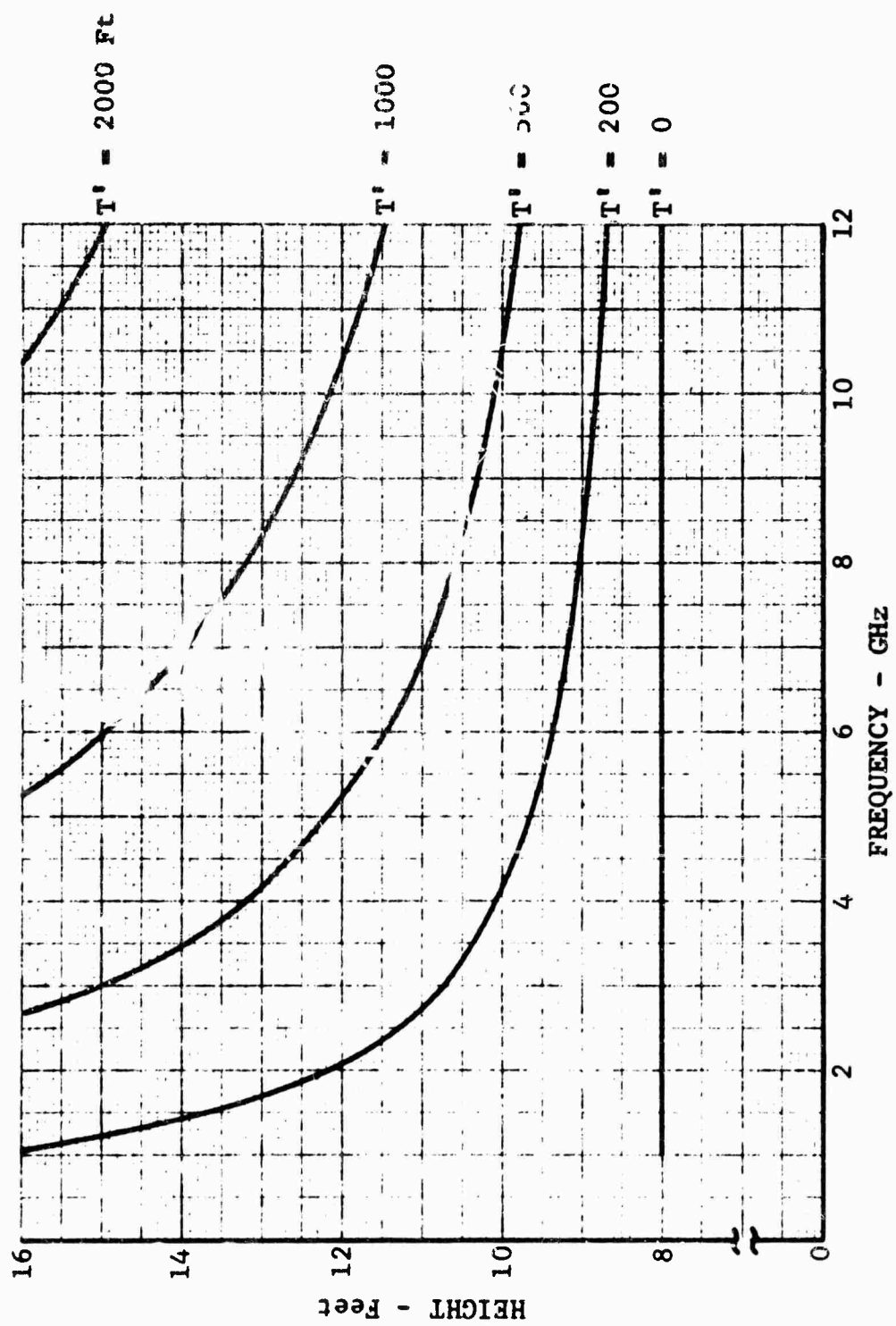


Fig. 1.3-10 LENS HEIGHT REQUIREMENTS

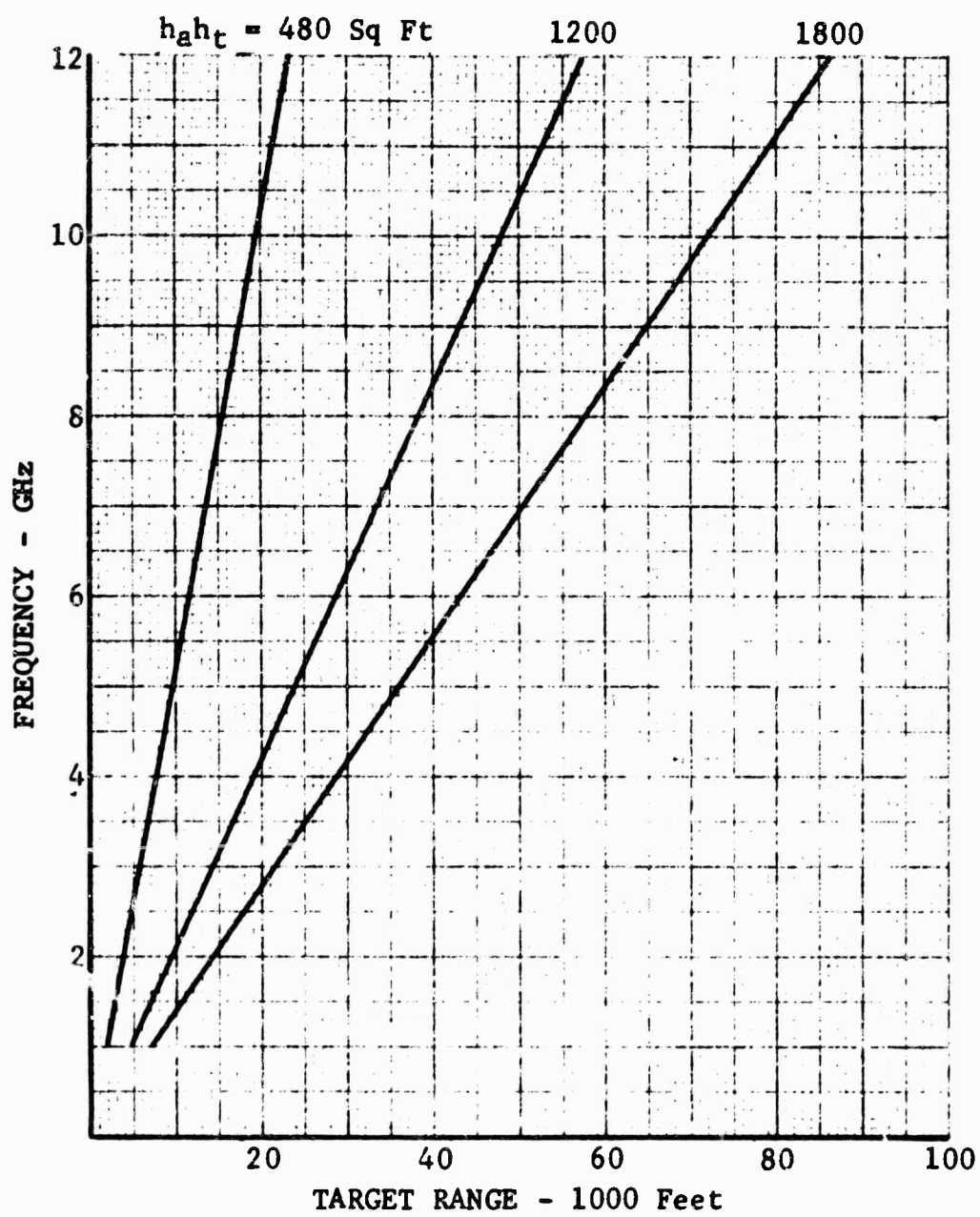


Fig. 1.3-11 FREQUENCY LIMITATION IN FIXED RANGE OPERATION USING LENS

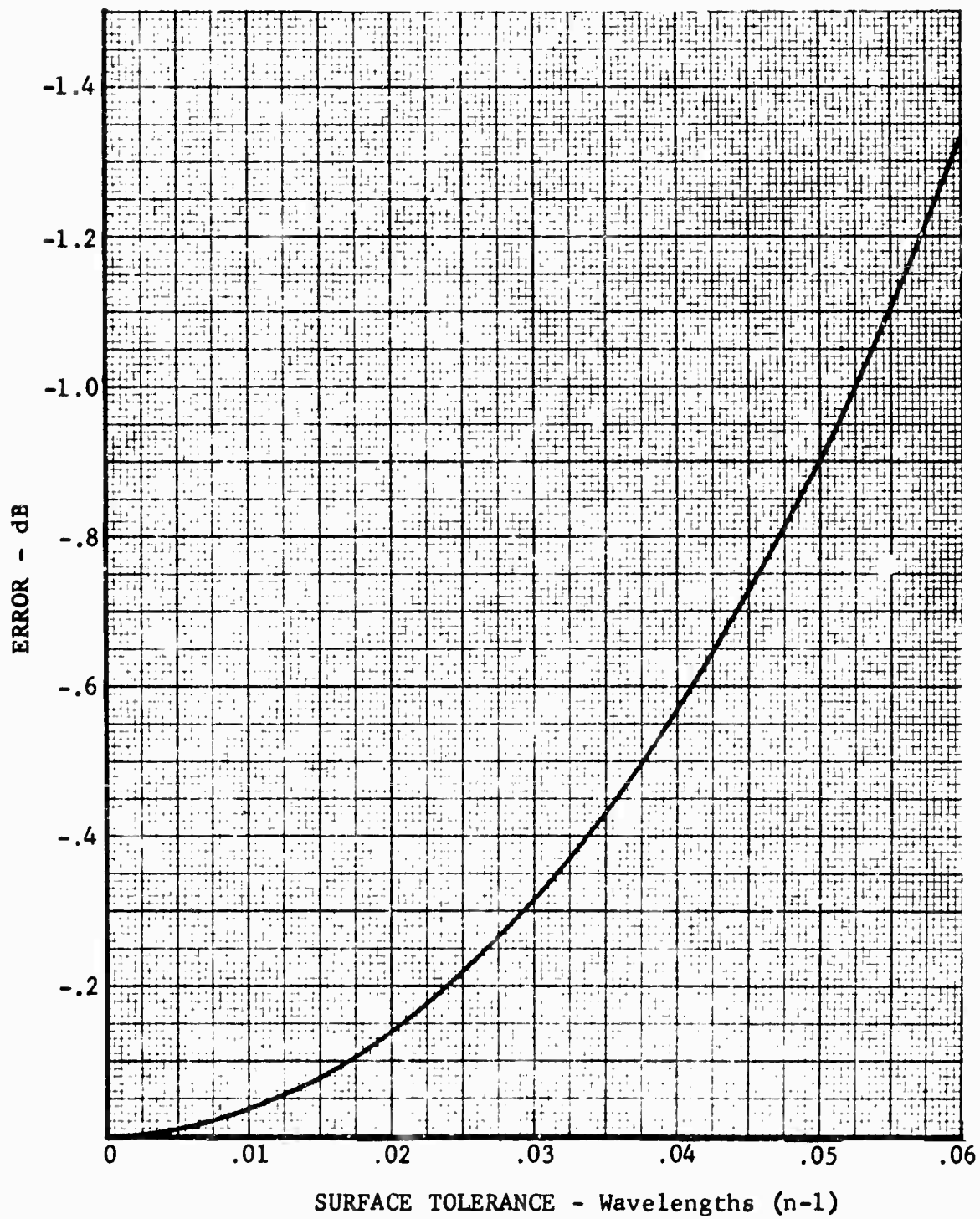


Fig. 1.3-12 LENS CONSTRUCTION TOLERANCE REQUIREMENTS

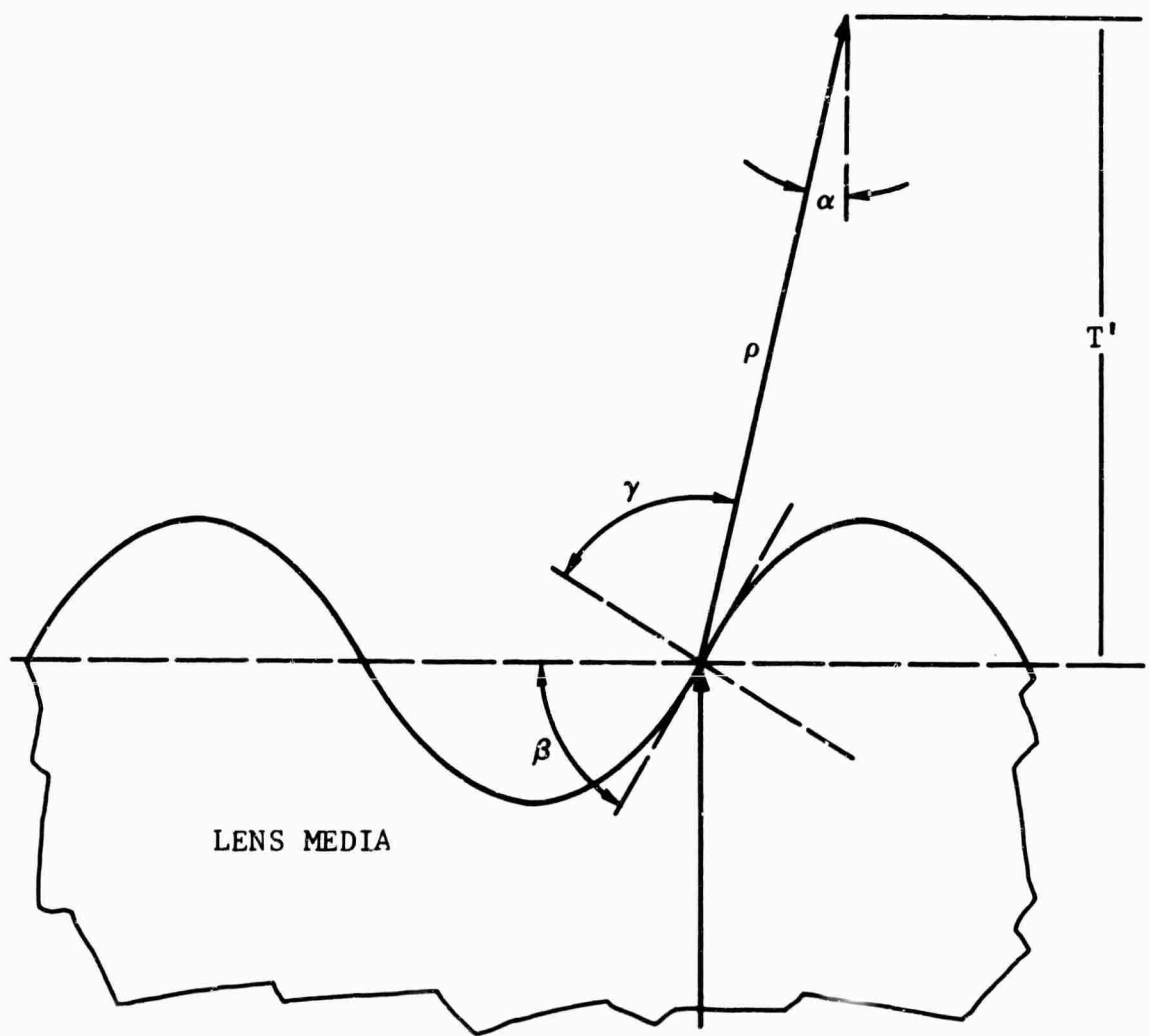


Fig. 1.3-13 LENS SURFACE VARIATION
GEOMETRY

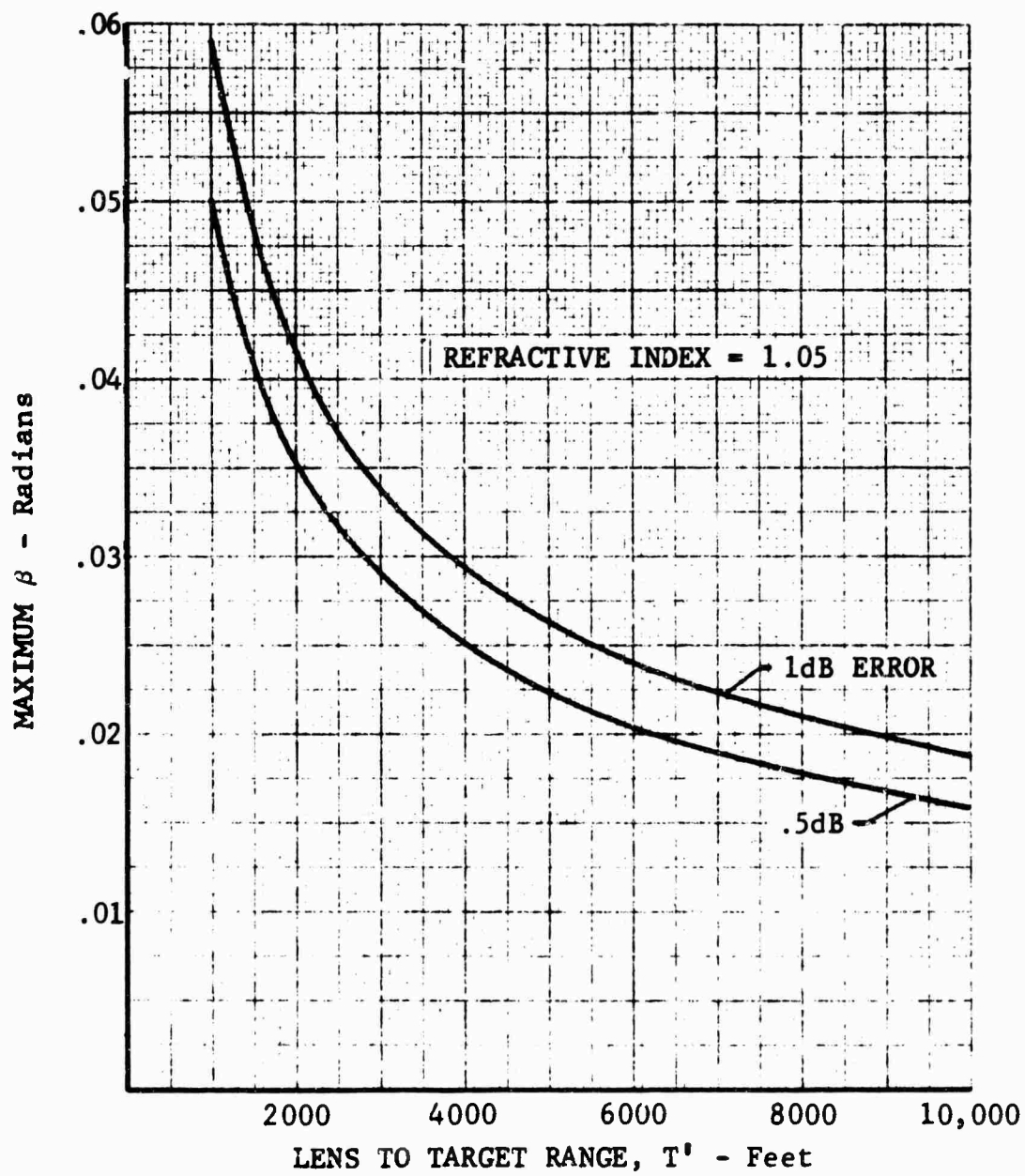


Fig. 1.3-14 LENS SURFACE VARIATION REQUIREMENTS

1.4 Analytical Correction of Near Field Data

1.4.1 General

A portion of the large object measurement study was oriented toward definition of the error forms resulting from measurements obtained in the near field and means of analytically reducing the resulting measurement errors. A detailed analysis of potential measurement errors caused by near field effects was made in terms of (1) the class of targets to be measured, (2) the antenna system, (3) the frequency range of interest, and (4) the anticipated range geometries. A general formulation of the near-field problem was implemented on the IBM 7090 digital computer and used to compute the near-field error related to selected targets, frequencies, and range geometries. The results obtained from these computations were used to assess the feasibility of analytically correcting measurement errors caused by measuring large targets at ranges less than the normally accepted values of $2D^2/\lambda$, where D is the maximum dimension of the target.

This technique was found to be unfeasible on the basis of the excessive error level and the erratic and unpredictable nature of the errors produced in the near field at ranges less than $2D^2/\lambda$. This degree of reduction was required in order for this approach to be competitive on a cost basis with other methods. Although the error levels defined in this study were excessive for the application defined herein, the levels were not as large as commonly expected. The most applicable region for use of this method is in Band 6, 40- to 60-foot target lengths. Details of significant features associated with this measurement method are presented in the following paragraphs.

1.4.2 Range Length Effects

The primary analysis of range length effects was based on the results obtained using a computer program written for use in calculating the error caused by near-field effects for the case of an elliptic cylinder. This program was used to obtain the data considered necessary for defining the representative measurements conditions encountered at RAT SCAT in measuring large targets. Four methods of computing the near-field error are included in the computer program to allow the error to be computed for the following cases:

- S₀ - Phase and amplitude curvature in the horizontal and vertical planes by using distributed antennas
- S₁ - Phase and amplitude curvature in the horizontal plane by using distributed antennas
- S₂ - Phase and amplitude curvature in the vertical plane by using distributed antennas
- S₃ - Phase and amplitude curvature in the vertical and horizontal planes by using point source antennas

These cases comprise the four subroutines used in the computer program. Appendix B contains a discussion of the basic equation from which the expressions used in the above four subroutines were derived. The basic computer program is illustrated in Figure 1.4-1 and the subroutines, along with the programmed equations, are presented in the appendix.

The input parameters indicated in Figure 1.4-1 are classified in terms of the part of the program quantities with which they are associated. The measurement condition parameters were defined above, the remaining parameters are defined below:

1. Target Size and Aspect

- L = Cylinder length in wavelengths
- θ_0 = Initial value in radians of the cylinder axis relative to broadside of $\theta_0 = 0$
- $\Delta\theta$ = Increment for stepping the cylinder aspect in radians
- N = Number of aspect increments
- A = Cylinder major axis in wavelengths
- B = Cylinder minor axis in wavelengths

2. Range and Antenna Geometry

- R₀ = Initial range to target in wavelengths
- β = Percent increase in range relative to R₀
- M = Number of range increases

- H_t = Height of beam maximum in wavelengths
- D_t = Transmit antenna diameter in wavelengths
- D_r = Receive antenna diameter in wavelengths
- α = Distance of target center below H_t in wavelengths.

The parameters were written in terms of wavelengths to obtain data which could be interpreted in terms of both target size and measurement frequency. The parameters and their values used in the various theoretical investigations of large objects are listed in Table 1.4-1 along with the subroutines which were used. As indicated in this table, the near-field error computer program was used to obtain data for use in the long-range and high-power study, as well as in the analytical correction investigation. To relate the normalized values of the problem parameters presented in Table 1.4-1 (target size, range length, target height, etc.) to frequency and dimensions in feet, the relationship plotted in Figure 1.4-2 can be used. For example, the value of A shown in Table 1.4-1 can be related to the cylinder radius (major axis) in feet with the aid of Figure 1.4-2 by selecting the frequency of interest.

Results obtained by using the values listed in Table 1.4-1 are plotted in Figures 1.4-3 through 1.4-14, for the case of the analytical correction study parameters. In Figures 1.4-3 through 1.4-10, cross section data is presented as a function of normalized range for the case of four aspect regions between broadside and 30 degrees from broadside. The data presented in Figures 1.4-3 through 1.4-6 are for the case of a 100λ length target at ranges of $\infty D^2/\lambda$, $3 D^2/\lambda$, $2 D^2/\lambda$, and D^2/λ . The data in Figures 1.4-7 through 1.4-10 are for the case of a 500λ length target at ranges of $\infty D^2/\lambda$, $5 D^2/\lambda$, and $4 D^2/\lambda$. The data in each of these figures was computed for the case of a point source, and as can be seen in the figures, the region of substantial error is the vicinity of the first side lobe. Except for this region (which corresponds to less than one percent of the aspects), the error incurred even at a range of D^2/λ is (on the average) quite small with the exception of the singularity points (nulls). Also, the feasibility of correcting these errors is questionable because of the fact that the errors introduced are not monotonic functions of aspect and range. In addition, the error is dependent upon the antenna size although in the case of large objects the antenna size will

Table 1.4-1 PARAMETER VALUES FOR NEAR FIELD ERROR PROGRAM

Computer Subroutine	Type Study	L	A	B	θ_o	$\Delta\theta$	N	R_o	β	M	Ht	Dt	Dr
S1 and S3	Analytical Correction	100	10	10	0	.025	50	10^4	1	3	20	10	10
			10	1	6.9 20.6 28.6							50 100	50 100
		200	20	20	0	.01	50	2×10^4	1	3	50	10	10
			20	1	6.9 20.6 28.6								
		500	50	50	0	.005	50	2.5×10^5	1	3	120	10	10
			50	1	6.9 20.6 28.6							100 250	100 250
S2	Long Range High Power	600	60	60	0	.008	50	2×10^5	1	5	150	50	50
			60	1	6.9 20.6 28.6								
			50	1	0								
			50		6.9 20.6 28.6							10	10

be a small fraction of the target length. To illustrate the effect of antenna size on the cross section, the data in Figures 1.4-11 and 1.4-12 were computed for the cases of (1) a point source, (2) an antenna diameter of one half target length, and (3) an antenna diameter equal to the target length (in Figure 1.4-11 only). On the basis of the data presented in Figures 1.4-11 and 1.4-12, it appears that a measurement range of $2(D + L)^2/\lambda$ should be used as a range criterion rather than $2(D^2 + L^2)/\lambda$ or $2X^2/\lambda$ where X is the larger of D or L; the experimental results indicate that the latter criterion is appropriate to the antenna-target site geometries of interest in the measurement of large objects.

Measured data obtained under Contract AF30(602)-3872 was used to validate the computed cross section, such as the data presented in Figures 1.4-3 through 1.4-10. Figures 1.4-13 and 1.4-14 contain measured data on cylinders measured at a range of D^2/λ and $4D^2/\lambda$, respectively. Also indicated in the figures are computed data for the same conditions. On the basis of the agreement between theory and measurement, exhibited by the data in Figures 1.4-13 and 1.4-14, the mathematical model used to examine near-field error is considered to be representative of that which would be experienced in practice in the case of simple cylindrical targets.

The portion of the experimental program directed to obtaining measurements at range lengths less than $2D^2/\lambda$ was conducted at three range lengths by using three basic target configurations, a number of ancillary targets, and two different sizes of antenna aperture. The basic target configurations (Figure 1.1-41) were measured at ranges of approximately $2D^2/\lambda$ (position 0), D^2/λ , (position 1), and $0.6 D^2/\lambda$ (position 2) where D is the basic target length. The experimental data closely approximate the theoretical cylinder results (Figure 1.4-15) which were obtained from the theoretical data previously presented in Figures 1.4-3 through 1.4-10. The cumulative error densities for the 3 targets are shown in Figures 1.4-16 through 1.4-20. Correlation of the data involves the adjustment of the anticipated 1σ (standard deviation) of 1 dB introduced by the measurement system. This adjustment is effected in the manner described by Equation 1.1- Experimental data on selected targets and range lengths are presented in Figures 1.4-19 through 1.4-22. An examination of these

data indicates that no severe null depth reduction occurs at the range lengths used. In addition, no sensible effect of antenna relative to target site is noted (refer to Figure 1.4-16).

1.4.3 Equipment Requirements

As presented in the results of the trade-off study (refer to Section 2), the optimum region for the use of this technique is in Band 6, 40- to 60-foot target lengths, and Band 7, 30- to 60-foot target lengths. The sensitivity requirement is reduced by a factor of 12 dB in the case of operation at a range length of D^2/λ . Thus the basic equipments are the same as those specified in paragraph 1.2.6 except for the reduced sensitivity. A tabulation of the components required to provide adequate sensitivity are presented in Table 1.4-2.

Table 1.4-2 EQUIPMENT REQUIREMENTS

Equipment	Area Cost (1000 Dollars)
1 MHz Bandwidth IF	2.5
Band 6, 7 - Phase Measurement	41
Band 6, 7 - Coherent Integration	6
Band 7 - Noise Subtraction	15

*Facility Equipments presented in Table 1.2-6 are applicable.

1.4.4 Conclusions

The conclusions reached in this portion of the investigation are delineated in the following paragraphs in terms of the factors (1) adaptability to range operation, (2) accuracy, and (3) cost. The trade-off study results indicate that this method is most applicable to the approximate region of Band 6 (40- to 60-foot targets) and (30- to 60-foot targets) Band 7. In these regions, the range length criterion is $R = \rho D^2/\lambda$ where $1 < \rho < 2$. This method was found to be less cost effective than others under consideration.

1.4.4.1 Adaptability to Field Operation. Inasmuch as this measurement exactly duplicates the present RAT SCAT operation, except for a direction extension of the range length and sensitivity requirements, no problem exists in terms of its application at RAT SCAT.

1.4.4.2 Accuracy. Study results indicates that analytical correction of near-field errors is not feasible because of the random nature of the errors introduced. The error levels are excessive at range lengths much less than $2D^2/\lambda$ which are required in order to be competitive on a cost-effective basis with other combinations of methods. Under these conditions, the error levels introduced are excessive. The average 1σ (standard deviation) of the error in the region of interest is 1.3 dB, and under the worst-case condition, $R = D^2/\lambda$, the 1σ error introduced is on the order of 2 dB.

1.4.4.3 Cost. The primary costs associated with implementation of this method are those associated with providing the required measurement equipment sensitivity and other range-length-associated costs. The equipment sensitivity costs are illustrated in Table 1.4-2. The other significant costs include roadway and signal and control cable costs which total \$2.5 per foot and are applicable over a range length of 43,200 feet.

1.4.4.4 Other Considerations. Other considerations associated with the use of this approach in the large D^2/λ region of interest include (1) the accessibility to adequate space at the White Sands Missile Range and (2) the potentially severe operational problem associated with the setting up measurement equipments at ranges in excess of 8 miles.

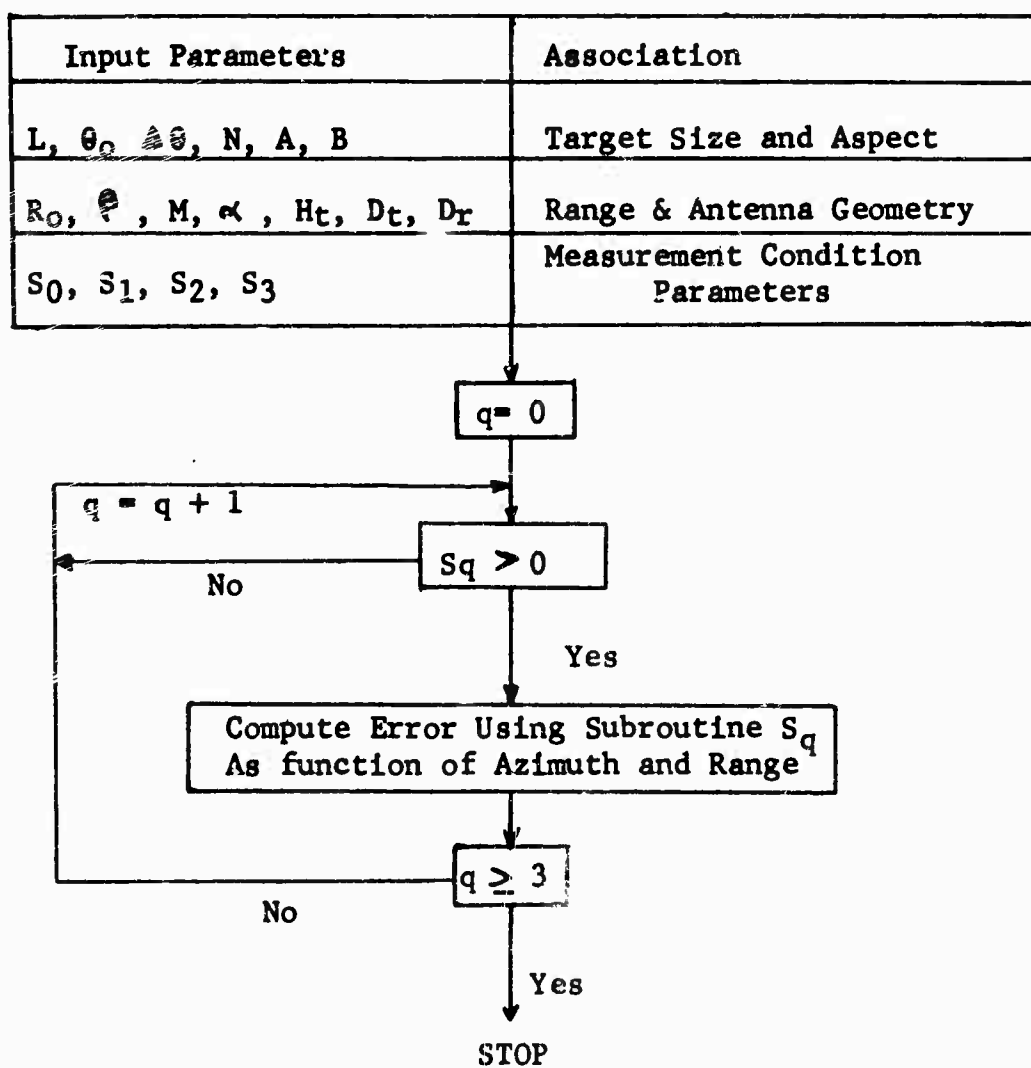


Fig. 1.4-1 NEAR-FIELD ERROR COMPUTER PROGRAM

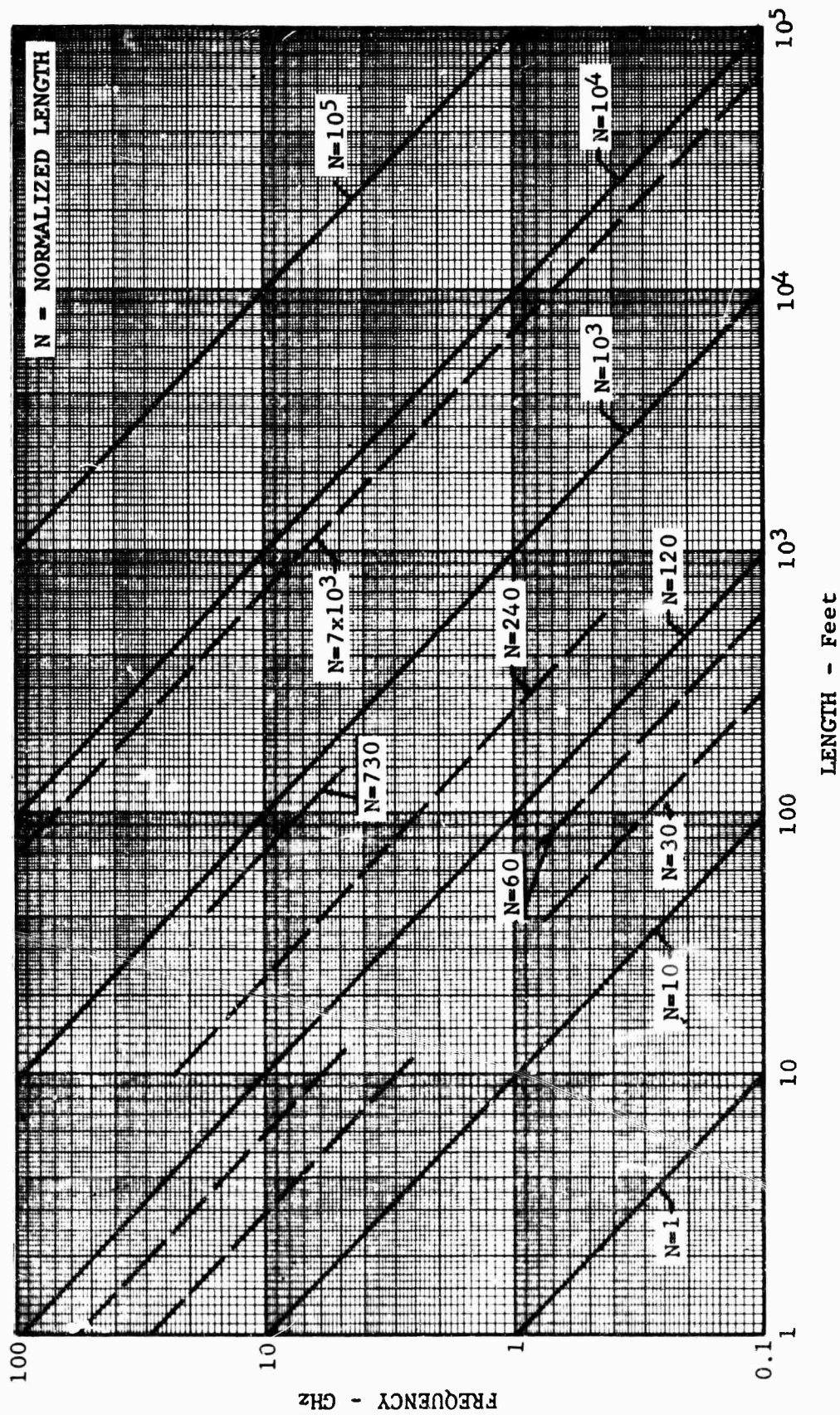


Fig. 1.4-2 NORMALIZED SIZE VS. FREQUENCY AND
TARGET LENGTH

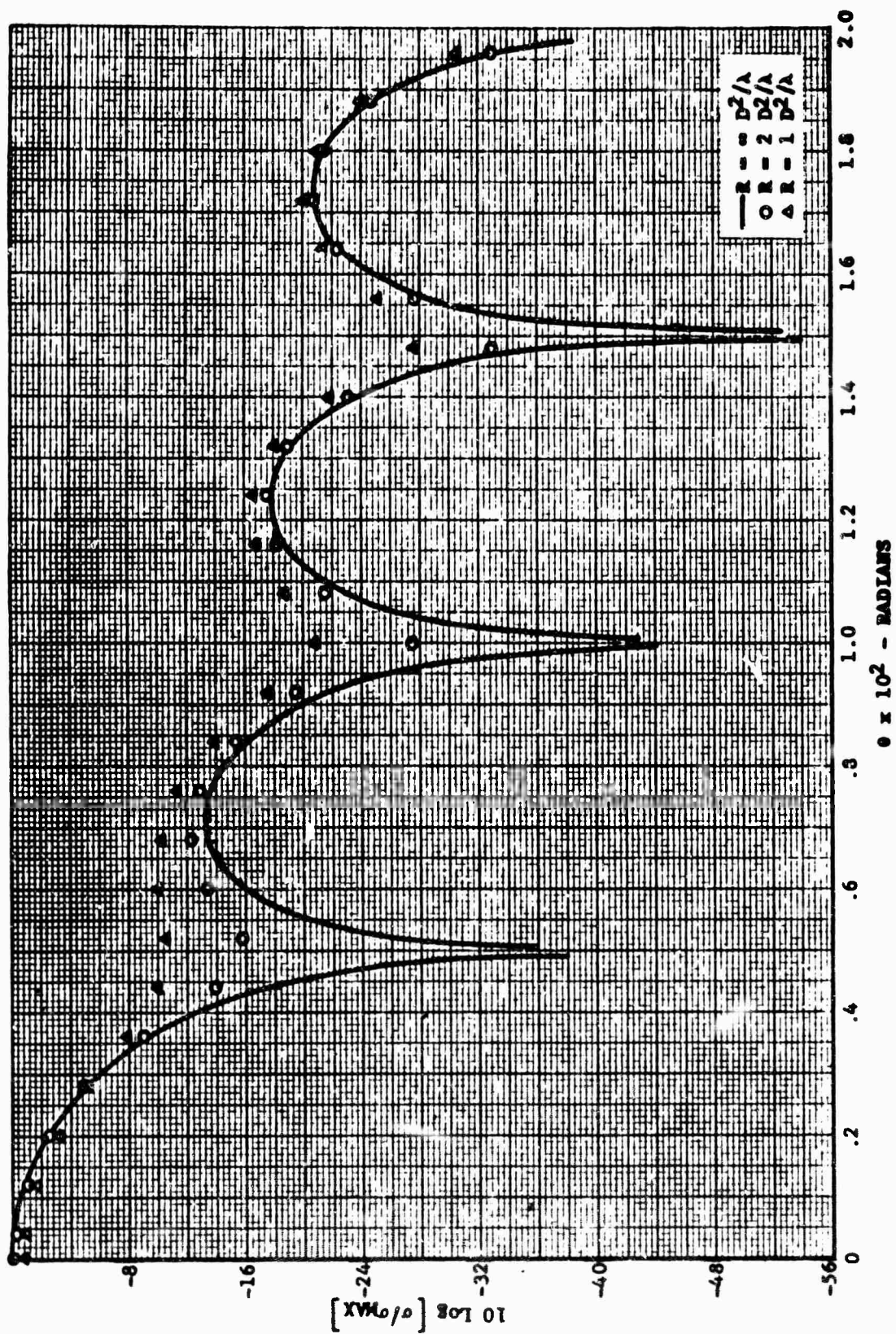


FIG. 1.4-3 CROSS SECTION AT SELECTED RANGES
(100 λ CYLINDER NEAR 0 DEGREES)

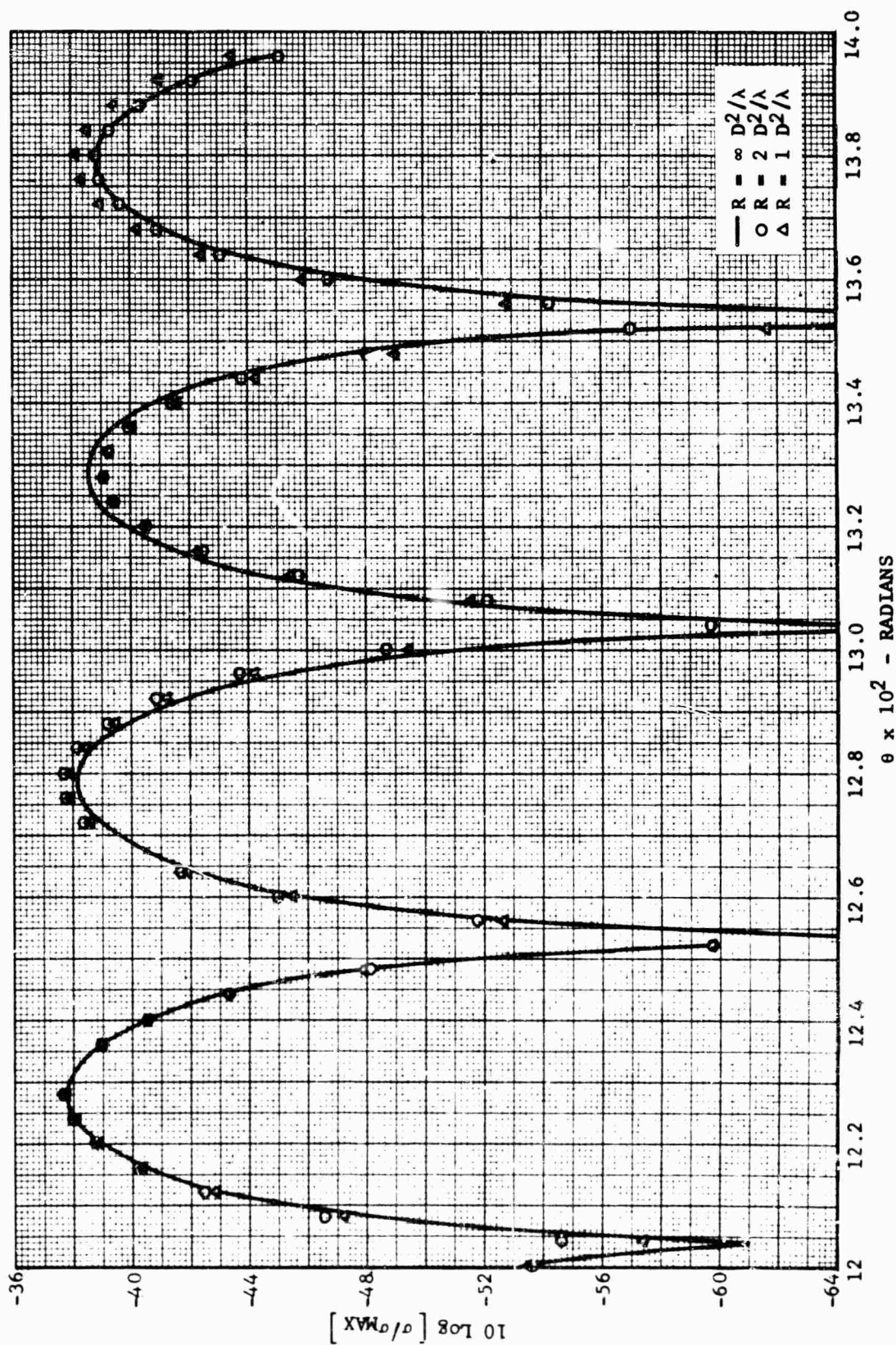


Fig. 1.4-4 CROSS SECTION AT SELECTED RANGES
(100 λ CYLINDER NEAR 7 DEGREES)

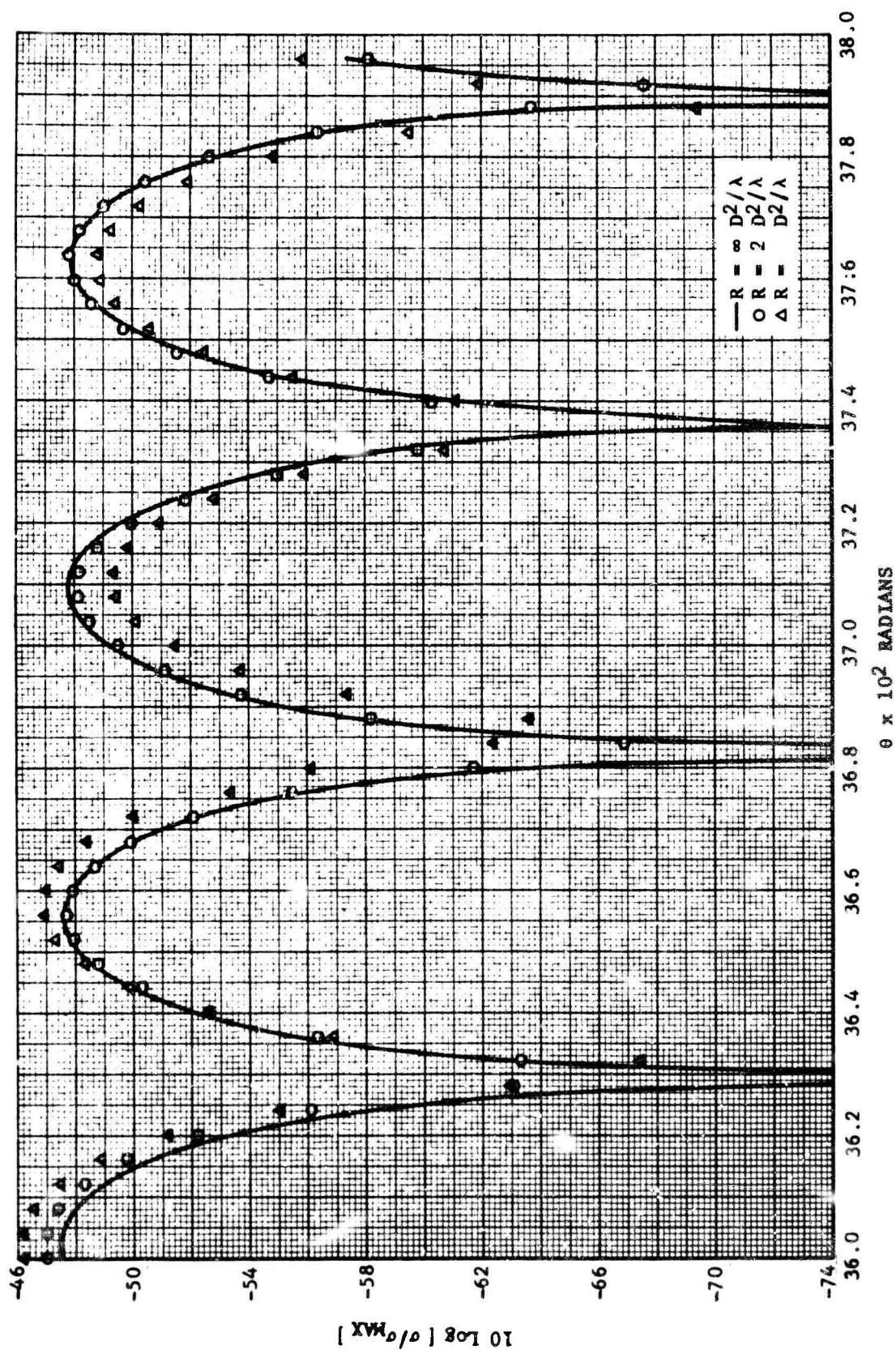


Fig. 1.4-5 CROSS SECTION AT SELECTED RANGES
(100 λ CYLINDER NEAR 20 DEGREES)

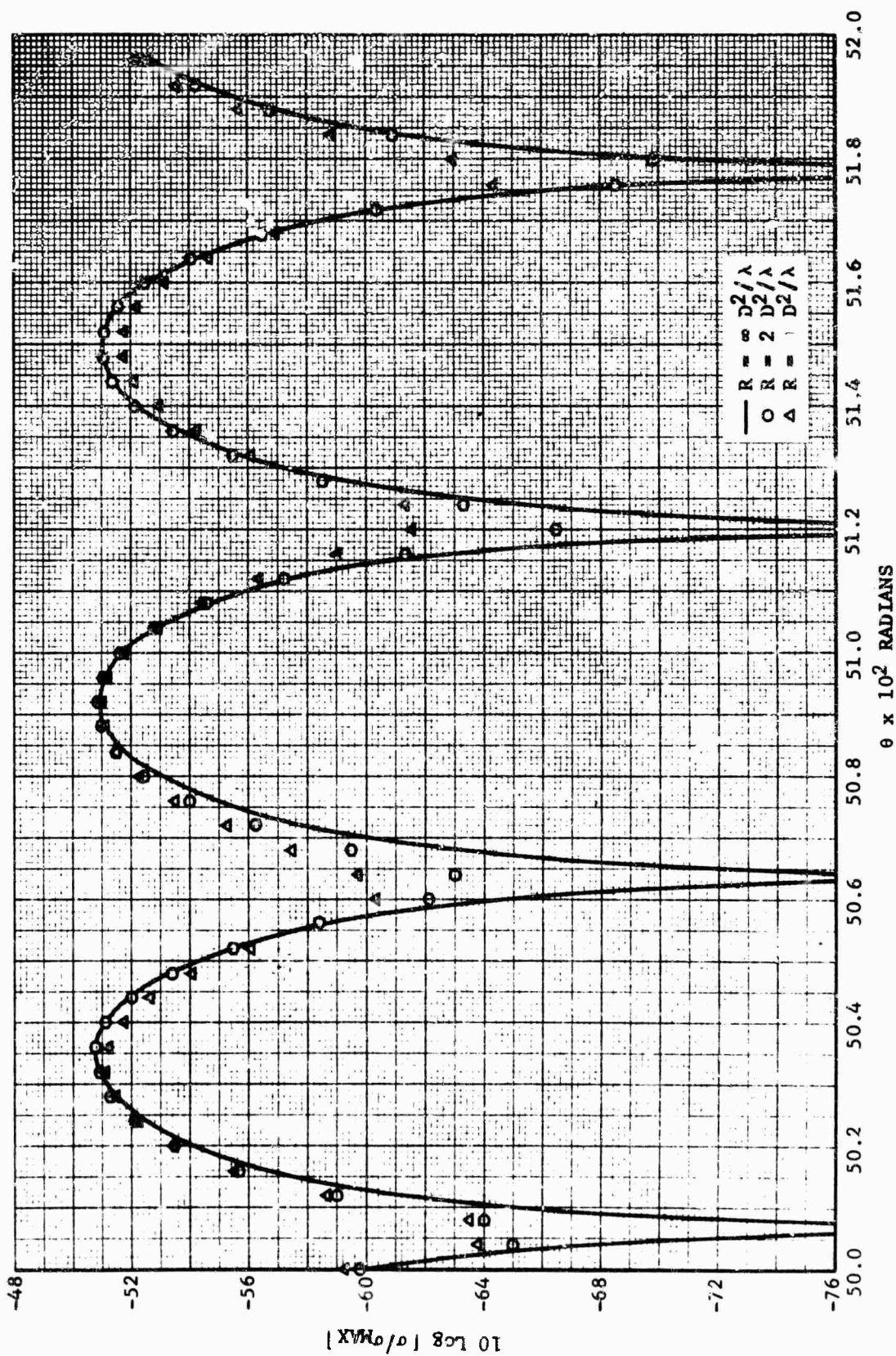


Fig. 1.4-6 CROSS SECTION AT SELECTED RANGES
(100λ CYLINDER NEAR 30 DEGREES)

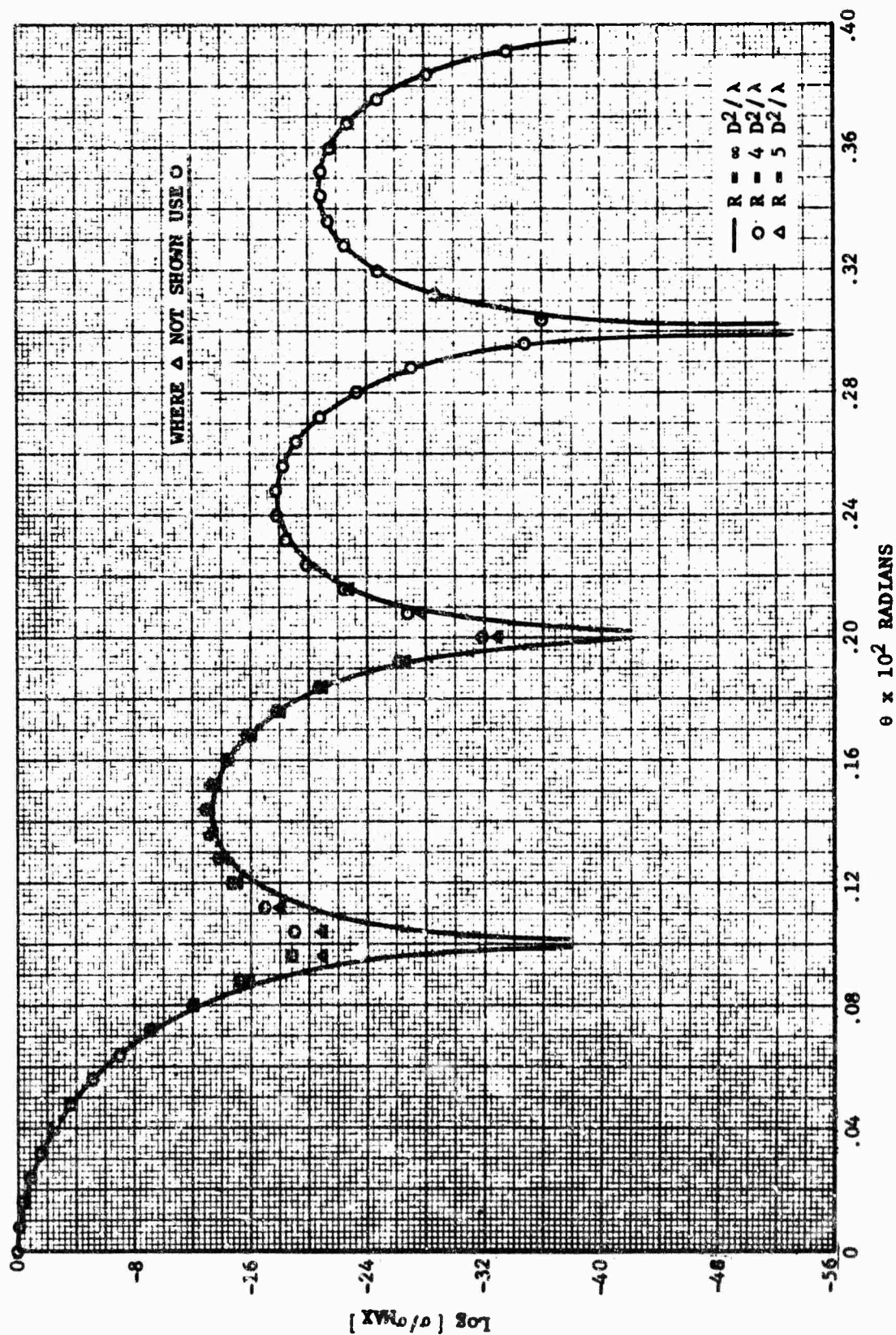


Fig. 1.4-7 CROSS SECTION AT SELECTED RANGES
(500 λ CYLINDER NEAR 0 DEGREES)

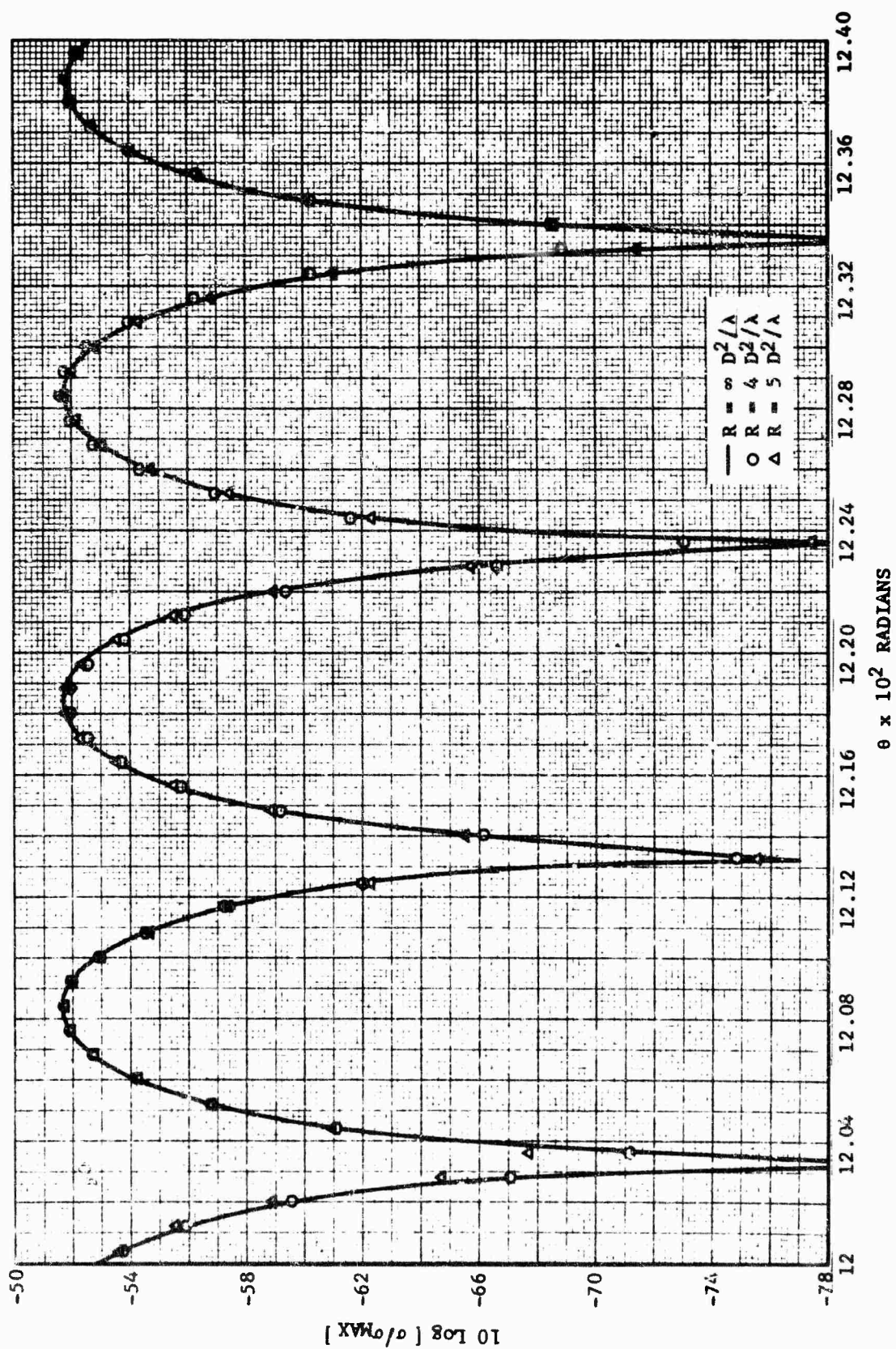


Fig. 1.4-8 CROSS SECTION AT SELECTED RANGES
(500 λ CYLINDER NEAR 7 DEGREES)

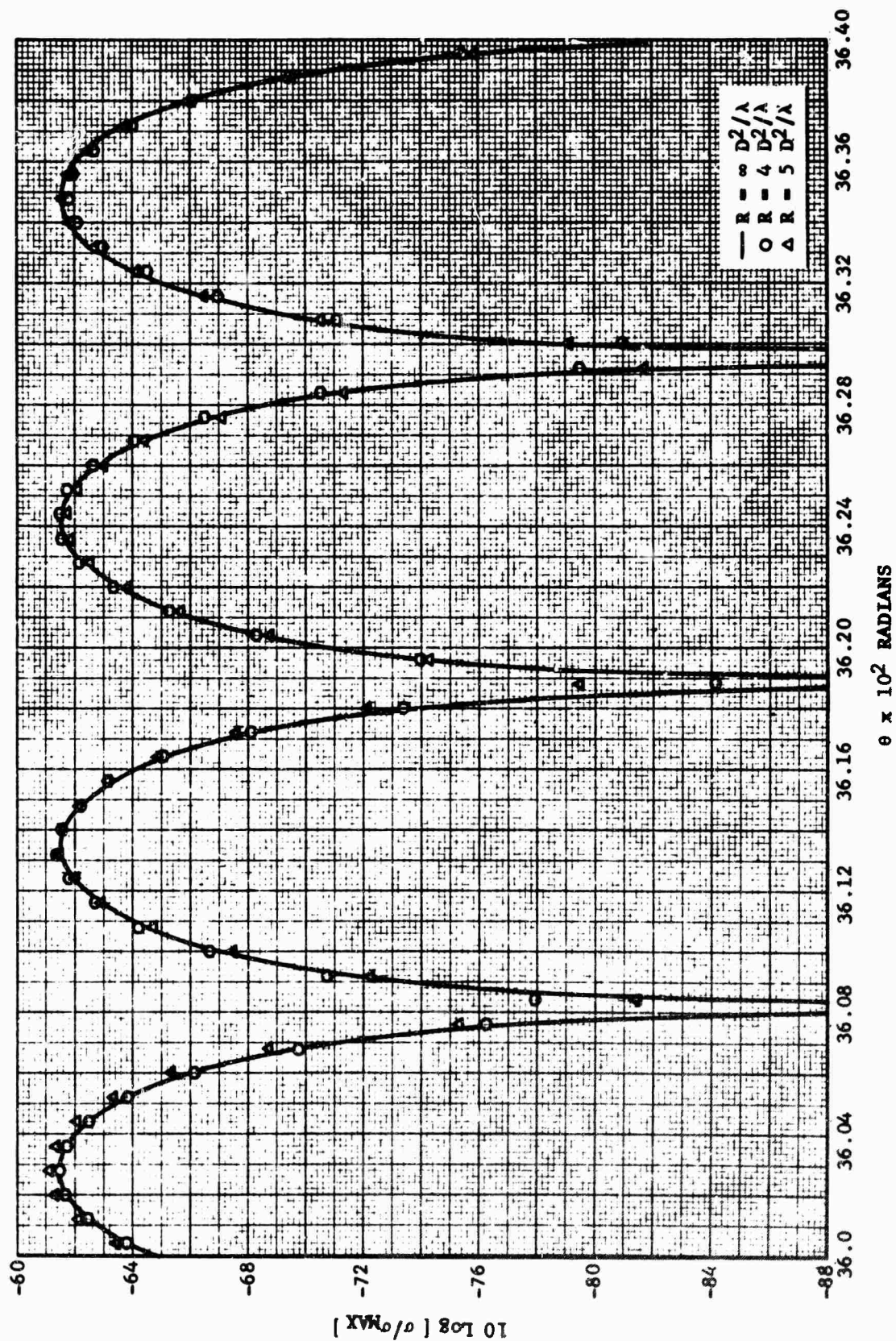


Fig. 1.4-9 CROSS SECTION AT SELECTED RANGES
(300 λ CYLINDER NEAR 20 DEGREES)

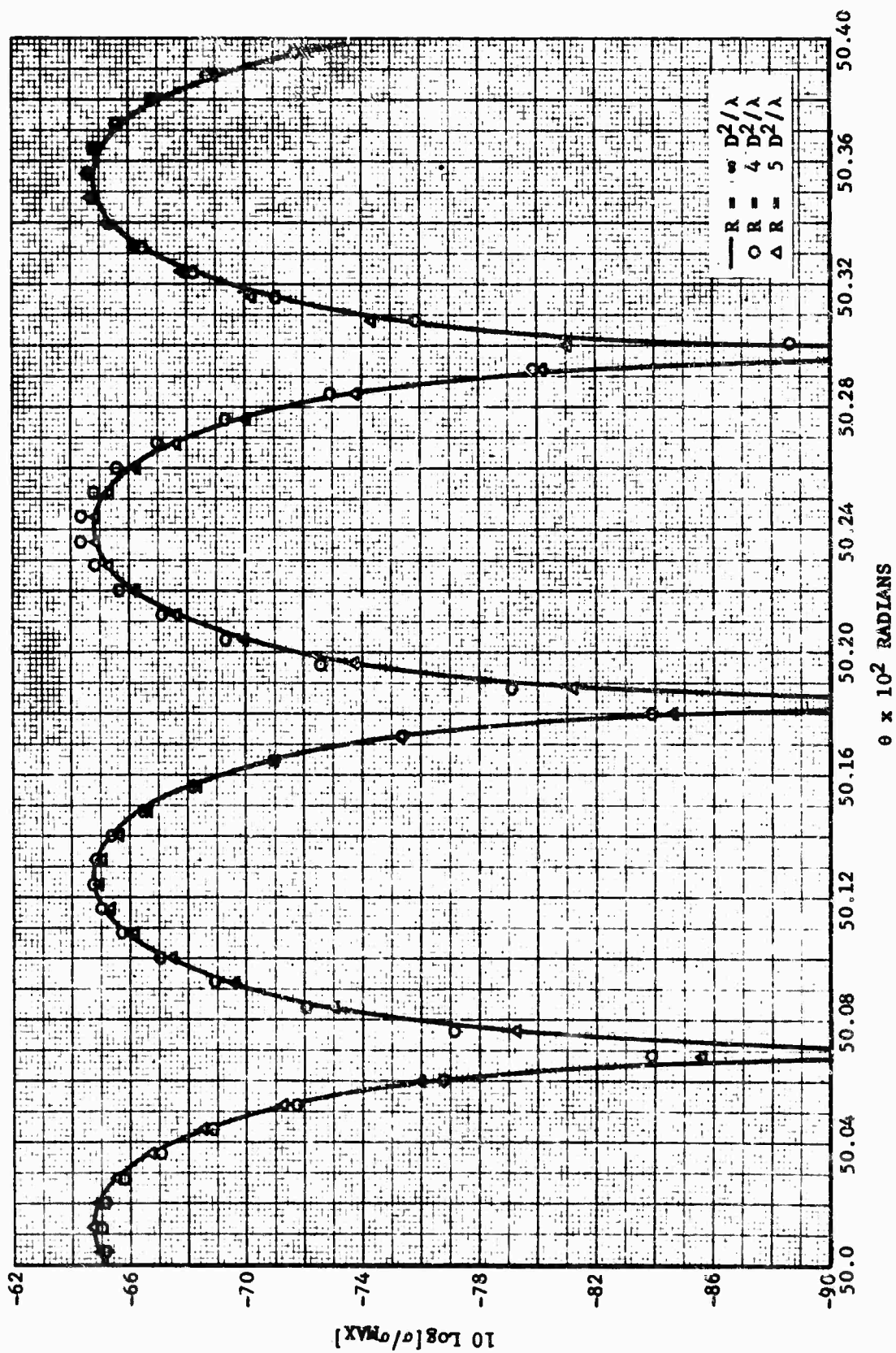


Fig. 1.4-10 CROSS SECTION AT SELECTED RANGES
(500 λ CYLINDER NEAR 30 DEGREES)

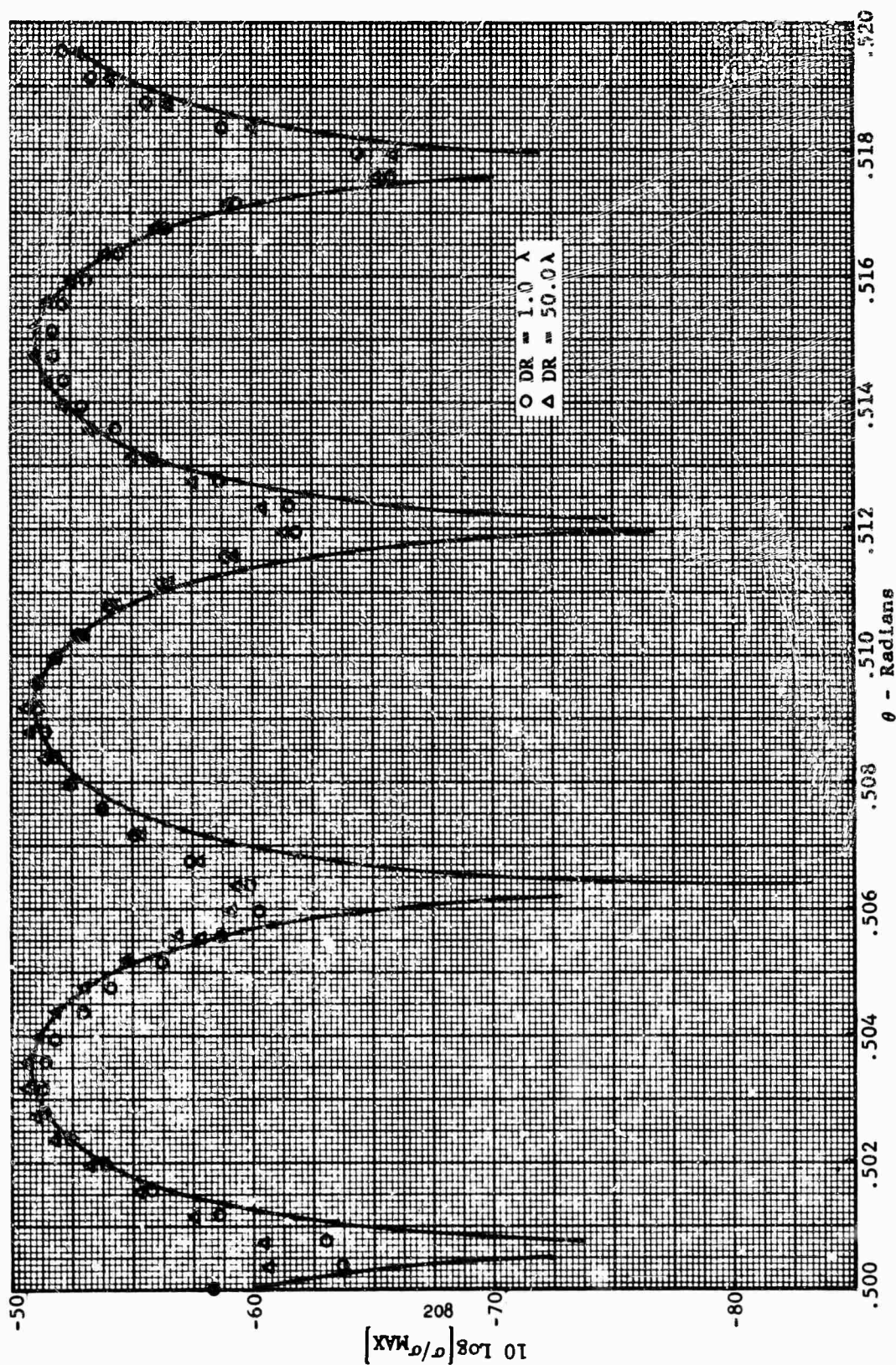


Fig. 1.4-11 CROSS SECTION FOR SELECTED ANTENNA SIZES (100λ CYLINDER NEAR 30 DEGREES)

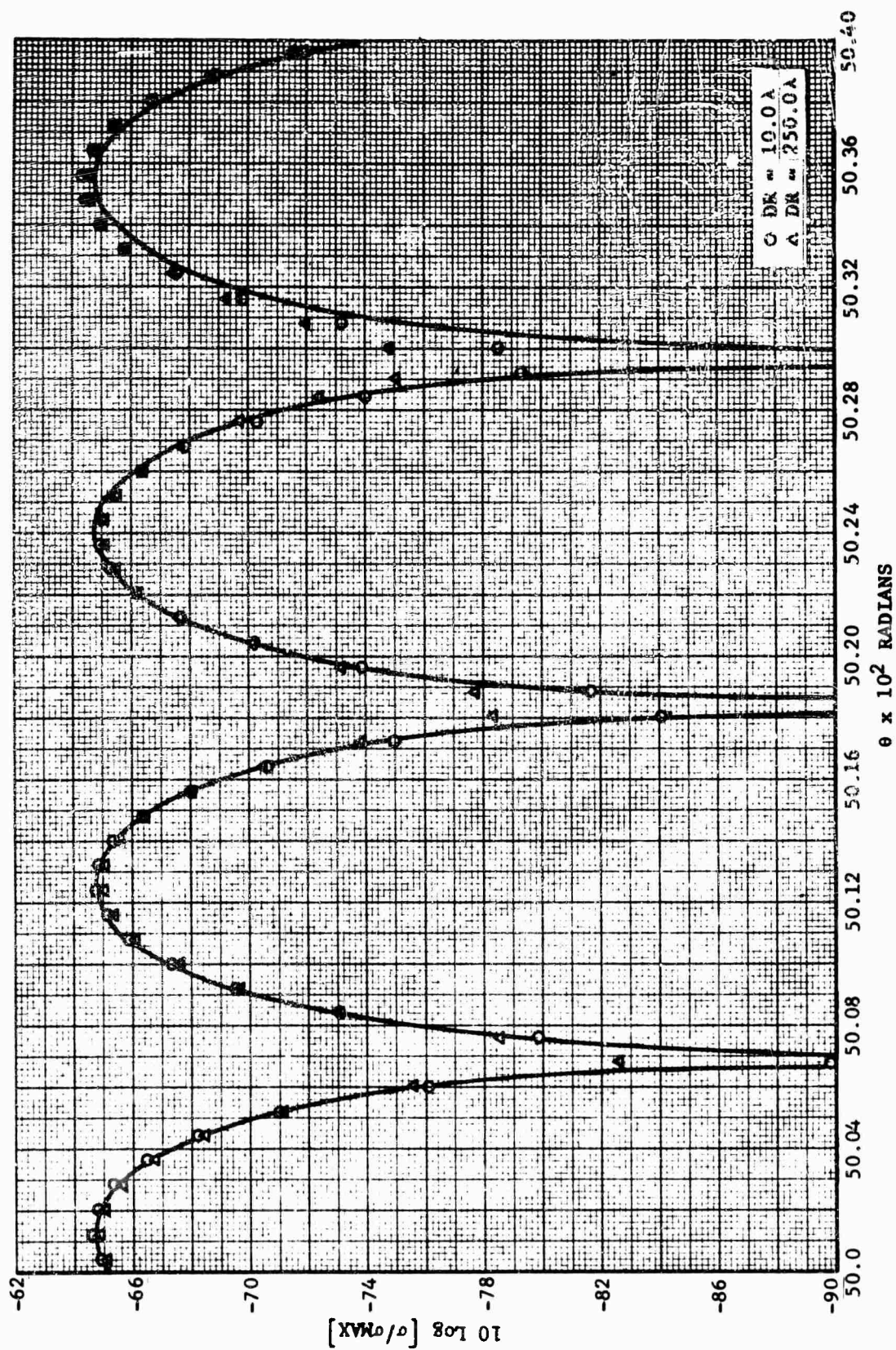


Fig. 1.4-12 CROSS SECTION AT SELECTED ANTENNA SIZES (500λ CYLINDER NEAR 30 DEGREES)

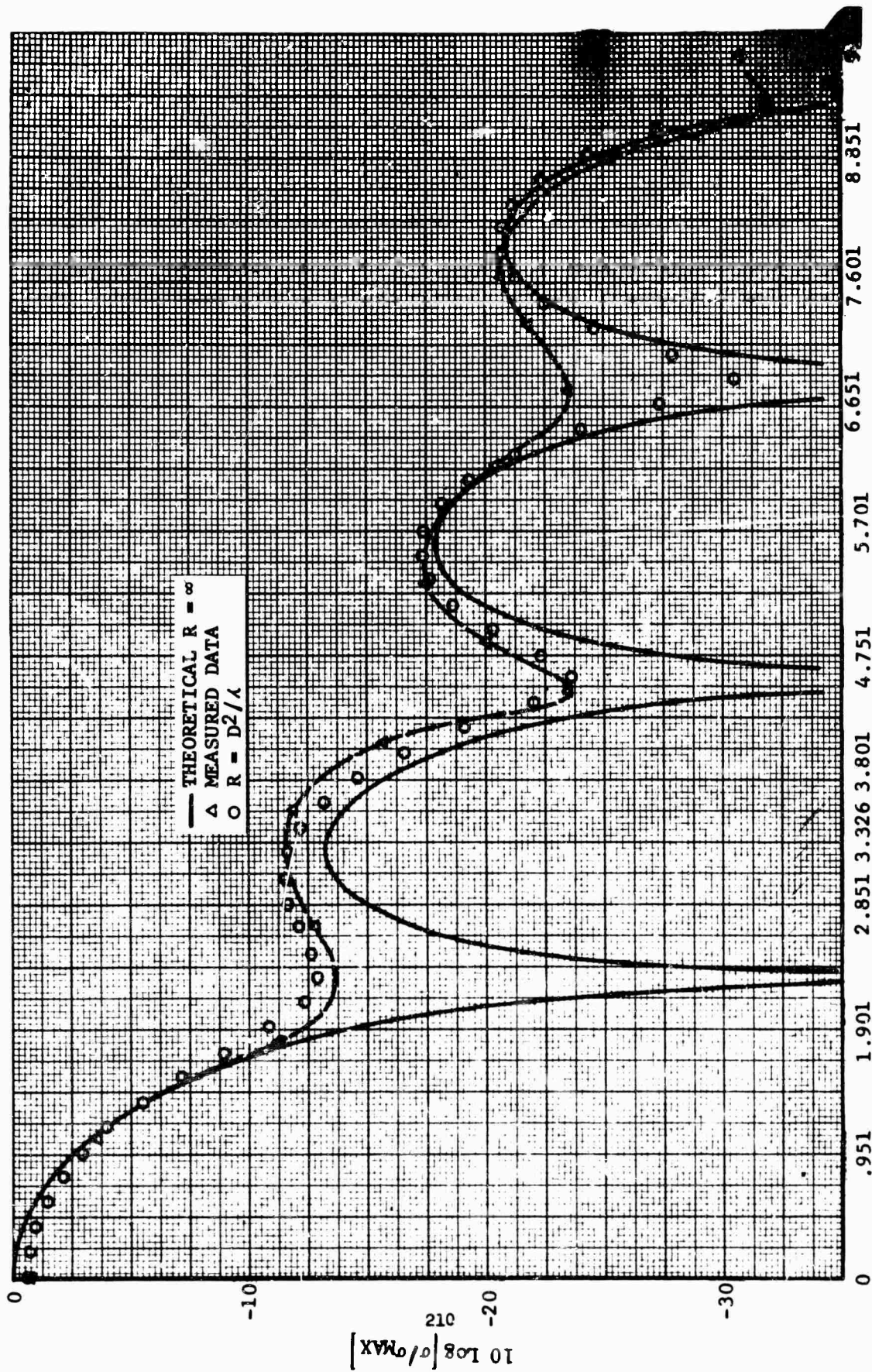


Fig. 1.4-13 MEASUREMENT VERSUS THEORY RANGE = D^2/λ
 $\theta \times 10^2$ - Radians

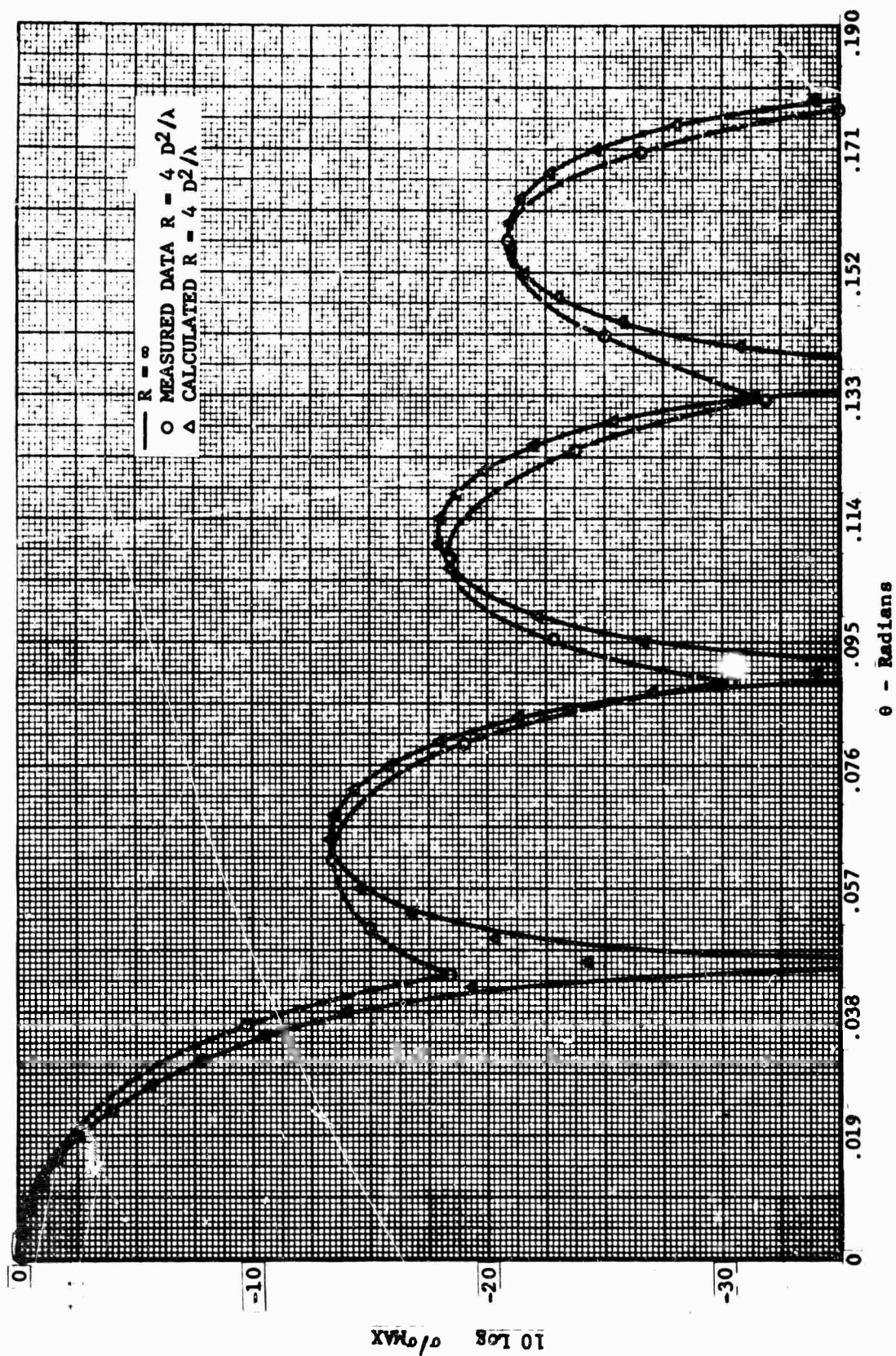


Fig. 1.4-14 MEASUREMENT VERSUS THEORY (RANGE = $4D^2/\lambda$)

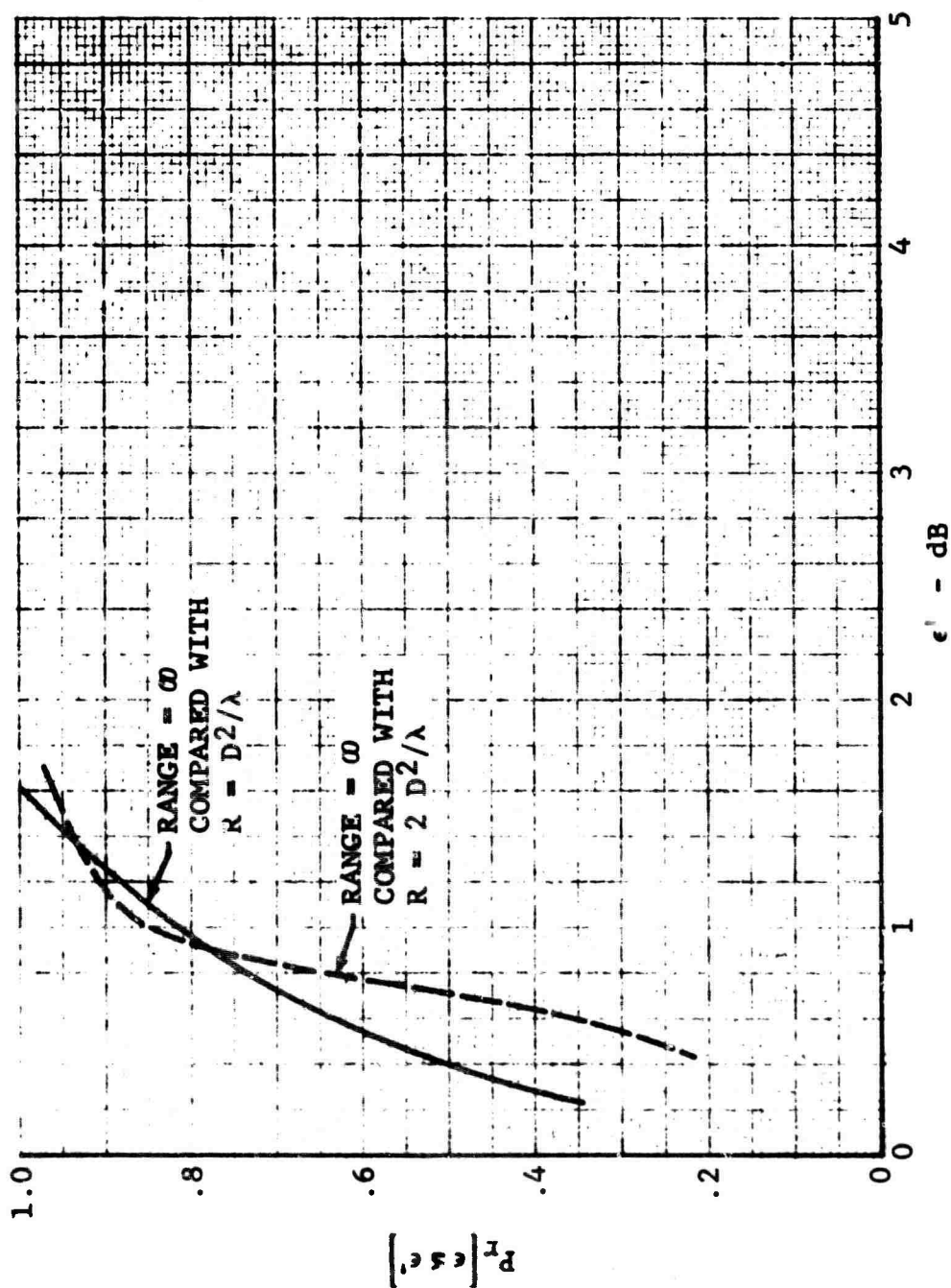


Fig. 1.4-15 CUMULATIVE ERROR DENSITY ON GENERAL CASE CYLINDER

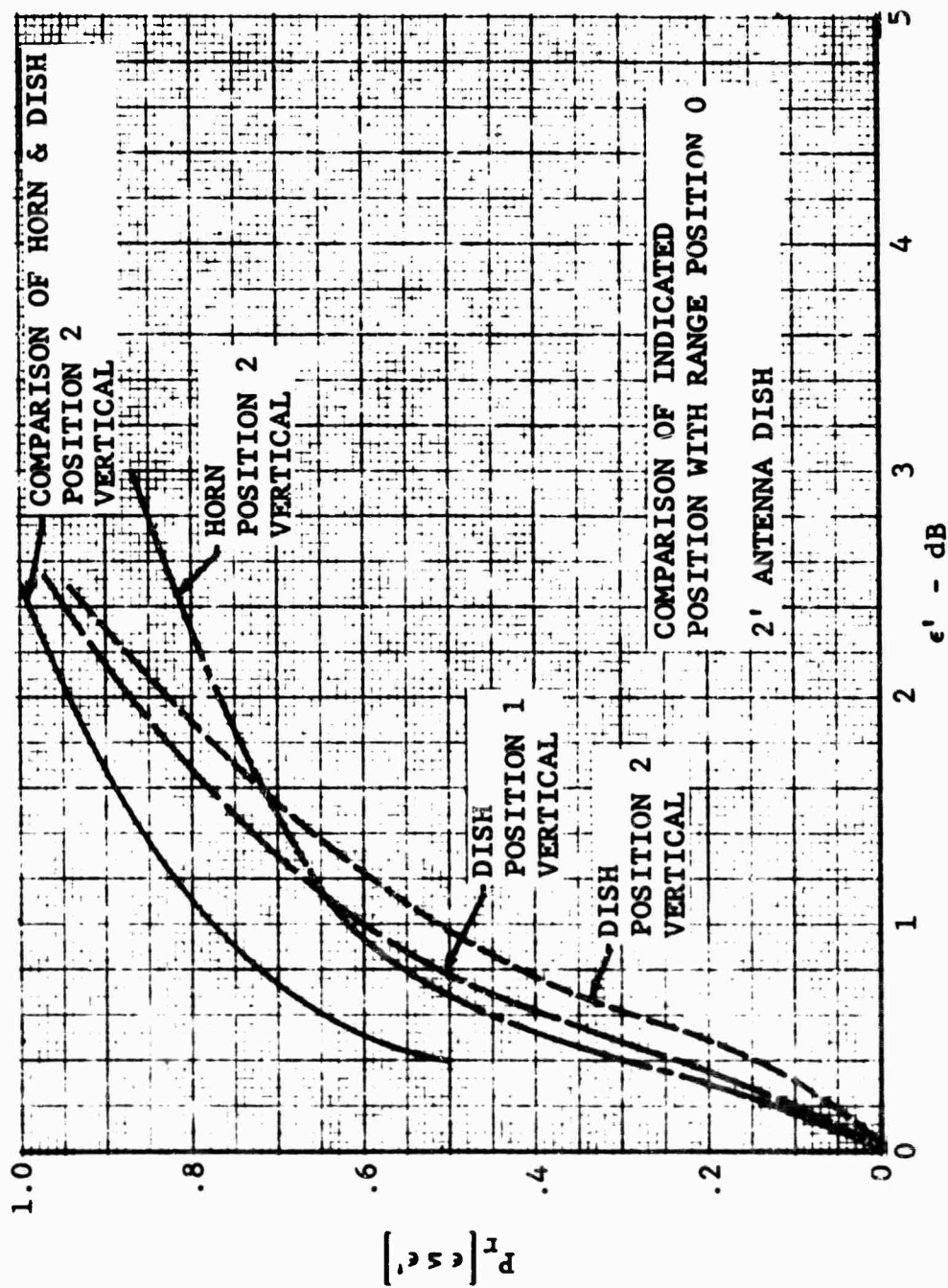


Fig. 1.4-16 CUMULATIVE ERROR DENSITY ON 60-INCH CYLINDER

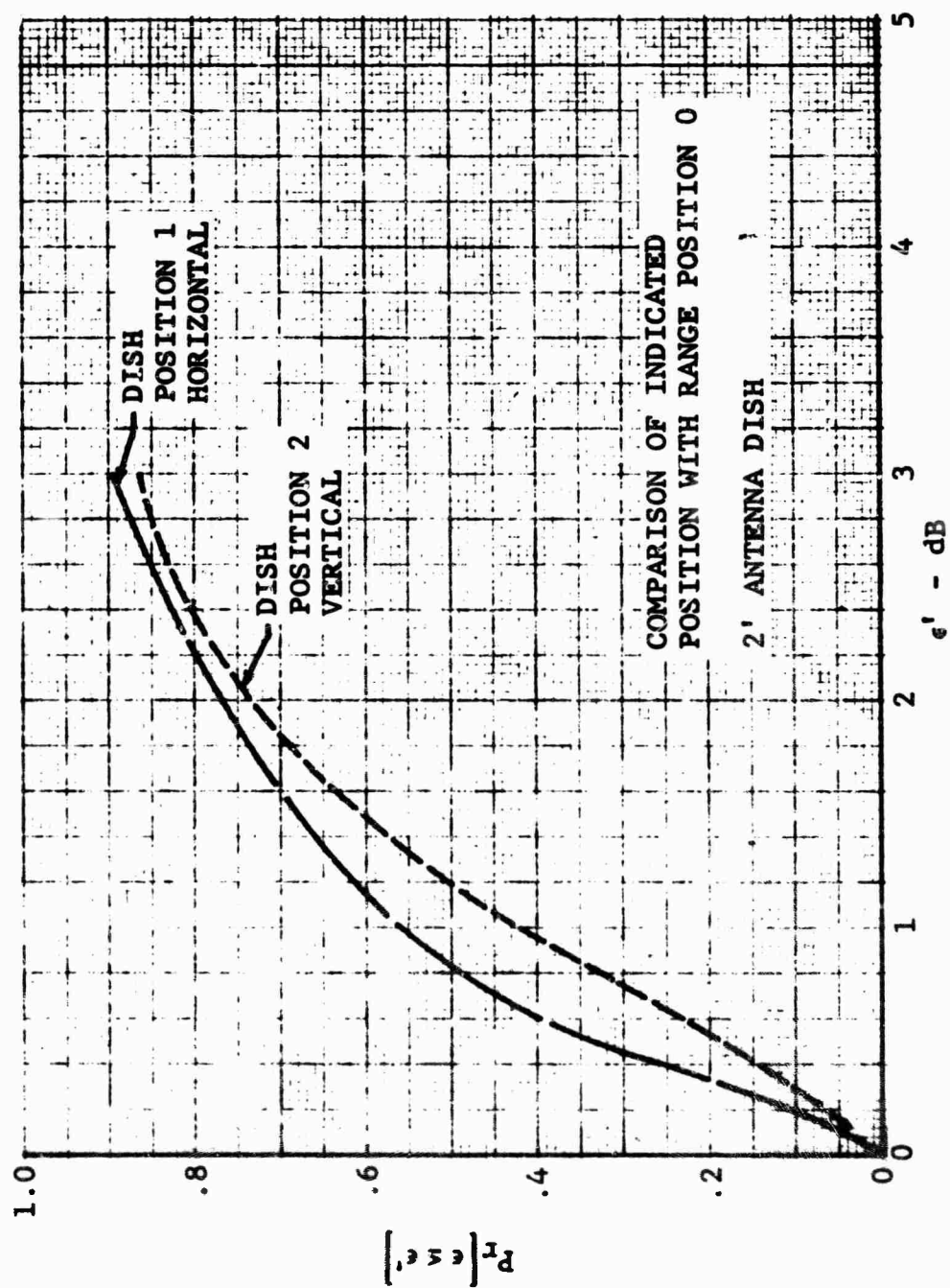


Fig. 1.4-17 CUMULATIVE ERROR DENSITY ON TARGET 2A

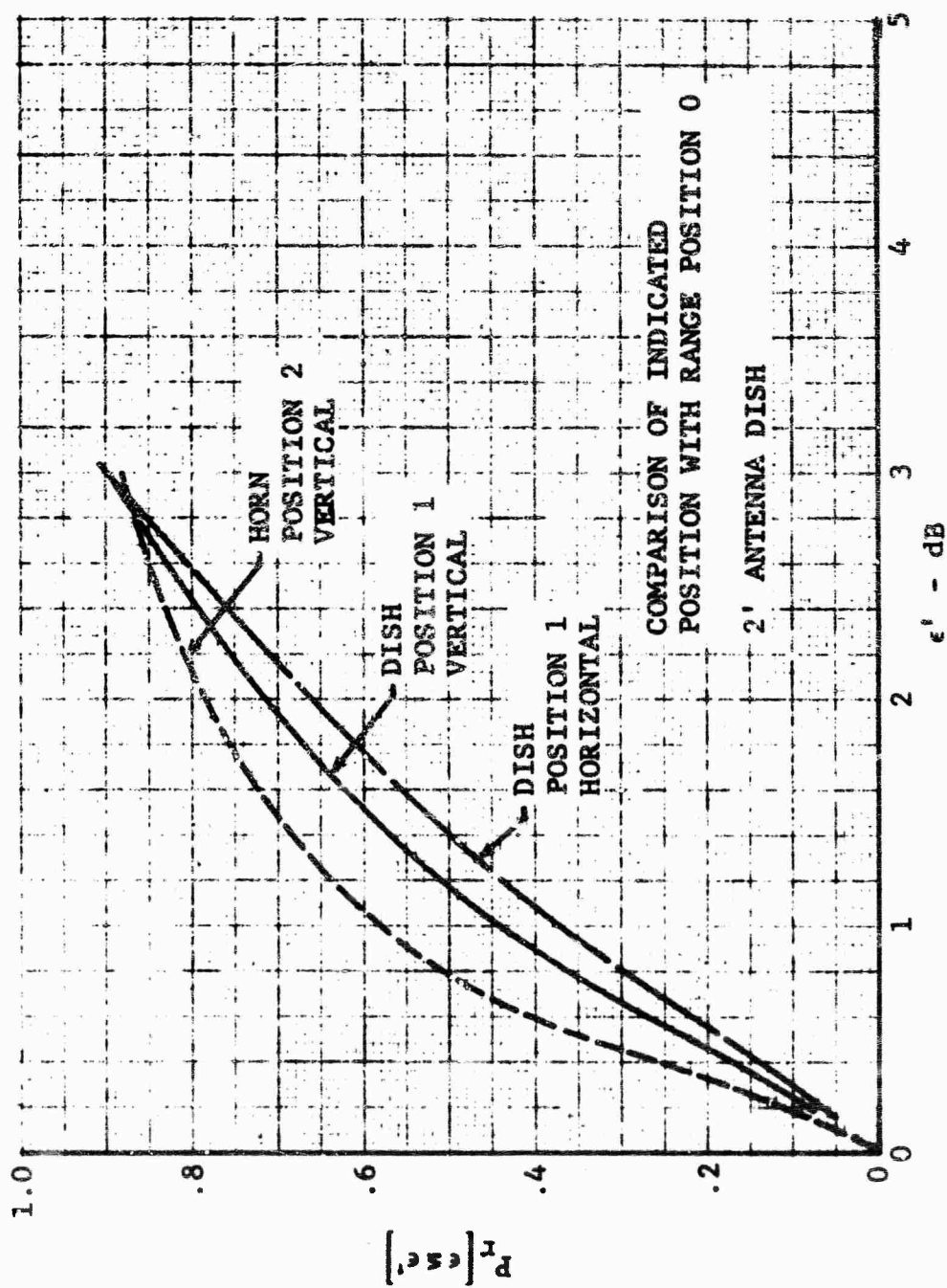


Fig. 1.4-18 CUMULATIVE ERROR DENSITY ON TARGET 9A

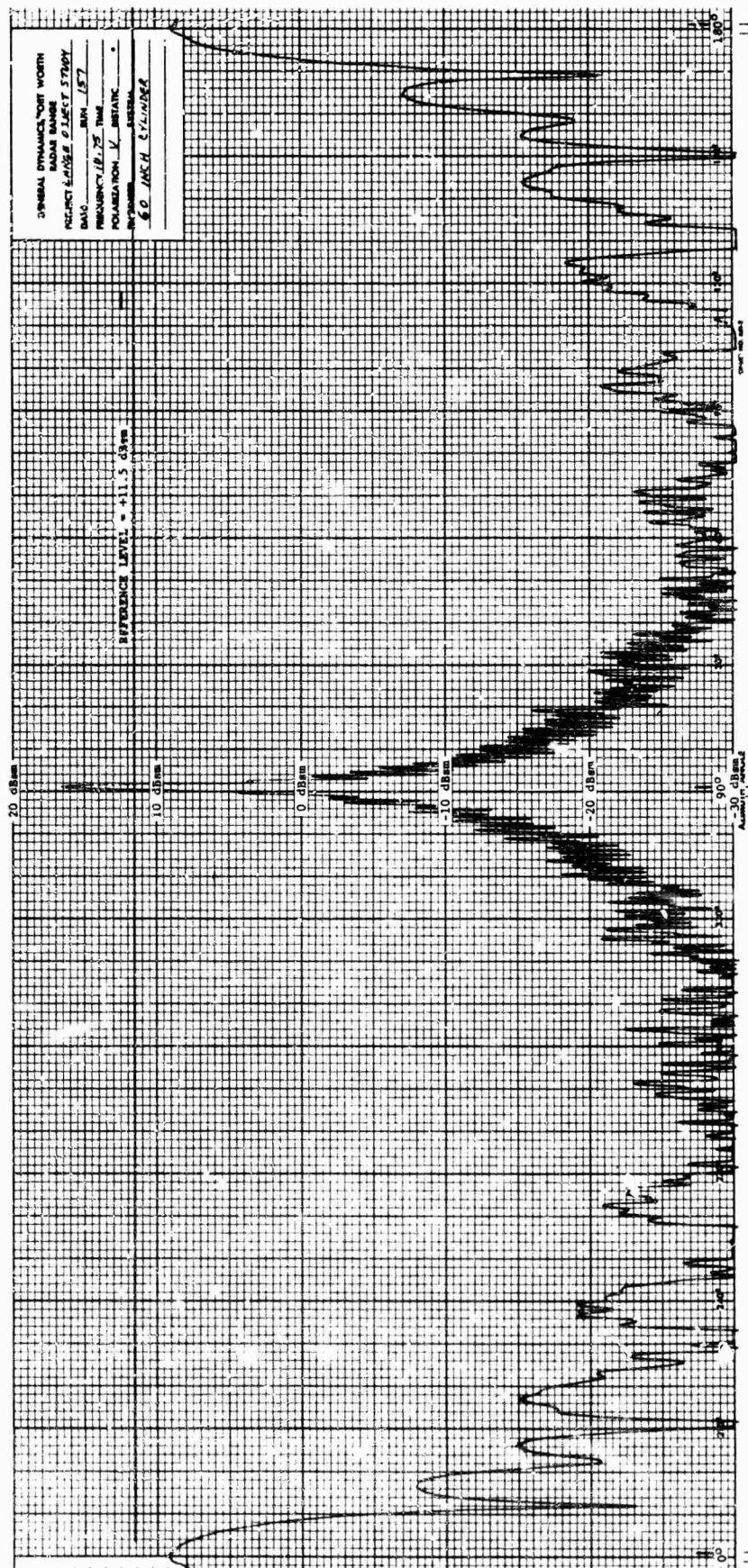


Fig. 1.4-19 EXPERIMENTAL DATA ON 60-INCH CYLINDER, RANGE POSITION 0

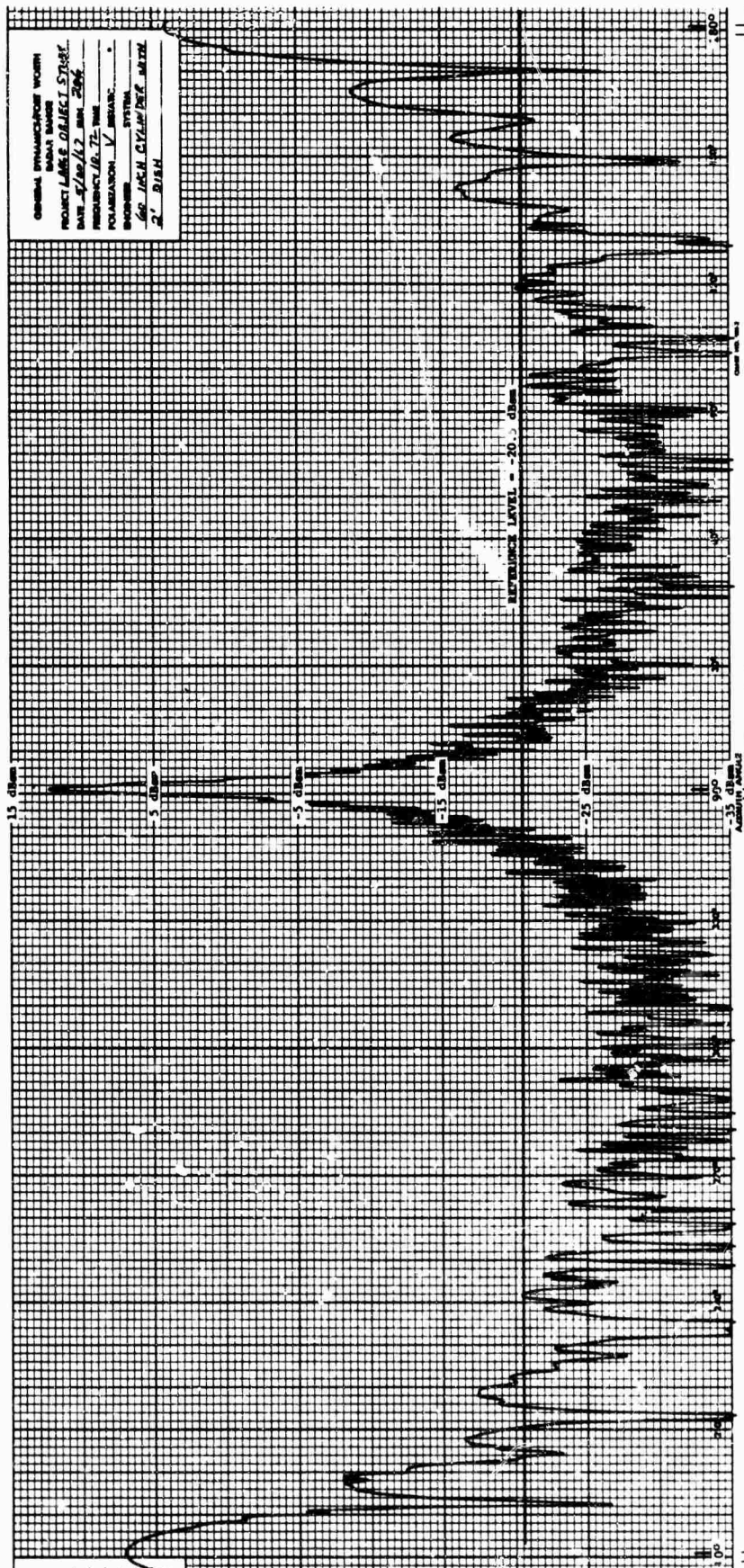


Fig. 1.4-20 EXPERIMENTAL DATA ON 60-INCH CYLINDER, RANGE POSITION 2

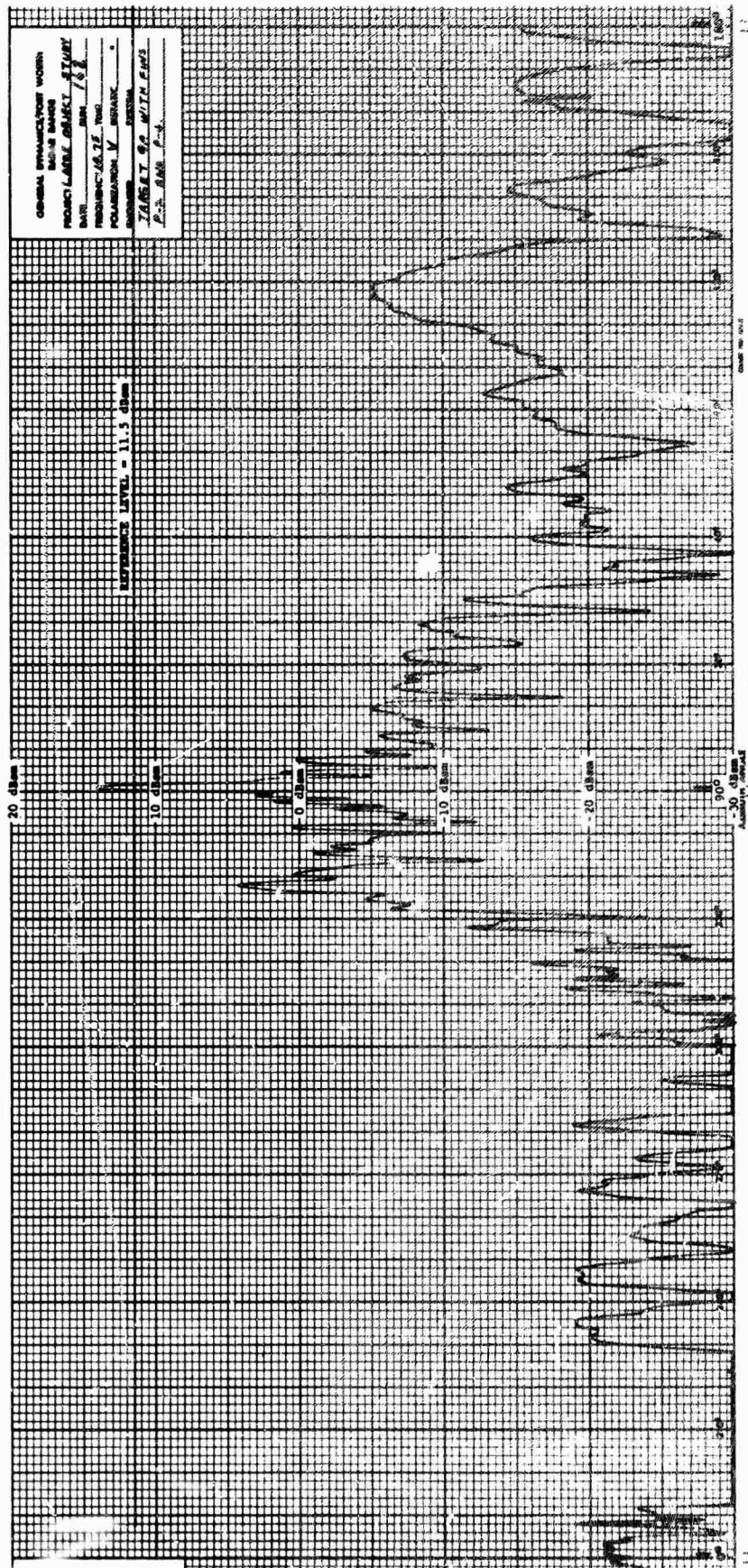


Fig. 1.4-21 EXPERIMENTAL DATA ON TARGET 9A, RANGE POSITION 0

SECTION 2

TRADE-OFF STUDY

2.1 General

The trade-off study was conducted on the basis of the requirement for evaluation of the following features of the techniques used:

1. Accuracy
2. Cost
3. Adaptability to field operations.

For the purpose of accomplishing the trade-off, results of an examination of these features in terms of the requirements of the individual techniques suggest further breakdown of accuracy and cost. In general, cost includes both initial and recurring costs, and recurring costs include that associated with features such as target construction, data acquisition time, range operating time, and the ratio of engineers to technicians required to obtain high-quality data.

The following trade-off discussion is oriented toward a final solution based on the use of the long-range and high-power technique over a significant portion of the D^2/λ region of interest. The use of this approach involves the provision of at least one long fixed-range length, a high-capacity rotator, 100-foot antenna towers, and a mobile operation capability. Consequently, in order to accentuate the actual cost differential, the cost of these items is not included in the trade-off study. The validity of this approach is based on the discussion presented in subsection 1.2 and the operational models discussed in this section. In addition, the cost of a phase measurement capability is not included since the final recommendations include provision of this capability for use in the general problem of reducing the target support cross section.

The procedure used in the trade-off analysis is shown in Figure 2.1-1, along with the primary features which have been evaluated and the evaluation process used in selecting candidate techniques or combinations. The primary input parameters are frequency, target

length, and target radar cross section. Associated with each technique is one or more sets of equipment requirements and an operational procedure requirement; satisfaction of these requirements will largely determine the initial cost and recurring cost. Recurring costs in this evaluation are limited to range hours required for measurement and special processing, such as target fabrication in the case of the scaling technique. The recurring costs are estimated for a five-year period in order to provide a reasonable basis for showing the relative significance of initial and recurring costs.

Accuracy is based on the appropriate combination of effective S/N, technique anomalies, and/or effective range length. The accuracy specification to be used in the evaluation matrixes (Tables 2.4-1 through 2.4-4) will be representative of the standard deviation (σ_T) of the error introduced by utilization of a technique.

In general, the accuracy obtained in the use of a technique will be the 1-dB level specified in the RFP as the present RAT SCAT capability. This value is interpreted as the standard deviation of a normal density distribution (i.e., the error is less than 1 dB 70 percent of the time). Thus the attainment of the RAT SCAT capability is based on the ability to reduce errors introduced by a particular technique to a negligible value. It is anticipated that the error sources (of the new technique) can be approximated by a normal distribution; and statistical independence of the processes can be assumed. Then the resultant error standard deviation, σ_R , is given by

$$\sigma_R = \left[1 + \sigma_T^2 \right]^{\frac{1}{2}} \quad (2-1)$$

where σ is the standard deviation and the R and T subscripts refer to the resultant error and the error introduced by the technique, respectively. On the basis that the density is described in logarithmic space, σ_R will be only 1.1 dB when $\sigma_T = 0.5$ dB. This value has been selected as the maximum acceptable error for routine evaluation. Special cases, wherein a large increase in effectiveness or reduction in cost can be achieved if a larger error is allowed, are indicated and discussed.

2.2 Operational Models

In order to minimize the subjective evaluation of the techniques of interest, a number of operational or statistical models have been defined for use in the trade-off analysis. These models are based in general on RAT SCAT operational data and in particular on present and past programs for measuring large objects (greater than 10 feet in length). Of specific interest are the probability of occurrence of a requirement for a measurement within a given frequency range, and target length and the time required for conducting a typical program.

Shown in Figure 2.2-1 is the cumulative density distribution of measurement frequency derived from previous RAT SCAT measurement programs. Although there is a concentration of measurement programs at the most common threat frequencies, data requests commonly include those for a wide range of frequency down to about 100 megahertz. The curve shown in this figure has been extended down to 30 megahertz in order to encompass the frequency range required in this study.

The cumulative probability of occurrence of a given target length is shown in Figure 2.2-2. However, it is further assumed that the size of the targets at RAT SCAT would increase if sufficient measurement capability were available. On this basis, the slope of the curve describing present RAT SCAT target length was decreased to place more emphasis on the larger target lengths. As shown in the figure, the target length density is assumed to be uniform between 10 and 60 feet. These data are interpreted in terms of the square of the target length in Figure 2.2-3. This parameter is of interest in defining the probability of occurrence of a given D^2/λ value. The cumulative density of D^2/λ can be readily determined by using an analytical approximation for the density of D^2 and F and a process involving a change of variables. The results obtained by use of this process are shown in Figure 2.2-4. It is evident from an examination of these data that the capability of a maximum range length much less than the $2D^2/\lambda$ for the measurement of a 60-foot target at X-Band will suffice for a very large percentage of the D^2/λ values expected.

Another significant operational feature is that of the time element involved in a measurement program. The results of an analysis of this feature, based on an extension of the present RAT SCAT capability, is shown in Figure 2.2-5 for the cases of both fixed and mobile operation by use of the long-range and high-power technique and for the case of mobile operation by use of the scaling technique. The basis of these data is the time required for the

present RAT SCAT measurement of 10-foot to 30-foot targets by use of an average number of frequencies and an average number of target orientations. Under these conditions, a large percentage of the total measurement time is required for equipment setup; this fact tends to mask the effect of the increased target handling time required for the larger targets. In addition, the handling time required apparently does not increase in direct proportion to target size (length) in the case of the larger targets. It is assumed that provision of a large-object measurement capability will increase the number of measurement programs by a factor of 1/2 and consequently increase the efficiency in using a measurement setup in more programs than at present. On this basis, a decrease in equipment setup time of 15 percent was imposed to obtain the long-range and high-power technique curves shown in Figure 2.2-5. This factor was not applied to the time required for use of the scaling technique since a relatively low rate of utilization is anticipated. The mobile operation curves are based on the time required for fixed range operation, plus a 10-percent increase in equipment setup time. The significant change in the time relative to the scaling and the long-range and high-power technique is the feature of target handling when a scaled target is used.

Another model used in the trade-off study was that of the number of targets to be handled and the associated time required. As previously indicated, the additional capability to be afforded by the implementation of the large-object program is expected to increase the number of programs at RAT SCAT. For the purpose of making this study, an increase of 1/2 has been used; this increase would involve a 3-pit and 2-shift or 2-pit and 3-shift operation, whereas present RAT SCAT operations are oriented toward 2-pit and 2-shift operation. This increase will allow use of a total number of 8780 range hours. This figure is based on previous RAT SCAT experience and includes time lost as a result of bad weather. The data shown in Figure 2.2-6 is the expected time required for the measurement of targets within 10-foot length intervals, and these data are based on an assumption of operation under the various conditions shown in Figure 2.2-5 and the imposition of the target length density shown in Figure 2.2-2. In each case, the total number of range hours is 8780. However, in order to obtain a measure of the impact of the measurement time required for use of the various methods, the total number of targets handled will be based on the time required in the long-range, high-power approach.

In order to provide a means of technique analysis on the basis of frequency band, it is necessary to establish the number and length of targets expected in each frequency band. The results of this process, based on an average of 5 measurement frequencies, are shown in Table 2.2-1 for a one-year period. The data in this table for target lengths from 30 to 60 feet and that in Figure 2.2-6 have been used in the trade-off study to assign a total measurement time in each band in terms of the applicability of each technique to a given target length.

Table 2.2-1 TARGET LENGTH AND FREQUENCY BAND ALLOCATION

Band	Frequency	Target Length						
		0 - 10	10 - 20	20 - 30	30 - 40	40 - 50	50 - 60	
0	.03 - 0.1	7.9	4.2	3.8	3.8	3.8	3.8	
1	0.1 - 0.25	7.9	4.2	3.8	3.8	3.8	3.8	
2	0.25 - 0.5	7.3	3.7	3.5	3.5	3.5	3.5	
3	0.5 - 1.0	6.4	3.3	3.1	3.1	3.1	3.1	
4	1.0 - 2.0	9	4.6	4.2	4.2	4.2	4.2	
5	2.0 - 4.0	12.1	6.2	5.8	5.8	5.8	5.8	
6	4.0 - 8.0	16	8.3	7.8	7.8	7.8	7.8	
7	8.0 - 12.0	12.1	6.2	5.8	5.8	5.8	5.8	

2.3 General Trade-Off Parameters

A number of the parameters under study are of interest in two or more of the basic techniques of interest. These parameters are associated with the dependent range geometry features of range length and antenna height and with the ancillary consideration of the choice of mobile or fixed range operation. The primary result of an examination of these features is specification of equipment sensitivity requirements under the various circumstances.

The range length and antenna height required for the antenna far-field simulation and the analytical correction of near-field data can be considered independently in that the required range length is dependent only on the degree of correction available and the antenna height requirement is, of course, the same as that for the usual ground-plane case. It should be noted, however, that the reduced range required in these techniques results in a relaxation of the requirements for antenna height related to the long-range and high-power method height requirements. The validity of this observation is limited if fixed range operation over a wide frequency range is attempted.

The range length requirements for the case of the long-range and high-power technique and the scaling technique are shown in Figure 2.3-1. The range reduction resulting from use of the scaling method is evident. The scaled frequencies were selected to be 12 and 35 gigahertz. The effects of target lengths from 20 to 60 feet are illustrated.

The relationship between the full-scale measurement frequency and the ideal antenna height-target height product is shown in Figure 2.3-2. Since the antenna height required for a $2D^2/\lambda$ range is proportional to the square of the scaling factor, the reduction in the required antenna height is extreme in the case of both 12- and 35-gigahertz scaling.

A significant feature needed in the costing analysis is that of the sensitivity required over the spectrum of target lengths, measurement frequencies, and operational approaches and techniques. These features are illustrated in Figure 2.3-3 wherein the required sensitivity is defined in terms of power, antenna gain, noise figure, and bandwidth as a function of full-scale frequency for the case of mobile and fixed range operation and the use of various

techniques. A number of significant observations can be made by using these data. As previously indicated, the primary sensitivity problem is in the high-frequency region, and in terms of the sensitivity required, mobile operation is a clear choice over fixed-range operation. Since the sensitivity requirement does not vary as a function of scaling factor when a range of $2D^2/\lambda$ is maintained, the 60-dB-per decade mobile operation curve is representative of the requirements for both the scaling and the long-range and high-power techniques. It can be seen that the use of full-scale and scaled, fixed-range operation involves an additional 12- and 24-dB sensitivity per octave of coverage, respectively. This fact clearly obviates any attempt at fixed-range operation by the use of scaling because of the limited sensitivity available at the scaling frequencies. There is, however, a region where the fixed-range approach can be used in the full-scale case inasmuch as the present RAT SCAT capability (and a small improvement) will provide adequate sensitivity. The influence of the use of the dielectric lens or analytical correction, in conjunction with a fixed-range length, can be seen as a 20-dB-per-decade line; in the specific example selected, the fixed range length if placed at $2D^2/\lambda$ in the case of a 60-foot target at 4 gigahertz although the effect in terms of the relative sensitivity requirement is independent of the range selected. The present RAT SCAT capability is superimposed in terms of the $PG^2/(NF)(B)$ factor (refer to paragraph 1.2.6).

The data in Figure 2.3-4 is included to illustrate the required improvement in sensitivity relative to the present RAT SCAT capability. The data is presented as a function of full-scale frequency and target lengths from 30 to 60 feet. These data illustrate that the present RAT SCAT sensitivity is adequate for 60-foot targets up to a frequency of 2.6 gigahertz and for 30-foot targets up to 5.9 gigahertz, except in small, isolated regions.

2.4 Trade Off Evaluation Matrices

The results of the technical developments and cost survey presented in this report and are subsequently displayed in Tables 2.4-1 and 2.4-2 in the form of trade-off evaluation matrices. As previously indicated, the purpose of the trade-off is that of demonstrating the relative cost-effectiveness of the various basic techniques and combinations thereof. The evaluation displays are based on the selection of optimum approaches to implementation of techniques or combinations of techniques. The application of a particular method is based on selected frequency bands and target lengths in 10-foot intervals within the frequency band.

The accuracy data displayed in these tables is based on the error analysis of the various methods. These data represent the standard deviation of the error in excess of the present RAT SCAT capabilities. Road construction and control cable costs are significant cost items in the matrices which vary in magnitude as a function of the several measurement methods. These costs have been established at 0.5 dollar per foot for a road similar for mobile van transportation, and 2 dollars per foot for rotator control and signal cable.

Consideration of the following evaluation matrices and the related discussion will reveal that each candidate technique option exhibits a degree of cost-effectiveness although the final selection is a clear choice. Method evaluation is limited herein to application of the various methods in Bands 6 and 7. Adequate sensitivity and range lengths are readily available for long range and high power measurements through Band 5.

2.4.1 Technique-Option I

The data presented in Table 2.4-1 illustrate the basic differential cost and accuracy information related to the long-range and high-power measurement approach which has been selected as Option I for evaluation purposes. These data are based on the lowest cost approach to implementing this measurement technique. As previously indicated, the costs of such items as a high-capacity rotator, mobile van, and fixed antenna tower have been omitted since provision of this capability is necessary in any practical combination of techniques which may be selected. The accuracy

Table 2.4-1 TECHNIQUE - OPTION I

Major Solution: Long Range and High Power Method			
Minor Solution: None			
Standard Evaluation Criteria	Frequency Bands (gigahertz)		Average or Total
	6 (4 - 8)	7 (8 - 12)	
Relative Accuracy, dB(1σ)	0	0	0
Initial Cost of Implement- ing Technique, 1000 Dollars	111.5	72	183.5
Average Data Acquisition Range Hours (5-year basis) 1000 Dollars	1369	1018	2387
Other Recurring Costs (5- year basis) 1000 Dollars	-	-	-
			Cost 2570.5
Matrix Qualifications 2D ² /λ mobile range length			
Extension of Present RAT SCAT Capability			
1. All Bands: 1 MHz Bandwidth IF			
2. Band 6, 7: Phase measurement, coherent integration, low noise preamp, noise subtraction			
3. Band 7: High gain antennas			
4. Roads, signal cable			
Other Considerations			
1. Operational Problems at long ranges (16 miles)			
2. Equipment maintenance costs			

data are based on the present RAT SCAT accuracy since the method is identical to the RAT SCAT method.

The cost data are based on provision of the items tabulated and the data in Table 1.2-3 and 1.2-5. The cost data shown exclude all fixed costs applicable and common to the bands of interest. The cost data are also presented in a noncumulative manner so that omission of this method at the highest frequency band will not influence any cost associated with lower bands. The signal and control cable costs are based on the maximum $2D^2/\lambda$ range associated with a frequency band. The road costs are based on the provision of a lower quality road of the appropriate length for the purpose of mobile van transportation.

2.4.2 Technique-Option II

The use of the long-range and high-power method and the scaling method has been selected as measurement Technique-Option II as shown in Table 2.4-2. In this approach, the long-range and high-power technique is used for the measurement of all targets through Band 5 where sufficient equipment sensitivity is readily available, the range length required at $2D^2/\lambda$ is practical, and no additional error is introduced. In Bands 6 and 7, the scaling technique is used in the measurement of targets whose lengths are in excess of 40 and 30 feet, respectively. Adequate sensitivity is available in the case of other target lengths in these bands, and measurements can be readily made by using the long-range and high-power method.

The accuracy data is based on the discussion presented in paragraph 1.1.4 for the cases where scaling is used. The values shown are based on the average of the errors introduced by perturbation level 1, averaged over the appropriate ka range in each frequency band. In cases where the long-range and high-power technique is used, it is assumed that no additional error is introduced since the measurement procedure is identical to that presently in use at RAT SCAT.

The equipment and target fabrication cost data is based on that described in paragraph 1.2.6 for the case of the long-range and high-power measurements and that in paragraphs 1.1.2 and 1.1.4 for the case of the scaling measurements. Target

Table 2.4-2 TECHNIQUE - OPTION II

Major Solution: Long Range and High Power Method			
Minor Solution: Scaling Method			
<u>Standard Evaluation Criteria</u>	Frequency Bands (gigahertz)		Average or Total
	6 (4 - 8)	7 (8 - 12)	
Relative Accuracy, dB(1σ)	< 1.1	< 1.5	< 1.3
Initial Cost of Implement- ing Technique, 1000 Dollars	200	0	200
Average Data Acquisition Range Hours (5-year basis) 1000 Dollars	1035	661	1696
Other Recurring Costs (5- year basis) 1000 Dollars	176	609	785
Matrix Qualifications		Cost	2681
1. $2D^2/\lambda$ range length through Band 5, Band 6 ($30' \leq D \leq 40'$) 2. Scaling $2D^2/\lambda$ in Band 6 ($40' \leq D \leq 60'$), Band 7 3. Accuracy Averaged over ka range in each band			
Extension of Present RAT SCAT Capability 1. Scaling measurement radar system 2. All Bands: 1 MHz Bandwidth IF 3. Band 6, 7: Phase measurement, coherent integration 4. Signal cable and roads			
Other Considerations 1. Excessive target support cross section levels 2. 35 GHz measurement in stability			

measurement time costs are based on the data shown in Figure 2.2.-5 and Table 2.2-1 on the basis of the discussion in Sub-section 2.2, an average of 1 model was selected for each two targets measured in Bands 6 and 7. The items discussed in paragraph 2.4 have been omitted since these items are common to the various combinations.

The data indicates that an insignificant cost differential but an excessive measurement error level relative to that obtained using Option I.

2.4.3 Technique-Option III

Table 2.4-3 contains the basic cost and accuracy data for the Option III approach to large-object measurement. In this approach, the major solution is the long-range and high-power method, and the minor solution involves the use of a lens for the purpose of providing a reduced range length. The normal RAT SCAT operation method is employed through Band 5 since adequate power can easily be made available in this region. In Band 6 the dielectric lens is used for target lengths above 40 feet since sensitivity is adequate in this band for use of the long-range and high-power technique in the case of smaller targets by using a $2D^2/\lambda$ range length (Figure 2.3-4). The measurements in Bands 6 and 7 are based on using the lens for the 40- to 60- and 30- to 60-foot target lengths, respectively. The accuracy data are based on the discussion presented in paragraph it is assumed that the lens design will be such that it will introduce a 1-sigma error of less than 0.5 dB.

The cost data are based on items listed in Table 2.4-4 and the frequency band-target length allocation discussed previously. The primary cost features involved in utilization of the lens are the initial cost and the recurring cost (lens placement and orientation) established as equivalent to the range time cost of placement of a 60-foot target. The items common to the various combinations have been omitted.

2.4.4 Technique-Option IV

The data shown in Table 2.4-4 illustrate the basic cost and accuracy data for the Option IV approach to large-object measurement. In this approach, the long-range and high-power technique

Table 2.4-3 TECHNIQUE - OPTION III

Major Solution: Long Range and High Power Method			
Minor Solution: Antenna Far Field Simulation			
<u>Standard Evaluation Criteria</u>	<u>Frequency Bands (gigahertz)</u>		Average or Total
	6 (4 - 8)	7 (8 - 12)	
Relative Accuracy, dB (1σ)	< .5	< .5	< .5
Initial Cost of Implement- ing Technique, 1000 Dollars	44.5	0	44.5
Average Data Acquisition Range Hours (5-year basis) 1000 Dollars	1369	1018	2387
Other Recurring Costs (5- year basis) 1000 Dollars	20	22	42
Matrix Qualifications		Cost	2473.5
1. $2D^2/\lambda$ range length through Band 5, Band 6 ($30' \leq D \leq 40'$) 2. 21,000 foot maximum range in Band 6 ($40' \leq D \leq 60'$), Band 7			
Extension of Present RAT SCAT Capability: 1. Dielectric Lens and Shelter 2. All Bands: 1 MHz Bandwidth IF 3. Band 6, 7: Phase measurement, coherent integration 4. Band 7: Low noise preamp 5. Signal Cable and roads			
Other Considerations:			
Weather Limitations			

Table 2.4-4 TECHNIQUE - OPTION IV

Major Solution: Long Range and High Power Method			
Minor Solution: Analytical Correction of Near Field Data			
<u>Standard Evaluation Criteria</u>	<u>Frequency Bands(gigahertz)</u>		Average or Total
	6 (4 - 8)	7 (8 - 12)	
Relative Accuracy, dB(1σ)	< .6	< .8	< .7
Initial Cost of Implement- ing Technique, 1000 Dollars	87	72	159
Average Data Acquisition Range Hours (5-year basis) 1000 Dollars	1369	1018	2387
Other Recurring Costs (5- year basis) 1000 Dollars	-	-	-
		Cost	2546
Matrix Qualifications			
1. $2D^2/\lambda$ range length through Band 5, Band 6 ($30' \leq D \leq 60'$)			
2. $< 2D^2/\lambda$ range in Band 6 ($40' \leq D \leq 60'$), Band 7			
Extension of Present RAT SCAT Capability			
1. All Bands: 1 MHz Bandwidth IF			
2. Bands 6,7: Phase measurement, coherent integration			
3. Band 7: Noise subtraction			
4. Roads, signal cable			
Other Considerations:			
Operational problems at long ranges (8 miles)			

is used in conjunction with a $2D^2/\lambda$ range length through Band 5 since adequate power is available in this region. In Bands 6 and 7, the method of analytical correction of near-field data is employed in conjunction with a maximum range of D^2/λ in order to reduce cost through a reduction of sensitivity requirements and other costs associated with range length. The cost items described in paragraph 2.4 have been omitted from this matrix since these items are common to the various combinations.

The accuracy data are based on the discussion in Subsection 1.4. Through Band 5 and for target lengths from 30- to 40-feet in Band 6, no additional error is introduced because the measurement technique is identical to that presently used at the RAT SCAT Site. It is assumed that the primary concern is obtaining data on the peak envelope and lobe structure of the target scattering pattern; in this case, errors in the vicinity of the pattern singularities (nulls) are not of interest.

The cost data are based on the items listed in Table 1.4-2 and the range lengths specified. It will be noted that, relative to other options, a substantial reduction in cost will result from use of the measurement approach described although the error levels are significantly higher.

2.5 Conclusions

On the basis of the data previously presented in the trade-off matrices, the most cost-effective approach to the measurement of large-object radar cross section is a combination of the long-range and high-power method and the antennas far-field simulation method. The long-range and high-power method involves the use of an approach which is a duplicate of the present operational procedures used at the RAT SCAT site. The antenna far-field simulation method involves the use of a dielectric lens in the vicinity of the target. The primary disadvantage in the recommended approach is the operational problem associated with the lens setup time. However, the cost reduction in terms of costs associated with range length and the small error level anticipated offset this potential disadvantage.

All methods considered exhibit a degree of cost effectiveness which may warrant consideration in other more specialized applications. The complete coverage of the target length - frequency spectrum of interest by using the long-range and high-power method imposes potentially severe operational problems in that a maximum range length of 16 miles is required and the cost to achieve the required sensitivity is excessive. A significant reduction in range length and target handling cost can be realized by the use of the scaling method, but these advantages are effectively offset by the high initial cost of a high-frequency (35 gigahertz) measurement system and the high cost of suitable accurate scale models of the full-scale targets. Only a small reduction in costs associated with range length can be realized by employing a range length criterion of less than $2D^2/\lambda$, and the errors introduced by the resulting phase curvature of the illuminating field partially nullify the cost advantages.

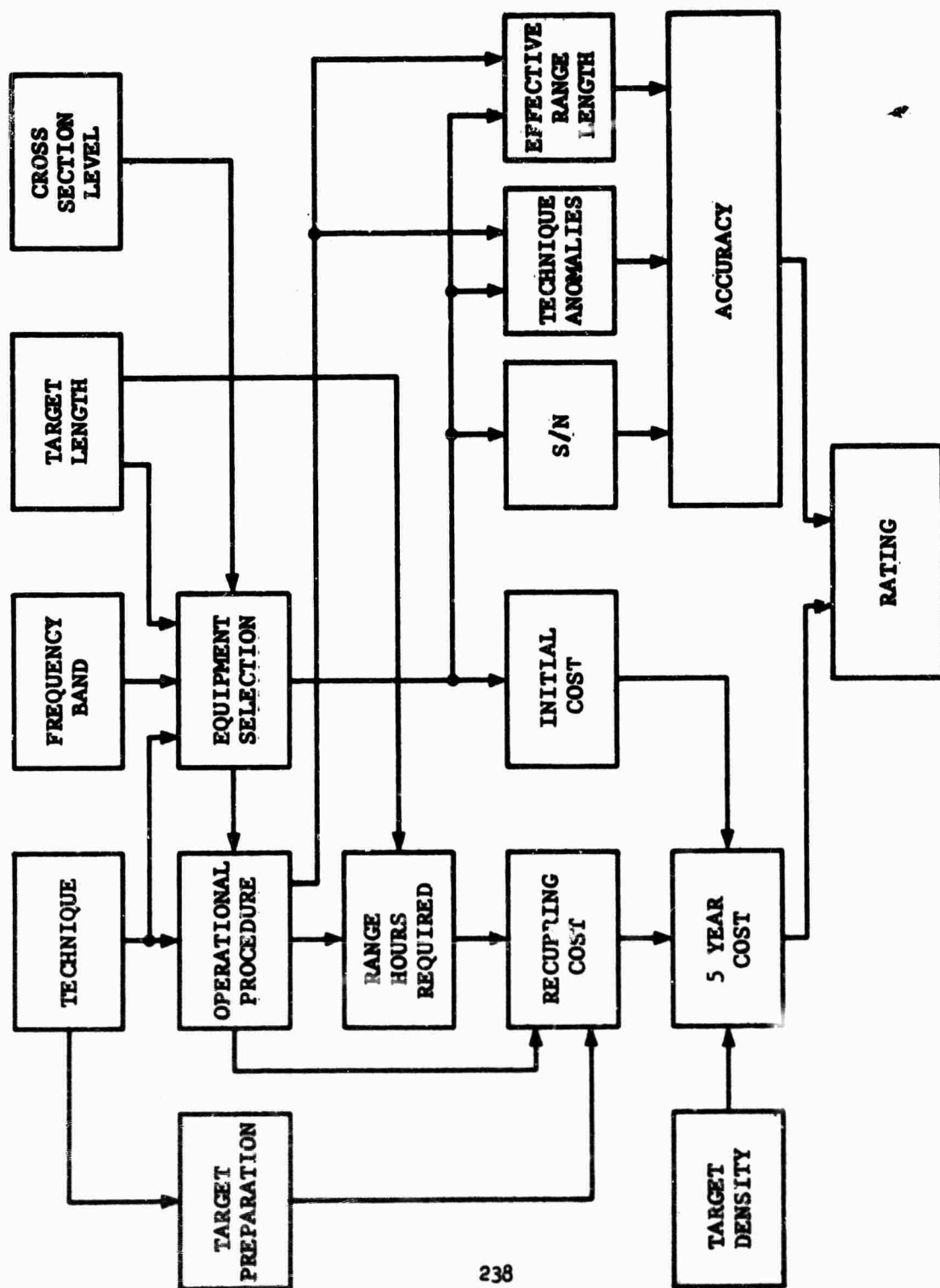


Fig. 2.1.1-1 PROCEDURE FLOW DIAGRAM FOR TRADE OFF STUDY

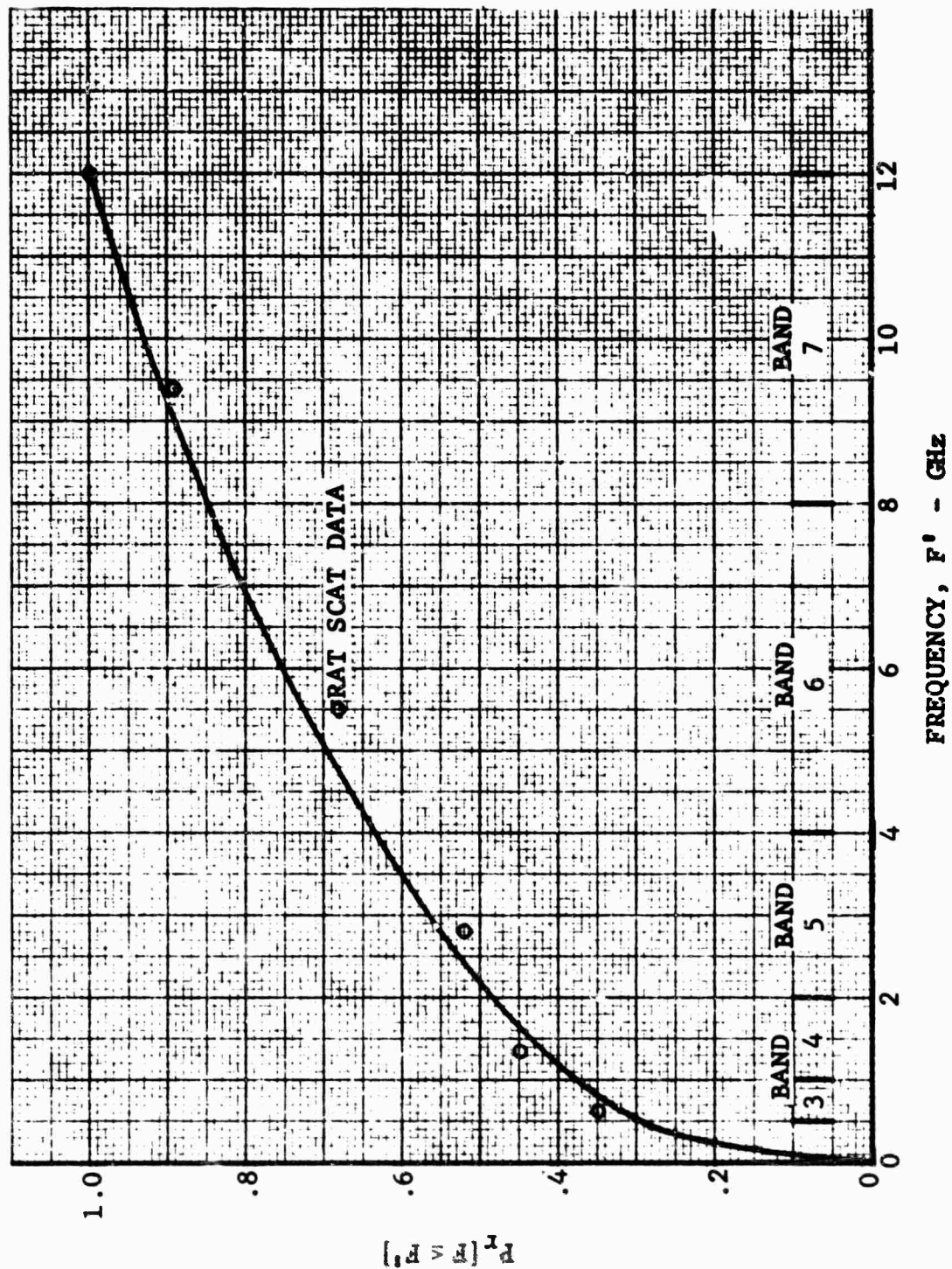


Fig. 2.2-1 CUMULATIVE DENSITY ON MEASUREMENT FREQUENCY

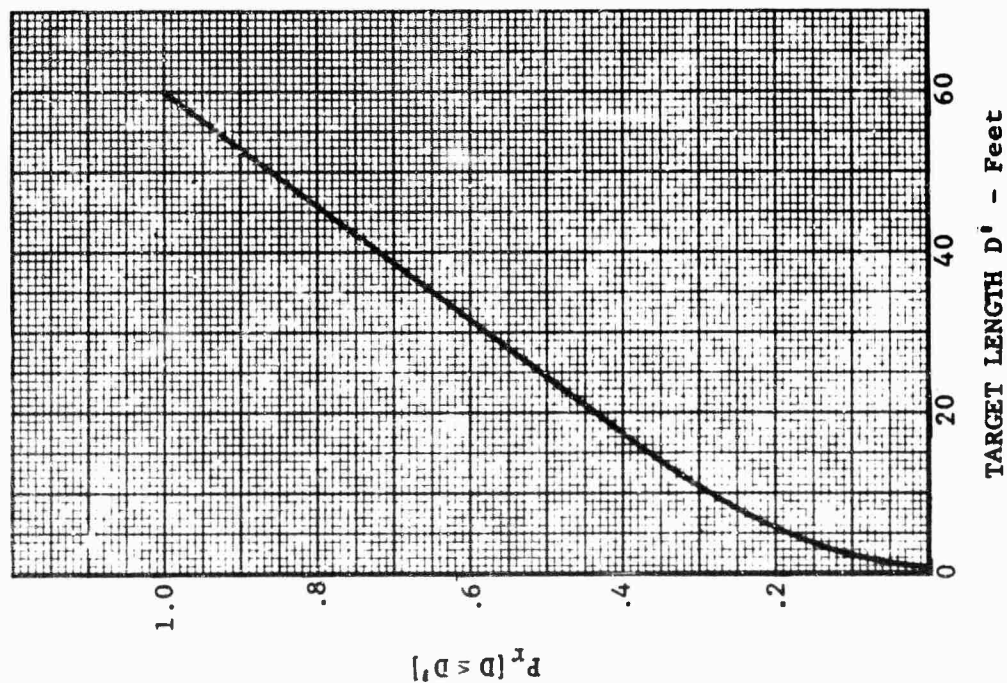


Fig. 2.2-2 CUMULATIVE DENSITY ON
TARGET LENGTH

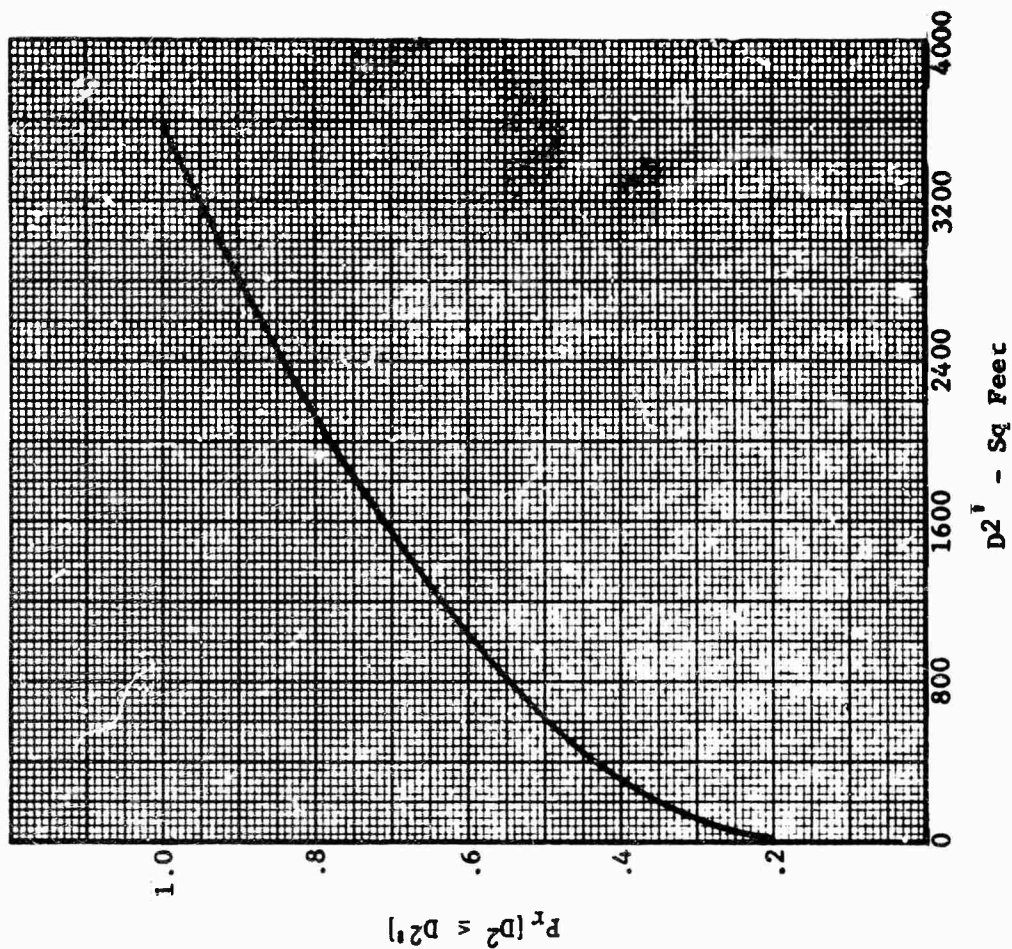


Fig. 2.2-3 CUMULATIVE DENSITY ON
TARGET LENGTH SQUARED

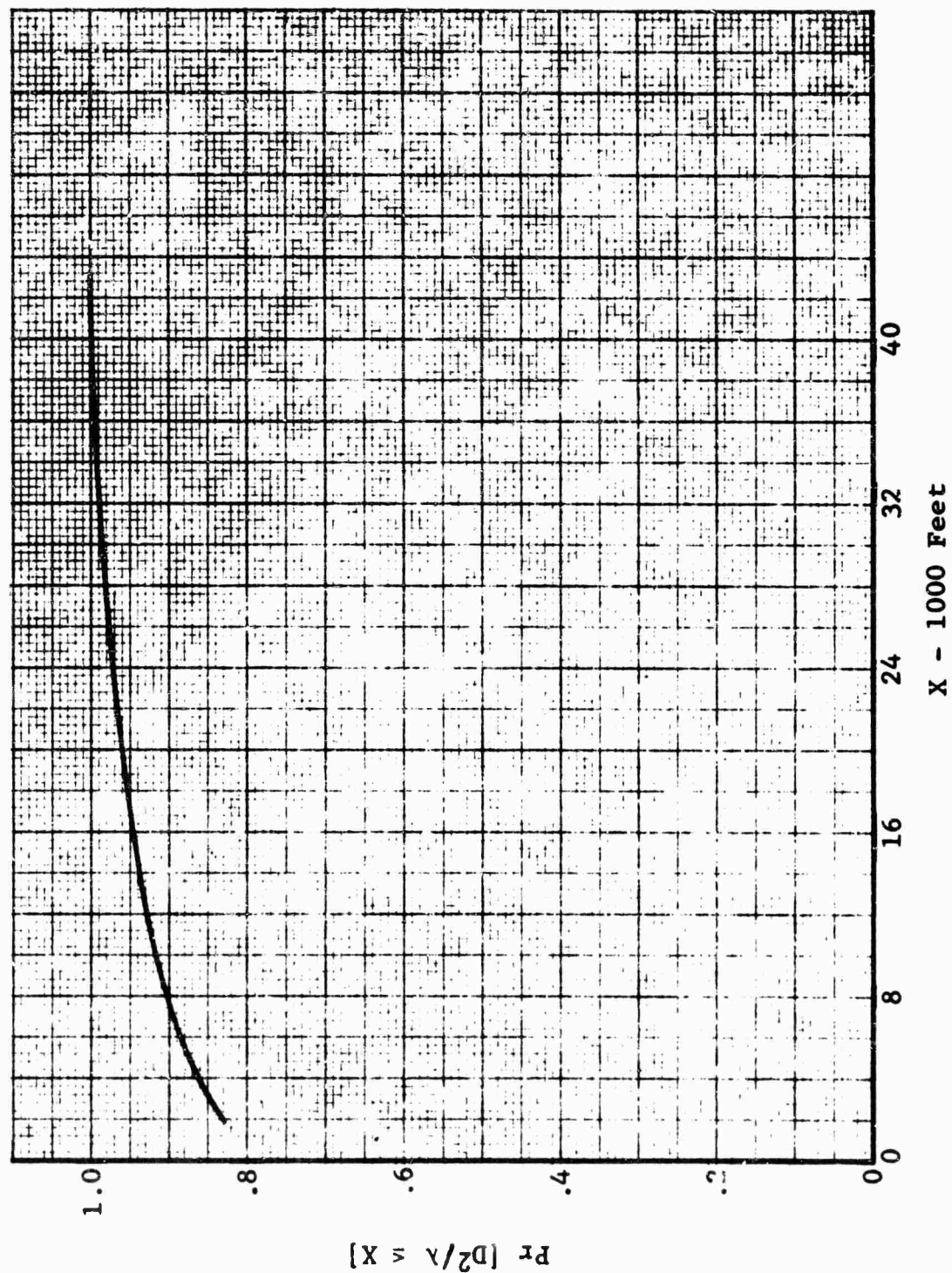


Fig. 2.2-4 CUMULATIVE DENSITY OF D^2/λ

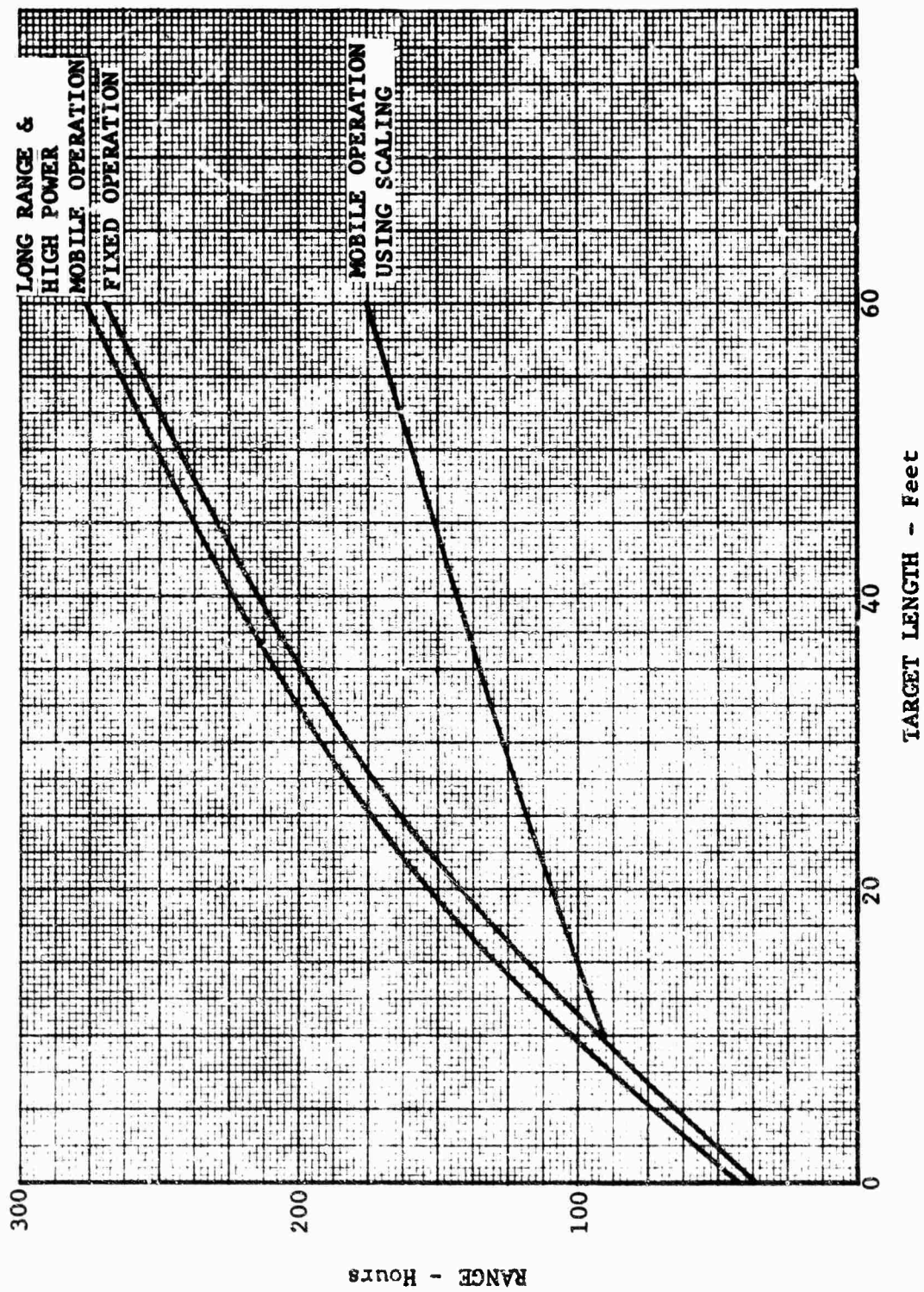


Fig. 2.2-5 MEASUREMENT TIME AS A FUNCTION OF TARGET LENGTH

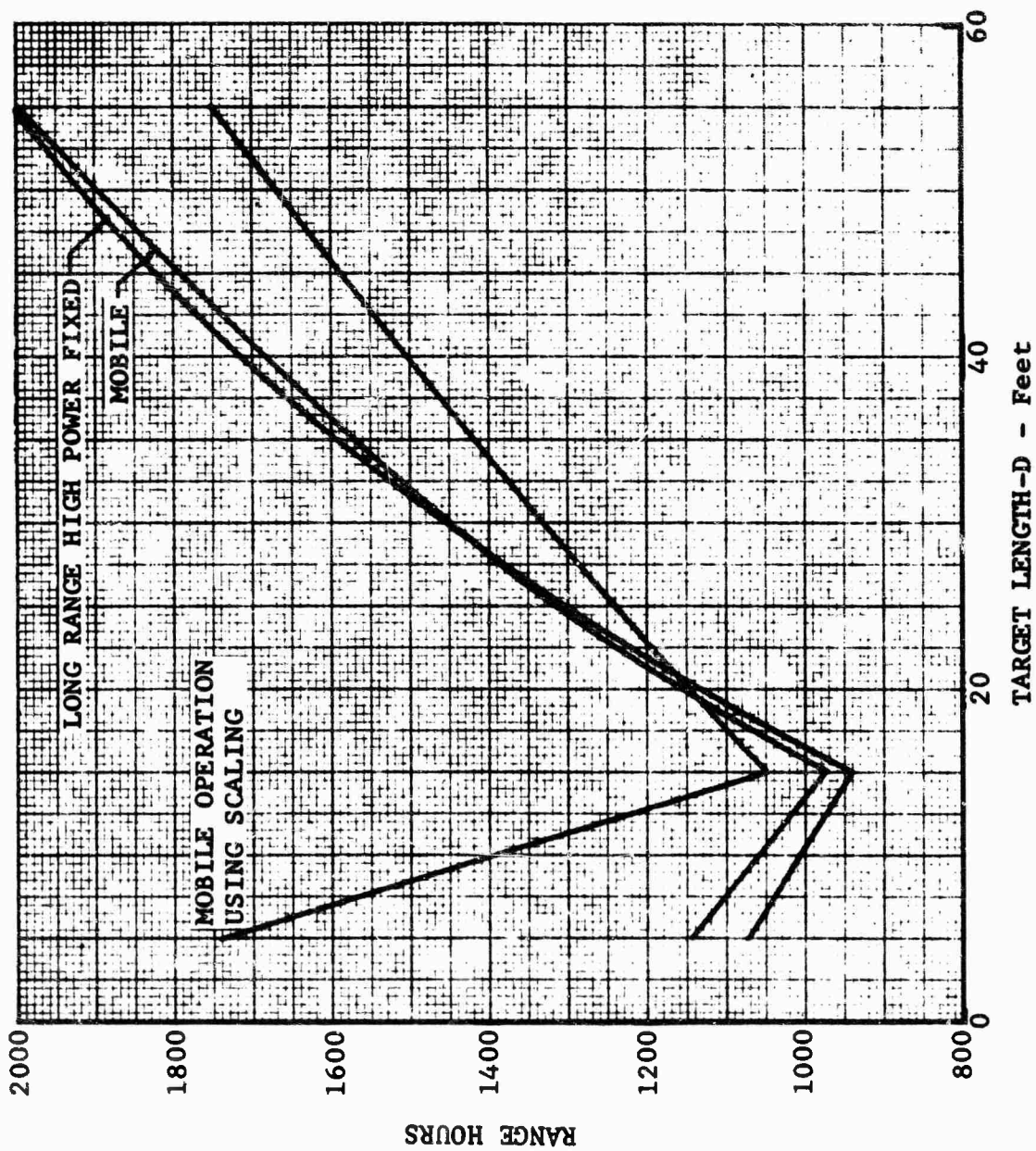


Fig. 2.2-6 TOTAL RANGE HOURS AS A FUNCTION OF TARGET LENGTH

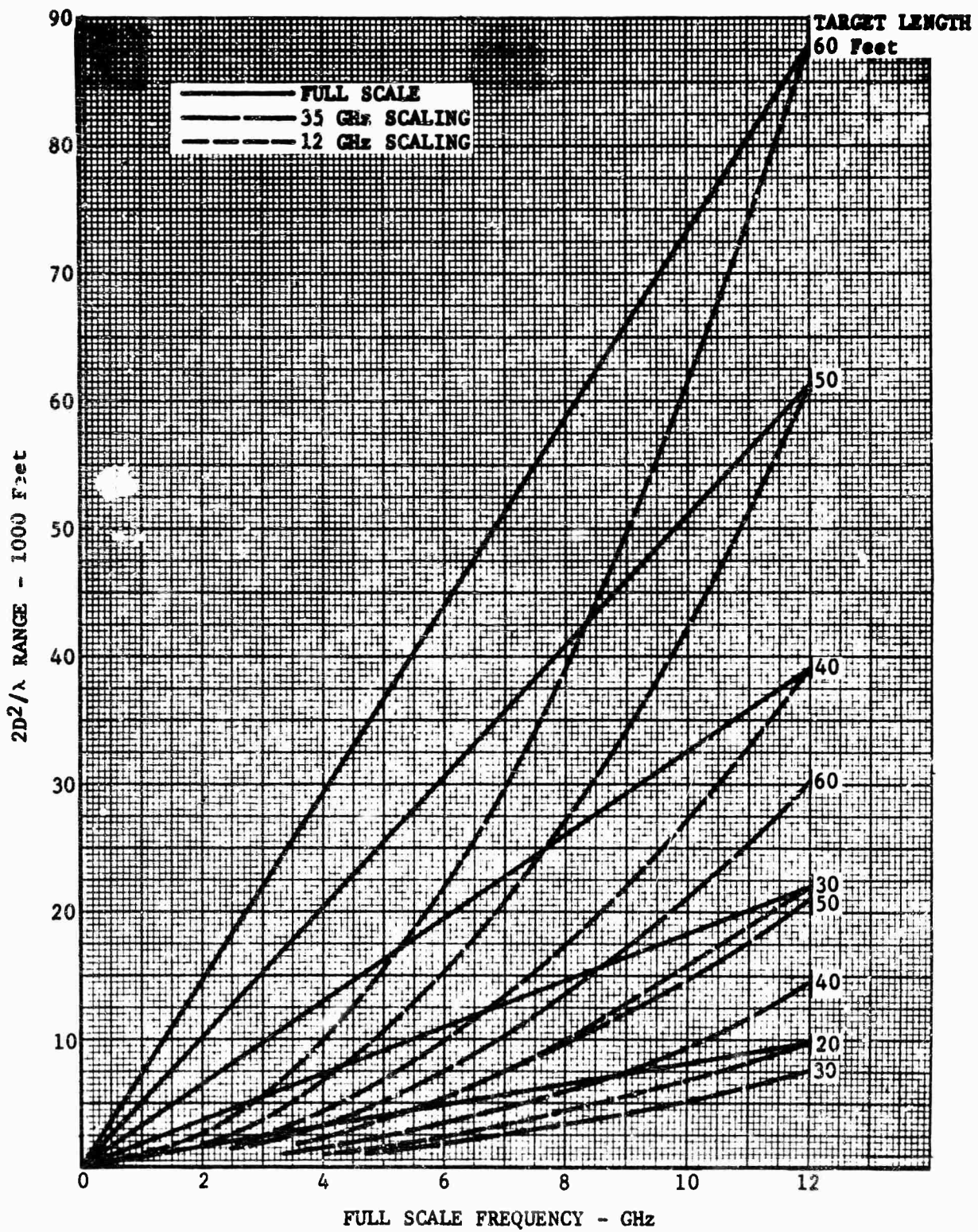


Fig. 2.3-1 RANGE LENGTH REQUIREMENT

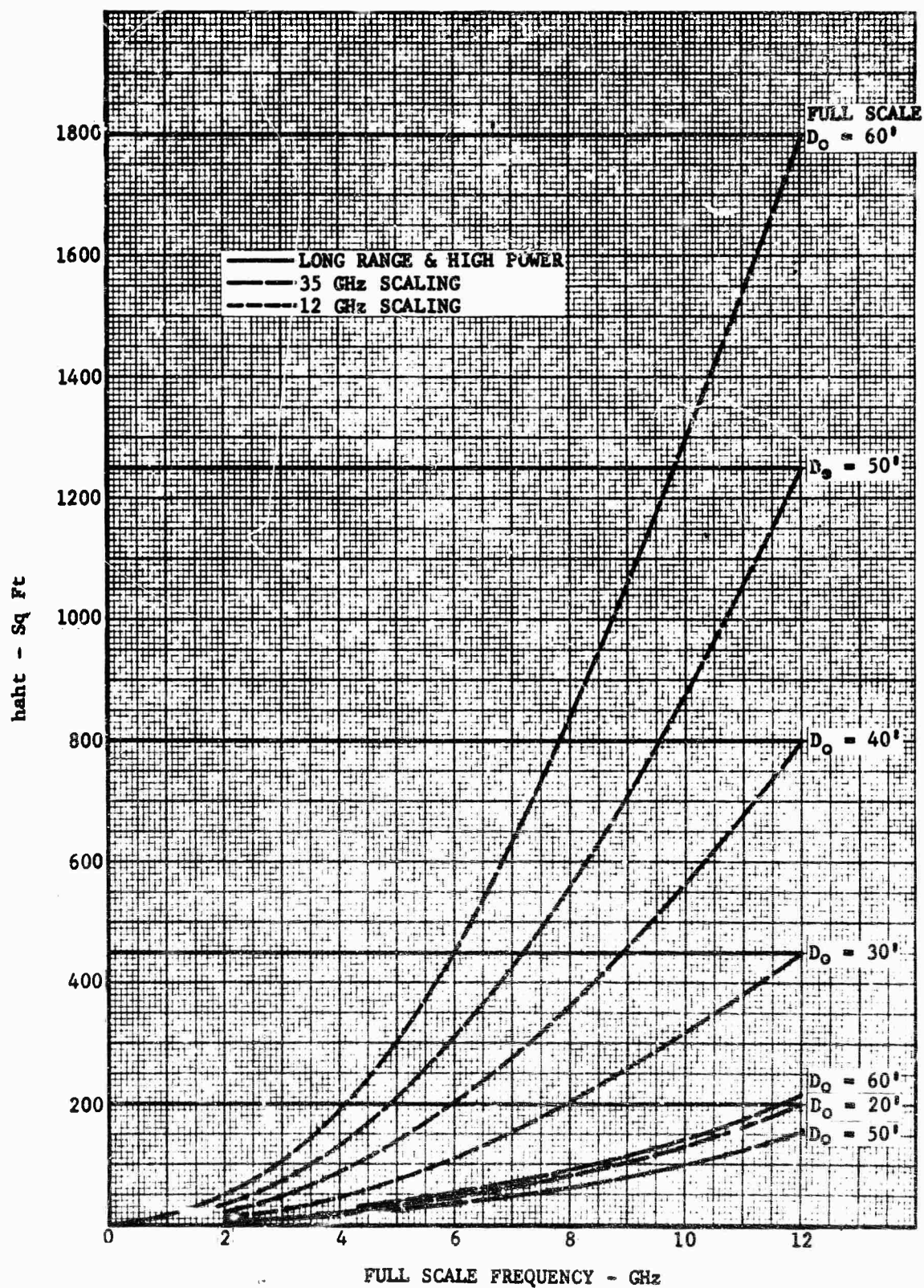


Fig. 2.3-2 ANTENNA-TARGET HEIGHT REQUIREMENT

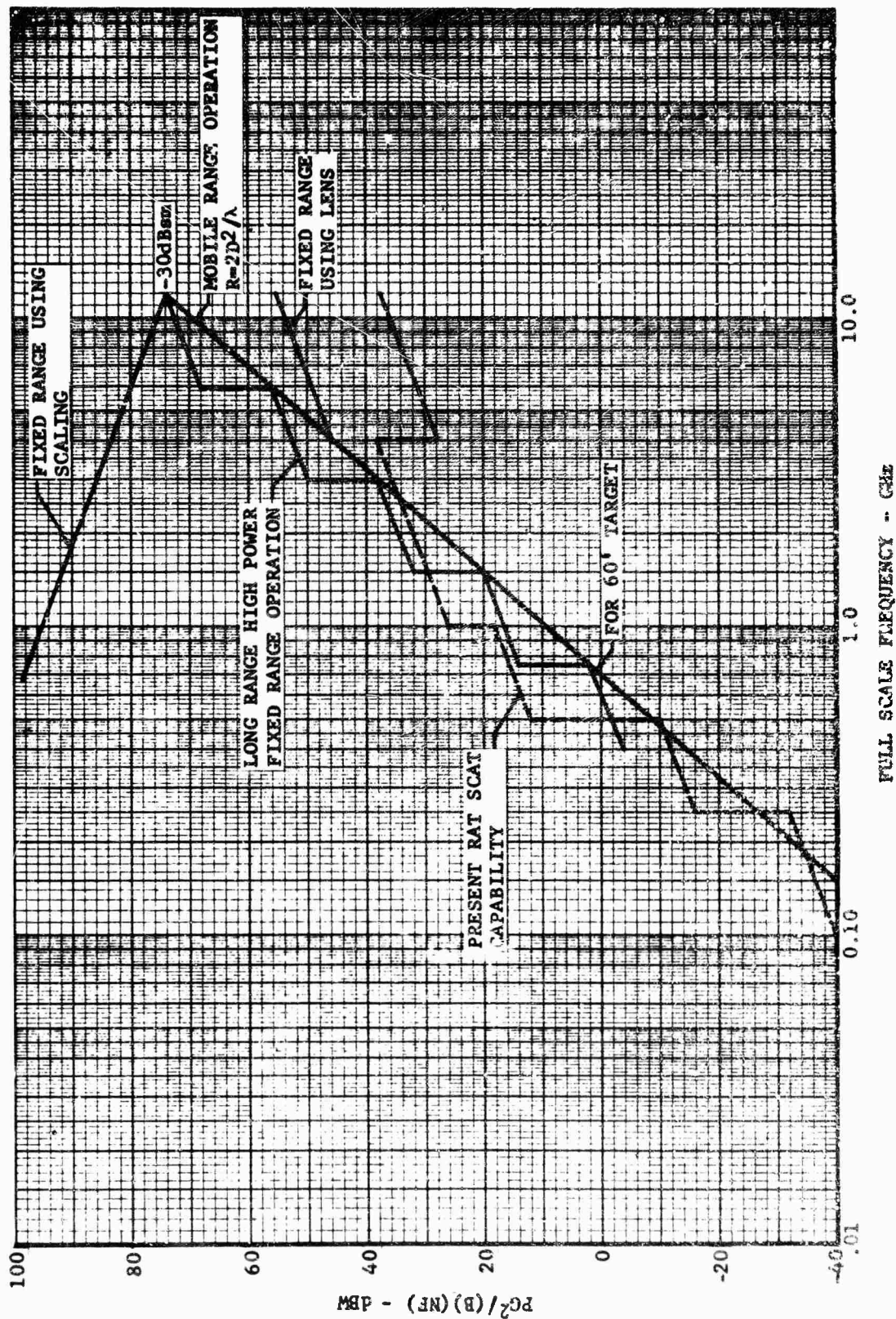


Fig. 2.5-3 SENSITIVITY REQUIREMENTS

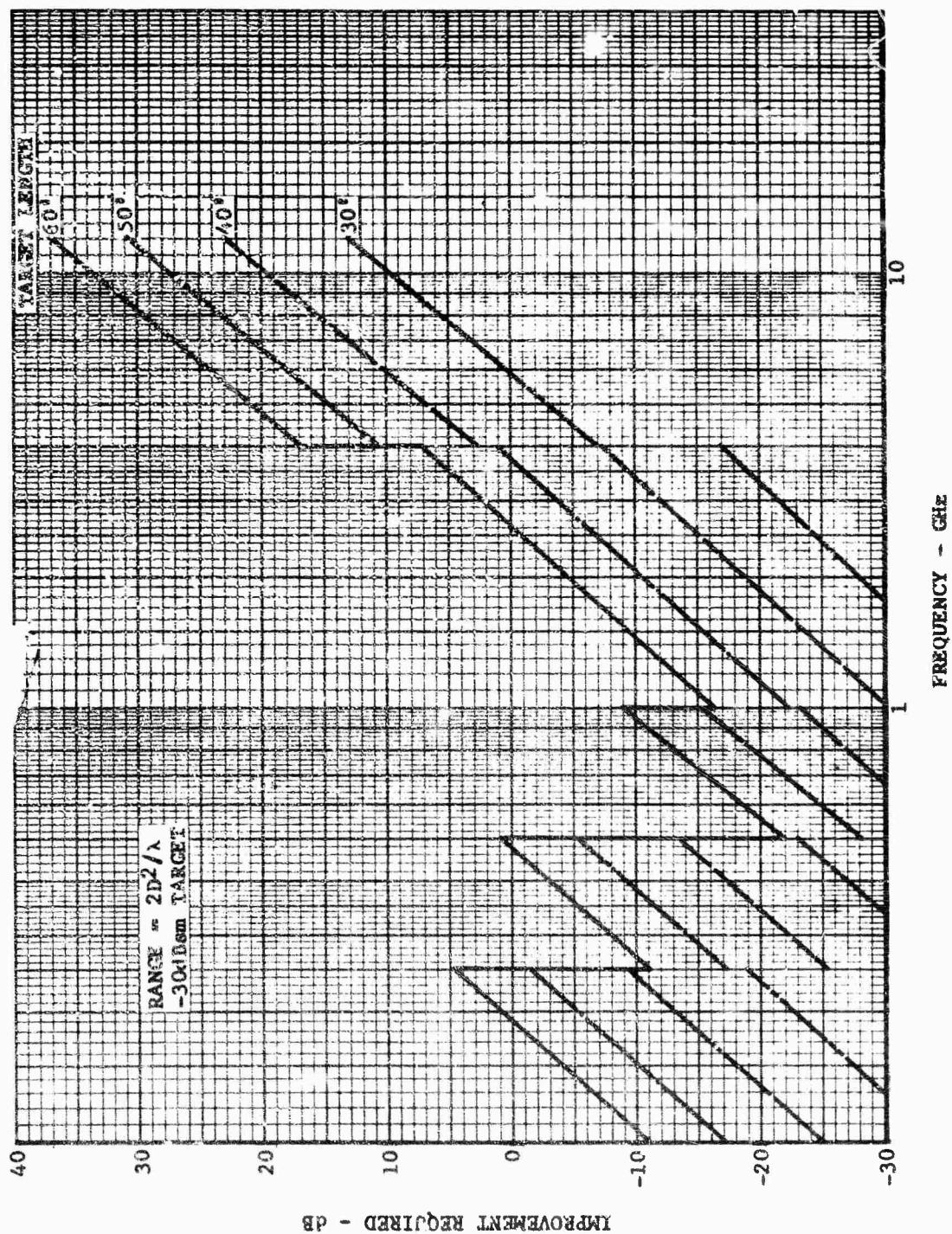


Fig. 2.3-4 SENSITIVITY IMPROVEMENT REQUIREMENTS

SECTION 3

RECOMMENDATIONS

3.1 General

This section contains a description of the equipment and operating procedures recommended for providing an optimum means of large-object measurement. Specific recommendations are made for all the necessary new equipments, modification of existing RAT SCAT equipments, and interface connections, as appropriate. The description of recommended equipments which are germane to the selection of the basic methods includes a breakdown of major components to be used by manufacturer name and part number and block diagram drawings of the functional concept of the equipments.

3.2 Measurement Subsystem

The necessary additions to the present RAT SCAT equipments and the basic interface connections are presented in Figure 3.2-1 in conjunction with the present RAT SCAT equipments. As indicated in previous subsections, the 1-megahertz bandwidth IF amplifier (applicable to all frequency bands), the Band-7, low-noise preamplifier, and the coherent integration capabilities in Bands 6 and 7 are required in order to achieve the necessary equipment sensitivity. The basic phase measurement capability in Bands 6 and 7 is required to utilize the coherent integration subsystem. The purpose and area cost of these items are presented in Table 3.2-1. The only other component required on the basis of the basic measurement method selection is the dielectric lens. References to selected equipments and components are presented in Table 3.2-2.

Required facility improvements include the appropriate antenna tower, a mounting pad for the dielectric lens, a large target rotator, the rotator signal and control cables required for use in mobile van operation and a lens shelter significant features of these components and facilities are discussed in the following paragraphs.

Table 3.2-1 LARGE OBJECT IMPLEMENTATION DESIGN SUMMARY

EQUIPMENT	ITEM	PURPOSE	COST (1000 Dollars)
Sensitivity Impact Items	RF preamplifier	Increase sensitivity	5
	1 MHz IF amplifier	Increase sensitivity	2.5
	Phase measurement capability	Coherent integration & background reduction*	75
	Coherent integra- tion	Increased sensitivity	8.5
Range Impact Items	Lens	Reduce range length	30
	Mobile towers	Optimize sensitivity	60
	Mobile equipment van	Optimize sensitivity	6
	Rotator & azimuth encoder	Provide range length, weight capability, azimuth speed, and resolution	310
	Generator	Rotator power and control signals	77.6
	Roadway	Provide access to rotator	14.4
	Lens shelter	Protect dielectric lens	10
	Gantry	Provide target handling capability	50
Budgetary Cost			647.5

*Bands 3, 4, 5, 6, 7

Table 3.2-2 SYSTEM IMPLEMENTATION COMPONENTS

Item	Components	Reference
1 MHz IF Amplifier	Modified present 2 MHz IF Amplifier	
RF Preamplifier	WJ 240	Watkins Johnson
Phase Measurement Capability	MHS-400 Synthesizer TFM-101 Multiplier 2650A Synchronizer	Manson Labs Manson Labs Dymec
Mobile Antenna Towers	-	Andrews Tower Co. Dallas, Texas
Lens	(Refer to Fig. 3.2-4)	Plastics Structures, Inc. Menlo Park, California
Rotator and Azimuth Encoder	(refer to Table 3.4-1)	C. W. Jones Engineering Los Angeles, California

3.2.1 Phase Measurement

The basic block diagram of the phase measurement subsystem is presented in Figure 3.2-2. The basic system tie-in is also shown. Basic components required in this subsystem are shown in Table 3.2-2. The synthesizer is the stable signal source required in phase measurements. The synchronizers are commercial units modified with a varicap unit to pull the crystal oscillator, thereby providing a frequency modulation input. The feedback circuit from the transmitter output is included for the purpose of minimizing the effects of phase shift in the transmitter components. The process illustrated results in providing a coherent reference and local oscillator signal to the present RAT SCAT receiver and phase servo. Details of the operation of the present phase-measurement subsystems can be found in Reference 14.

3.2.2 Coherent Integration

The basic block diagram of the coherent integration subsystem is shown in Figure 3.2-3; present RAT SCAT components are cross hatched. Basic system operation and the required tie-in to the phase-measurement subsystem, are also illustrated in this figure. As seen in Figure 3.2-3, the majority of the components required are presently used RAT SCAT equipments. The input signals required are the normal gated IF signal and the target phase reference signal which is obtained from the phase sensitive detector in the phase servo. The coherent detector recommended is a modification of the phase detector in the present phase servo. The AGC circuit requirements will consist of a modification to the present AGC to increase the dynamic range. By using this approach, essentially no changes to the sigma servo are required except for optimizing incoherent integration, and interface problems are therefore reduced.

3.2.3 Dielectric Lens

The preliminary specifications on the dielectric lens are shown in Figure 3.2-4. These specifications are based on the provision of a polyfoam material with a dielectric constant of 1.05. The basic configuration is formed from a polyurethane foam; a fiberglass supporting ring (I beam or box) is incorporated to provide structural rigidity and a means of attaching guy

lines. A 1/64-inch-thick mylar sheet or similar material is used to provide a degree of protection for the foam surface from sand and rain effects. The equation of the recommended lens surface is shown in the figure.

3.2.4 Antenna Towers

Antenna towers for use in mobile operation are recommended on the basis of the requirement for mobile operation. The basic tower preliminary requirements include

1. Utilization of the present RAT SCAT antennas
2. A maximum antenna height of 150 feet
3. A capability to withstand a 50 knot wind with 28 foot antennas emplaced.
4. The incorporation of a servo to orient the antenna dishes over a ± 10 -degree angular region in the principal planes.

The requirement for the mobile antenna includes provisions of a telescoping configuration. Although additional flexibility is provided by the availability of 150 foot fixed antennas, the optimum capability afforded by the use of mobile antennas suggests eliminating the additional cost of fixed towers.

3.3 Measurement Procedures

If the proposed measurement methods are used, the only deviations from the present procedure will be associated with the use of a dielectric lens and operation at the long range lengths required.

3.3.1 Lens Utilization

A number of steps must be accomplished in obtaining the proper range geometry for utilization of the lens. These steps include emplacing the lens at the proper position relative to the target or target pit, and properly placing the mobile van and associated equipments relative to the target or lens position.

The mounting recommended for the dielectric lens is shown in Figure 3.3-1. A shelter similar to that presently used at RAT SCAT to move large targets will be required for the purpose of emplacing and providing protection during inclement weather.

The envelope of the separation required between the lens and the target extremities is shown in Figure 3.3-2 as a function of frequency at a range length of 21,000 feet. The envelope is limited to a separation of 600 feet in order to provide adequate system recovery time and thereby essentially eliminate the effects of the radar cross section of the lens on the signal received from the target. The longest separation distance is limited by the loss of signal strength or the amplitude gradients expected.

The envelope, presented in Figure 3.3-3 as a function of target length and frequency indicates the bounds imposed by the recommended equipment sensitivity and the effective antenna system aperture. However, operation at a range length of 21,000 feet is recommended.

Both of the envelopes discussed above are established in a manner designed to insure the proper operation of the lens; therefore, some operational experience with the lens is expected to enable expansion of these envelopes.

3.3.2 Long Range Operation

The geometrical parameters associated with measurements at long-range lengths are identical to those presently used at RAT SCAT although adjustments may have to be made in the antenna height in order to obviate the effects of the earth curvature and atmospheric refractions. The terrain elevation contour will tend to reduce the effects. Tests conducted at RAT SCAT indicate that no significant amount of terrain preparation will be required. However, operation based on the use of mobile equipment will normally be required in order to realize adequate sensitivity; excluding lens utilization, sensitivity recommendations have been based on a range length of $2D^2/\lambda$, although some flexibility has been provided in this area. The range length envelope present in Figure 3.3-4 is established on the basis of antenna height limits and $2D^2/\lambda$ criterion.

The map presented in Figure 3.3-5 illustrates the recommended range layout. This layout was selected on the basis of terrain features and the utilization of existing roads.

The recommended position of the rotator pit is along the dashed line shown in Figure 3.3-5 at a range of 5000 feet from the operations building. The criteria used for selecting this location were the proximity of the rotator to the storage locations of the larger targets and the lens which are expected to be in the vicinity of the operations building. This location allows a 2500-foot separation between the subject rotator and the pit 3 rotator; this distance should be adequate to avoid any significance conflict between measurements being conducted on pit 3 from the operation building and from this down-range location of the mobile equipment.

The recommended location of the mobile unit with and without the use of the dielectric lens is along the dashed shown in Figure 3.3-5. The approximate maximum range required using the lens is 21,000 feet, and the maximum range required without the lens is 28,800 feet. These conditions coincide with the measurement of a 60-foot target at 12 and 4 gigahertz, respectively. The basic region for use of the lens is from 30- to 60-foot targets in Band 7 and 40- to 60-foot targets in Band 6.

3.4 Ancillary Equipments

In this subsection, a number of ancillary equipments are recommended for implementation for use in the large-object measurement program. The recommendation of these equipments is based on general requirements that are not related to the selection of a specific method of large-object measurement. These equipments include a target rotator, a data recording subsystem, and a vector subtraction subsystem.

3.4.1 Target Rotator

A set of preliminary rotator specifications are presented in Table 3.4-1. The most significant of these specifications are those for the weight bearing capability (refer to subsection 1.2), the rotation rate, the digital encoder readout resolution, and backlash. Each of these items are related to basic requirements for expected target weights and data resolution. The 0.02-degree resolution and the backlash specified are compatible with the data-recording interval recommended.

Table 3.4-1 PRELIMINARY ROTATOR SPECIFICATIONS

Item	Specification
Capacity	50,000 lbs
Table width	40 feet
Table tilt	0 to 3 degrees
Rotation rate	.01 to .5 rpm
Gear backlash	.02 degrees
Table surface tolerance	.01 inch
Encoder readout	0.02 degrees

3.4.2 Data Recording

The provision of additions to the recording equipment is required for large-object measurement programs. This requirement is independent of the measurement method employed (refer to paragraph 1.2.6). Previous studies by the Fort Worth Division and RAT SCAT personnel have resulted in implementation proposals and equipment testing in this area. The projected capability in the area of analog and digital recording is adequate for large-object measurement programs. An all-electric (digitally controlled) Sigma Servo prototype has been delivered to RAT SCAT and is currently undergoing testing. This unit has a maximum capability of 10,000 dB per second, which is far in excess of the anticipated requirements.

It appears that the analog recorder whose required data rate is on the order of 1000 dB per second, 10-inch readout (60 inches per second) cannot be reasonably achieved by using a mechanical recorder similar to that presently used at the RAT SCAT site. The present capability is approximately 300 dB per second. The most appropriate means of providing the required capability is the use of a "light pen" unit, such as the Hewlett Packard 4508B, whose writing speed is in excess of 1000 dB per second (2-kilohertz bandwidth). This type of unit is relatively expensive in terms of both initial and operating cost, but it is required if the necessary analog-recording resolution is to be provided.

The projected RAT SCAT capability in the area of on-line magnetic tape recording will provide the necessary digital recording capability (Reference 14). This capability is provided in the new data console configuration. The only significant requirements in this area are the provision of the correct RAT SCAT formulating and a data rate on the order of 30 data blocks per second.

3.4.3 Vector Subtraction

The implementation of a vector subtraction process is recommended in order to enhance the RAT SCAT target support level of capability. The recommended process is identical to that presently available at RAT SCAT in Band 4 (Reference 6). The implementation of the process imposes a requirement for phase measurement capability and a computer. The PB 250 pre-

sently used at RAT SCAT does not contain adequate storage capacity for the large-object measurements. The required capacity is on the order of 40,000 data blocks for programming and data storage. This figure includes a capacity of 36,000 words (phase and cross section data, indexed on azimuth degree) for a 0.02-degree sampling interval (refer to paragraph 1.2.6). A SDS 910 computer will provide adequate storage and the necessary computation for this approach although the most cost effective approach may be that of programming and utilizing an existing computer facility.

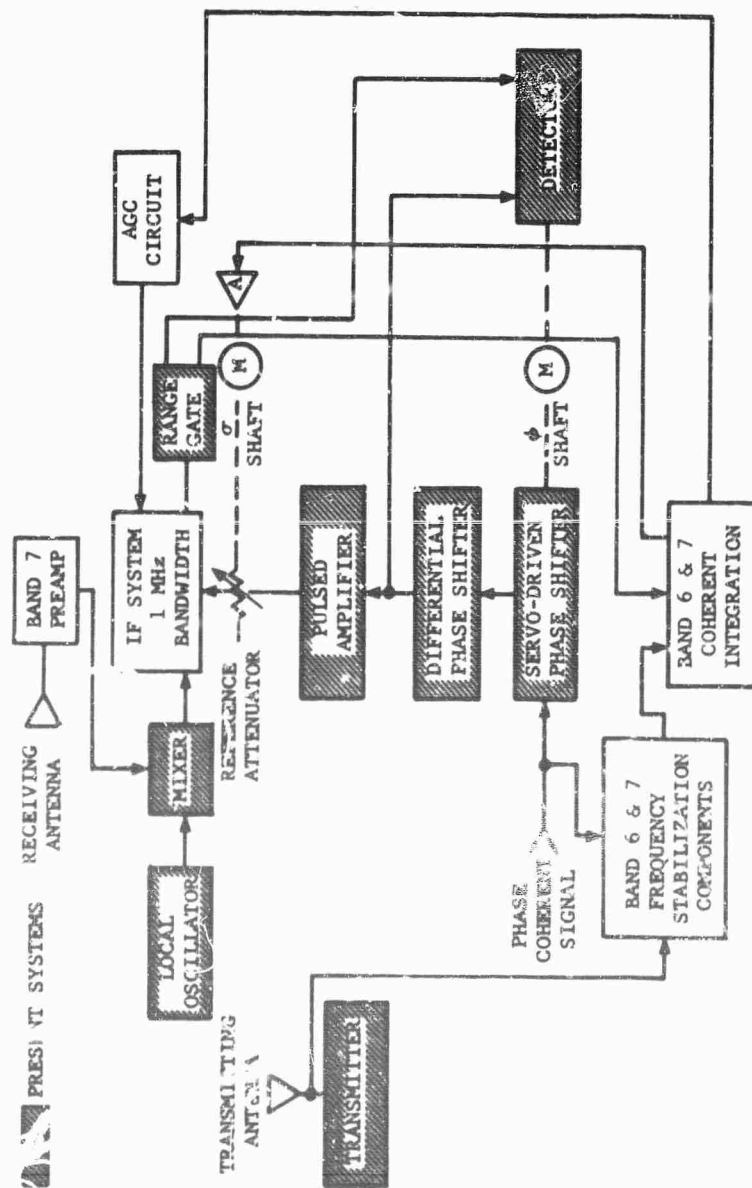


Fig. 3 -1 BASIC RAT SCAT EQUIPMENT ADDITIONS

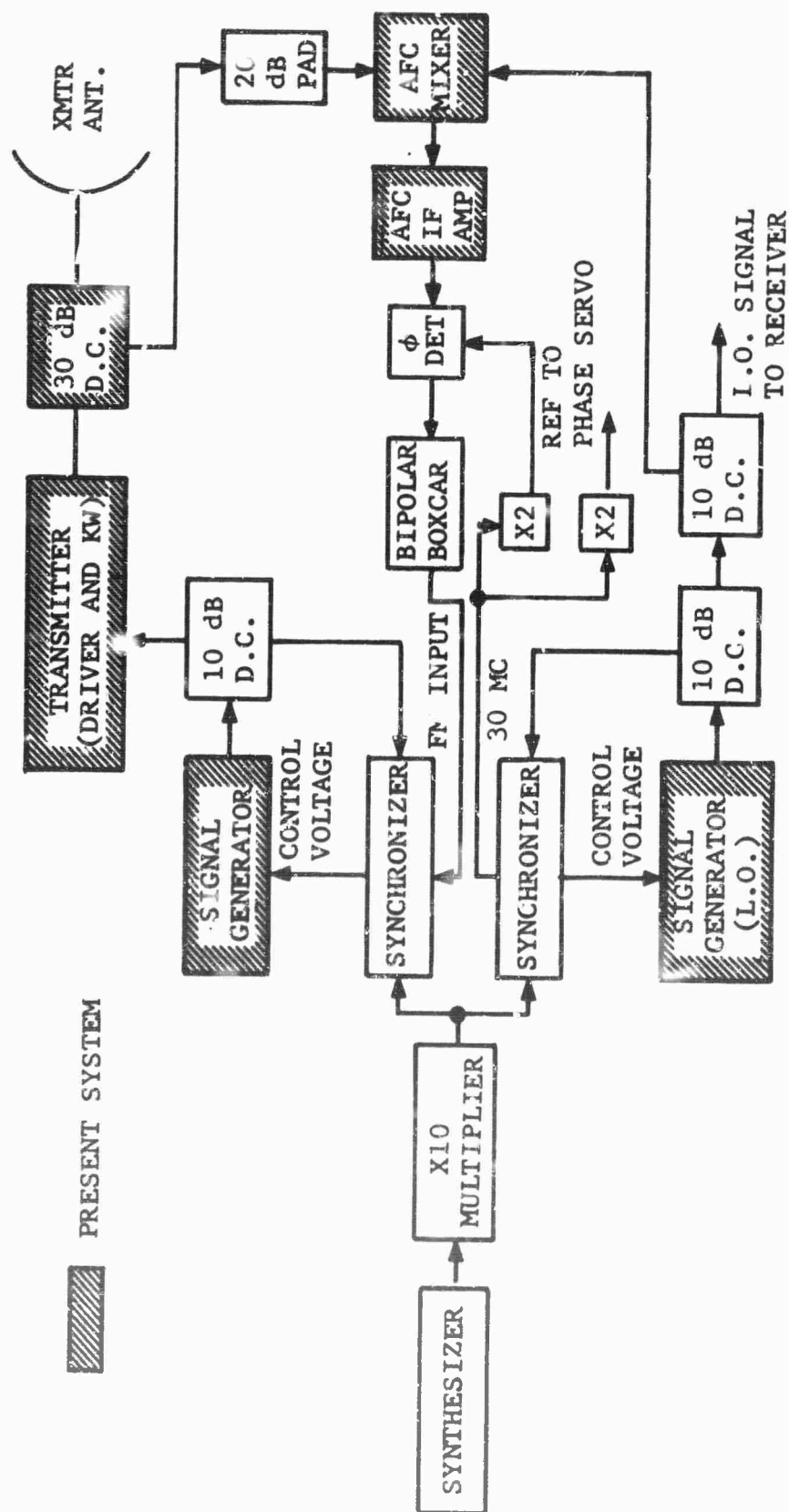


Fig. 3.2-2 PHASE MEASUREMENT BLOCK DIAGRAM

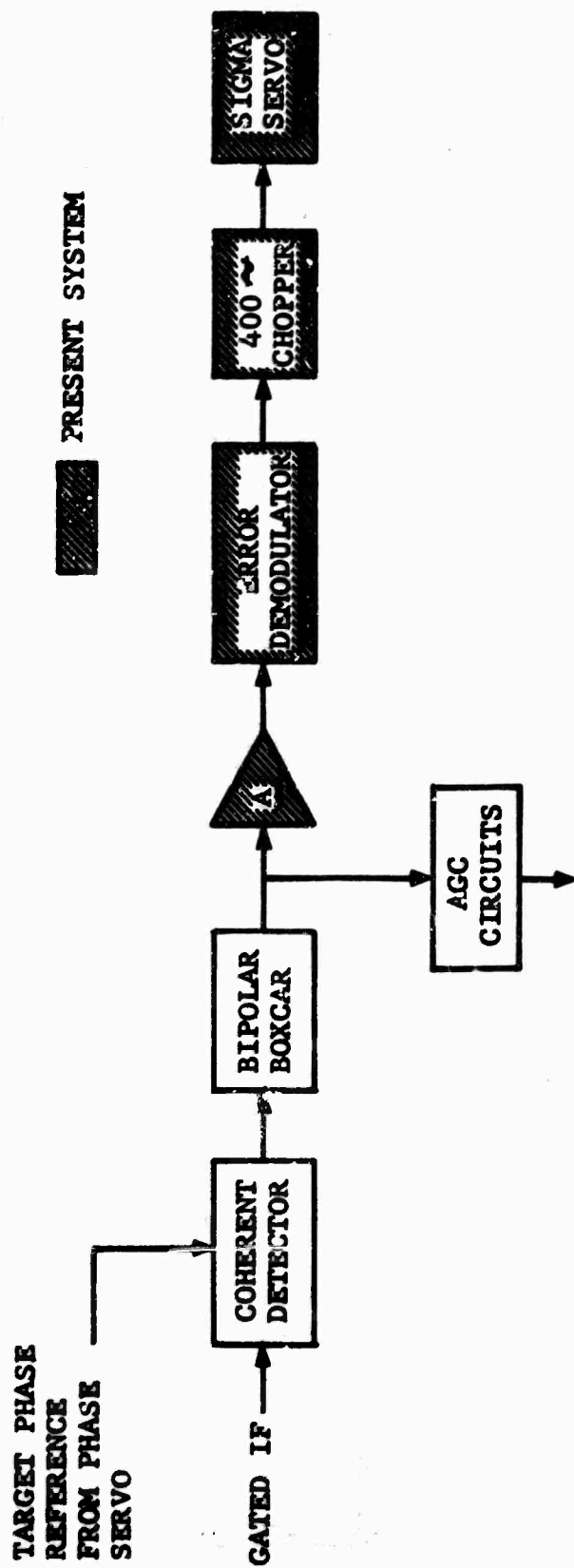
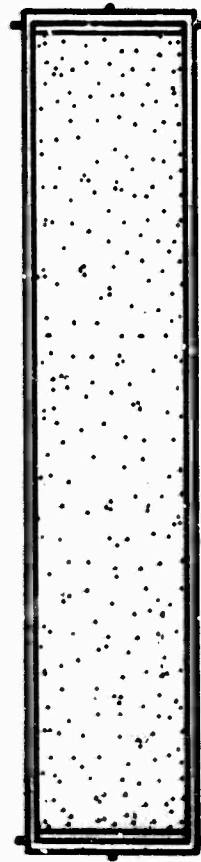


Fig. 3.2-3 BASIC COHERENT INTEGRATION BLOCK DIAGRAM

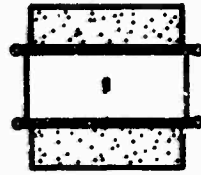
$$-(10.235)x^2 = (y^2 - 1) - (21,000)(y - 1)$$



Top View



Front View



Side View

Preliminary Specifications	
Dielectric Constant	1.05
Surface Tolerance	0.03"
Total Length	65'
Aperture Length	63'
Aperture Height	10'
Thickness	2'
Weight	2000 lb

Figure 3.2-4 DIELECTRIC LENS SPECIFICATIONS

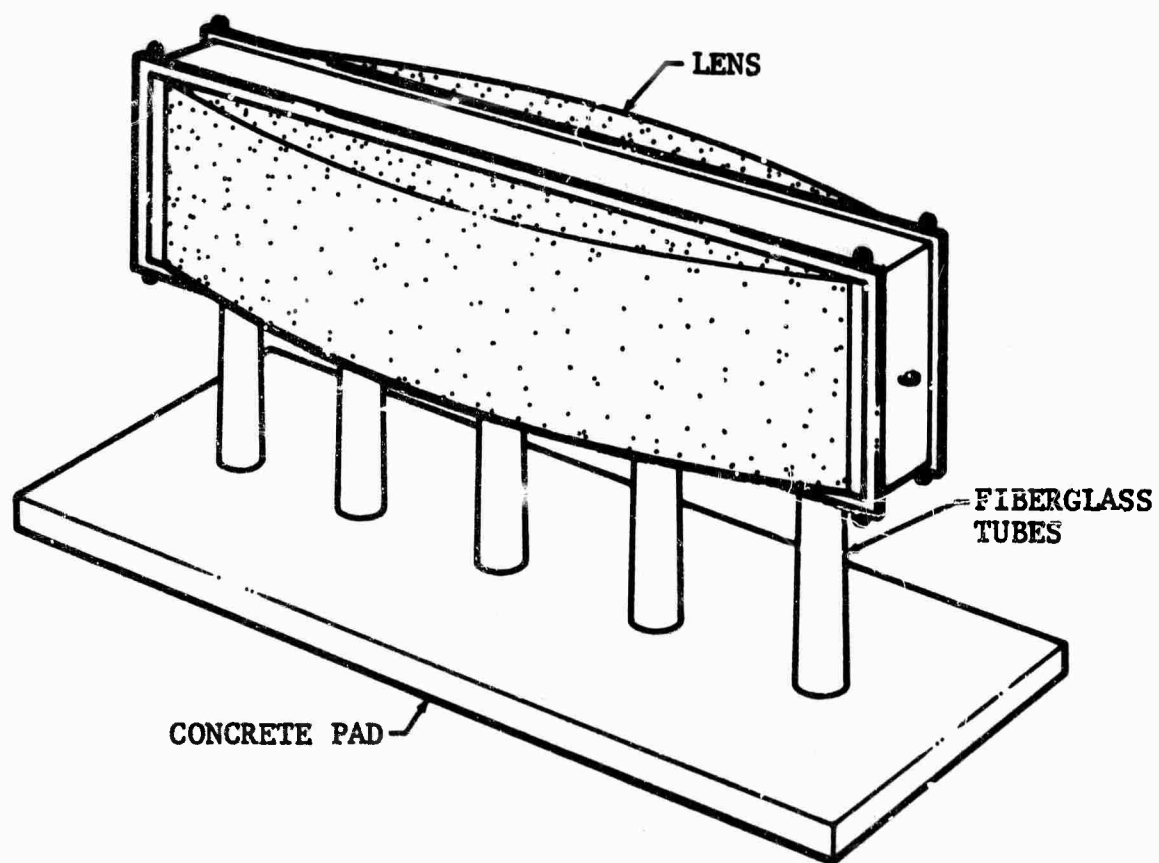


Fig. 3.3-1 DIELECTRIC LENS MOUNTING

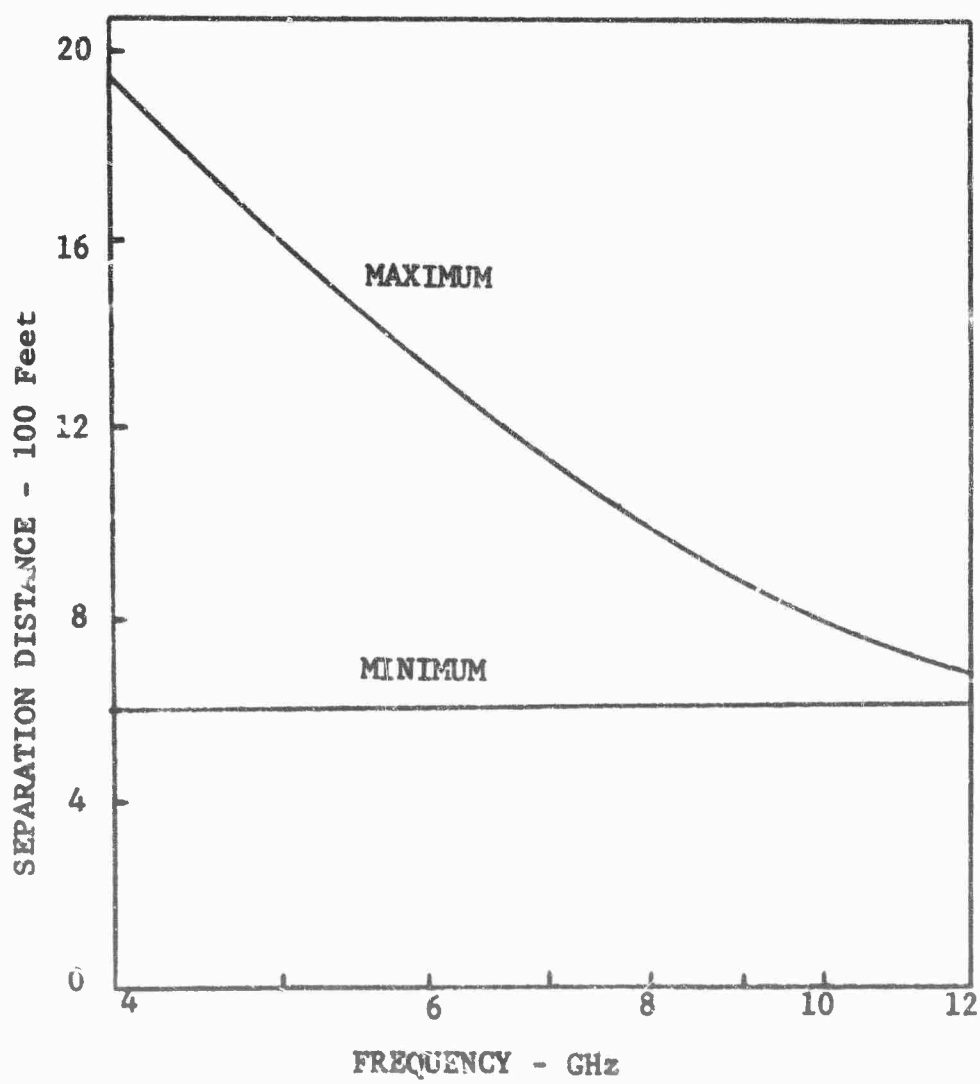


Fig. 3.3-2 TARGET-LENS SEPARATION

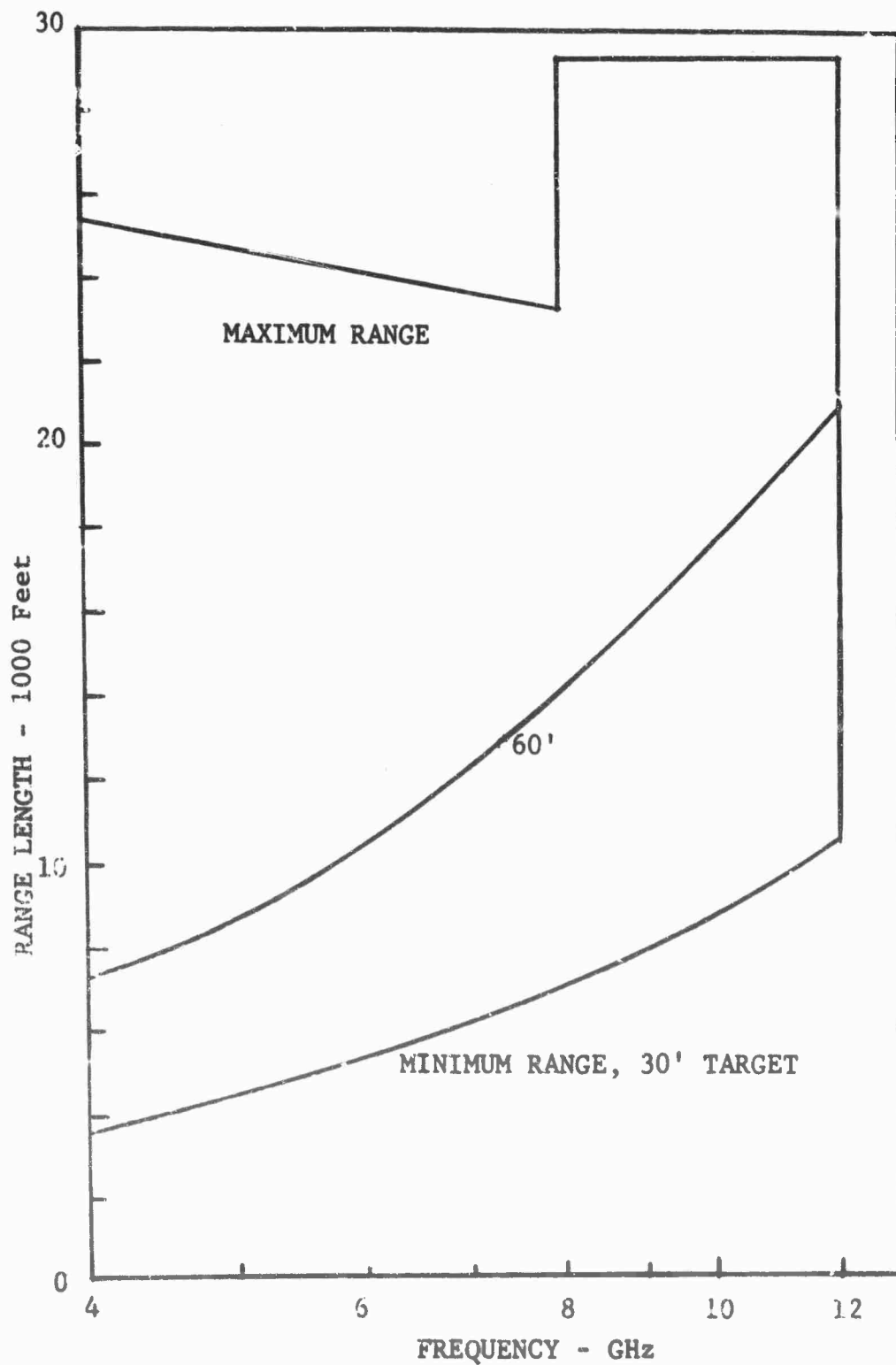


Fig. 3.3-3 ANTENNA-LENS SEPARATION ENVELOPE

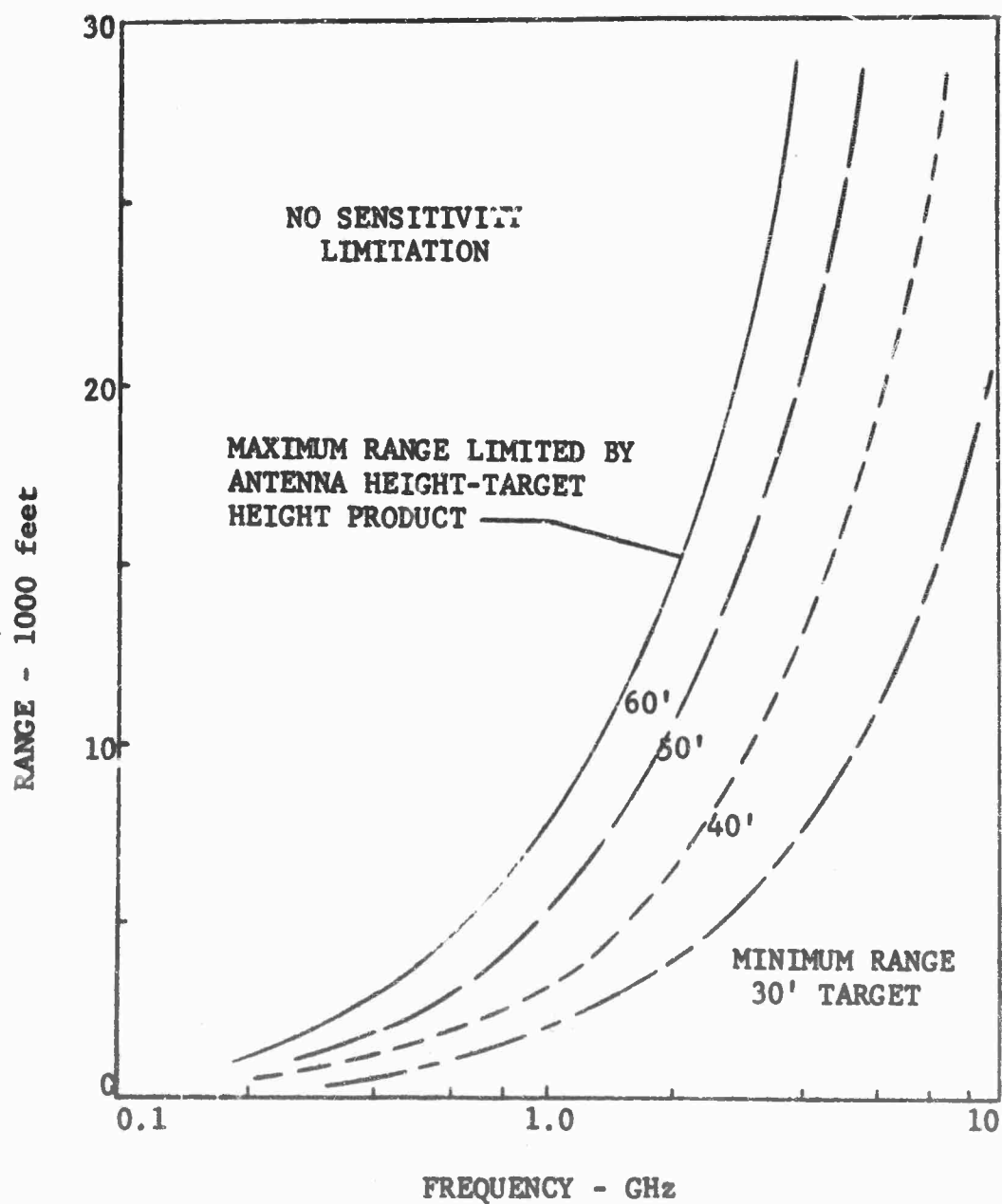
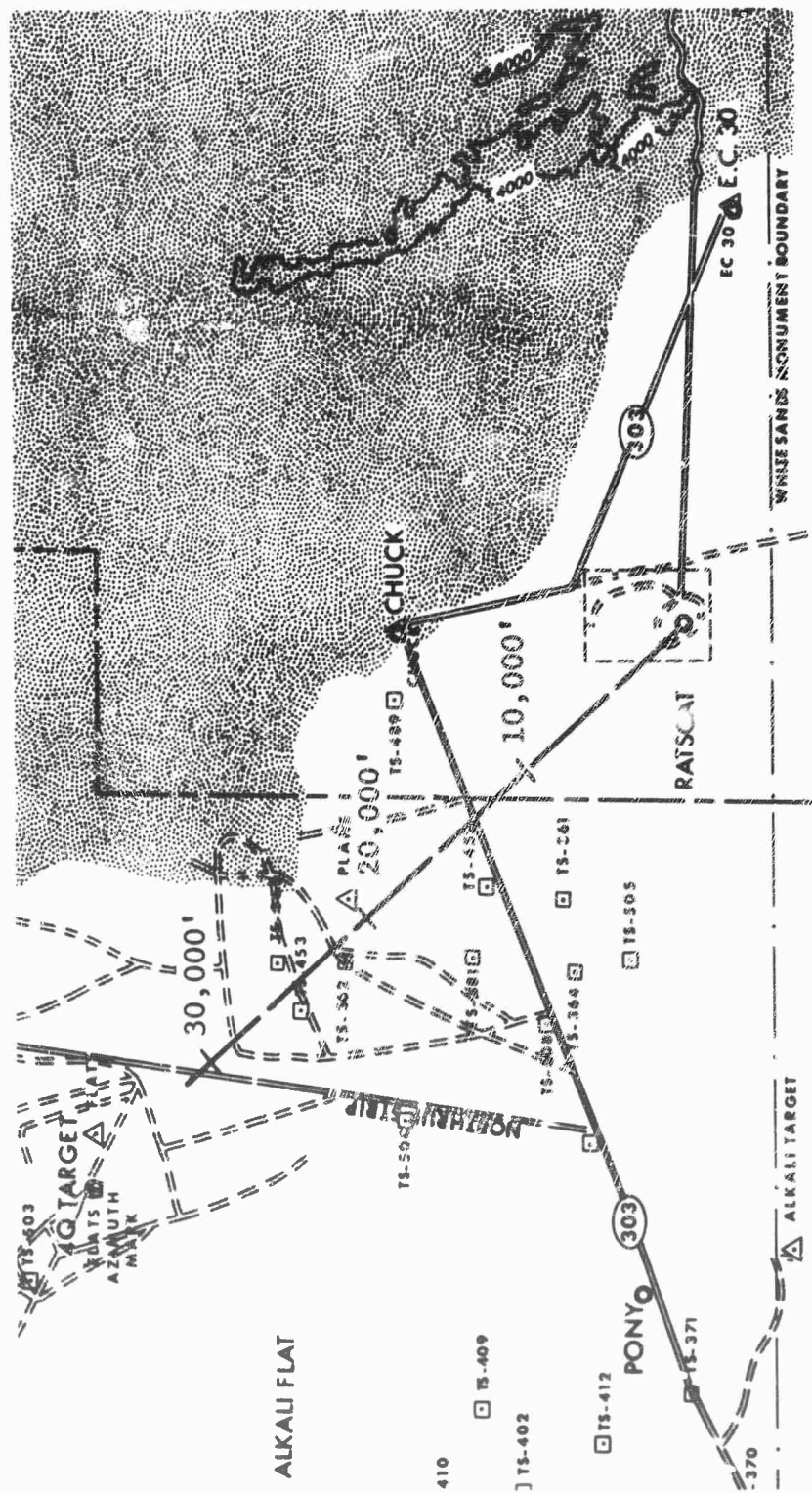


Fig. 3.3-4 LONG-RANGE OPERATIONAL ENVELOPE



APPENDIX A

SCALING ERROR COMPUTER PROGRAM

The scaling error investigation was conducted with the aid of an existing physical optics computer program (Fort Worth Division Procedure H-25) written at this division. This program was modified to allow the computation of theoretical scaling errors as presented in subsection 1.1 of this report. A comprehensive description of the general computer program is presented in Reference 15 and in a description of that portion of the computer program used in the large-object scaling-error investigation is presented in this appendix.

The basic program logic is presented in Figure A-1 along with the definitions of the index parameters. It is evident from the figure that the program logic basically consists of making individual cross section computations (k index) vectorially combined at each of a selected number of aspect intervals (i index) and then repeating this process for a selected number of geometrical perturbations (n index) which represent scale factor errors.

The k^{th} cross section computation is performed by using the physical optics expression for the k^{th} type of generic shape used to describe the composite target being studied (see Figure 1.1-2). At present, expressions for six types of surfaces are available, and these are listed in Equations A-1 through A-6 (Table A-1). Note that the frustrum expression (Equation A-5) represents the frustrum, cone, and right circular cylinder in the broadside region, whereas the cone represents the cone only in the nose-on region.

APPENDIX A

SCALING ERROR COMPUTER PROGRAM

The scaling error investigation was conducted with the aid of an existing physical optics computer program (Fort Worth Division Procedure H-25) written at this division. This program was modified to allow the computation of theoretical scaling errors as presented in subsection 1.1 of this report. A comprehensive description of the general computer program is presented in Reference 15 and in a description of that portion of the computer program used in the large-object scaling-error investigation is presented in this appendix.

The basic program logic is presented in Figure A-1 along with the definitions of the index parameters. It is evident from the figure that the program logic basically consists of making individual cross section computations (k index) vectorially combined at each of a selected number of aspect intervals (i index) and then repeating this process for a selected number of geometrical perturbations (n index) which represent scale factor errors.

The k^{th} cross section computation is performed by using the physical optics expression for the k^{th} type of generic shape used to describe the composite target being studied (see Figure 1.1-2). At present, expressions for six types of surfaces are available, and these are listed in Equations A-1 through A-6 (Table A-1). Note that the frustrum expression (Equation A-5) represents the frustrum, cone, and right circular cylinder in the broadside region, whereas the cone represents the cone only in the nose-on region.

Table A-1 EQUATIONS FOR FIVE BASIC
TYPES OF SURFACE (Continued)

a = small radius of frustrum in wavelengths

L = length of frustrum

α = half angle

$$f(t, a, \theta, \alpha) = \int_0^1 \left[a + L \tan \alpha \right]^{\frac{1}{2}} \left[e^{(4\pi i \sin(\theta - \alpha)/\cos \alpha)V} \right] dv$$

X, Y = dependent on constants a, L, α

Cone - Equation A-E

$$\sqrt{\sigma} = \lambda \sqrt{\pi} \tan^2 \alpha L \quad 0 \leq \theta \leq X$$

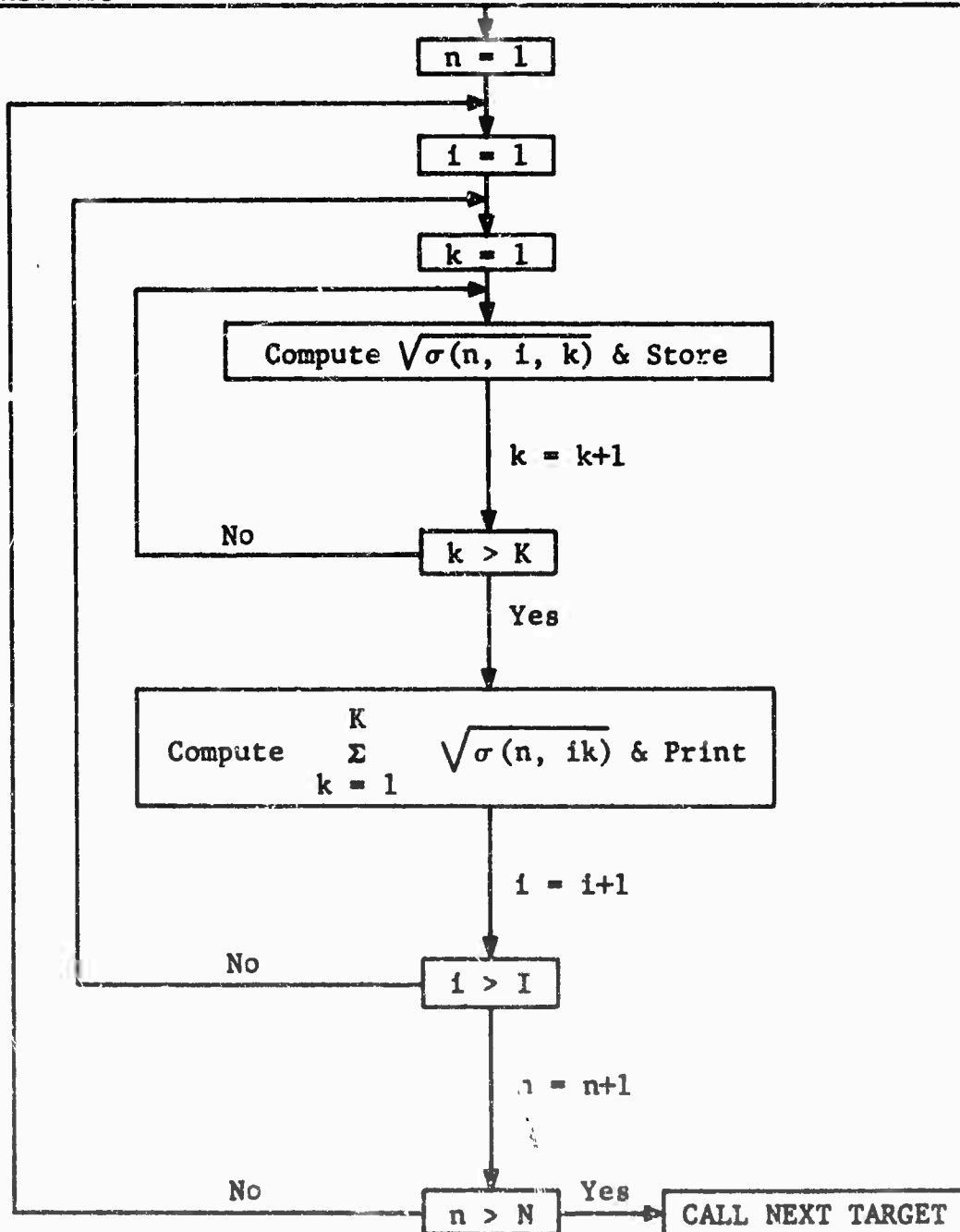
L = cone length in wavelengths

α = cone half angle

X = compatible with Equation E

INPUT DATA

Target designation, frequency, scale factor, number of generic shapes (K), number of aspect angles (I), number of geometrical perturbations (N), size of geometrical perturbations, generic shape size constants, generic shape geometrical position constants



Basic Computer Logic
Figure A-1

APPENDIX B

NEAR-FIELD ERROR COMPUTER PROGRAM

B.1 Development of Equations

The Fort Worth Division has written a computer program for predicting the near-field error associated with the measurement of an elliptical cylinder target. The equations were written for programming on an IBM 7090/7040 and have been incorporated in the subroutines of program H86 of this division.

The basic near-field error expression in the case of an ideal ground plane range can be written as in Equation B-1.

$$E = \frac{\left| \int_x \int_z A_r(x,z) e^{-\frac{1\pi}{R_0} [x^2 - 2x(h_t - h_a) + z^2]} \left[\int_S e^{-12\pi y'} I(x',z') \cos \frac{2\pi}{R_0} (x'x + xh_t + x'h_a) e^{-\frac{12\pi}{R_0} (x'^2 + z'^2 - x'x - z'z)} N_y ds \right] dx dz \right|^2}{\left| \int_x \int_z A_r(x,z) e^{-\frac{1\pi}{R_0} [x^2 - 2x(h_t - h_a) + z^2]} I(0,0) \cos \frac{2\pi x h_t}{R_0} dx dz \right|^2} \quad (B-1)$$

$$\left| \int_S e^{-14\pi y'} N_y ds \right|^2$$

$$-\frac{D_r}{2} \leq x \leq \frac{D_r}{2}, \quad -\frac{D_r}{2} \leq z \leq \frac{D_r}{2}$$

where

$$A_T(x, z) = \left[1 - \left(\frac{2x}{D_r} \right)^2 \right]^{\frac{1}{2}} \left[1 - \left(\frac{2z}{D_r} \right)^2 \right]^{\frac{1}{2}}, \quad D_r = \text{diameter of receiver antenna in wavelengths}$$

$$I(x', z') = \left[1 - \frac{1}{2} \left(\frac{D+z'\pi'}{2R_0} \right)^2 \right] \cos \frac{\pi' x'}{2h_t},$$

D_t = diameter of transmit antenna in wavelengths

$$z' \leq \frac{R_0}{\pi D_t}, \quad -h_t \leq x' \leq h_t$$

In the case of an elliptic cylinder oriented with the major and minor axes aligned with the x' and y' coordinates, the value of the y component of the unit normal N_y times ds can be written in terms of θ by using the expression

$$\left(\frac{\partial s}{\partial y'} \times \frac{\partial s}{\partial z'} \right)_y$$

where $s(x', y', z')$ describes the surface of the elliptic cylinder. The resulting expression is given in Equation B-2.

$$\int_S e^{-i2\pi y'} N_y ds = \frac{2A}{B^2} \int \frac{L \cos \theta}{2} - \frac{L \cos \theta}{2} \quad (B-2)$$

$$-z' \tan \theta$$

$$\int e^{-i4\pi y'} \frac{(y' \cos \theta + z' \sin \theta) dy' dz'}{\left(1 - \frac{1}{B^2} [y' \cos \theta + z' \sin \theta]^2 \right)^{\frac{1}{2}}}$$

$$-(z' \tan \theta + B / \cos \theta)$$

The 2 in the integral multiplier appears because of the double value representation of the cylinder x' coordinate by y' , where

A = radius of major axis in wavelengths

B = radius of minor axis in wavelengths.

The limits of the integrals are determined from the geometry of a finite cylinder under the assumption that the end plates are always parallel to the radar line of sight and there are no currents past the shadow boundary.

Since Equation B-2 represents the cross section of the cylinder unmodified by near-field and antenna effects, it is convenient to evaluate this equation in closed form to avoid repeated numerical integration. Closed-form evaluation can be accomplished in the large-object case by evaluating Equation B-2 as B becomes large. To take this limit, it is convenient to replace $y'\cos\theta + z'\sin\theta$ by W and z' by V . This transformation results in Equation B-3.

$$\int_S e^{-i2\pi y'} N_y ds = \frac{2A}{B^2 \cos\theta} \left[\begin{array}{l} \frac{L \cos\theta}{2} \\ \frac{-L \cos\theta}{2} \end{array} \right] e^{+i4\pi V \tan\theta} \quad (B-3)$$

$$\left[\int_{-B}^0 e^{\frac{-14\pi W}{\cos\theta}} \frac{W dW}{\left[1 - \left(\frac{W}{B}\right)^2\right]^{\frac{1}{2}}} \right] dv$$

Equation B-3 can be integrated to obtain Equation B-4 for which the large B value limit is given in Equation B-5.

$$\int_S e^{-i2\pi y'} N_y ds = \left[\frac{-A \sin(2L\pi \sin\theta)}{\sin\theta} \right] \quad (B-4)$$

$$\cdot \left[1 - \frac{\pi}{2} \left(H_1 \left(\frac{2\pi B(1)^2}{\cos\theta} \right) + i J_1 \left(\frac{2\pi B(1)^2}{\cos\theta} \right) \right) \right]$$

where the J_1 and H_1 represent the Bessel and Struve functions of order 1, respectively.

$$\int_S e^{-i2\pi y'} N_y ds = i \sqrt{\frac{\cos\theta}{8B}} \frac{A \sin(2L\pi \sin\theta)}{\pi \sin\theta} \quad (B-5)$$

Note that the validity of the expression in Equation B-5 can be checked for the case of a circular cylinder by letting $B = A$, and after multiplication by $2\sqrt{\pi}$ to obtain cross section, the result is the standard physical optics $\sqrt{\sigma}$ expression for a cylinder.

The next expression to be considered is the other term in the denominator of Equation B-1. This term can be written as the product of two integrals as given in Equation B-6 and B-7.

$$I_1 = \int_{-D_r/2}^{D_r/2} \left[1 - \left(\frac{2x}{D_r} \right)^2 \right]^{\frac{1}{2}} \left(\cos \frac{\pi\alpha}{2h_t} \cos \frac{2\pi}{R_c} [x(h_t - \alpha) - \alpha h_a] \right) \quad (B-6)$$

$$\cdot \left(e^{\frac{-i\pi}{R_0}} [x^2 - 2x(h_t - h_a - \alpha) + 2\alpha^2] \right) dx$$

$$I_2 = \int_{-D_r/2}^{D_r/2} \left[1 - \left(\frac{2z}{D_r} \right)^2 \right]^{\frac{1}{2}} e^{-\frac{i\pi}{R_0} z^2} dz \quad (B-7)$$

where x' has been changed to $x' - \alpha$ and α denotes the distance between the center of the cylinder and the center of the beam in the vertical direction in wavelengths.

The expressions in equations (B-6) and (B-7) are programmed in subroutines 2 and 1, respectively, by using numerical integration. The criterion used to determine the integration interval was that of phase variation across the antenna aperture. The aperture was divided into intervals so that the phase variation over each of the intervals was less than 1.0 degree. In particular, the aperture is divided as indicated in Equation B-8.

$$K = 72 D_r^2 / R \quad (B-8)$$

where K is the number of intervals.

Equations B-5, B-6, and B-7 were used to represent the denominator of Equation B-1. The combinations of these equations used in the four subroutines will be discussed after the numerator of Equation B-1 is reduced to a form similar to Equations B-6 and B-7. This step was accomplished to reduce the number of integration intervals and to simplify the programming. By retracing the steps used to separate the variables to obtain Equation B-9, the numerator of Equation B-1 can be written as shown in Equations B-9 and B-10.

$$I_3 = \int_{-D_r/2}^{D_r/2} \left[1 - \left(\frac{2x}{D_r} \right)^2 \right]^{\frac{1}{2}} e^{-\frac{i\pi}{R_0} [x^2 - 2x(h_t - h_a - \alpha) + 2\alpha^2]} \quad (B-9)$$

$$\left(\sum_{-B}^{+} \int_{-B}^0 e^{-\frac{4\pi i w}{\cos \theta}} \cos f_1^{\pm}(w) \cos f_2^{\pm}(w, x) \frac{e^{\pm f_3(w, x)} (A/B^2) W dW}{\cos \theta \left[1 - \left(\frac{W}{B} \right)^2 \right]^{\frac{1}{2}}} \right) dx$$

where

$$f_1^{\pm}(w) = \frac{\pi}{2h_t} \left(\pm A \left[1 - \left(\frac{W}{B} \right)^2 \right]^{\frac{1}{2}} - \alpha \right)$$

$$f_2^{\pm}(w, x) = \frac{2\pi}{R_0} \left(\pm A \left[1 - \left(\frac{W}{B} \right)^2 \right]^{\frac{1}{2}} [x+h_a] + x[h_t - \alpha] - h_a \alpha \right)$$

$$f_3^{\pm}(w, x) = \frac{-12\pi}{R_0} \left(A \left[1 - \left(\frac{W}{B} \right)^2 \right]^{\frac{1}{2}} \right) \left(A \left[1 - \left(\frac{W}{B} \right)^2 \right]^{\frac{1}{2}} \mp [x + 2\alpha] \right)$$

and the \pm occurs because of the double-valued relation between x' and y', z' and the \sum^{\pm} denotes summing the integral for the case of the (+) and the (-) integral function.

$$I_4 = \int_{-D_r/2}^{D_4/2} \left[1 - \left(\frac{2z}{D_r} \right)^2 \right]^{\frac{1}{2}} \epsilon^{-\frac{i\pi Z^2}{R_0}} \left(\int_{-\frac{L \cos \theta}{2}}^{\frac{L \cos \theta}{2}} \epsilon^{i4\pi v \tan \theta} \left[1 - \frac{1}{2} \left(\frac{D_t v}{2R_0} \right)^2 \right] \epsilon^{\frac{-12\pi}{R_0} (v^2 - vz)} dv \right) dz \quad (B-10)$$

It can be seen that the form of Equations B-9 and B-10 is identical to that of Equations B-6 and B-7. However, to evaluate the inside integral in Equations B-9 and B-10, denoted by (*) and (**), numerical integration must be used, whereas the corresponding terms in Equations B-6 and B-7 are simple expressions.

To numerically integrate the (*) term in Equation B-9, it was noted that, except for the term

$$\epsilon^{\frac{-4\pi iw}{\cos \theta}},$$

the integral was slowly varying. Hence, the (*) term of Equation B-9 was put in the form of Equation B-11 in order to perform the numerical integration. (To obtain Equation B-11 from Equation B-9, let $W/B = \sin \phi$.)

$$(A/\cos \theta) D(\phi, x) \left(\int_{-\pi/2}^0 \epsilon^{\frac{-4}{\cos \theta} B i \sin \phi} d\phi \right) \quad (B-11)$$

$$\text{where } D(\phi, x) = \left(\left[\cos f_1^+ (B \sin \phi) \cos f_2^+ (B \sin \phi, x) \right. \right. \\ \left. \left. e^{f_3^+ (B \sin \phi, x)} \right] + \left[\cos f_1^- (B \sin \phi) \right. \right. \\ \left. \left. \cos f_2^- (B \sin \phi, x) e^{f_3^- (B \sin \phi, x)} \right] \right) \sin$$

Since $4B/\cos\theta$ will in general be quite large in the case of the large-object study, the integral in Equation B-11 was evaluated by changing variables to $\bar{\phi} = 4B \sin \phi / \cos \theta$ and integrating between $\bar{\phi}_i$ and $\bar{\phi}_{i+1}$ so that $\bar{\phi}_{i+1} - \bar{\phi}_i = 1$. Use of this technique gives a Stieltjes type of integral rather than a Riemann integral. Using this technique reduces the number of integration intervals by better than an order of magnitude. The form of the equation obtained by using the above change of variables is given in Equation B-12.

$$(*) = - \frac{2}{\pi} \frac{A}{\cos \theta} e^{i\pi s} \sum_{r=1}^{r=s} D(\phi_r, x) \Delta \phi_r (-1)^r \quad (\text{B-12})$$

where

$$\Delta \phi_r = \sin^{-1} \left(1 - \frac{r}{s} \right) - \sin^{-1} \left(1 - \frac{r+1}{s} \right)$$

$$\phi_r = \sin^{-1} \left(\frac{r}{s} - 1 \right) + \frac{\Delta \phi_r}{2} \quad \begin{array}{l} \text{(Use of this equality} \\ \text{allows the function} \\ D(\phi_r, x) \text{ to be evaluated} \\ \text{at the midpoint of the} \\ \text{integration interval)} \end{array}$$

$$S = 4B/\cos \theta$$

Equation B-12 was used to evaluate the (*) term in Equation B-9 although the term $e^{i\pi s}$ was omitted because of the absolute magnitude signs in Equation B-1.

To evaluate the (**) term in Equation B-10, a process similar to that used to arrive at Equation B-12 was used. It was noted that the rapid changing term could be integrated

$$e^{i4\pi v \left(\tan \theta + \frac{z}{2R_0} \right)}$$

Hence the numerical integration should be carried out over the phase variation of the term

$$e^{-i2\pi v^2/R_0}$$

Making the change of variable from v to $u = 2v/L\cos\theta$ and reducing the limits of integration from -1 to 1 to 0 to 1 give the form of the expression used to evaluate the (**) term of Equation B-10. This expression is written in Equation B-13.

$$(**) = \frac{2\cos\theta}{\pi(2\sin\theta + z\cos\theta)} \left(\sum_{r=1}^{r=s} \left[1 - \frac{1}{2} \left(\frac{D_t u'_r L \cos\theta}{4R_0} \right)^2 \right] \right) \quad (B-13)$$

$$\left[e^{\frac{-i\pi L^2 \cos^2\theta (u'_r)^2}{2R_0}} \right] \left[\sin \left(\frac{\pi L}{2} \Delta u_r \left(2\sin\theta + \frac{z\cos\theta}{R_0} \right) \right) \right]$$

$$\left[\cos \frac{\pi L}{2} \left(2\sin\theta + \frac{z\cos\theta}{R_0} \right) \left(u_r + \sqrt{u_r^2 + 1/S} \right) \right]$$

where

$$S = 36L^2 \cos^2 \theta_1 / R_0 \quad (s \text{ is the number of 5-degree, two-way phase variations across half of the cylinder length projected onto the } z' \text{ axis.})$$

$$\Delta u_r = \left(\sqrt{u_r^2 + 1/S} - u_r \right) \quad (\Delta u_r \text{ is such that each integration interval is 5 degrees})$$

$$u_r' = u_r + \Delta u_r / 2 \quad (\text{Use of this equality } u_r' \text{ allows the function to be evaluated in the middle of the integration interval.})$$

Equation B-13 was used to evaluate the (**) term of Equation B-10, but special consideration was given to the last integration interval. The reason for this is that a major contribution can come from the last integration interval; consequently, the computer program was written so that the integration was performed over each 5-degree phase interval, and the contribution from the last interval, which was not necessarily 5 degrees, but never greater than 5 degrees, was added.

B.2 Program Summary

The derivation of Equations B-5 through B-13 constitutes the basic steps used to reduce the general near-field error expression to several basic subforms which can be used to study the near-field error for the major measurement conditions of interest.

B.2.1 Subroutines

The equations indicated above were used in various combinations to obtain the four computer programs (subroutines) used to investigate the near field error in the large object study. To explain how the four subroutines were generated it is convenient to represent Equations B-5, B-6, B-7, B-9 and B-10 by the symbols A' , B' , C' , D' , and F , respectively. By using this representation, Equation B-1 can be written as

$$E = \frac{|D'|^2 |F|^2}{|A'|^2 |B'|^2 |C'|^2} \quad (B-14)$$

B.2.1.1 Subroutine I. In the case of horizontal field curvature only, note that D'^2 becomes equal to $B'^2 A^2/2 \cos \theta B$ and therefore B-14 is reduced to

$$\begin{aligned} E &= \frac{|F|^2 A^2/2 \cos \theta B}{|C'|^2 \frac{\cos \theta}{8B} \frac{4A^2 L^2 \sin^2 2L\pi \sin \theta}{(2\pi L \sin \theta)^2}} \\ &= \frac{|F|^2 (2\pi L \sin \theta)^2}{|C'|^2 \cos^2 \theta L^2 \sin^2 (2L\pi \sin \theta)} \end{aligned} \quad (B-15)$$

This expression ($10 \log E$) was programmed for subroutine I in which the technique represented by Equation B-13 was used to numerically integrate F along with the technique described for C' .

B.2.1.2 Subroutine II. In the case of vertical field curvature only, note that $|F|^2$ becomes equal to $|C'|^2$

$$\frac{\cos^2 \theta L^2 \sin^2 2L\pi \sin \theta}{(2\pi L \sin \theta)^2}$$

and B-14 is therefore reduced to the expression

$$E = \frac{|D'|^2 (\cos^2 \theta L^2 \sin^2 [2L\pi \sin \theta]) / (2\pi L \sin \theta)^2}{|B'|^2 \frac{\cos \theta}{8B} \frac{A^2 \sin^2 (2L\pi \sin \theta)}{\pi^2 \sin^2 \theta}} \quad (B-16)$$

$$= \frac{|D'|^2 2B \cos \theta}{|B'|^2 A^2}$$

This expression (10LogE) is equivalent to that programmed for subroutine II although the actual expression for $|D'|^2$ which was programmed was equal to $(A^2/\cos^2 \theta) |D'|^2$. To evaluate the expression for D' , the technique represented by Equation B-12 was used along with the numerical technique described for B' (Equation B-6).

B.2.1.3 Subroutine III. In the case of the point source antennas, if field variations appear in both the vertical and horizontal planes, note that $|D'|^2$ and $|F|^2$ are reduced to $|B'|^2$ (bracket term of D') $^2/|F(\alpha)|^2$ and $|C'|^2$ (bracket term of F) 2 , respectively. Equation B-14 is reduced to

$$E = |{(12)}|^2 |{(13)}|^2 / \frac{\cos \theta A^2 \sin^2 (2L\pi \sin \theta)}{8B \left(\cos \frac{\pi \alpha}{2H_t} \right)^2 \pi^2 \sin^2 \theta \left(\cos \frac{2\pi H_a \alpha}{R} \right)^2} \quad (B-17)$$

$$F(\alpha) = \cos \frac{\pi \alpha}{2H_t} \cos \frac{2\pi H_a \alpha}{R}$$

This expression (10 Log E) is equivalent to that programmed for subroutine III although as in subroutine II the programmed $|{(12)}|^2$ was equal to $(A^2/\cos^2 \theta) |{(12)}|^2$.

B.2.1.4 Subroutine IV. In the case of finite antennas and curvature in both the vertical and horizontal planes, note that the product of Equations B-15 and B-16 give Equation B-14 which is the general expression. Hence subroutine IV is the sum of the results of subroutines I and II.

B.2.2 Additional Computations and Variables

B.2.2.1 Cross Section. In addition to the error computations which can be made using any or all of the four subroutines, the cross section of the cylinder was computed and normalized to the broadside value. This expression is given in Equation B-18.

$$\sigma/\sigma_{\max} = \cos \theta \left[\frac{\sin (2 \pi L \sin \theta)}{(2 \pi L \sin \theta)} \right]^2 \quad (\text{B-18})$$

The value of σ/σ_{\max} was included in subroutines I and II only.

B.2.2.2 Variables. In order to compute error as a function of range and azimuth, the computer program was designed to increment these variables by replacing all of the R_0 and θ variables in the equations by the range and azimuth variables to obtain

$$R = R_0 [1 + \beta(M-1)] \quad M \leq 10, \quad \beta \text{ chosen to represent the desired range step}$$

$$\theta = \theta_0 [1] + \Delta \theta(N-1) \quad N \leq 50, \quad \Delta \theta \text{ in radians chosen to represent the desired azimuth change.}$$

Also the antenna height h_a is adjusted automatically to compensate for changes in range. This compensation is accomplished by using the relationship given in Equation B-19 which is the standard ground plane relation for determining the center of the beam:

$$h_a = \frac{R \lambda}{4 h_t} \quad (\text{B-19})$$

The computer program flow diagrams are presented in Figures B-1 through B-4.

B.2.3 Checkout

The validity of the computer program was checked against the equations listed in the subroutines by using two basic

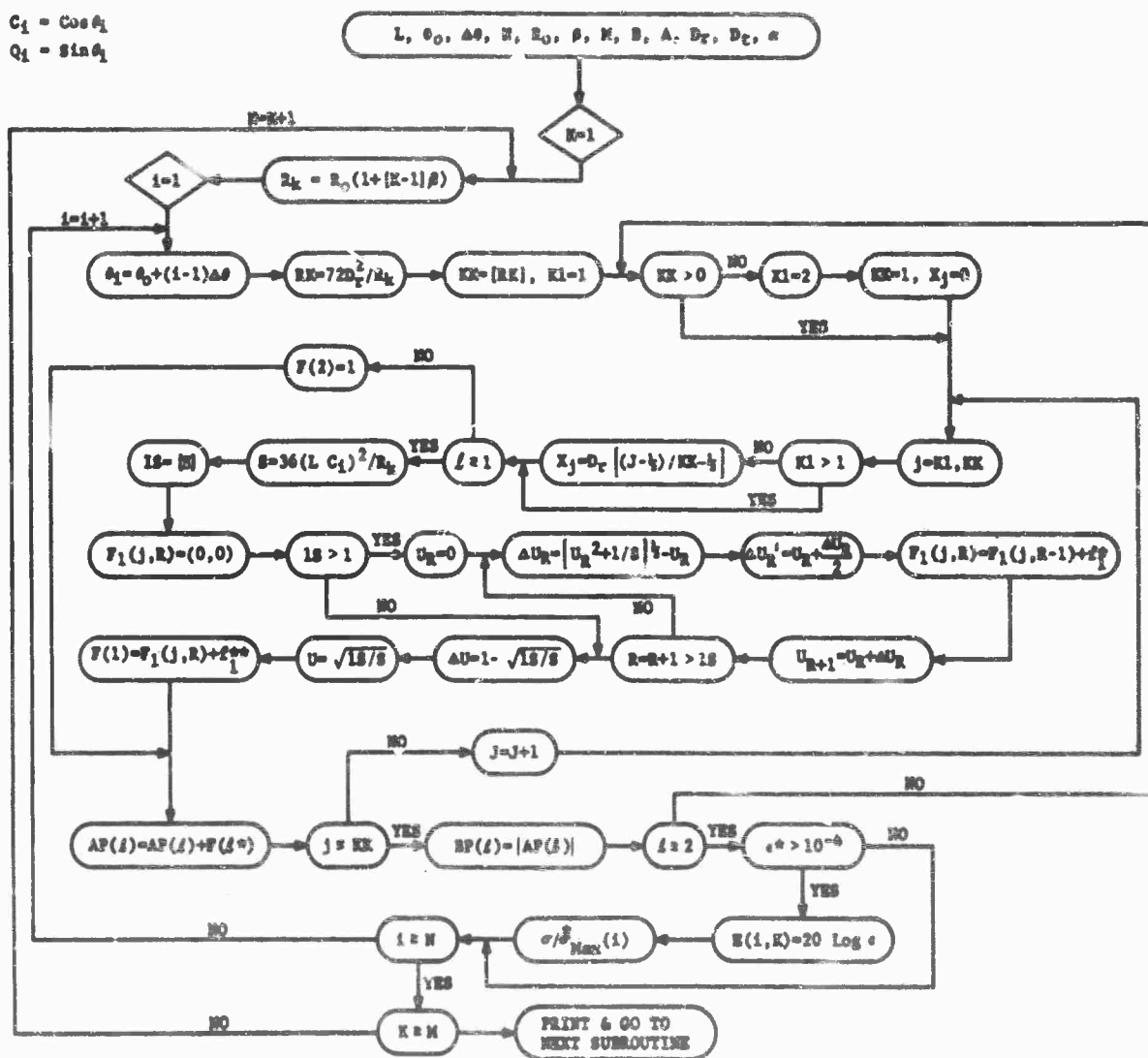
techniques. The first technique was that of comparing the computed data with hand calculations, and the second was that of comparing the outputs of related subroutines. The first method was used for checking subroutines I and II and the second for subroutines III and IV. The relationships between subroutines I and II and III and IV are (1) the error computed for subroutine III should equal the sum of the errors from subroutines I and II when small antennas are used and (2) the error computed for subroutine IV should equal the sum of the errors from subroutines I and II.

The hand calculations used to check subroutine I were taken from RADC Report TDR-64-397 pp. 13. By using the curve presented in the referenced report, the computed data checked within the resolution of the ability to read the error from the curve.

The hand calculations used to check subroutine II are listed in Table B-1 for the more complex operations shown in the flow diagram in Figure B-2. The input parameters for this problem are also listed in Table B-1.

Table B-1 VALIDATION DATA FOR SUBROUTINE II

Input Parameters		
$L=10^2$, $\theta_0=10^{-4}$, $R_0=5 \times 21 \times 10^3$, $A=B=10$, $D_t=D_r=25$, $H_t=39$, $\alpha=0$		
Operation	Slide Rule Computation	Computer Value
$kK = RK$	0	0
$IS = S$	40	40
$D^*(1,0)$	$-2.0 + j0$	$-1.98 + j0.000148$
$D^*(40,0)$	$-0.02 + j0$	$-0.0212 + j0.000127$
$F^*(2,0)$	$1 + j0$	$1 + j0$
$AP(2)$	$1 + j0$	$1 + j0$
$BP(2)$	1	1
$E(1,3)$	-0.28 db	-0.2799 db

$$\begin{aligned} C_1 &= \cos \theta_1 \\ Q_1 &= \sin \theta_1 \end{aligned}$$


$$f_1 = \frac{2C_1}{\sqrt{k_1}} \left[1 - \frac{(D_0 C_1 U_1 L_0)^2}{4 k_1} \right] \left[\frac{-1 + (U_1^2)_2 / 72}{\sin \frac{L_0}{2} U_1 (2Q_1 + K_1 C_1)} \right] \left[\frac{\cos \frac{L_0}{2} (2U_1 + aU_1) (2Q_1 + K_1 C_1)}{\frac{1}{k_1}} \right] \sqrt{\frac{2Q_1 + K_1 C_1}{k_2}}$$

$$z_1^{**} = \frac{2C_1}{\pi} \left[1 - \frac{1}{2} \left(\frac{D_0 C_1 L \pi}{4 R_k} \right)^2 \right] \left[e^{-L\pi/72} \left| \sin \frac{L\pi \sin U}{2} (2Q_1 + K_1 C_1) \right| \left| \frac{\cos L\pi (2U + \pi U)}{2} (2Q_1 + K_1 C_1) \right| \right] \left| \frac{2Q_1 + K_1 C_1}{\frac{1}{R_k}} \right|$$

$$F^*(f) = \left[1/K_2 \right] \left[1 - \left(\frac{2x_j}{\sqrt{\pi}} \right)^2 \right]^{1/2} \left[e^{-1/2 x_j^2 / R_k} \right] F(f), \quad c = \left| \frac{BP(1) 2\pi Q_1}{BP(2) C_1 \sin(2\pi L Q_1)} \right|$$

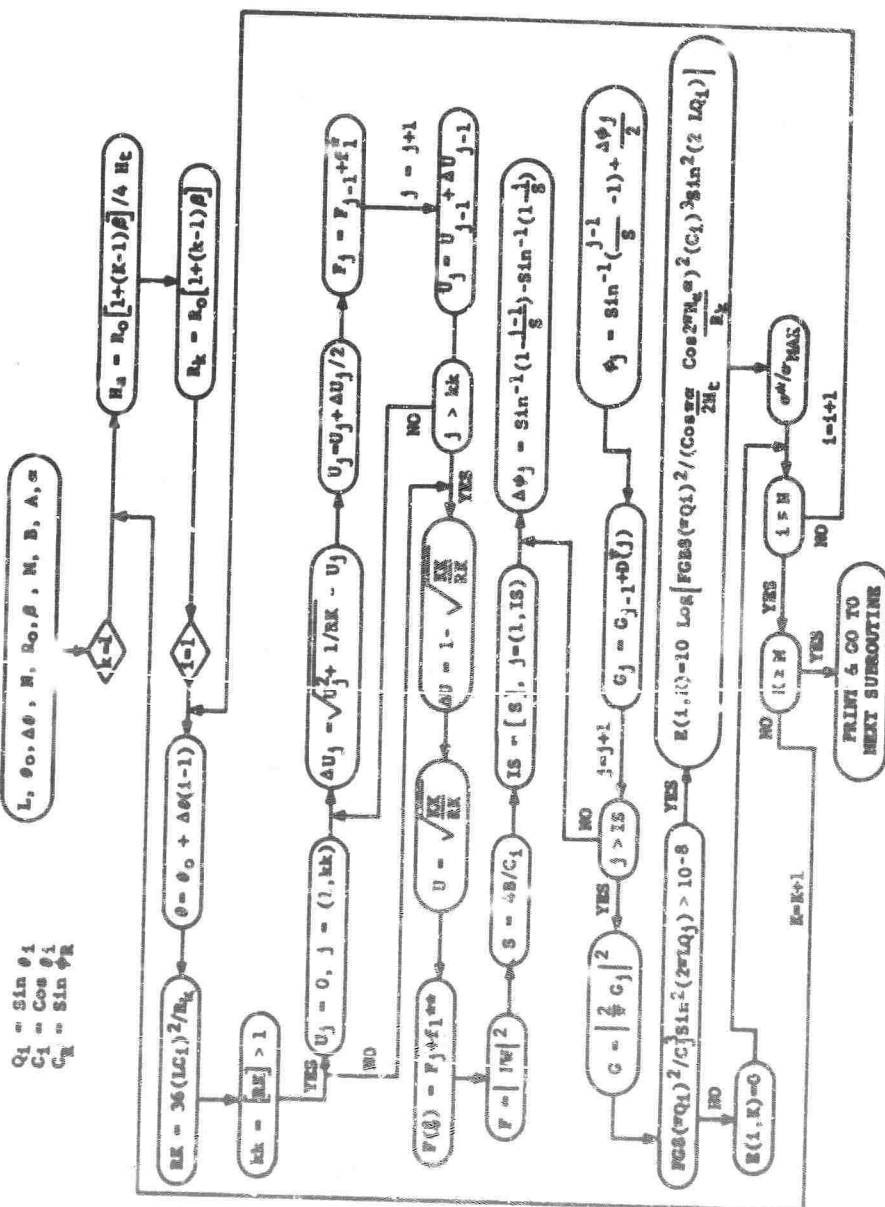
$$\sigma/\sigma_{\text{max}} = 20 \log \left| \sqrt{\epsilon_1} \sin(2\pi LQ_1) / 2\pi LQ_1 \right|$$

Fig. B-1 SUBROUTINE 1 PROGRAM H-86

[illegible]

$$\begin{aligned}
F^{\pm}(2, j) &= \left[\cos \frac{\pi \alpha}{2H_t} \right] \left[\cos \frac{2\pi(X_j[H_t - \alpha] - H_a \alpha)}{2H_t} \right] \\
D^{\pm}(R, j) &= \sin \theta_{Rj} \left[\left(\left| \cos \pi(AC_R - \alpha) / 2H_t \right| \cos \frac{2\pi(AC_R[X_j + H_a] + X_j[H_t - \alpha] - H_a \alpha)}{2H_t} \right) \left[e^{-2i\pi AC_R(AC_R - 2\alpha + X_j)} \right]^{\frac{1}{R_k}} + \right. \\
&\quad \left. \left(\cos \pi(AC_R + \alpha) / 2H_t \right) \left[\cos \frac{2\pi(AC_R[X_j + H_a] + X_j[\alpha - H_t] + H_a \alpha)}{2H_t} \right] \left[e^{-2i\pi AC_R(A/R + \frac{2\alpha + X_j}{R_k})} \right]^{\frac{1}{R_k}} \right] \left[\frac{2\Delta C_R(-1)^{R-1}}{R} \right] \\
F^{\pm}(j) &= \left| 1 / EK \right| \left[1 - (2X_j / D_r)^2 \right]^{\frac{1}{2}} \left[e^{-i\pi(X_j^2 - 2X_j[H_t - H_a - \alpha] + 2\alpha^2) / H_t} \right] \left[F / \delta \right]
\end{aligned}$$

FIG. B-2 SUBROUTINE 2 PROGRAM H-86



$\epsilon_1^0 = \text{SAME AS SUBROUTINE 1 WITH } X_j = 0,$
 $\epsilon_1^0 = \text{SAME AS SUBROUTINE 1 WITH } X_j = 0$
 $D^0(j) = \frac{1}{2}(D^0(R, j)) \text{ OF SUBROUTINE 2 WITH } X_j = 0, \phi^0/\phi_{MAX} = \text{SAME AS SUBROUTINES 1 \& 2}$

Fig. B-3 SUBROUTINE 3 PROGRAM H-86

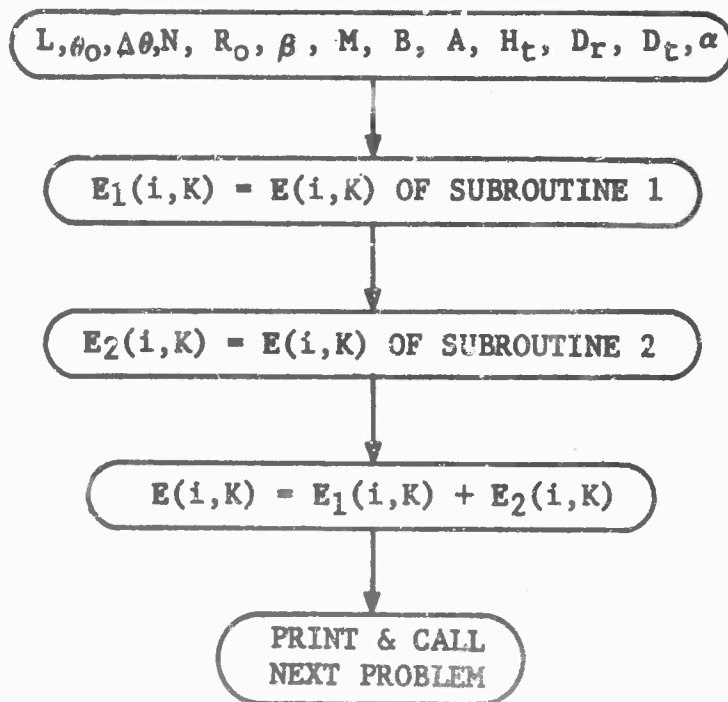


Fig. B-4 SUBROUTINE 4 PROGRAM H-86

REFERENCES

1. STRATTON, J. A., Electromagnetic Theory, McGraw-Hill Book Company, Inc., New York, 1941.
2. FREENY, C. C., "Target Support Parameters Associated With Radar Reflectivity Measurements," Proceedings of the I.E.E.E., Volume 53, pp 929-936, August 1965.
3. Investigation of Measurement Errors of the RAT SCAT Cross Section Facility, Technical Documentary Report No. RADC-TDR-64-397, July 1964.
4. Radar Cross Section Target Supports-Plastic Materials, Technical Documentary Report No. RADC-TDR-64-381, June 1964.
5. Background Subtraction Investigation, General Dynamics, Fort Worth Division Report No. FZE-645, 3 April 1967.
6. Theoretical and Experimental Investigation of a Technique For Reducing Extraneous Signals in Radar Scattering Measurements, Technical Documentary Report No. RADC-TDR-64-418, July 1964.
7. Scattering Matrix Utilization Study, Final Report, General Dynamics, Fort Worth Division Report No. FZE-666, 15 July 1967.
8. BARTON, DAVID K., Radar Systems Analysis, Prentice-Hall, Inc., New Jersey, 1964.
9. MENTZER, J. R., "The Use of Dielectric Lenses in Reflection Measurements," Proceedings of the I.R.E., Volume 41, pp. 254-256, February, 1953.
10. Short Pulse Model Measurement Studies, Technical Documentary Report No. RADC-TR-66-785, Volume 1, December, 1966.
11. COHEN, EDWARD, "Wind Load On Towers," Meteorological Monographs, Vol. 4, No. 22, May 1960.
12. Techniques for Airborne Radome Design, Vol. I, Air Force Avionics Laboratory Research and Technology Division Report AFAL-TR-66-391, December, 1966.

13. RAT SCAT Phase Measurement System, General Dynamics, Fort Worth Division Report No. FZE-344, 29 August 1964.
14. Proposal for Operation and Maintenance of the Air Force Radar Target Scatter Site, General Dynamics, Fort Worth Division Report No. FZP-813, 26 April 1966.
15. (RAT SCAT) Large Object Study, Quarterly Status Report, 23 September - 23 December 1966, General Dynamics, Fort Worth Division Report No. FZR-016-2, 23 December 1966.

UNCLASSIFIED

Security Classification

DOCUMENT CONTROL DATA - R & D

(Security classification of title, body of abstract and indexing annotation must be entered when the overall report is classified)

1. ORIGINATING ACTIVITY (Corporate author)		2a. REPORT SECURITY CLASSIFICATION	
General Dynamics P.O. Box 748 Fort Worth, Texas 76101		UNCLASSIFIED	
3. REPORT TITLE		2b. GROUP	
(RAT SCAT) LARGE OBJECT STUDY		N/A	
4. DESCRIPTIVE NOTES (Type of report and inclusive dates)			
FINAL			
5. AUTHOR(S) (First name, middle initial, last name)			
Dr. Charles C. Freeny Mr. William P. Cahill			
6. REPORT DATE		7a. TOTAL NO. OF PAGES	7b. NO. OF REFS
October 1967		306	15
8. CONTRACT OR GRANT NO.		9a. ORIGINATOR'S REPORT NUMBER(S)	
AF30(602)-4300		JFE-670	
a. PROJECT NO.		9b. OTHER REPORT NO(S) (Any other numbers that may be assigned this report)	
6503		RADC-TR-67-465	
c. Task No.			
650301			
d. Unit No.			
02			
10. DISTRIBUTION STATEMENT			
This document is subject to special export controls and each transmittal to foreign governments, foreign nationals or representatives thereto may be made only with prior approval of RADC (EMLI), GAFB, N.Y. 13440			
11. SUPPLEMENTARY NOTES		12. SPONSORING MILITARY ACTIVITY	
		Rome Air Development Center (EMASP) Griffiss AFB, N.Y. 13440	
13. ABSTRACT			
<p>The investigation reported herein has been directed to defining an optimum means of implementing a capability for measurement of large-object radar cross section at the Radar Target Scattering Site, White Sands Missile Range. The required capability is that of accommodating targets up to 60 feet in length, over a frequency range of 0.03 to 12 gigahertz, and maintaining the present RAT SCAT measurement accuracy. The primary trade-off feature in this study was the requirement for range length, which exceeded 16 miles in the case of the most straight-forward approach to large-object measurement. This condition is commonly defined by $R > 2D^2/\lambda$ when D is the minimum target dimension and λ is the radar wavelength.</p> <p>Four basic measurement methods were analyzed in this investigation: (1) scaling, wherein the target size and range length are reduced via the well-known scaling laws, (2) long range and high power, wherein a range length of $2D^2/\lambda$ is used, (3) antenna far field simulation, wherein a dielectric lens is used to partially correct the phase of the incident illuminating field, and (4) analytical correction of near field data, wherein data obtained at $R < 2D^2/\lambda$ is analytically processed to obtain data equivalent to that at $R = 2D^2/\lambda$.</p> <p>The study conclusions are based on extensive theoretical investigation and experimental testing. Over 200,000 IBM 7090 computations and 250 experiments were performed. A trade-off study was conducted in order to uniformly evaluate the impact of the selection of the several methods. The final selection represents a combination</p> <p style="text-align: center;">continued</p>			

DD FORM 1 NOV 66 1473

UNCLASSIFIED

Security Classification

UNCLASSIFIED

Security Classification

14. KEY WORDS	LINK A		LINK B		LINK C	
	ROLE	WT	ROLE	WT	ROLE	WT
<p>Radar Reflectivity</p> <p>Static Range Cross Section</p> <p>Near Field Effects</p> <p>Lens Correction</p> <p>Analytic Correction</p> <p>Full-size Targets</p> <p>Scaled Targets</p> <p>Abstract (contd)</p> <p>of the long-range, and high-power, and antenna far-field simulation methods. The sensitive target length and frequency regions were determined to be 30 feet $\leq D \leq$ 60 feet and 4 gigahertz $\leq F \leq$ 12 gigahertz. With these bounds, the latter method is specified for the regions (1) $D >$ 40 feet, $F >$ 4 gigahertz and (2) $F >$ 8 gigahertz. Other methods were eliminated in the trade-off study on the basis of the cost required to achieve the necessary range length or measurement accuracy.</p>						

UNCLASSIFIED

Security Classification